GENETIC, ENVIRONMENTAL AND SYNERGISTIC GENE-ENVIRONMENT CONTRIBUTIONS TO CRANIOFACIAL DEFECTS

EDITED BY: Sebastian Dworkin, Peter John Anderson, Karen Liu and Mary L. Marazita

PUBLISHED IN: Frontiers in Cell and Developmental Biology

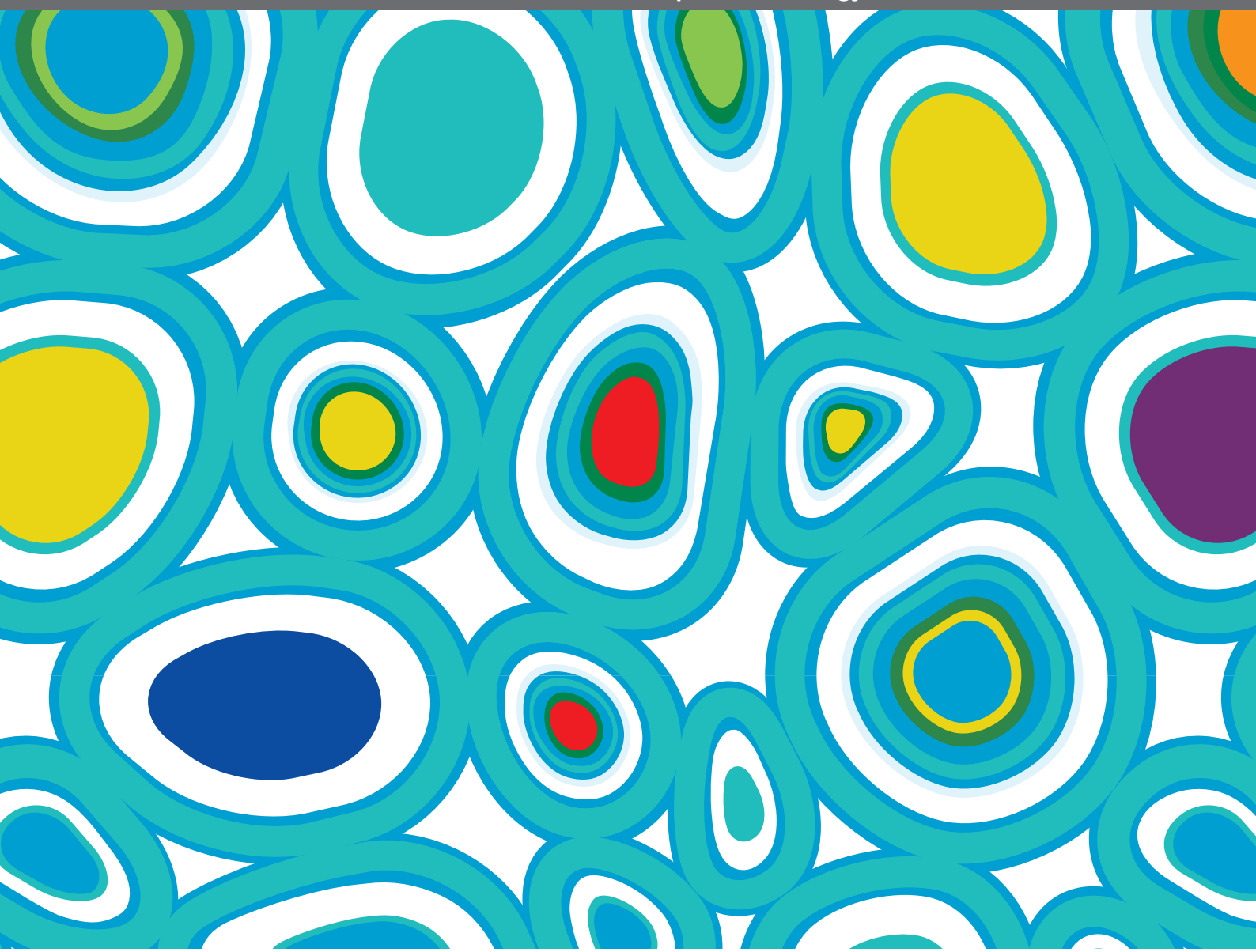

frontiers Research Topics

ISSN 1664-8714
ISBN 978-2-88974-929-4
DOI 10.3389/978-2-88974-929-4

About Frontiers

Frontiers is more than just an open-access publisher of scholarly articles: it is a pioneering approach to the world of academia, radically improving the way scholarly research is managed. The grand vision of Frontiers is a world where all people have an equal opportunity to seek, share and generate knowledge. Frontiers provides immediate and permanent online open access to all its publications, but this alone is not enough to realize our grand goals.

Frontiers Journal Series

The Frontiers Journal Series is a multi-tier and interdisciplinary set of open-access, online journals, promising a paradigm shift from the current review, selection and dissemination processes in academic publishing. All Frontiers journals are driven by researchers for researchers; therefore, they constitute a service to the scholarly community. At the same time, the Frontiers Journal Series operates on a revolutionary invention, the tiered publishing system, initially addressing specific communities of scholars, and gradually climbing up to broader public understanding, thus serving the interests of the lay society, too.

Dedication to Quality

Each Frontiers article is a landmark of the highest quality, thanks to genuinely collaborative interactions between authors and review editors, who include some of the world's best academicians. Research must be certified by peers before entering a stream of knowledge that may eventually reach the public - and shape society; therefore, Frontiers only applies the most rigorous and unbiased reviews.
Frontiers revolutionizes research publishing by freely delivering the most outstanding research, evaluated with no bias from both the academic and social point of view. By applying the most advanced information technologies, Frontiers is catapulting scholarly publishing into a new generation.

What are Frontiers Research Topics?

Frontiers Research Topics are very popular trademarks of the Frontiers Journals Series: they are collections of at least ten articles, all centered on a particular subject. With their unique mix of varied contributions from Original Research to Review Articles, Frontiers Research Topics unify the most influential researchers, the latest key findings and historical advances in a hot research area! Find out more on how to host your own Frontiers Research Topic or contribute to one as an author by contacting the Frontiers Editorial Office: frontiersin.org/about/contact

GENETIC, ENVIRONMENTAL AND SYNERGISTIC GENE-ENVIRONMENT CONTRIBUTIONS TO CRANIOFACIAL DEFECTS

Topic Editors:
Sebastian Dworkin, La Trobe University, Australia
Peter John Anderson, University of Adelaide, Australia
Karen Liu, King's College London, United Kingdom
Mary L. Marazita, University of Pittsburgh, United States

Citation: Dworkin, S., Anderson, P. J., Liu, K., Marazita, M. L., eds. (2022). Genetic, Environmental and Synergistic Gene-Environment Contributions to Craniofacial Defects. Lausanne: Frontiers Media SA. doi: 10.3389/978-2-88974-929-4

Table of Contents

frontiers in Cell and Developmental Biology

EDITORIAL
published: 24 March 2022
doi: 10.3389/fcell.2022.887051

Editorial: Genetic, Environmental and Synergistic Gene-Environment Contributions to Craniofacial Defects

Peter J. Anderson[1,2,3], *Karen J. Liu*[4], *Mary L. Marazita*[5,6,7] *and Sebastian Dworkin*[8]*

[1]Australian Craniofacial Unit, Women's and Children's Hospital, Adelaide, SA, Australia, [2]Faculty of Health Sciences, University of Adelaide, Adelaide, SA, Australia, [3]Nanjing Medical University, Nanjing, China, [4]Centre for Craniofacial and Regenerative Biology, King's College London, London, United Kingdom, [5]Department of Oral Biology, School of Dental Medicine, Center for Craniofacial and Dental Genetics, University of Pittsburgh, Pittsburgh, PA, United States, [6]Department of Human Genetics, Graduate School of Public Health, University of Pittsburgh, Pittsburgh, PA, United States, [7]Department of Psychiatry and Clinical and Translational Science Institute, School of Medicine, University of Pittsburgh, Pittsburgh, PA, United States, [8]Department of Physiology, Anatomy and Microbiology, La Trobe University, Melbourne, VIC, Australia

Keywords: craniofacial, gene-environment interaction, genetic, cleft palate, craniosynostosis

Editorial on the Research Topic

Genetic, Environmental and Synergistic Gene-Environment Contributions to Craniofacial Defects

Of the defects that affect formation of the craniofacial skeleton (the skull, face and jaws of vertebrates), the most common are those that affect fusion of the lip and secondary (hard) palate (resulting in cleft lip/palate) (Dixon et al., 2011), and those that lead to premature fusion of the bones of the skull (craniosynostosis). As a research and clinical field, we know that both genetic mutations (Wilkie and Morriss-Kay, 2001; Twigg and Wilkie, 2015; Weinberg et al., 2018) and fetal exposure to environmental toxins (Brent, 2004) individually may lead to craniofacial defects (CFD), although, in general, the synergistic nature of genetic predisposition to CFD and maternal toxin intake remains largely understudied.

In general, there are two approaches for identifying novel Gene-Environment Interactions (GxE). One approach utilises large-scale big data analyses at the population level; these can unearth both genetic polymorphisms and differences in genetic background (e.g., ethnicity), to identify risk-factors associated with increased susceptibility to craniofacial defects (Marazita, 2012; Leslie and Marazita, 2013). Often, these population studies may be further combined with understanding relevant societal and behavioural risk-factors, such as national living standards, socioeconomic background, intake of alcohol, drugs and tobacco smoke and environmental pollutants. Combining such datasets allows strong GxE risk factors for CFD to be identified (Dixon et al., 2011).

The second approach relies on utilising animal models harbouring defined genetic mutations that lead to congenital abnormalities during embryogenesis (Liu, 2016). By exposing these animal models to bioactive compounds (under carefully controlled supplementation regimes), novel compounds may be discovered that either exacerbate or reduce the incidence and penetrance of those defects (Greene and Copp, 2005).

Both approaches have yielded substantial advances, and understanding these GxE is critical for patient healthcare. Prospective parents carrying sensitising genetic mutations or polymorphisms can be advised to avoid certain foods, alcohol, medications etc., to minimise the risk of exacerbating an otherwise mild defect in their offspring, resulting in a much healthier start to life for these babies. Moreover, understanding how to overcome defects of genetic origin (that would otherwise lead to severe CFD) provides even more far-reaching possibilities—dramatically reducing the need for extensive, expensive and frequently inaccessible post-natal surgical intervention and post-operative care.

OPEN ACCESS

Edited and reviewed by:
Ramani Ramchandran, Medical College of Wisconsin, United States

***Correspondence:**
Sebastian Dworkin
s.dworkin@latrobe.edu.au

Specialty section:
This article was submitted to Molecular and Cellular Pathology, a section of the journal Frontiers in Cell and Developmental Biology

Received: *01 March 2022*
Accepted: *09 March 2022*
Published: *24 March 2022*

Citation:
Anderson PJ, Liu KJ, Marazita ML and Dworkin S (2022) Editorial: Genetic, Environmental and Synergistic Gene-Environment Contributions to Craniofacial Defects. Front. Cell Dev. Biol. 10:887051. doi: 10.3389/fcell.2022.887051

This special issue of 10 articles (comprising eight original studies and two reviews) explores some exciting advances in understanding GxE in the aetiology of craniofacial defects, utilising *in vitro*, *in silico*, zebrafish and mouse models as well as employing Genome-Wide Association Studies (GWAS) and human genetic approaches to obtain population-level data from disparate patient cohorts and datasets.

Firstly, this issue comprises two excellent reviews on factors that affect the fetal environment *in utero*, and consequences of exposure to both exogenous and endogenous stressors on craniofacial development, particularly on the fidelity, survival and functional differentiation of neural crest cells (NCCs). Fitriasari and Trainor explore the features of neural crest cells that make them uniquely sensitive to replication stress. They review the link between maternal diabetes, oxidative stress, genotoxic damage and the resultant death of NCCs as a means by which the penetrance and phenotypic variability of various craniofacial disorders is determined. Sánchez et al. review the emerging link between anti-depressant use during pregnancy (typically those medications used to maintain or increase levels of serotonin) and the incidence of craniofacial disorders. Together these reviews highlight the importance of maternal health and well-being during pregnancy as an important contributing factor to normal embryonic and fetal craniofacial development.

Secondly, we present four excellent studies centring on the rich data to be mined from human genetic approaches, GWAS and patient trios, in understanding GxE more broadly at the population level. Carlson et al. show a significant association between genetic predisposition of patients with certain Single Nucleotide Polymorphisms (SNPs) near the genes VGLL2 and PRL with adverse outcomes on craniofacial development following maternal exposure to alcohol and smoking respectively. Zhang et al. utilised two large databases of case-parent trios (comprising over 3,300 patients) to investigate GxE in patients of diverse ethnic backgrounds, and similarly identified novel risk loci following exposure to smoking, alcohol and multivitamin supplementation. The group of Mukhopadhyay et al. utilised the extensive resource of the Pittsburgh Orofacial Clefts Multiethnic study, comprising ~12,000 individuals, to determine the statistical power in identifying and characterising common, disparate and novel risk loci predisposing to orofacial clefting based on individual ancestry. In a complementary approach, Machado et al. used whole exome sequencing (WES) to identify putative polymorphisms in genetic protein-coding regions associated with non-syndromic oral clefts in a multiethnic Brazilian population, and found significant associations between cleft lip and palate in the folic-acid associated metabolism genes LRP6 and methyltransferase (MTR).

These studies elegantly highlight the rich potential of GWAS and WES to not only identify novel genetic risk factors, but importantly, to also apply these genetic discoveries to identifying novel GxE following *in utero* toxin exposure. The emerging applications of big data to identifying biologically relevant risk-factors present an extremely promising approach to unravel novel deleterious GxE in the manifestation of CFD in newborns.

Finally, the development of novel, non-human, experimental models for increasing our understanding of craniofacial disorders is also paramount. Narumi et al. explore the relationship between chemical exposure and the *Wnt*-signalling pathway, using the excellent and highly-tractable zebrafish embryo model as a screening tool for investigating novel GxE. Johnson et al. report an elegant *in vitro* assay to model interaction between epithelial and mesenchymal tissue and the chemical modulation of *Shh*-gradients, providing a novel tool to investigate the complex cross-talk that occurs between these tissues during development, classically, in the context of the developing hard palate. Cross et al. have developed a ground-breaking new computational model to predict the clinical outcomes (head and skull shape) following reconstructive surgery for craniosynostosis , and this interesting study may serve as a strong foundation for further extensive studies. We look forward with anticipation to see if the outcomes of this sophisticated approach will positively impact on future patient healthcare. Lastly, the group of Yoshioka et al. explore the relationship between microRNA signalling, cell proliferation, and all-trans retinoic acid (*at*RA), elegantly demonstrating that inhibiting miR-124-3p activity in mice rescues cleft palate caused by *at*RA exposure. Together, these studies present novel findings from non-human approaches, highlighting the utility and conservation of animal and predictive models to enhance our understanding of craniofacial defects.

Ultimately, the identification and investigation of novel genes identified from patient datasets, together with functional characterisation in animal models presents the best combined strategy to rapidly increase our understanding of GxE in the context of the aetiology of craniofacial defects.

AUTHOR CONTRIBUTIONS

All authors were involved in drafting and writing the review; all authors have approved the final version of this editorial.

REFERENCES

Brent, R. L. (2004). Environmental Causes of Human Congenital Malformations: the Pediatrician's Role in Dealing with These Complex Clinical Problems Caused by a Multiplicity of Environmental and Genetic Factors. *Pediatrics* 113 (4 Suppl. l), 957–968. doi:10.1542/peds.113.s3.957

Dixon, M. J., Marazita, M. L., Beaty, T. H., and Murray, J. C. (2011). Cleft Lip and Palate: Understanding Genetic and Environmental Influences. *Nat. Rev. Genet.* 12 (3), 167–178. doi:10.1038/nrg2933

Greene, N. D. E., and Copp, A. J. (2005). Mouse Models of Neural Tube Defects: Investigating Preventive Mechanisms. *Am. J. Med. Genet.* 135C (1), 31–41. doi:10.1002/ajmg.c.30051

Leslie, E. J., and Marazita, M. L. (2013). Genetics of Cleft Lip and Cleft Palate. *Am. J. Med. Genet.* 163 (4), 246–258. doi:10.1002/ajmg.c.31381

Liu, K. J. (2016). Animal Models of Craniofacial Anomalies. *Developmental Biol.* 415 (2), 169–170. doi:10.1016/j.ydbio.2016.06.008

Marazita, M. L. (2012). The Evolution of Human Genetic Studies of Cleft Lip and Cleft Palate. *Annu. Rev. Genom. Hum. Genet.* 13, 263–283. doi:10.1146/annurev-genom-090711-163729

Twigg, S. R. F., and Wilkie, A. O. M. (2015). New Insights into Craniofacial Malformations. *Hum. Mol. Genet.* 24 (R1), R50–R59. doi:10.1093/hmg/ddv228

Weinberg, S. M., Cornell, R., and Leslie, E. J. (2018). Craniofacial Genetics: Where Have We Been and where Are We Going? *Plos Genet.* 14 (6), e1007438. doi:10.1371/journal.pgen.1007438

Wilkie, A. O. M., and Morriss-Kay, G. M. (2001). Genetics of Craniofacial Development and Malformation. *Nat. Rev. Genet.* 2 (6), 458–468. doi:10.1038/35076601

Conflict of Interest: The authors declare that the research was conducted in the absence of any commercial or financial relationships that could be construed as a potential conflict of interest.

Publisher's Note: All claims expressed in this article are solely those of the authors and do not necessarily represent those of their affiliated organizations, or those of the publisher, the editors and the reviewers. Any product that may be evaluated in this article, or claim that may be made by its manufacturer, is not guaranteed or endorsed by the publisher.

frontiers in Cell and Developmental Biology

ORIGINAL RESEARCH
published: 14 December 2020
doi: 10.3389/fcell.2020.592967

Chemical-Induced Cleft Palate Is Caused and Rescued by Pharmacological Modulation of the Canonical Wnt Signaling Pathway in a Zebrafish Model

*Rika Narumi[1], Shujie Liu[2], Naohiro Ikeda[1], Osamu Morita[2] and Junichi Tasaki[1]**

[1] R&D, Safety Science Research, Kao Corporation, Kawasaki, Japan, [2] R&D, Safety Science Research, Kao Corporation, Ichikai-machi, Japan

OPEN ACCESS

Edited by:
Sebastian Dworkin,
La Trobe University, Australia

Reviewed by:
Brooke Elizabeth Chambers,
University of Notre Dame,
United States
James Alan Marrs,
Indiana University–Purdue University
Indianapolis, United States

***Correspondence:**
Junichi Tasaki
tasaki.junichi2@kao.com
orcid.org/0000-0003-1798-5160

Specialty section:
This article was submitted to Molecular Medicine, a section of the journal Frontiers in Cell and Developmental Biology

Received: 08 August 2020
Accepted: 02 November 2020
Published: 14 December 2020

Citation:
Narumi R, Liu S, Ikeda N, Morita O and Tasaki J (2020) Chemical-Induced Cleft Palate Is Caused and Rescued by Pharmacological Modulation of the Canonical Wnt Signaling Pathway in a Zebrafish Model. Front. Cell Dev. Biol. 8:592967. doi: 10.3389/fcell.2020.592967

Cleft palate is one of the most frequent birth defects worldwide. It causes severe problems regarding eating and speaking and requires long-term treatment. Effective prenatal treatment would contribute to reducing the risk of cleft palate. The canonical Wnt signaling pathway is critically involved in palatogenesis, and genetic or chemical disturbance of this signaling pathway leads to cleft palate. Presently, preventative treatment for cleft palate during prenatal development has limited efficacy, but we expect that zebrafish will provide a useful high-throughput chemical screening model for effective prevention. To achieve this, the zebrafish model should recapitulate cleft palate development and its rescue by chemical modulation of the Wnt pathway. Here, we provide proof of concept for a zebrafish chemical screening model. Zebrafish embryos were treated with 12 chemical reagents known to induce cleft palate in mammals, and all 12 chemicals induced cleft palate characterized by decreased proliferation and increased apoptosis of palatal cells. The cleft phenotype was enhanced by combinatorial treatment with Wnt inhibitor and teratogens. Furthermore, the expression of *tcf7* and *lef1* as a readout of the pathway was decreased. Conversely, cleft palate was prevented by Wnt agonist and the cellular defects were also prevented. In conclusion, we provide evidence that chemical-induced cleft palate is caused by inhibition of the canonical Wnt pathway. Our results indicate that this zebrafish model is promising for chemical screening for prevention of cleft palate as well as modulation of the Wnt pathway as a therapeutic target.

Keywords: teratogen, environmental factors, cleft palate, canonical Wnt signaling pathway, zebrafish

INTRODUCTION

Cleft palate and/or lip is one of the most frequent birth defects, occurring in 1 out of 800 to 2500 live births, and induces severe eating and speaking problems, dental defects, ear infections, and hearing loss (Parker et al., 2010; Mezawa et al., 2019). The patients require long-term treatments, including surgeries, dental treatment, speech rehabilitation and psychological treatment, which impose huge a lifetime burden estimated at $200,000 on their family and social support system (Boulet et al., 2009;

Wehby and Cassell, 2010). Thus, prevention and treatment of cleft palate is a worldwide health and medical issue. Cleft palate has complicated etiology and its causation involves both genetic and environmental risk factors (Dixon et al., 2011). To date, over 500 Mendelian syndromes have been reported as congenital diseases, including cleft palate, in Online Mendelian Inheritance in Man (OMIM)[1], and also over 60 chemicals have been categorized as teratogens that induce cleft palate in ToxRefDB (Martin et al., 2009). Recent studies point out that cleft palate patients have various mutations in components of specific signaling pathways, i.e., the Wnt, Hedgehog, FGF, and TGF-beta signaling pathways (Riley et al., 2007; Lipinski et al., 2010; Liu and Millar, 2010; Parada and Chai, 2012; Stanier and Pauws, 2012; Iwata et al., 2014; Kurosaka, 2015; Reynolds et al., 2019). Thus, for prenatal prevention and therapy of cleft palate, regulation of such signaling pathways will be a central target. In a mouse model with a consistent cleft palate phenotype, the cleft phenotype is partially or completely recovered by chemical modulation of the canonical Wnt signaling pathway (Liu et al., 2007; Jia et al., 2017; Li et al., 2017).

Prenatal exposure to environmental risk factors such as alcohol, cigarette smoking, pharmaceuticals and chemical reagents also leads to cleft palate in mammals, including humans (Shaw et al., 1996; Brent, 2004; DeRoo et al., 2008; Beaty et al., 2016). Some of these chemicals are reported to target the Wnt signaling pathway: excess retinoic acid or dexamethasone exposure induces cleft palate via inhibition of the canonical Wnt pathway in a mouse model (Hu et al., 2013; Okano et al., 2014; Wang et al., 2019). These reports suggest that chemical modulation of the Wnt signaling pathway will be a promising approach for prenatal prevention of cleft palate. The mammalian model has enabled great progress for investigating the etiology and pathology of cleft palate. However, at present, there are few therapies or medications directed at reducing the risk of cleft palate during prenatal development. Thus, a zebrafish screening model could provide another approach for prenatal prevention of cleft palate as well as teratogenicity testing aimed at preventing cleft palate.

As an emerging model organism for human disease, zebrafish provides excellent opportunities for investigating fundamental mechanisms causing common birth defects as well as screening and discovering small molecules that impact human disease (Mork and Crump, 2015; Rennekamp and Peterson, 2015; Wiley et al., 2017; Weinberg et al., 2018; Patton and Tobin, 2019). Zebrafish has several experimental advantages for high-throughput genetic and chemical screening, including evolutionarily conserved developmental programs, cost effectiveness, rapid external development, and transparency during the embryonic stage. Zebrafish ethmoid plate is considered to be a mammalian palate model because the zebrafish palate is composed of cells derived from the frontonasal and maxillary domain, which is similar to the palatogenesis of mammals (Jugessur et al., 2009; Kague et al., 2012; Mongera et al., 2013; Mork and Crump, 2015; Duncan et al., 2017). Moreover, the fundamental signaling pathways and cellular events during craniofacial development, including palatogenesis, are conserved between fish and mammals (Swartz et al., 2011). Recently, the responsible genes, such as *irf6*, *tgfβ3*, *smad5* and *faf1*, causing cleft palate have been identified, and disruption of these genes is phenocopied in the zebrafish model, validating the genetic relevance of cleft palate in zebrafish to mammalian cleft palate (Cheah et al., 2010; Ghassibe-Sabbagh et al., 2011; Swartz et al., 2011; Dougherty et al., 2013). Furthermore, genetic disruption of the Wnt signaling pathway in zebrafish causes craniofacial anomalies such as cleft palate and micrognathia, suggesting involvement of the Wnt signaling pathway in cleft palate both in fish and mammals (Curtin et al., 2011; Jackson et al., 2015; Duncan et al., 2017; Neiswender et al., 2017). This accumulating knowledge of the genetic phenocopying of cleft palate in the zebrafish palate model indicates the relevance of this model to mammalian cleft palate.

Recently we reported that in a zebrafish model, several teratogens recapitulated craniofacial anomalies found in mammals and some defects phenocopied neurocristopathy, indicating that the zebrafish model is amenable for high-throughput prediction of teratogen-induced craniofacial anomalies of mammals (Liu et al., 2020). Many teratogens that induce cleft palate have been identified by epidemiological studies or teratogenicity testing; however, only a few chemicals, such as retinoic acid and alcohol, have been employed for analyzing detailed cellular and molecular mechanisms of cleft palate in a mammalian model (Kietzman et al., 2014; Okano et al., 2014; Wang et al., 2019). For use in chemical screening for prenatal prediction and prevention of chemical-induced cleft palate, a zebrafish model should be useful in addition to a mouse model, which has been used to detect phenocopied cleft palate and its rescue based on mechanistic insights (Sive, 2011; Hahn and Sadler, 2020). Although our previous study suggested that teratogen-treated zebrafish phenocopied mammalian craniofacial anomalies, the biological relevance of chemical-induced cleft palate in this zebrafish model to mammals still remained unclear. Notably, the causal relationship between the canonical Wnt signaling pathway and chemical-induced cleft palate remained to be examined.

In the present study, we consolidate our previous proof-of-principle study by Liu et al., 2020 showing that zebrafish can be utilized as a discovery platform to investigate chemical-induced neurocristopathies. Zebrafish embryos were exposed to 12 chemical compounds (caffeine, 5-fluorouracil, salicylic acid, hydroxyurea, warfarin, valproic acid, methotrexate, imatinib, thalidomide, phenytoin, dexamethasone, and retinoic acid), which have been identified as teratogens causing cleft palate by epidemiological research and teratogenicity testing in mammals (**Table 1**). All 12 teratogens induced a series of palate malformations of zebrafish palate dose-dependently, suggesting the phenotypic relevance of this zebrafish model to chemical-induced cleft palate in mammals. Moreover, IWP-L6, a specific inhibitor of the canonical Wnt signaling pathway, also induced clefting phenotypes, which were enhanced by

[1]https://omim.org

TABLE 1 | Chemicals used in the current study.

Category	Compound	Abbreviation	Birth defects		References
			Rodents	Human	
Antiepileptic drug	Valproic acid	VPA	Cleft palate, spina bifida occulta, and delay in ossification	Cleft palate, spina bifida, atrial septal defect, and hypospadias	Faiella et al., 2000; Jentink et al., 2010
	Phenytoin	PHT	Cleft lip, tetralogy of Fallot, short neck, and diaphragmatic hernia	Cleft lip and palate, congenital heart disease, and microcephaly	Speidel and Meadow, 1972; Czeizel, 1976
Antithrombotic drug	Warfarin	WAF	Maxillonasal hypoplasia and skeletal abnormalities	Cleft palate, nasal hypoplasia, and skeletal abnormalities	Howe and Webster, 1992; Starling et al., 2012; D'Souza et al., 2017
Antineoplastic drug	5-Fluorouracil	5FU	Cleft lip and/or palate, clubbed leg, and polydactyly	Radial aplasia, imperforate anus, esophageal aplasia, and hypoplasia	Stephens et al., 1980; National Toxicology, 2008
	Hydroxyurea	HU	Cleft palate, cleft lip, exencephaly, and clubbed leg	–	Chaube and Murphy, 1966
	Imatinib	IM	Cleft lip, exencephaly, and contraction of forelimb	Cleft palate, polydactyly, hypospadias, scoliosis, and small exomphalos	Pye et al., 2008; El Gendy et al., 2015
	Methotrexate	MTX	Cleft palate, skull defects, and severe fore- and hindlimb dysplasia	Cleft palate, ear malformation, and multiple cardiac malformations	Jordan et al., 1977; Granzow et al., 2003
Immunosuppressive drug	Thalidomide	THA	–	Limb defects, cleft lip and palate, ear defects, and small eyes	Newman, 1985; Speirs, 1962; Taussig, 1962; Smithells and Newman, 1992
Anti-inflammatory drug	Dexamethasone	DEX	Cleft lip, and cleft palate	Cleft lip and palate	Hviid and Mølgaard-Nielsen, 2011; Zhou et al., 2011; Kemp et al., 2016
	Salicylic acid	SA	Cleft palate, spina bifida, cranioschisis, spondyloschisis, and abdominal fissure	Neural tube defects, gastroschisis, and cleft lip/palate	Trasler, 1965; Tagashira et al., 1981; Kozer et al., 2002
Non-pharmaceutical chemical	Caffeine	CAF	Cleft palate, and digital defect	Cleft palate, hydrocephalus, and interventricular septal defect	Nishimura and Nakai, 1960; Collier et al., 2009
	Retinoic acid	RA	Cleft lip and palate, ear defects, and limb and lower-body duplications	Cleft palate, ear defects, hydrocephalus, and teratology of Fallot	Benke, 1984; Lammer et al., 1988; Rutledge et al., 1994; Padmanabhan and Ahmed, 1997
	Boric acid	BA	Rib defects (short rib and wavy rib)	-	Moore, 1997

All chemicals have been reported to induce birth defects in rodents and human.

combinatorial treatment with the Wnt inhibitor and teratogens. These results suggested that teratogens inhibited the canonical Wnt signaling pathway, which was confirmed by observation of decreased expression levels of downstream effectors of canonical Wnt signaling (*tcf7* and *lef1*). Cellular defects of teratogen-induced cleft palate were characterized by inhibition of cell proliferation and viability in the palate. Furthermore, cleft palate induced by teratogens was abrogated by three Wnt agonists (BIO, CHIR-99021, and WAY-262611). These findings suggest that inhibition of canonical Wnt signaling in the zebrafish model contributes critically to chemical-induced cleft palate, which is the same etiology as in mammalian models. Taken together, our findings indicate that the zebrafish palate is a suitable model for investigating the etiology of chemical-induced cleft palate as well as for high-throughput chemical screening for prevention of cleft palate and teratogenicity. Additionally, our results provide insights into chemical modulation of the canonical Wnt signaling pathway as a potential target for prenatal prevention of cleft palate.

MATERIALS AND METHODS

Zebrafish Maintenance

Zebrafish (*Danio rerio*), strain RIKEN WT (RW), were maintained with a 14-h light/10-h dark cycle and water temperature at 28 (±1)°C. Water quality conditions were maintained according to The Zebrafish Book (Westerfield, 2000) and the Guide for the Care and Use of Laboratory Animals 8th edition (National Research Council, 2011).

Test Compounds

Test compounds used in this study are listed in **Table 1**. These tested compounds are known to be teratogens inducing cleft palate in mammals and have been classified into various

categories as a result of being tested in zebrafish experiments or chemical safety assays (Hillegass et al., 2008; Selderslaghs et al., 2009; Ito and Handa, 2012; Lee et al., 2012; Teixido et al., 2013; Yamashita et al., 2014; Inoue et al., 2016; Martinez et al., 2018; Cassar et al., 2019). The test compounds and exposure concentrations were determined based on Liu et al., 2020. The exposure concentrations were as follows: hydroxyurea (1 mM, Sigma-Aldrich), valproic acid (7.5–30 μM, Wako), salicylic acid (100–400 μM, Wako), boric acid (1 mM, Wako), and caffeine (0.5–2 mM, Wako), which were diluted from stock solutions prepared with distilled water (Life Technologies), and imatinib (250 μM, Tokyo Chemical Industry), retinoic acid (10–50 nM, Tokyo Chemical Industry), thalidomide (400 μM, Tocris Bioscience), methotrexate (50–200 μM, Wako), warfarin (15–60 μM, Wako), phenytoin (1 mM, Wako), dexamethasone (1 mM, Wako), 5-fluorouracil (1 mM, Wako), and isoniazid (1 mM, LKT Laboratories), which were diluted from stock solutions prepared with dimethyl sulfoxide (DMSO, Wako).

Egg Production and Chemical Exposure

Adult male and female zebrafish (4–10 months after fertilization) were placed in a breeding tank with a separator in the late afternoon the day before spawning. The separator was removed in the morning and spawning was stimulated when the light was turned on. Fertilized eggs were collected within 1 h after removal of the separator. The eggs were incubated in E3 medium (5 mM NaCl, 0.17 mM KCl, 0.33 mM $CaCl_2$, 0.33 mM $MgSO_4$, 0.1 mM NaOH) at 28°C and dechorionated by 1 mg/mL Protease type XIV (Sigma-Aldrich) for 10 min at room temperature and washed several times with E3 medium. Dechorionation was done within an hour after fertilization. The dechorionated embryos were incubated with E3 medium and were exposed to the test compounds at 4 hpf. Embryos were treated with Wnt antagonist (IWP-L6, 15 μM, Merck) or Wnt agonist [BIO (100 nM, Sigma-Aldrich), CHIR99021 (300 nM, Abcam) or WAY-262611 (250 nM, Wako)]. Embryos were treated with these small molecules starting at 50 hpf, when the onset of palatogenesis occurs (DeLaurier et al., 2012). The exposure medium was replaced daily and samples were collected at 96 hpf.

Fluorescence Imaging and Immunofluorescence Staining

Prior to nucleic staining, zebrafish embryos were fixed at 96 hpf with 4% paraformaldehyde (PFA, Wako) for 1 h and Alcian blue cartilage staining was performed as previously described (Liu et al., 2020). Samples were washed twice with PBS-T (phosphate buffered saline containing 0.1% Triton X-100) for 5 min and stained with DAPI (1/5000, DOJINDO) diluted with PBS-T on a shaker for 1 h. After nucleic staining, samples were dissected with fine forceps and embedded in 1% low-melting agarose (Sigma-Aldrich) and then mounted on a 35-mm non-coated glass bottom dish (Matsunami).

For immunofluorescence staining, zebrafish embryos were fixed at 96 hpf with 4% PFA for 1–2 h(s). Samples were washed twice with PBS-T for 5 min and placed in 100% ice-cold methanol (MeOH, KANTO CHEMICAL) and stored for more than 2 h at −20°C to accomplish complete dehydration. Then, samples were gradually rehydrated with 75%, 50%, 25% MeOH in PBS-T (volume percent) for 5 min per wash on ice and processed to remove pigmentation by bleaching in 3% hydrogen peroxide and 0.5% potassium hydroxide under light. After bleaching, samples were incubated in 10 μg/mL Protease type XIV (Sigma-Aldrich) in PBS-T for 30 min and then post-fixed with 4% PFA for 20 min. Samples were washed with 150 mM Tris–HCl (pH 8.5) for 5 min and then heated for 15 min at 70°C following by washing twice with PBS-T for 5 min. Samples were incubated in ice-cold acetone (Wako) for 20 min at −20°C and washed twice with PBS-T for 5 min. Samples were blocked with 3% bovine serum albumin in PBS for 2 h and incubated with rabbit anti-active caspase3 (1/1000, BD Pharmingen: 559565), rabbit anti-phospho-histone H3 (Ser10) (1/500, EMD Millipore: 06-570), mouse anti-collagen type II (anti-coll2, 1/20, DSHB: AB_528165) primary antibody or lectin PNA Alexa Fluor 488 conjugate (1/1000, Thermo) overnight at 4°C, washed six times with PBS-T for 15 min, and then stained with Alexa Fluor 568-goat anti-rabbit, or Alexa Fluor 647-IgG1 kappa-goat anti-mouse secondary antibodies (1/1000, Life Technologies) for 2 h. After washing six times with PBS-T for 15 min, samples were embedded in 1% low-melting agarose and mounted on a 35-mm non-coated glass bottom dish. All immunofluorescence images were acquired by the Zeiss LSM880 or LSM800 system equipped with Zeiss ZEN black or blue software. Z-sections of the images were stacked by Z-projection (projection type: Max intensity) of ImageJ (National Institutes of Health). All procedures were performed at room temperature unless otherwise specified.

Quantification of Immunofluorescence Image

After nucleic staining, quantification of palate morphology was performed. The phenotypes were categorized based on the criteria shown in **Supplementary Figure 1A**. Lengths of zebrafish palate and cleft were analyzed using ImageJ. For quantification of the frequency of pH3- or active caspase3-positive cells, the number of proliferative or apoptotic cells in the palate was normalized to 10^{-4} μm^2. The area of the palate was measured using the ImageJ Measure option. All analysis was performed after the Z-projection. All experiments were performed in triplicate and sample sizes are stated in each figure legend.

Dissection, RNA Preparation and RT-qPCR Analysis

Zebrafish embryos were stained with 5 μM diaminofluorescein-FM diacetate (DAF-FM DA, GORYO Chemical) in E3 medium at 28°C overnight to visualize cranial cartilage. After the trunk and yolk were removed, the head region of the embryo was treated with 5 mg/ml pancreatin (Wako) for several minutes at room temperature. The fluorescence-positive region of the head region was dissected using Disponano needles (Saito Medical Instruments) under a fluorescence stereomicroscope. Total RNA

of each sample was extracted using Trizol (Invitrogen) and an RNeasy Mini Kit (QIAGEN) followed by reverse transcription with a QuantiTect Reverse Transcription Kit (QIAGEN). RT-qPCR analysis was performed with TaqMan Master Mix (Thermo Fisher Scientific), TaqMan probes and gene-specific primers for *tcf7l1a*, *lef1*, and *gapdh* (Bio-Rad) using the 7500 Fast Real-Time PCR System (Thermo Fisher Scientific). For data analysis, relative quantification analysis was performed using the comparative CT ($2^{-\Delta\Delta CT}$) method. For each sample, mRNA levels of the target genes were normalized to the *gapdh* mRNA.

Statistics

Two-tailed Welch's *t*-tests were used to determine *P*-values for RT-PCR experiments. Multiple comparison tests were performed using Graph Pad Prism version 8 for Windows (La Jolla). *P*-values were calculated with one-way ANOVA followed by Dunnett's multiple comparison tests for quantification of pH3- and Cas3-positive cells. *P*-values less than 0.05 were considered to be statistically significant. All data are presented as the mean ± SD unless otherwise specified.

RESULTS

Chemical-Induced Cleft Palate Is Recapitulated in Zebrafish Embryo Model

To examine the effects of teratogens on zebrafish palatogenesis, embryos from blastula to larval stage (4–96 hpf) were exposed to 14 chemical reagents, which included 12 teratogens that induce cleft palate, a teratogen that does not induce cleft palate and a non-teratogen, according to (Kimmel et al., 1995; **Figure 1A** and **Table 1**). These teratogens have been reported to induce orofacial clefts in humans and/or rodents. Morphological analysis of the palate was carried out at 96 hpf by nuclear staining after soft tissue removal and dissection of the neurocranium (**Figures 1A,B**). All teratogens induced palate malformation, which was classified into four types of defects as follows: rough edge, moderate clefting, severe clefting, and rod-like (**Supplementary Figure 1A**). Cleft at the center of the anterior edge of the palate (moderate clefting and severe clefting) was frequently observed in CAF-, 5FU-, SA-, HU-, WAF-, VPA-, and MTX-treated embryos (**Figures 1C,D,G–M**). Rough edge consisting of several small clefts was frequently induced by IM, THA, PHT, and DEX treatment (**Figures 1C,D,N–Q,S**). These palatal defects were quantified and summarized in **Figure 1T**. Dose-response analysis revealed that these phenotypes were observed in a dose-dependent manner (**Supplementary Figure 1B**). RA induced a rod-like malformation (**Figure 1R**). This defect was only observed in RA-treated embryos (**Figure 1T** and **Supplementary Figure 1B**). Non-teratogens (DMSO as vehicle control and isoniazid; INA) and a teratogen that does not induce cleft palate (boric acid; BA) did not induce palate abnormalities (**Figures 1C–F,T**). These results suggest that specific teratogens induce cleft palate and chemical-induced cleft palate is recapitulated in the zebrafish model.

Inhibition of the Canonical Wnt Signaling Pathway Induces Chemical-Induced Cleft Palate

Next, we investigated the contribution of canonical Wnt signaling to chemical-induced cleft palate because the canonical Wnt signaling pathway is critically associated with cleft palate in mammals (Song et al., 2009; Kurosaka et al., 2014; Reynolds et al., 2019). We performed morphological analysis after pharmacological inhibition of the canonical Wnt signaling pathway using a specific Porcn inhibitor, IWP-L6 (Wang et al., 2013; Grainger et al., 2016). To focus on the effect on the zebrafish palate, IWP-L6 added specifically during palatogenesis (50–96 hpf) (**Figure 2A**). Cleft phenotypes were observed in IWP-L6-treated embryos dose-dependently (**Figures 2B–D,I**). Moreover, these palatal malformations were phenocopied by teratogen-treated embryos (**Figures 1G–Q**), suggesting that the teratogens disturbed the canonical Wnt signaling pathway. To test this, combinatorial treatment with the Wnt antagonist and the teratogens was performed (**Figure 2A**). Warfarin (WAF) and valproic acid (VPA) were selected as suitable chemicals among the teratogens to verify the combinatorial effect on cleft palate because of their dose-dependent phenotypic severity and their different pharmacodynamics (**Supplementary Figure 1B**; Holford, 1986; Ghodke-Puranik et al., 2013). The low dosage of WAF (5 μM) and VAP (5 μM) induced a small number of palatal defects (**Figures 2E,G,J**). Combinatorial treatment with a low dose of IWP-L6 (15 μM, which alone induced a small number of palatal defects) increased the number of palatal defects in the treated embryos (**Figures 2F,H,J**). Furthermore, to obtain a readout of the effect of disturbing the canonical Wnt signaling pathway, we analyzed the expression levels of *transcription factor 7* (*tcf7*) and *lymphoid enhancer binding factor 1* (*lef1*), which are two of the downstream effectors by quantitative real-time PCR (Veien et al., 2005; Wang et al., 2009; Hagemann et al., 2014). After WAF and VAP treatment, the neurocranium was dissected to enrich for the neurocranial progenitors at 72 and 96 hpf, at which time basic morphogenesis of the palate is completed (DeLaurier et al., 2012). The expression levels of both *tcf7l1a* and *lef1* in the neurocranium were significantly reduced by teratogen exposure (**Figures 2K,L**). These results suggest that inhibition of canonical Wnt signaling contributes to chemical-induced cleft palate in zebrafish.

Decreased Proliferation and Increased Apoptosis Are Observed in Chemical-Induced Cleft Palate

The proper regulation of cell proliferation and cell death is one of the key factors for developing the proper size and shape of organs during morphogenesis, and disruption of such regulation of proliferation and apoptosis in palatal shelves induces cleft palate in mammalian models (He et al., 2011; Bush and Jiang, 2012). Thus, the induction of cleft palate by teratogens raised the possibility that cell proliferation and/or viability were inhibited

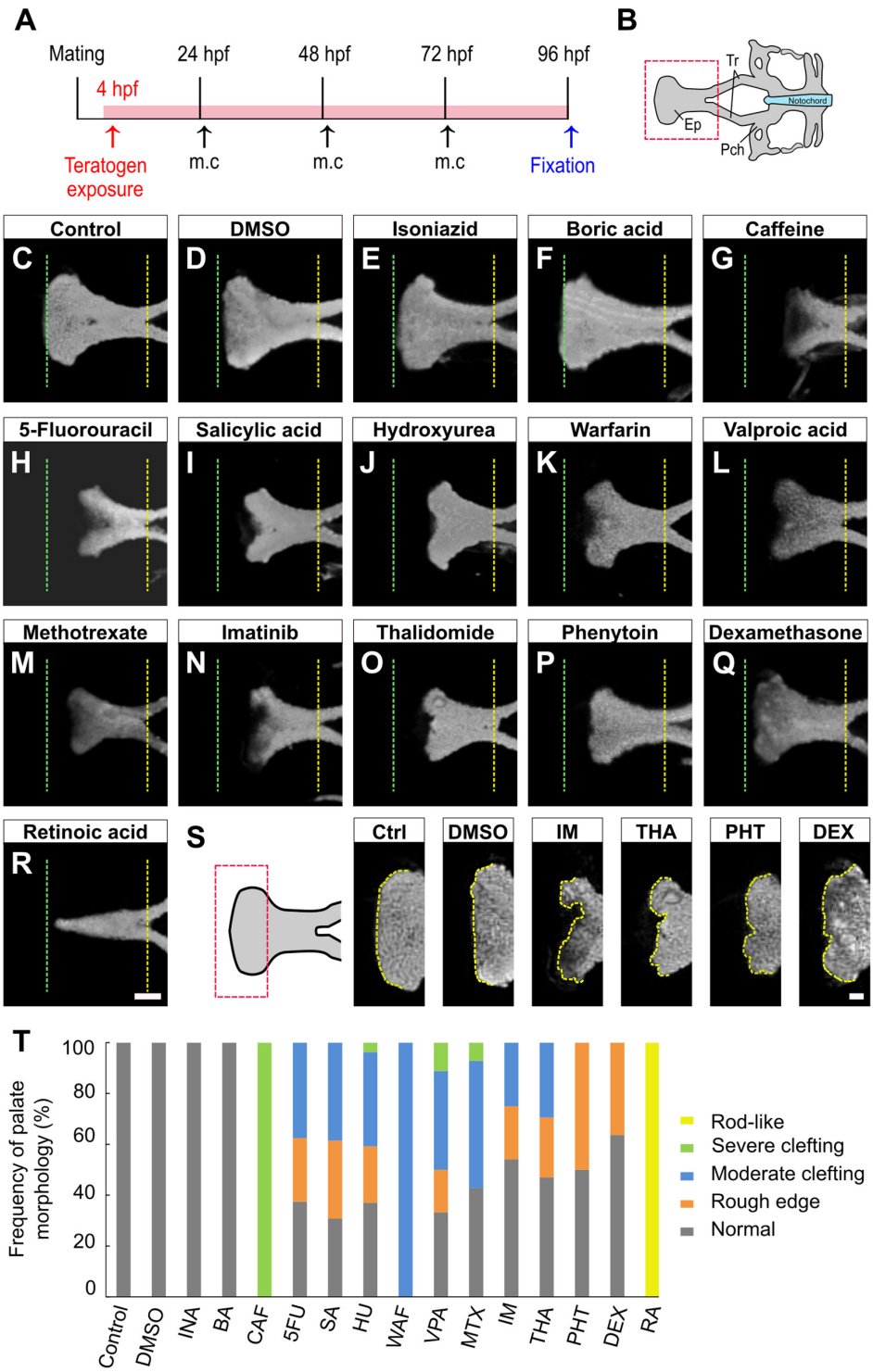

FIGURE 1 | Morphological phenotype of chemical-induced cleft palate in zebrafish embryos. **(A)** Experimental time course m.c.: medium change. **(B)** Atlas of the neurocranial cartilage. Ep, Ethmoid plate; Tr, Trabecula; Pch, Parachordal. **(C–R)** Fluorescence images of the ethmoid palate (zebrafish palate) at 96 hpf. Nuclei of cartilage cells were stained with DAPI. The anterior and posterior edges of the palate are indicated by green and yellow dotted lines, respectively. Exposure concentration was as follows: DMSO as vehicle control (0.1%), isoniazid (INA, 1 mM), boric acid (BA, 1 mM), caffeine (CAF, 1 mM), 5-fluorouracil (5FU, 1 mM), salicylic acid, (SA, 200 μM), hydroxyurea (HU, 1 mM), warfarin (WAF, 30 μM), valproic acid (VPA, 15 μM), methotrexate (MTX, 200 μM), imatinib (IM, 250 μM), thalidomide (THA, 400 μM), phenytoin (PHT, 1 mM), dexamethasone (DEX, 1 mM), and retinoic acid (RA, 10 nM). **(S)** Highly magnified images of the anterior edge of the palate. Ctrl, control; IM, imatinib; THA, thalidomide; PHT, phenytoin; DEX, dexamethasone. Yellow dotted line traces the shape of anterior edge. **(T)** Frequency of palate morphology. *n* = 19 (Control), 18 (DMSO), 11 (INA), 14 (BA), 17 (CAF), 8 (5FU), 16 (SA), 27 (HU), 11 (WAF), 18 (VPA), 14 (MTX), 24 (IM), 17 (THA), 10 (PHT), 22 (DEX), 16 (RA). Scale bars: 50 μm in **(C–R)**, 20 μm in **(S)**.

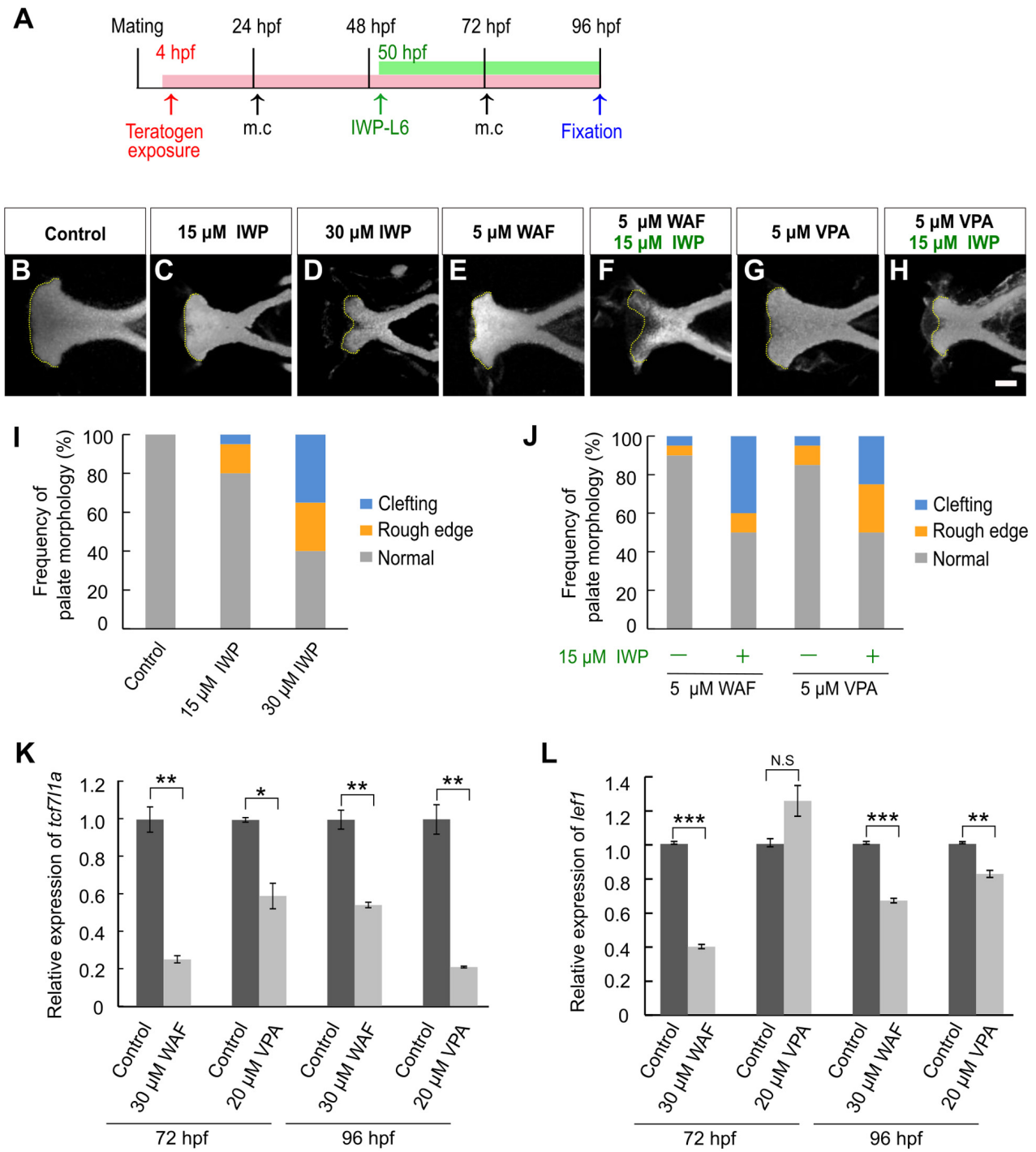

FIGURE 2 | Chemical-induced cleft palate was induced by inhibition of the canonical Wnt signaling pathway. **(A)** Experimental time-course. m.c.: medium change. **(B–H)** Fluorescence images of the palate at 96 hpf. Nuclei of cartilage cells were stained with DAPI. Yellow dotted line indicates the anterior edge of the palate. **(I,J)** Frequency of palate morphology. $n = 20$ for each sample. **(K,L)** Quantification of relative levels of *tcf7l1a* **(K)** and *lef1* **(L)** mRNA isolated from the neurocranium at 72 and 96 hpf. Each mRNA level was normalized by *gapdh* mRNA by the comparative CT ($2^{-\Delta\Delta CT}$) method. Data are shown as mean ± SD from triplicate experiments. $^{*}P < 0.05$, $^{**}P < 0.01$, $^{***}P < 0.001$ (two-tailed Welch's *t*-tests). Scale bar: 50 μm.

by the teratogens. To examine the effect of teratogens on cell proliferation and apoptosis, we performed immunofluorescence staining with anti-phospho-Histone H3 (pH3) antibody as a mitotic marker and anti-active Caspase-3 (active Cas-3) antibody as an apoptosis marker. After WAF and VPA treatment, the numbers of proliferative and apoptotic cells in zebrafish palate

were quantified (**Figure 3**). Palatal morphology was marked by double staining with anti-Collagen type 2 antibody and lectin PNA (**Figure 3A**). WAF (30 μM) and VAP (20 μM) treatment induced cleft palate and significantly decreased the number of pH3-positive cells in the palate (**Figures 3A,B**). In contrast, the number of active Cas-3-positive cells was markedly increased in

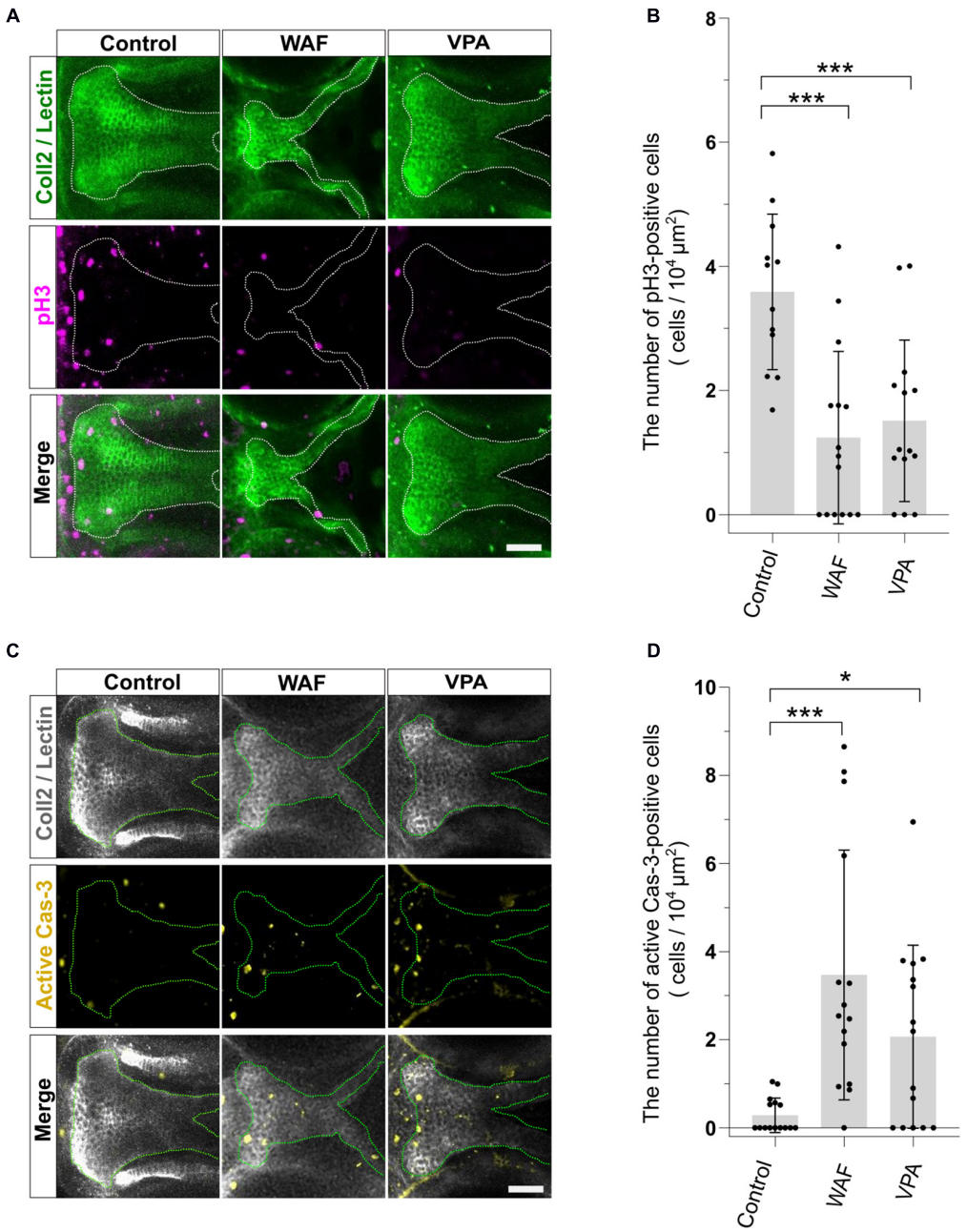

FIGURE 3 | The pattern of proliferation and apoptosis in the cleft palate induced by teratogens. **(A)** Immunofluorescence images of proliferative cells in the palate at 96 hpf. Embryos were treated with WAF (30 μM) or VPA (20 μM) and stained with anti-coll2 antibody, lectin PNA and anti-phospho-histone H3 (pH3) antibody. Green indicates cartilage cells double stained with anti-coll2 antibody and lectin PNA. White dotted lines trace the shape of the palate. Magenta indicates proliferative cells stained with anti-pH3 antibody. **(B)** The number of pH3-positive cells in the palate. Numerical value is normalized by 10^4 μm^2. n = 12 (Control), 15 (WAF), 14 (VPA), $^{***}P < 0.001$ (one-way ANOVA followed by Dunnett's multiple comparison test). **(C)** Immunofluorescence images of apoptotic cells in the palate at 96 hpf. Embryos were treated with WAF (30 μM) or VPA (20 μM) and stained with anti-coll2, lectin PNA anti-active caspase 3 (active Cas-3) antibody. White indicates cartilage cells double stained with anti-coll2 antibody and lectin PNA. Green dotted lines trace the shape of ethmoid plate. Yellow indicates apoptotic cells stained with anti-caspase3 antibody. **(D)** The number of active caspase3-positive cells in the palate. Numerical value was normalized to 10^4 μm^2. n = 15 (Control), 15 (WAF), 15 (VPA), $^{*}P < 0.05$, $^{***}P < 0.001$ (one-way ANOVA followed by Dunnett's multiple comparison test). Scale bars: 50 μm.

the palate (**Figures 3C,D**). No cellular changes were observed in the embryos exposed to INA, which is a non-teratogenic chemical (**Supplementary Figure 2**). These results indicate that disruption of the balance between cell proliferation and apoptosis occurs in teratogen-treated embryos, leading to cleft palate.

Wnt Agonists Rescue Chemical-Induced Cleft Palate

We showed that inhibition of the canonical Wnt signaling pathway is a contributor to chemical-induced cleft palate in our zebrafish model. Several lines of evidence suggested that modulation of the canonical Wnt signaling pathway would induce or correct chemical-induced cleft palate. Next, to test this hypothesis, we analyzed the effect of simultaneous treatment with the teratogens and small molecule Wnt agonists: two glycogen synthase kinase-3 (Gsk-3) inhibitors: (2′Z,3′E)-6-bromoindirubin-3′-oxime (BIO) and CHIR-99021 (CHIR), and one Dickkopf1 (Dkk1) inhibitor: WAY-262611 (WAY) (**Figure 4A**). These two types of small molecules specifically inhibit components of the canonical Wnt signaling pathway and lead to activation of the Wnt signaling pathway in zebrafish and mammals (Chen et al., 2014; Nishiya et al., 2014; Jia et al., 2017). These agonists were administered from 50 hpf, a critical

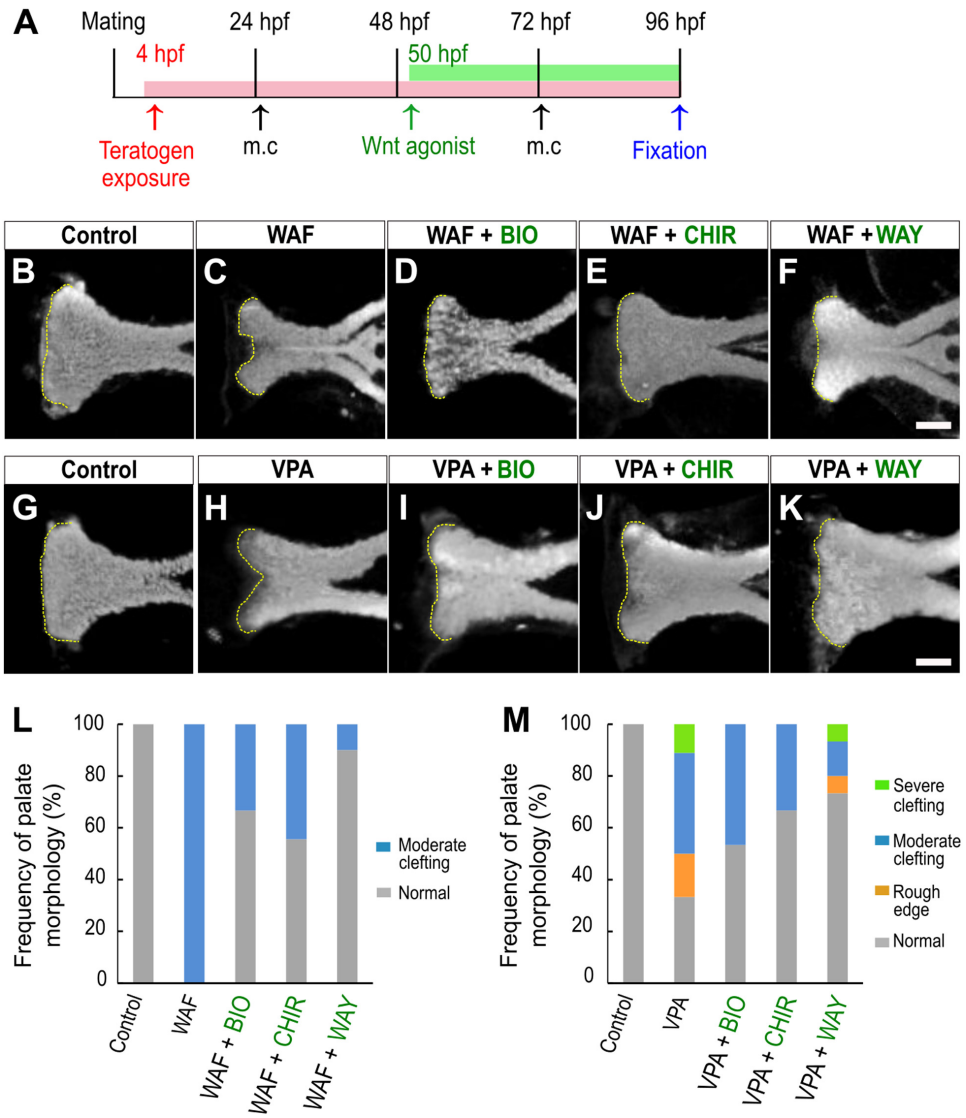

FIGURE 4 | Restoration of chemical-induced cleft palate by Wnt agonists. **(A)** Experimental time course. m.c.: medium change. **(B–K)** Fluorescence images of the palate at 96 hpf. **(B,C)** WAF (30 μM) exposure induced cleft palate. **(D–F)** The cleft palate was rescued by combinatorial treatment with BIO (100 nM), CHIR99021 (300 nM) or WAY-262611 (250 nM). **(G,H)** VPA (20 μM) exposure induced cleft palate. **(I–K)** The cleft palate caused by VPA was rescued by combinatorial treatment with BIO (100 nM), CHIR99021 (300 nM) or WAY-262611 (250 nM). White indicates nuclei stained with DAPI. Yellow dotted lines trace the shape of the anterior edge of the plate. **(L,M)** Frequency of rescued cleft palate. *n* = 18 (Control), 11 (WAF), 12 (WAF + BIO), 9 (WAF + CHIR), 10 (WAF + WAY) in **(L)**, *n* = 19 (Control), 18 (VPA), 15 (VPA + BIO), 18 (VPA + CHIR),15 (VPA + WAY) in **(M)**. Scale bar: 50 μm.

developmental window for zebrafish palatogenesis (DeLaurier et al., 2012). Cleft phenotype was induced by WAF and VPA exposure (**Figures 4B,C,G,H,L,M**). These cleft palate phenotypes were rescued by the Wnt agonist treatment (**Figures 4D–F,I–K**). Moreover, quantitative analysis showed that the frequency of the severe phenotype was reduced by the Wnt agonist treatment (**Figures 4L,M**). In contrast, the rod-like phenotype induced by RA treatment was not rescued in the presence of the Wnt agonists (**Supplementary Figure 3**). Therefore, the cleft palate phenotype alone was specifically restored by the Wnt agonist treatment. These results suggest that activation of the canonical Wnt signaling pathway corrects a certain type of cleft palate induced by teratogens.

Palate Rescued by Wnt Agonists Shows Restored Cell Proliferation and Apoptosis

Chemical-induced cleft palate was rescued phenotypically by Wnt agonist treatment (**Figure 4**). Our results showed that teratogens caused decreased cell proliferation and increased apoptosis in the palate and led to disturbance of proper palatogenesis (**Figure 3**). To confirm the restoration of cell proliferation and apoptosis to the normal levels in the rescued palate, we performed simultaneous treatment with the teratogens and the Wnt agonists, followed by immunostaining with anti-pH3 antibody and anti-active Cas3 antibody (**Figures 5**, **6**). WAF treatment significantly lowered cell proliferation in the palate; however, cell proliferation was restored to a level which appeared adequate for developing normal palatal morphology by BIO, CHIR, and WAY treatment (**Figures 5A,B**). Restoration of cell proliferation was also observed upon combinatorial treatment with VPA and the Wnt agonists (**Figure 5C**). Consistent with this, the number of anti-pH3-positive cells recovered as compared with the control (**Figure 5D**).

Next, we investigated the apoptosis in the recovered palate by anti-active Caspase-3 staining and its quantification. WAF treatment resulted in a significant increase of apoptosis in the zebrafish palate (**Figures 6A,B**). CHIR and WAY treatment significantly rescued this WAF-induced apoptosis and BIO treatment tended to decrease it (**Figures 6A,B**). In VPA-exposed embryos, the apoptosis in the palate was significantly increased, and this increase was blocked by BIO, CHIR, and WAY treatment (**Figures 6C,D**). These results suggest that inhibition of the canonical Wnt signaling pathway contributes to both decreased cell proliferation and increased apoptosis and leads to cleft palate.

DISCUSSION

Our results revealed that: (1) Cleft palate in zebrafish was specifically induced by the teratogens. (2) Inhibition of the canonical Wnt pathway caused cleft palate. (3) Chemical-induced cleft palate is characterized by decreased cell proliferation and increased apoptosis in the palate. (4) Wnt agonist treatment rescued chemical-induced cleft palate (**Figure 7A**).

We selected 12 teratogens to examine the relevance of cleft palate in the zebrafish model to mammalian cleft palate. These teratogens are known to induce cleft palate in mammals, including human (**Table 1**). Zebrafish embryos were exposed to these 12 teratogens, and all of them induced palatal defects dose dependently, ranging from a rough edge to a cleft at the anterior edge of the palate. Furthermore, the zebrafish model showed potential for distinguishing teratogens from non-teratogens. Isoniazid (INA), which is an anti-tubercular drug, does not induce teratogenicity (Snider et al., 1980). Boric acid (BA) is known to be a teratogen, but does not induce cleft palate in mammalian models (Heindel et al., 1994; Price et al., 1996). Zebrafish embryos did not show cleft palate after INA or BA treatment, and precisely detected teratogens inducing cleft palate. BA-treated zebrafish showed other types of teratogenicity, such as micrognathia, reported in mammalian models (Liu et al., 2020). Therefore, although further accumulation of evidence about various chemicals is required to substantiate the validity of the zebrafish model for prediction of chemical-induced cleft palate, our results suggest that the zebrafish model detects phenotypically similar teratogenic responses to mammals' and indicates conserved responses to teratogens between fish and mammals.

Retinoic acid (RA) alone induced a rod-like phenotype in a dose-dependent manner and did not induce clefting in the palate. It is reported that RA induces holoprosencephaly (HPE), which is a birth defect with various degrees of both defects in the brain and facial abnormalities such as cleft palate, in zebrafish, mouse, and human (Gongal and Waskiewicz, 2008; Maurus and Harris, 2009; Roessler and Muenke, 2010; Billington et al., 2015). It is reported that the palatal morphology of *sonic you* (*syu*) mutant zebrafish embryos, which have disruption of the *sonic hedgehog* gene, and of embryos treated with the Hedgehog (Hh) signaling inhibitor cyclopamine (CyA) show a rod-like structure like that observed in the RA-exposed embryos (Wada et al., 2005). Corresponding to those reports, our previous study showed a decreased expression level of *zic2a*, which is a gene responsible for HPE, in RA-treated embryos (Gongal and Waskiewicz, 2008; Maurus and Harris, 2009; Solomon et al., 2010; Liu et al., 2020). Thus, our results indicate that the zebrafish model detects and recapitulates chemical-induced HPE.

Furthermore, we showed that chemical modulation of the canonical Wnt pathway did not rescue the RA-induced defect, suggesting that RA-induced palatal abnormality was induced as a consequence of complicated signaling cross-talk. The RA signaling pathway plays an essential role in normal palatogenesis and interacts with other signaling pathways, such as the canonical Wnt signaling pathway, Hedgehog signaling pathway and Fgf signaling pathways (Rhinn and Dolle, 2012). In a mouse model, interplay between the Hh signaling pathway and the Wnt signaling pathway is required for cleft palate (Kurosaka et al., 2014). In accord with that previous report, we also found that RA treatment disturbed the expression of downstream effectors of both the canonical Wnt pathway (*tcf7l1a* and *lef1*) and the Hh pathway (*gli1*) (data not shown). This evidence indicates that RA interferes with the Hh pathway and canonical Wnt pathway, which has also been reported in mouse palatogenesis (Hu et al., 2013; Wang et al., 2019). Our finding suggests that partial rescue of the RA phenotype by Wnt agonist treatment could

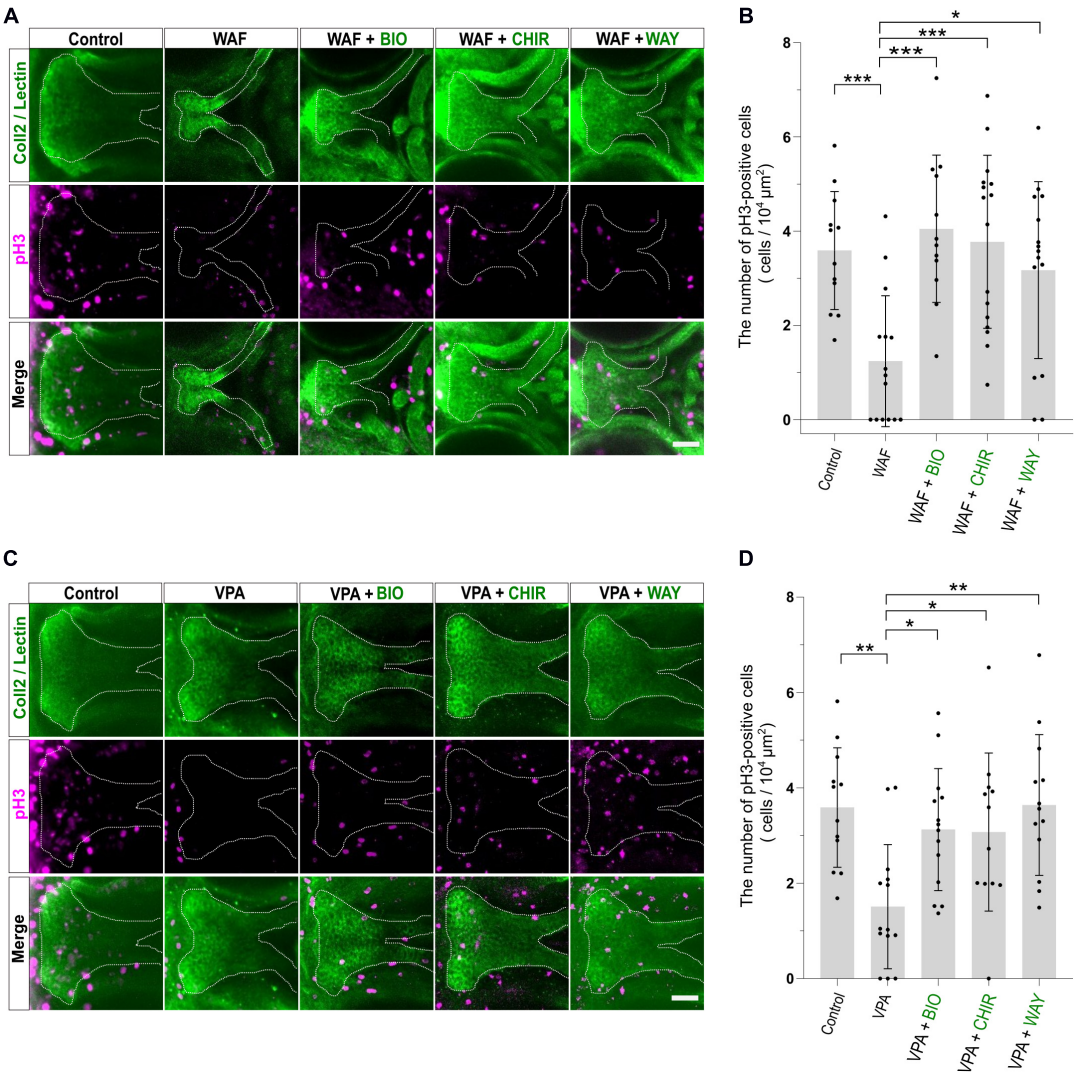

FIGURE 5 | Cell proliferation in the palate was restored by combinatorial treatment with the teratogen and Wnt agonists. **(A)** Immunofluorescence images of proliferative cells of the plate at 96 hpf. Experimental time course is the same as in **Figure 4A**. WAF (30 μM) exposure induced cleft palate and decreased the number of pH3-positive cells in the palate. The number of pH3-positive cells was restored by combinatorial treatment with BIO (100 nM), CHIR99021 (300 nM) or WAY-262611 (250 nM). Green indicates cartilage cells double stained with anti-coll2 antibody and lectin PNA. White dotted lines trace the shape of the palate. Magenta indicates proliferative cells stained with anti-pH3 antibody. **(B)** Quantification of the number of pH3-positive cells in the palate. Numerical value was normalized to 10^4 μm^2. **(C)** VPA (20 μM) exposure induced cleft palate and the number of pH3-positive cells was decreased. The number of pH3-positive cells was restored by combinatorial treatment with BIO (100 nM), CHIR99021 (300 nM) or WAY-262611 (250 nM). **(D)** Quantification of the number of pH3-positive cells in the palate. Numerical value was normalized to 10^4 μm^2. n = 12 (Control), 15 (WAF), 12 (WAF + BIO), 16 (WAF + CHIR), 15 (WAF + WAY) in **(B)**, n = 12 (Control), 14 (VPA), 14 (VPA + BIO), 12 (VPA + CHIR), 13 (VPA + WAY) in **(D)**, $^*P < 0.05$, $^{**}P < 0.01$, $^{***}P < 0.001$ (one-way ANOVA followed by Dunnett's multiple comparison test). Scale bar: 50 μm.

be strengthened to complete rescue by simultaneous activation of the Hh and the Wnt pathway. This evidence indicates that the zebrafish model has potential for analyzing complicated etiology, such as signaling cross-talk, leading to birth defects. Collectively, our findings demonstrate that the zebrafish model detects chemical-induced cleft palate found in mammals and will be applicable mechanism-based prediction of chemical-induced cleft palate.

In addition to the phenotypic relevance, our findings showed that chemical-induced cleft palate is induced by inhibition of the canonical Wnt pathway in the zebrafish model. Low doses of Wnt antagonists enhanced the cleft phenotype induced by teratogens (warfarin: WAF and valproic acid: VPA) and caused decreased expression of downstream effectors of the canonical Wnt signaling pathway. These results imply that teratogens disrupt canonical Wnt signaling, which is a target signaling pathway of cleft palate in mammals (Reynolds et al., 2019). In addition, these results support a previous *in vitro* study that showed that disruption of Wnt signaling is one of the important mechanisms underlying VPA-induced teratogenicity (Langlands et al., 2018).

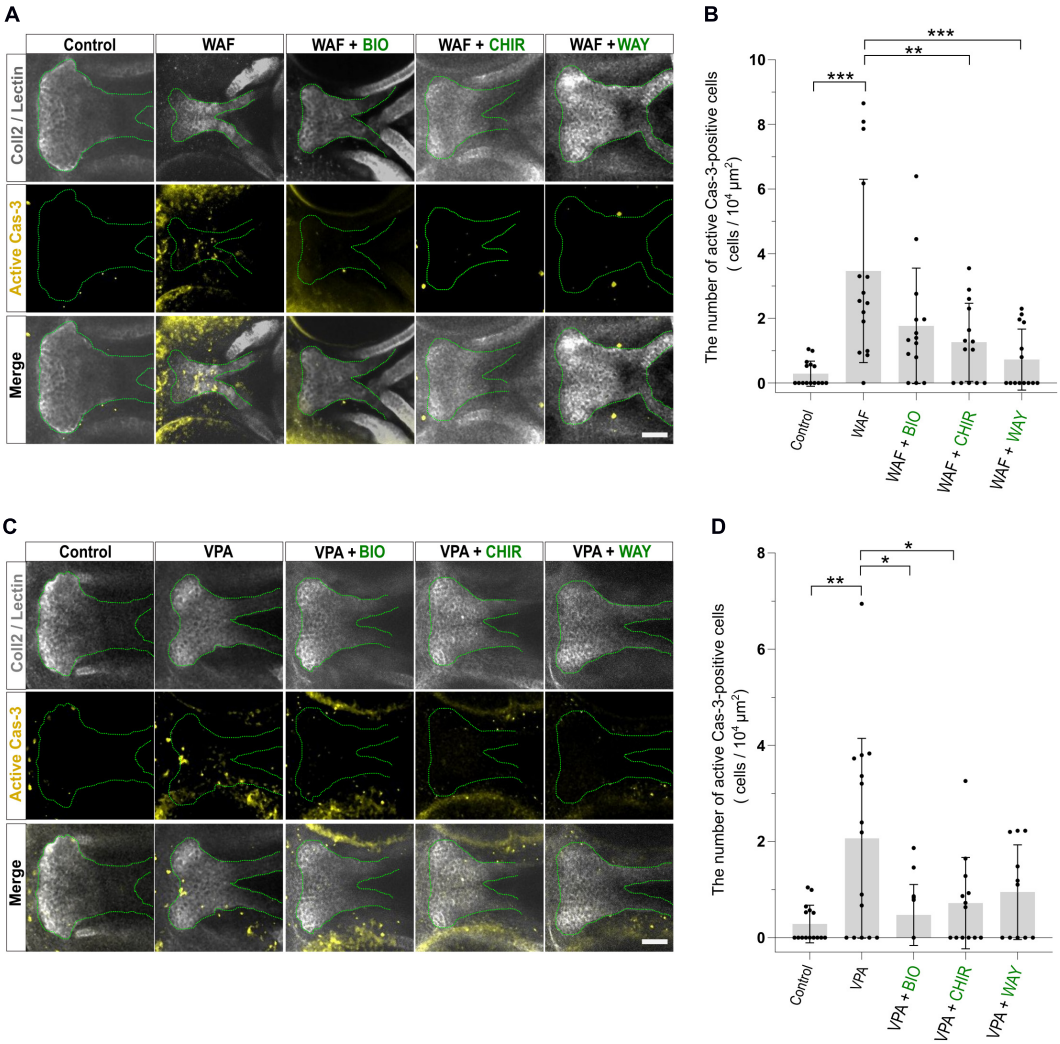

FIGURE 6 | Apoptosis level was restored by combinatorial treatment with teratogen and Wnt agonists. **(A)** Immunofluorescence images of apoptotic cells in the palate at 96 hpf. Experimental time course is the same as in **Figure 4A**. WAF (30 μM) exposure induced cleft palate and increased the number of active Cas3-positive cells in the palate. The number of active Cas3-positive cells was restored to normal by combinatorial treatment with BIO (100 nM), CHIR99021 (300 nM) or WAY-262611 (250 nM). White indicates cartilage cells double stained with anti-coll2 antibody and lectin PNA. Green dotted lines trace the shape of the palate. Yellow indicates apoptotic cells stained with anti-caspase3 antibody. **(B)** Quantification of the number of active Cas3-positive cells in the palate. Numerical value is normalized to 10^4 μm^2. **(C)** VPA (20 μM) exposure induced cleft palate and increased the number of active Cas3-positive cells. The number of active Cas3-positive cells was restored to normal by combinatorial treatment with BIO (100 nM), CHIR99021 (300 nM) or WAY-262611 (250 nM). **(D)** Quantification of the number of active Cas3-positive cells in the palate. Numerical value is normalized to 10^4 μm^2. n = 15 (Control), 15 (WAF), 14 (WAF + BIO), 14 (WAF + CHIR), 14 (WAF + WAY) in **(B)**, n = 15 (Control), 15 (VPA), 14 (VPA + BIO), 13 (VPA + CHIR), 11 (VPA + WAY) in **(D)**, $^*P < 0.05$, $^{**}P < 0.01$, $^{***}P < 0.001$ (one-way ANOVA followed by Dunnett's multiple comparison test). Scale bar, 50 μm.

Thus, considering the dose-dependent severity of the chemical-induced cleft phenotypes, our findings indicate that the teratogens examined here target the canonical Wnt pathway. Moreover, we investigated the cellular response associated with Wnt inhibition during palatogenesis. In zebrafish embryos, WAF and VPA exposure inhibited both cell proliferation and viability in the palate. These results suggest that inhibition of the canonical Wnt pathway causes cleft palate via altered cell proliferation and apoptosis in the zebrafish model. Similar observations are also found in mammalian models: Pax9-deficient mice show inhibition of the canonical Wnt pathway as well as retardation of palatal growth marked by decreased cell proliferation (Jia et al., 2017; Li et al., 2017). Another study showed that Wnt-mediated Tgf-β3 activation regulates palatal shelf closure, and inhibition of the Tgf-β3 pathway causes cleft palate via reduced cell proliferation and increased apoptosis (He et al., 2011). Thus, the zebrafish model recapitulates mammalian cleft palate etiology at the cell signaling and cellular levels.

To achieve accurate prediction and reveal the etiology and pathology of chemical-induced cleft palate, detailed analysis of the developmental origin of proliferative and apoptotic cells in chemical-induced cleft palate and target cells adversely affected

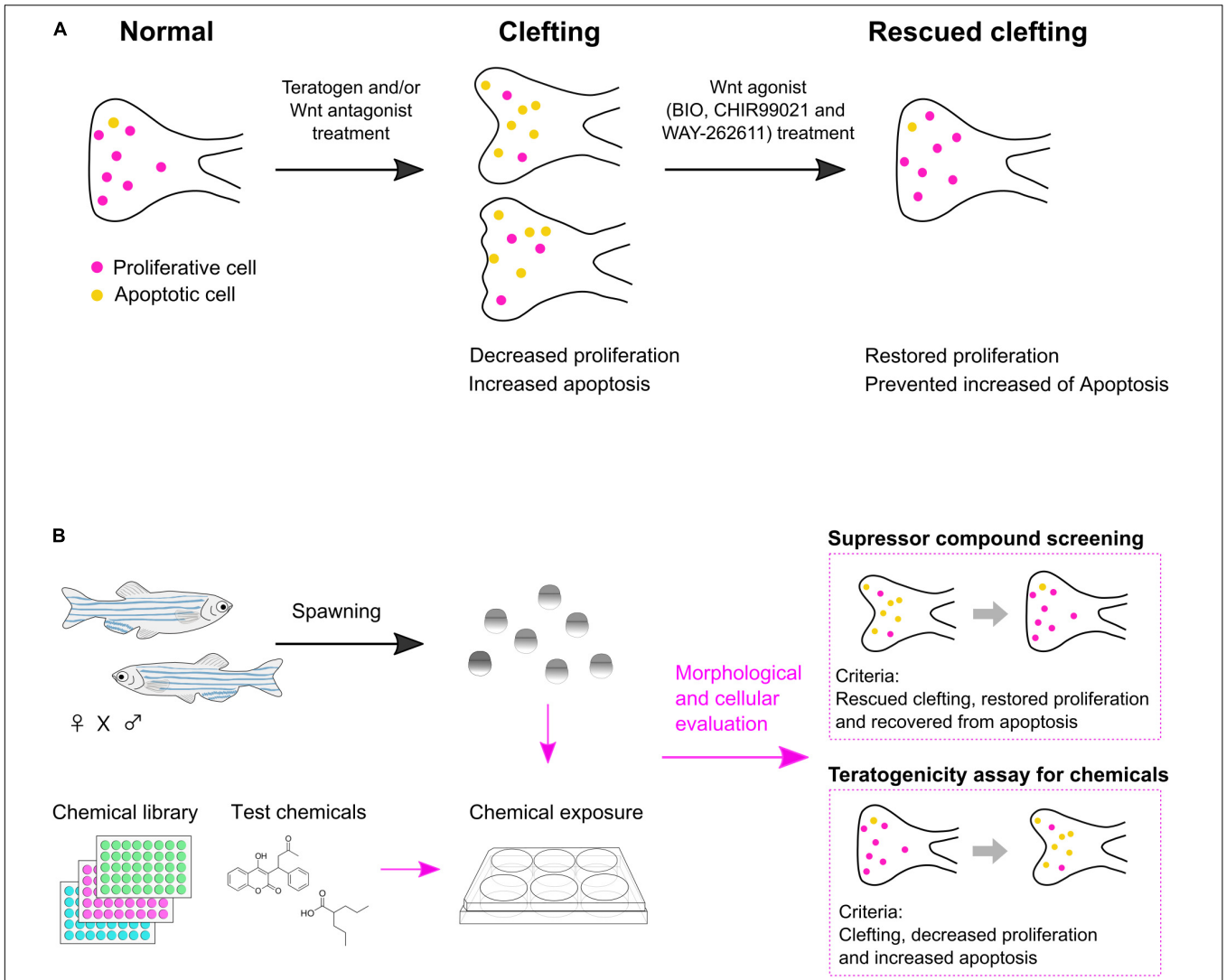

FIGURE 7 | Summary of chemical-induced cleft palate. **(A)** Teratogen induces cleft palate by inhibition of the canonical Wnt signaling pathway. This defect is characterized by decreased proliferation and increased apoptosis in the zebrafish palate. Chemical-induced cleft palate is prevented by Wnt agonist treatment. **(B)** Application of a zebrafish model for suppressor screening as well as teratogenicity assay for chemicals.

by teratogens will be needed. The cells composing the zebrafish palate are progenies of neural crest cells migrating from the frontonasal and maxillary domain to form the palate, a process which is conserved between fish and mammals (Swartz et al., 2011; Dougherty et al., 2013; Mork and Crump, 2015). In our previous report, we demonstrated that 12 teratogens disrupted cranial neural crest cell development. Besides chemical-induced craniofacial anomalies, developmental defects in eye, otic vesicles, the heart and/or body axis were observed as a result of teratogen treatment (Liu et al., 2020). Thus, to discriminate teratogen effects on neural crest cells from effects on other cell types will be required in order to eliminate the possibility that secondary effect(s) on neural crest cells development are caused by the teratogens. For this purpose, we have set up experimental systems such as transgenic lines of cranial neural crest cells and target organs for applying spatio-temporal analysis. In addition to utilizing these lines, we will perform teratogen treatment at different time points to define the specific effects on neural crest cells and their descendants. These analyses will reveal whether chemical-induced cleft palate is caused by primary defect(s) in neural crest cells and will provide insights into the relevance to mammals, including human.

We investigated the effect of cleft palate prevention by chemical modulation of the canonical Wnt pathway. Treatment with small molecule Wnt agonists (BIO, CHIR99021, WAY-262611) rescued chemical-induced cleft palate at the morphological and cellular level. This result supports the conclusion that inhibition of Wnt signaling has a significant role in chemical-induced cleft palate via decreased cell proliferation and viability in the zebrafish palate. In a mouse model with cleft palate, Wnt agonist treatment also corrected cleft palate (Liu et al., 2007; Jia et al., 2017; Li et al., 2017). Therefore,

our results demonstrate the relevance of our zebrafish model to the development of mammalian cleft palate. However, chemical-induced cleft palate was not completely prevented by chemical modulation of the canonical Wnt pathway, implying insufficient penetrance of the small molecules or the existence of another signaling pathway(s) for complete prevention of cleft palate. To strengthen the prevention of cleft palate, genetic modification of the canonical Wnt signaling could be effective. In addition, modulation of an additional signaling pathway should also be considered. In the zebrafish model, disruption of the non-canonical Wnt pathway also caused cleft phenotype, and cross-talk between the non-canonical and canonical Wnt pathway was previously reported (Curtin et al., 2011; Duncan et al., 2017). To obtain higher efficacy, simultaneous chemical modulation or chemical and genetic modulation with other signaling pathways will be a next step toward prevention of cleft palate. The present results demonstrate the usefulness of the zebrafish model for mechanism-based suppressor chemical screening as well as the promising potential of the Wnt pathway as a therapeutic target.

In this report, we investigated the biological relevance of a zebrafish experimental model of chemical-induced cleft palate to cleft palate in mammals at the morphological, cellular and signaling levels. The results support the usefulness of the zebrafish model for teratogenicity screening. Also, the rescue experiments further indicated the usefulness of the zebrafish model: chemical modulation of the Wnt pathway showed the possibility of using this zebrafish model for chemical screening for prevention or treatment of cleft palate (**Figure 7B**).

In sum, we show a proof of concept for this zebrafish palate model for chemical screening for prediction and prevention of chemical-induced cleft palate. Also, our findings show that the canonical Wnt signaling pathway would be a therapeutic target.

DATA AVAILABILITY STATEMENT

The raw data supporting the conclusions of this article will be made available by the authors, without undue reservation.

ETHICS STATEMENT

Ethical review and approval was not required for the animal study because according to the Council Directive 2010/63/EU, zebrafish embryos and larvae up to 5 day old are excepted. However, we performed any experiments and fish husbandry according to the Zebrafish Book (Westerfield, 2000) and the Guide for the Care and Use of Laboratory Animals 8th edition (National Research Council, 2011). Written informed consent was obtained from the owners for the participation of their animals in this study.

AUTHOR CONTRIBUTIONS

RN performed conceptualization, methodology, validation, formal analysis, investigation, writing – original draft preparation, writing, and visualization. SL performed methodology and investigation. NI and OM performed original draft preparation. JT performed conceptualization, methodology, validation, formal analysis, writing – original draft preparation, writing – review and editing, visualization, and supervision. All authors contributed to the article and approved the submitted version.

ACKNOWLEDGMENTS

We are grateful to the National BioResource Project for providing RIKEN WT strain. We thank Dr. Elizabeth Nakajima for critical reading of the manuscript; Dr. Shinichi Meguro for helpful discussions and zebrafish support; Dr. Atsuko Shimada for technical support of dissection; Dr. Takashi Ieki for helpful discussions; and Mr. Yuji Takemura, Mr. Takahito Arai, Jun Kitayama, and Toshiyuki Iwama for fish care.

SUPPLEMENTARY MATERIAL

The Supplementary Material for this article can be found online at: https://www.frontiersin.org/articles/10.3389/fcell.2020.592967/full#supplementary-material

Supplementary Figure 1 | Phenotypic severity of teratogen treatment in a dose-dependent manner. **(A)** Definition of phenotypic severity. Anterior is to the left. Green dotted lines indicate the anterior **(left)** and posterior **(right)** edge of the zebrafish palate, respectively. The palate length between the green dotted lines is defined as 100% length. Red dotted line indicates 40% length line of the palate length. Each phenotype was defined as follows: rough edge; several small nicks existing at the anterior edge, moderate clefting; under 40% clefting at the center of the palate, severe clefting; over 40% clefting of at the center of the palate, and rod-like; the palate showing rod-like structure. **(B)** Frequency of palatal defects in dose-dependent manner. n = 11 (VPA 7.5 μM), 18 (VPA 15 μM), 20 (VPA 30 μM), 10 (WAF 15 μM), 14 (WAF 30 μM), 14 (WAF 60 μM), 10 (SA 100 μM), 13 (SA 200 μM), 13 (SA 400 μM), 11 (MTX 50 μM), 14 (MTX 100 μM), 8 (MTX 200 μM), 13 (CAF 500 μM), 17 (CAF 1 mM), 10 (CAF 2 mM), 16 (RA 10 nM), 12 (RA 30 nM), 11 (RA 50 nM).

Supplementary Figure 2 | Proliferation and apoptosis in the palate of INA-exposed embryos. **(A)** Immunofluorescence images of proliferative cells in the palate. Control is the same as **Figure 3A**. Embryos were treated with isoniazid (1 mM) and then examined by fluorescent immunohistochemistry. No striking difference was observed between the control and treated embryos. Green indicates cartilage cells double stained with anti-coll2 antibody and lectin PNA. White dotted lines trace the shape of the palate. Magenta indicates proliferative cells stained with anti-pH3 antibody. **(B)** Immunofluorescence images of apoptotic cells in the palate at 96 hpf. Control is the same as in **Figure 3C**. Embryos were treated with isoniazid (1 mM) and then examined by fluorescent immunohistochemistry. No striking difference was observed between the control and treated embryos. White indicates cartilage cells double stained with anti-coll2 antibody and lectin PNA. Green dotted lines trace the shape of the palate. Yellow indicates proliferative cells stained with anti-caspase3 antibody. Scale bar: 50 μm.

Supplementary Figure 3 | Rod-like phenotype was not rescued by Wnt agonists. **(A–E)** Fluorescence images of palate at 96 hpf. Nuclei of cartilage cells were stained with DAPI. Embryos were treated with retinoic acid (RA, 10 nM). **(A,B)** Retinoic acid (RA) induced rod-like phenotype. **(C–E)** The rod-like phenotype was not rescued by combinatorial treatment with Wnt agonists [BIO (100 nM), CHIR99021 (300 nM) or WAY-262611 (250 nM)]. Scale bar: 50 μm.

REFERENCES

Beaty, T. H., Marazita, M. L., and Leslie, E. J. (2016). Genetic factors influencing risk to orofacial clefts: today's challenges and tomorrow's opportunities. *F1000Res* 5:2800. doi: 10.12688/f1000research.9503.1

Benke, P. J. (1984). The isotretinoin teratogen syndrome. *JAMA* 251, 3267–3269. doi: 10.1001/jama.251.24.3267

Billington, C. J. Jr., Schmidt, B., Marcucio, R. S., Hallgrimsson, B., Gopalakrishnan, R., et al. (2015). Impact of retinoic acid exposure on midfacial shape variation and manifestation of holoprosencephaly in Twsg1 mutant mice. *Dis. Model. Mech.* 8, 139–146. doi: 10.1242/dmm.018275

Boulet, S. L., Grosse, S. D., Honein, M. A., and Correa-Villasenor, A. (2009). Children with orofacial clefts: health-care use and costs among a privately insured population. *Public Health Rep.* 124, 447–453. doi: 10.1177/003335490912400315

Brent, R. L. (2004). Environmental causes of human congenital malformations: the pediatrician's role in dealing with these complex clinical problems caused by a multiplicity of environmental and genetic factors. *Pediatrics* 113, 957–968.

Bush, J. O., and Jiang, R. (2012). Palatogenesis: morphogenetic and molecular mechanisms of secondary palate development. *Development* 139, 231–243. doi: 10.1242/dev.067082

Cassar, S., Beekhuijzen, M., Beyer, B., Chapin, R., Dorau, M., Hoberman, A., et al. (2019). A multi-institutional study benchmarking the zebrafish developmental assay for prediction of embryotoxic plasma concentrations from rat embryo-fetal development studies. *Reprod. Toxicol.* 86, 33–44. doi: 10.1016/j.reprotox.2019.02.004

Chaube, S., and Murphy, M. L. (1966). The effects of hydroxyurea and related compounds on the rat fetus. *Cancer Res.* 26, 1448–1457.

Cheah, F. S., Winkler, C., Jabs, E. W., and Chong, S. S. (2010). Tgf β3 regulation of chondrogenesis and osteogenesis in zebrafish is mediated through formation and survival of a subpopulation of the cranial neural crest. *Mech. Dev.* 127, 329–344. doi: 10.1016/j.mod.2010.04.003

Chen, E. Y., DeRan, M. T., Ignatius, M. S., Grandinetti, K. B., Clagg, R., McCarthy, K. M., et al. (2014). Glycogen synthase kinase 3 inhibitors induce the canonical WNT/beta-catenin pathway to suppress growth and self-renewal in embryonal rhabdomyosarcoma. *Proc. Natl. Acad. Sci. U.S.A.* 111, 5349–5354. doi: 10.1073/pnas.1317731111

Collier, S. A., Browne, M. L., Rasmussen, S. A., Honein, M. A., and National Birth Defects Prevention, S. (2009). Maternal caffeine intake during pregnancy and orofacial clefts. *Birth Defects Res. A Clin. Mol. Teratol.* 85, 842–849. doi: 10.1002/bdra.20600

Curtin, E., Hickey, G., Kamel, G., Davidson, A. J., and Liao, E. C. (2011). Zebrafish wnt9a is expressed in pharyngeal ectoderm and is required for palate and lower jaw development. *Mech. Dev.* 128, 104–115. doi: 10.1016/j.mod.2010.11.003

Czeizel, A. (1976). Letter: Diazepam, phenytoin, and aetiology of cleft lip and/or cleft palate. *Lancet* 1:810. doi: 10.1016/s0140-6736(76)91654-8

DeLaurier, A., Nakamura, Y., Braasch, I., Khanna, V., Kato, H., Wakitani, S., et al. (2012). Histone deacetylase-4 is required during early cranial neural crest development for generation of the zebrafish palatal skeleton. *BMC Dev. Biol.* 12:16. doi: 10.1186/1471-213x-12-16

DeRoo, L. A., Wilcox, A. J., Drevon, C. A., and Lie, R. T. (2008). First-trimester maternal alcohol consumption and the risk of infant oral clefts in Norway: a population-based case-control study. *Am. J. Epidemiol.* 168, 638–646. doi: 10.1093/aje/kwn186

Dixon, M. J., Marazita, M. L., Beaty, T. H., and Murray, J. C. (2011). Cleft lip and palate: understanding genetic and environmental influences. *Nat. Rev. Genet.* 12, 167–178. doi: 10.1038/nrg2933

Dougherty, M., Kamel, G., Grimaldi, M., Gfrerer, L., Shubinets, V., Ethier, R., et al. (2013). Distinct requirements for wnt9a and irf6 in extension and integration mechanisms during zebrafish palate morphogenesis. *Development* 140, 76–81. doi: 10.1242/dev.080473

D'Souza, R., Ostro, J., Shah, P. S., Silversides, C. K., Malinowski, A., Murphy, K. E., et al. (2017). Anticoagulation for pregnant women with mechanical heart valves: a systematic review and meta-analysis. *Eur. Heart J.* 38, 1509–1516. doi: 10.1093/eurheartj/ehx032

Duncan, K. M., Mukherjee, K., Cornell, R. A., and Liao, E. C. (2017). Zebrafish models of orofacial clefts. *Dev. Dyn.* 246, 897–914. doi: 10.1002/dvdy.24566

El Gendy, M. M., Kandil, A. M., Helal, M. A., and Zahou, F. M. (2015). The teratogenic effects of imatinib mesylate on rat fetuses. *Toxicol. Rep.* 2, 654–663. doi: 10.1016/j.toxrep.2015.05.001

Faiella, A., Wernig, M., Consalez, G. G., Hostick, U., Hofmann, C., Hustert, E., et al. (2000). A mouse model for valproate teratogenicity: parental effects, homeotic transformations, and altered HOX expression. *Hum. Mol. Genet.* 9, 227–236. doi: 10.1093/hmg/9.2.227

Ghassibe-Sabbagh, M., Desmyter, L., Langenberg, T., Claes, F., Boute, O., Bayet, B., et al. (2011). FAF1, a gene that is disrupted in cleft palate and has conserved function in zebrafish. *Am. J. Hum. Genet.* 88, 150–161. doi: 10.1016/j.ajhg.2011.01.003

Ghodke-Puranik, Y., Thorn, C. F., Lamba, J. K., Leeder, J. S., Song, W., Birnbaum, A. K., et al. (2013). Valproic acid pathway: pharmacokinetics and pharmacodynamics. *Pharmacogenet. Genomics* 23, 236–241. doi: 10.1097/fpc.0b013e32835ea0b2

Gongal, P. A., and Waskiewicz, A. J. (2008). Zebrafish model of holoprosencephaly demonstrates a key role for TGIF in regulating retinoic acid metabolism. *Hum. Mol. Genet.* 17, 525–538. doi: 10.1093/hmg/ddm328

Grainger, S., Richter, J., Palazon, R. E., Pouget, C., Lonquich, B., Wirth, S., et al. (2016). Wnt9a is required for the aortic amplification of nascent hematopoietic stem cells. *Cell Rep.* 17, 1595–1606. doi: 10.1016/j.celrep.2016.10.027

Granzow, J. W., Thaller, S. R., and Panthaki, Z. (2003). Cleft palate and toe malformations in a child with fetal methotrexate exposure. *J. Craniofac. Surg.* 14, 747–748. doi: 10.1097/00001665-200309000-00027

Hagemann, A. I., Kurz, J., Kauffeld, S., Chen, Q., Reeves, P. M., Weber, S., et al. (2014). In vivo analysis of formation and endocytosis of the Wnt/beta-catenin signaling complex in zebrafish embryos. *J. Cell Sci.* 127, 3970–3982. doi: 10.1242/jcs.148767

Hahn, M. E., and Sadler, K. C. (2020). Casting a wide net: use of diverse model organisms to advance toxicology. *Dis. Model. Mech.* 13:dmm.043844.

He, F., Xiong, W., Wang, Y., Li, L., Liu, C., Yamagami, T., et al. (2011). Epithelial Wnt/beta-catenin signaling regulates palatal shelf fusion through regulation of Tgf β3 expression. *Dev. Biol.* 350, 511–519. doi: 10.1016/j.ydbio.2010.12.021

Heindel, J. J., Price, C. J., and Schwetz, B. A. (1994). The developmental toxicity of boric acid in mice, rats, and rabbits. *Environ. Health Perspect.* 102(Suppl. 7), 107–112. doi: 10.2307/3431972

Hillegass, J. M., Villano, C. M., Cooper, K. R., and White, L. A. (2008). Glucocorticoids alter craniofacial development and increase expression and activity of matrix metalloproteinases in developing zebrafish (Danio rerio). *Toxicol. Sci.* 102, 413–424. doi: 10.1093/toxsci/kfn010

Holford, N. H. (1986). Clinical pharmacokinetics and pharmacodynamics of warfarin. Understanding the dose-effect relationship. *Clin. Pharmacokinet.* 11, 483–504. doi: 10.2165/00003088-198611060-00005

Howe, A. M., and Webster, W. S. (1992). The warfarin embryopathy: a rat model showing maxillonasal hypoplasia and other skeletal disturbances. *Teratology* 46, 379–390. doi: 10.1002/tera.1420460408

Hu, X., Gao, J., Liao, Y., Tang, S., and Lu, F. (2013). Retinoic acid alters the proliferation and survival of the epithelium and mesenchyme and suppresses Wnt/beta-catenin signaling in developing cleft palate. *Cell Death Dis.* 4:e898. doi: 10.1038/cddis.2013.424

Hviid, A., and Mølgaard-Nielsen, D. (2011). Corticosteroid use during pregnancy and risk of orofacial clefts. *CMAJ* 183, 796–804. doi: 10.1503/cmaj.101063

Inoue, A., Nishimura, Y., Matsumoto, N., Umemoto, N., Shimada, Y., Maruyama, T., et al. (2016). Comparative study of the zebrafish embryonic toxicity test and mouse embryonic stem cell test to screen developmental toxicity of human pharmaceutical drugs. *Fundamental Toxicol. Sci.* 3, 79–87. doi: 10.2131/fts.3.79

Ito, T., and Handa, H. (2012). Deciphering the mystery of thalidomide teratogenicity. *Congenit. Anom.* 52, 1–7. doi: 10.1111/j.1741-4520.2011.00351.x

Iwata, J., Suzuki, A., Yokota, T., Ho, T. V., Pelikan, R., Urata, M., et al. (2014). TGF β regulates epithelial-mesenchymal interactions through WNT signaling activity to control muscle development in the soft palate. *Development* 141, 909–917. doi: 10.1242/dev.103093

Jackson, H. E., Ono, Y., Wang, X., Elworthy, S., Cunliffe, V. T., and Ingham, P. W. (2015). The role of Sox6 in zebrafish muscle fiber type specification. *Skelet Muscle* 5:2. doi: 10.1186/s13395-014-0026-2

Jentink, J., Loane, M. A., Dolk, H., Barisic, I., Garne, E., Morris, J. K., et al. (2010). Valproic acid monotherapy in pregnancy and major congenital malformations. *N. Engl. J. Med.* 362, 2185–2193. doi: 10.1056/nejmoa0907328

Jia, S., Zhou, J., Fanelli, C., Wee, Y., Bonds, J., Schneider, P., et al. (2017). Small-molecule Wnt agonists correct cleft palates in Pax9 mutant mice in utero. *Development* 144, 3819–3828. doi: 10.1242/dev.157750

Jordan, R. L., Wilson, J. G., and Schumacher, H. J. (1977). Embryotoxicity of the folate antagonist methotrexate in rats and rabbits. *Teratology* 15, 73–79. doi: 10.1002/tera.1420150110

Jugessur, A., Farlie, P. G., and Kilpatrick, N. (2009). The genetics of isolated orofacial clefts: from genotypes to subphenotypes. *Oral Dis.* 15, 437–453. doi: 10.1111/j.1601-0825.2009.01577.x

Kague, E., Gallagher, M., Burke, S., Parsons, M., Franz-Odendaal, T., and Fisher, S. (2012). Skeletogenic fate of zebrafish cranial and trunk neural crest. *PLoS One* 7:e47394. doi: 10.1371/journal.pone.0047394

Kemp, M. W., Newnham, J. P., Challis, J. G., Jobe, A. H., and Stock, S. J. (2016). The clinical use of corticosteroids in pregnancy. *Hum. Reprod. Update* 22, 240–259.

Kietzman, H. W., Everson, J. L., Sulik, K. K., and Lipinski, R. J. (2014). The teratogenic effects of prenatal ethanol exposure are exacerbated by Sonic Hedgehog or GLI2 haploinsufficiency in the mouse. *PLoS One* 9:e89448. doi: 10.1371/journal.pone.0089448

Kimmel, C. B., Ballard, W. W., Kimmel, S. R., Ullmann, B., and Schilling, T. F. (1995). Stages of embryonic development of the zebrafish. *Dev. Dyn.* 203, 253–310. doi: 10.1002/aja.1002030302

Kozer, E., Nikfar, S., Costei, A., Boskovic, R., Nulman, I., and Koren, G. (2002). Aspirin consumption during the first trimester of pregnancy and congenital anomalies: a meta-analysis. *Am. J. Obstet. Gynecol.* 187, 1623–1630. doi: 10.1067/mob.2002.127376

Kurosaka, H. (2015). The roles of hedgehog signaling in upper lip formation. *Biomed. Res. Int.* 2015:901041.

Kurosaka, H., Iulianella, A., Williams, T., and Trainor, P. A. (2014). Disrupting hedgehog and WNT signaling interactions promotes cleft lip pathogenesis. *J. Clin. Invest.* 124, 1660–1671. doi: 10.1172/jci72688

Lammer, E. J., Schunior, A., Hayes, A. M., and Holmes, L. B. (1988). Isotretinoin dose and teratogenicity. *Lancet* 2, 503–504. doi: 10.1016/s0140-6736(88)90143-2

Langlands, A. J., Carroll, T. D., Chen, Y., and Nathke, I. (2018). Chir99021 and Valproic acid reduce the proliferative advantage of Apc mutant cells. *Cell Death Dis.* 9:255.

Lee, M. S., Bonner, J. R., Bernard, D. J., Sanchez, E. L., Sause, E. T., Prentice, R. R., et al. (2012). Disruption of the folate pathway in zebrafish causes developmental defects. *BMC Dev. Biol.* 12:12. doi: 10.1186/1471-213x-12-12

Li, C., Lan, Y., Krumlauf, R., and Jiang, R. (2017). Modulating Wnt signaling rescues palate morphogenesis in Pax9 mutant mice. *J. Dent Res.* 96, 1273–1281. doi: 10.1177/0022034517719865

Lipinski, R. J., Song, C., Sulik, K. K., Everson, J. L., Gipp, J. J., Yan, D., et al. (2010). Cleft lip and palate results from Hedgehog signaling antagonism in the mouse: phenotypic characterization and clinical implications. *Birth Defects Res. A Clin. Mol. Teratol.* 88, 232–240.

Liu, F., and Millar, S. E. (2010). Wnt/beta-catenin signaling in oral tissue development and disease. *J. Dent. Res.* 89, 318–330. doi: 10.1177/0022034510363373

Liu, K. J., Arron, J. R., Stankunas, K., Crabtree, G. R., and Longaker, M. T. (2007). Chemical rescue of cleft palate and midline defects in conditional GSK-3beta mice. *Nature* 446, 79–82. doi: 10.1038/nature05557

Liu, S., Narumi, R., Ikeda, N., Morita, O., and Tasaki, J. (2020). Chemical-induced craniofacial anomalies caused by disruption of neural crest cell development in a zebrafish model. *Dev. Dyn.* 249, 794–815. doi: 10.1002/dvdy.179

Martin, M. T., Judson, R. S., Reif, D. M., Kavlock, R. J., and Dix, D. J. (2009). Profiling chemicals based on chronic toxicity results from the U.S. EPA ToxRef Database. *Environ. Health Perspect.* 117, 392–399. doi: 10.1289/ehp.0800074

Martinez, C. S., Feas, D. A., Siri, M., Igartua, D. E., Chiaramoni, N. S., Del, V. A. S., et al. (2018). In vivo study of teratogenic and anticonvulsant effects of antiepileptics drugs in zebrafish embryo and larvae. *Neurotoxicol. Teratol.* 66, 17–24. doi: 10.1016/j.ntt.2018.01.008

Maurus, D., and Harris, W. A. (2009). Zic-associated holoprosencephaly: zebrafish Zic1 controls midline formation and forebrain patterning by regulating Nodal, Hedgehog, and retinoic acid signaling. *Genes Dev.* 23, 1461–1473. doi: 10.1101/gad.517009

Mezawa, H., Tomotaki, A., Yamamoto-Hanada, K., Ishitsuka, K., Ayabe, T., Konishi, M., et al. (2019). Prevalence of congenital anomalies in the Japan environment and Children's study. *J. Epidemiol.* 29, 247–256.

Mongera, A., Singh, A. P., Levesque, M. P., Chen, Y. Y., Konstantinidis, P., and Nusslein-Volhard, C. (2013). Genetic lineage labeling in zebrafish uncovers novel neural crest contributions to the head, including gill pillar cells. *Development* 140, 916–925. doi: 10.1242/dev.091066

Moore, J. A. (1997). An assessment of boric acid and borax using the IEHR Evaluative Process for Assessing Human Developmental and Reproductive Toxicity of Agents. Expert Scientific Committee. *Reproduct. Toxicol.* 11, 123–160. doi: 10.1016/s0890-6238(96)00204-3

Mork, L., and Crump, G. (2015). Zebrafish craniofacial development: a window into early patterning. *Curr. Top. Dev. Biol.* 115, 235–269. doi: 10.1016/bs.ctdb.2015.07.001

National Research Council (2011). *Guide for the Care and Use of Laboratory Animals*, 8th Edn. Washington, DC: National Academies Press.

National Toxicology, P. (2008). NTP-CERHR monograph on the potential human reproductive and developmental effects of hydroxyurea. *NTP Cerhr Mon* 7–8, 9–31.

Neiswender, H., Navarre, S., Kozlowski, D. J., and LeMosy, E. K. (2017). Early Craniofacial Defects in Zebrafish That Have Reduced Function of a Wnt-Interacting Extracellular Matrix Protein, Tinagl1. *Cleft Palate Craniofac J.* 54, 381–390. doi: 10.1597/15-283

Newman, C. G. (1985). Teratogen update: clinical aspects of thalidomide embryopathy–a continuing preoccupation. *Teratology* 32, 133–144. doi: 10.1002/tera.1420320118

Nishimura, H., and Nakai, K. (1960). Congenital malformations in offspring of mice treated with caffeine. *Proc. Soc. Exp. Biol. Med.* 104, 140–142. doi: 10.3181/00379727-104-25757

Nishiya, N., Oku, Y., Kumagai, Y., Sato, Y., Yamaguchi, E., Sasaki, A., et al. (2014). A zebrafish chemical suppressor screening identifies small molecule inhibitors of the Wnt/beta-catenin pathway. *Chem. Biol.* 21, 530–540. doi: 10.1016/j.chembiol.2014.02.015

Okano, J., Udagawa, J., and Shiota, K. (2014). Roles of retinoic acid signaling in normal and abnormal development of the palate and tongue. *Congenit. Anom.* 54, 69–76. doi: 10.1111/cga.12049

Padmanabhan, R., and Ahmed, I. (1997). Retinoic acid-induced asymmetric craniofacial growth and cleft palate in the TO mouse fetus. *Reprod. Toxicol.* 11, 843–860. doi: 10.1016/s0890-6238(97)00068-3

Parada, C., and Chai, Y. (2012). Roles of BMP signaling pathway in lip and palate development. *Front. Oral. Biol.* 16:60–70. doi: 10.1159/000337617

Parker, S. E., Mai, C. T., Canfield, M. A., Rickard, R., Wang, Y., Meyer, R. E., et al. (2010). Updated National Birth Prevalence estimates for selected birth defects in the United States, 2004-2006. *Birth Defects Res. A Clin. Mol. Teratol.* 88, 1008–1016. doi: 10.1002/bdra.20735

Patton, E. E., and Tobin, D. M. (2019). Spotlight on zebrafish: the next wave of translational research. *Dis. Model Mech.* 12:dmm039370. doi: 10.1242/dmm.039370

Price, C. J., Marr, M. C., Myers, C. B., Seely, J. C., Heindel, J. J., and Schwetz, B. A. (1996). The developmental toxicity of boric acid in rabbits. *Fundam. Appl. Toxicol.* 34, 176–187. doi: 10.1006/faat.1996.0188

Pye, S. M., Cortes, J., Ault, P., Hatfield, A., Kantarjian, H., Pilot, R., et al. (2008). The effects of imatinib on pregnancy outcome. *Blood* 111, 5505–5508. doi: 10.1182/blood-2007-10-114900

Rennekamp, A. J., and Peterson, R. T. (2015). 15 years of zebrafish chemical screening. *Curr. Opin. Chem. Biol.* 24, 58–70. doi: 10.1016/j.cbpa.2014.10.025

Reynolds, K., Kumari, P., Sepulveda Rincon, L., Gu, R., Ji, Y., Kumar, S., et al. (2019). Wnt signaling in orofacial clefts: crosstalk, pathogenesis and models. *Dis. Model Mech.* 12:dmm037051. doi: 10.1242/dmm.037051

Rhinn, M., and Dolle, P. (2012). Retinoic acid signalling during development. *Development* 139, 843–858. doi: 10.1242/dev.065938

Riley, B. M., Mansilla, M. A., Ma, J., Daack-Hirsch, S., Maher, B. S., Raffensperger, L. M., et al. (2007). Impaired FGF signaling contributes to cleft lip and palate. *Proc. Natl. Acad. Sci. U.S.A.* 104, 4512–4517.

Roessler, E., and Muenke, M. (2010). The molecular genetics of holoprosencephaly. *Am. J. Med. Genet. C Semin. Med. Genet.* 154C, 52–61. doi: 10.1002/ajmg.c.30236

Rutledge, J. C., Shourbaji, A. G., Hughes, L. A., Polifka, J. E., Cruz, Y. P., Bishop, J. B., et al. (1994). Limb and lower-body duplications induced by retinoic acid in mice. *Proc. Natl. Acad. Sci. U.S.A.* 91, 5436–5440. doi: 10.1073/pnas.91.12.5436

Selderslaghs, I. W., Van Rompay, A. R., De Coen, W., and Witters, H. E. (2009). Development of a screening assay to identify teratogenic and embryotoxic chemicals using the zebrafish embryo. *Reprod. Toxicol.* 28, 308–320. doi: 10.1016/j.reprotox.2009.05.004

Shaw, G. M., Wasserman, C. R., Lammer, E. J., O'Malley, C. D., Murray, J. C., Basart, A. M., et al. (1996). Orofacial clefts, parental cigarette smoking, and transforming growth factor-alpha gene variants. *Am. J. Hum. Genet.* 58, 551–561.

Sive, H. (2011). 'Model' or 'tool'? New definitions for translational research. *Dis. Model. Mech.* 4, 137–138. doi: 10.1242/dmm.007666

Smithells, R. W., and Newman, C. G. (1992). Recognition of thalidomide defects. *J. Med. Genet.* 29, 716–723. doi: 10.1136/jmg.29.10.716

Snider, D. E. Jr., Layde, P. M., Johnson, M. W., and Lyle, M. A. (1980). Treatment of tuberculosis during pregnancy. *Am. Rev. Respir. Dis.* 122, 65–79.

Solomon, B. D., Lacbawan, F., Mercier, S., Clegg, N. J., Delgado, M. R., Rosenbaum, K., et al. (2010). Mutations in ZIC2 in human holoprosencephaly: description of a novel ZIC2 specific phenotype and comprehensive analysis of 157 individuals. *J. Med. Genet.* 47, 513–524. doi: 10.1136/jmg.2009.073049

Song, L., Li, Y., Wang, K., Wang, Y. Z., Molotkov, A., Gao, L., et al. (2009). Lrp6-mediated canonical Wnt signaling is required for lip formation and fusion. *Development* 136, 3161–3171. doi: 10.1242/dev.037440

Speidel, B. D., and Meadow, S. R. (1972). Maternal epilepsy and abnormalities of the fetus and newborn. *Lancet* 300, 839–843. doi: 10.1016/s0140-6736(72)92209-x

Speirs, A. L. (1962). Thalidomide and congenital abnormalities. *Lancet* 1, 303–305.

Stanier, P., and Pauws, E. (2012). Development of the lip and palate: FGF signalling. *Front. Oral Biol.* 16:71–80. doi: 10.1159/000337618

Starling, L. D., Sinha, A., Boyd, D., and Furck, A. (2012). Fetal warfarin syndrome. *BMJ Case Rep.* 2012:bcr2012007344.

Stephens, J. D., Golbus, M. S., Miller, T. R., Wilber, R. R., and Epstein, C. J. (1980). Multiple congenital anomalies in a fetus exposed to 5-fluorouracil during the first trimester. *Am. J. Obstet. Gynecol.* 137, 747–749. doi: 10.1016/s0002-9378(15)33259-2

Swartz, M. E., Sheehan-Rooney, K., Dixon, M. J., and Eberhart, J. K. (2011). Examination of a palatogenic gene program in zebrafish. *Dev. Dyn.* 240, 2204–2220. doi: 10.1002/dvdy.22713

Tagashira, E., Nakao, K., Urano, T., Shikawa, S., Hiramori, T., and Yanaura, S. (1981). Correlation of teratogenicity of aspirin to the stagespecific distribution of salicylic acid in rats. *Jpn. J. Pharmacol.* 31, 563–571. doi: 10.1254/jjp.31.563

Taussig, H. B. (1962). A study of the German outbreak of phocomelia. The thalidomide syndrome. *JAMA* 180, 1106–1114.

Teixido, E., Pique, E., Gomez-Catalan, J., and Llobet, J. M. (2013). Assessment of developmental delay in the zebrafish embryo teratogenicity assay. *Toxicol. In Vitro* 27, 469–478. doi: 10.1016/j.tiv.2012.07.010

Trasler, D. G. (1965). Aspirin-induced cleft lip and other malformations in mice. *Lancet* 1, 606–607. doi: 10.1016/s0140-6736(65)91192-x

Veien, E. S., Grierson, M. J., Saund, R. S., and Dorsky, R. I. (2005). Expression pattern of zebrafish tcf7 suggests unexplored domains of Wnt/beta-catenin activity. *Dev. Dyn.* 233, 233–239. doi: 10.1002/dvdy.20330

Wada, N., Javidan, Y., Nelson, S., Carney, T. J., Kelsh, R. N., and Schilling, T. F. (2005). Hedgehog signaling is required for cranial neural crest morphogenesis and chondrogenesis at the midline in the zebrafish skull. *Development* 132, 3977–3988. doi: 10.1242/dev.01943

Wang, Q., Kurosaka, H., Kikuchi, M., Nakaya, A., Trainor, P. A., and Yamashiro, T. (2019). Perturbed development of cranial neural crest cells in association with reduced sonic hedgehog signaling underlies the pathogenesis of retinoic-acid-induced cleft palate. *Dis. Model Mech.* 12:dmm040279. doi: 10.1242/dmm.040279

Wang, X., Lee, J. E., and Dorsky, R. I. (2009). Identification of Wnt-responsive cells in the zebrafish hypothalamus. *Zebrafish* 6, 49–58. doi: 10.1089/zeb.2008.0570

Wang, X., Moon, J., Dodge, M. E., Pan, X., Zhang, L., Hanson, J. M., et al. (2013). The development of highly potent inhibitors for porcupine. *J. Med. Chem.* 56, 2700–2704.

Wehby, G. L., and Cassell, C. H. (2010). The impact of orofacial clefts on quality of life and healthcare use and costs. *Oral. Dis.* 16, 3–10. doi: 10.1111/j.1601-0825.2009.01588.x

Weinberg, S. M., Cornell, R., and Leslie, E. J. (2018). Craniofacial genetics: where have we been and where are we going? *PLoS Genet.* 14:e1007438. doi: 10.1371/journal.pgen.1007438

Westerfield, M. (2000). *The Zebrafish Book. A Guide for the Laboratory Use of Zebrafish (Danio rerio)*, 4th ed Edn. Eugene: University of Oregon Press.

Wiley, D. S., Redfield, S. E., and Zon, L. I. (2017). Chemical screening in zebrafish for novel biological and therapeutic discovery. *Methods Cell Biol.* 138, 651–679. doi: 10.1016/bs.mcb.2016.10.004

Yamashita, A., Inada, H., Chihara, K., Yamada, T., Deguchi, J., and Funabashi, H. (2014). Improvement of the evaluation method for teratogenicity using zebrafish embryos. *J. Toxicol. Sci.* 39, 453–464. doi: 10.2131/jts.39.453

Zhou, J., Xu, B., Shi, B., Huang, J., He, W., Lu, S., et al. (2011). A metabonomic approach to analyze the dexamethasone-induced cleft palate in mice. *J. Biomed. Biotechnol.* 2011:509043.

Conflict of Interest: All authors are employed by the company Kao Corporation.

frontiers in Cell and Developmental Biology

ORIGINAL RESEARCH
published: 09 February 2021
doi: 10.3389/fcell.2021.621442

A Microphysiological Approach to Evaluate Effectors of Intercellular Hedgehog Signaling in Development

Brian P. Johnson[1,2,3,4*†], *Ross A. Vitek*[1], *Molly M. Morgan*[1], *Dustin M. Fink*[5], *Tyler G. Beames*[4,5], *Peter G. Geiger*[1], *David J. Beebe*[1] *and Robert J. Lipinski*[4,5*]

[1] *Department of Biomedical Engineering, University of Wisconsin, Madison, WI, United States,* [2] *Department of Pharmacology and Toxicology, Michigan State University, East Lansing, MI, United States,* [3] *Department of Biomedical Engineering, Institute for Quantitative Health Science and Engineering, Michigan State University, East Lansing, MI, United States,* [4] *Molecular and Environmental Toxicology Center, University of Wisconsin, Madison, WI, United States,* [5] *Department of Comparative Biosciences, School of Veterinary Medicine, University of Wisconsin, Madison, WI, United States*

OPEN ACCESS

Edited by:
Sebastian Dworkin, La Trobe University, Australia

Reviewed by:
Marko Piirsoo, University of Tartu, Estonia
Gaofeng Xiong, University of Kentucky, United States

***Correspondence:**
Brian P. Johnson
bjohnson@msu.edu
Robert J. Lipinski
robert.lipinski@wisc.edu

†Present address:
Brian P. Johnson, Department of Pharmacology and Toxicology, Department of Biomedical Engineering, Institute for Quantitative Health Science and Engineering, East Lansing, MI, United States

Specialty section:
This article was submitted to Molecular Medicine, a section of the journal Frontiers in Cell and Developmental Biology

Received: *26 October 2020*
Accepted: *08 January 2021*
Published: *09 February 2021*

Citation:
Johnson BP, Vitek RA, Morgan MM, Fink DM, Beames TG, Geiger PG, Beebe DJ and Lipinski RJ (2021) A Microphysiological Approach to Evaluate Effectors of Intercellular Hedgehog Signaling in Development. Front. Cell Dev. Biol. 9:621442. doi: 10.3389/fcell.2021.621442

Paracrine signaling in the tissue microenvironment is a central mediator of morphogenesis, and modeling this dynamic intercellular activity *in vitro* is critical to understanding normal and abnormal development. For example, Sonic Hedgehog (Shh) signaling is a conserved mechanism involved in multiple developmental processes and strongly linked to human birth defects including orofacial clefts of the lip and palate. SHH ligand produced, processed, and secreted from the epithelial ectoderm is shuttled through the extracellular matrix where it binds mesenchymal receptors, establishing a gradient of transcriptional response that drives orofacial morphogenesis. In humans, complex interactions of genetic predispositions and environmental insults acting on diverse molecular targets are thought to underlie orofacial cleft etiology. Consequently, there is a need for tractable *in vitro* approaches that model this complex cellular and environmental interplay and are sensitive to disruption across the multistep signaling cascade. We developed a microplate-based device that supports an epithelium directly overlaid onto an extracellular matrix-embedded mesenchyme, mimicking the basic tissue architecture of developing orofacial tissues. SHH ligand produced from the epithelium generated a gradient of SHH-driven transcription in the adjacent mesenchyme, recapitulating the gradient of pathway activity observed *in vivo*. Shh pathway activation was antagonized by small molecule inhibitors of epithelial secretory, extracellular matrix transport, and mesenchymal sensing targets, supporting the use of this approach in high-content chemical screening of the complete Shh pathway. Together, these findings demonstrate a novel and practical microphysiological model with broad utility for investigating epithelial-mesenchymal interactions and environmental signaling disruptions in development.

Keywords: gene environment interaction, chemical screening, paracrine signaling, cleft lip and palate, embryonic morphogenesis, epithelial mesenchymal cross-talk, 3D extracellular matrix, signaling gradient

INTRODUCTION

Paracrine signaling factors play key roles in embryonic morphogenesis by establishing complex temporospatial gene expression patterns that drive cell differentiation and tissue outgrowth. The temporally dynamic and multicellular nature of developmental paracrine signaling poses challenges to studying this biology both *in vivo* and *in vitro*. Sonic hedgehog (Shh) is a classic example of an intercellular paracrine signaling pathway that is critically important for normal embryonic and fetal development. For example, Shh activity drives orofacial morphogenesis (Lan and Jiang, 2009; Kurosaka, 2015), while targeted pathway disruption results in orofacial clefts (OFCs) of the lip and palate in animal models (Lipinski et al., 2010; Heyne et al., 2015a). Normal development of the upper lip and palate requires the orchestrated proliferation and fusion of embryonic facial growth centers primarily composed of cranial neural crest-derived mesenchyme overlaid by an epithelial layer (Ferguson, 1988; Jiang et al., 2006). This tissue architecture facilitates epithelium-secreted SHH ligand producing a gradient of pathway activation in the cranial neural crest-derived mesenchyme (Lan and Jiang, 2009; Hu et al., 2015; Kurosaka, 2015).

Most birth defects are thought to be caused by interacting genetic and environmental influences (Beames and Lipinski, 2020). Isolated congenital malformations linked to Shh pathway disruption, including OFCs, holoprosencephaly, and hypospadias, are particularly etiologically complex (Murray, 2002; Carmichael et al., 2012; Krauss and Hong, 2016; Beames and Lipinski, 2020). Among the most common human birth defects, OFCs have been studied extensively, though our understanding of causative factors remains inadequate. Efforts to resolve OFC etiology using genetic approaches have identified dozens of associated risk loci (Leslie and Marazita, 2013), but recognized sequence variants are rarely causative. Furthermore, isolated OFC cases generally do not follow Mendelian inheritance patterns, suggesting an important role for environmental influences in OFC susceptibility (Murray, 2002; Roessler et al., 2003; Graham and Shaw, 2005; Juriloff and Harris, 2008; Lidral et al., 2008; Vieira, 2008). Identifying specific environmental factors that disrupt the signaling pathways that drive orofacial morphogenesis and may contribute to OFC risk is a route to prevention strategies and, therefore, an important focus of investigation.

The Shh signaling pathway is inherently sensitive to disruption by environmental chemicals. We have shown that the natural alkaloid cyclopamine inhibits Shh signaling, decreases mesenchymal proliferation, and prevents tissue outgrowth and fusion, leading to cleft lip and/or palate in mouse models (Heyne et al., 2015a; Everson et al., 2017). Numerous other environmental chemicals have been found to disrupt Shh pathway signaling, including cyclopamine-like dietary alkaloids, natural and synthetic pharmaceuticals, and a common pesticide component (Lipinski et al., 2007; Lipinski and Bushman, 2010; Wang et al., 2012; Everson et al., 2019; Rivera-González et al., 2021). Importantly, Shh signaling is sensitive to disruption by a variety of mechanistically distinct chemicals that affect signal transduction at multiple molecular targets within the signaling cascade. These targets range from secretory ligand modification and paracrine shuttling to downstream sensing and transduction events (Jeong and McMahon, 2002; Lauth et al., 2007; Petrova et al., 2013). However, efforts to identify Shh pathway effectors are limited by the simplicity of traditional *in silico* and *in vitro* assays and the time and cost of complex *in vivo* models. An ideal system would replicate key cellular and molecular interactions that, when disrupted, give rise to most isolated birth defects and be amenable to screening-based approaches to test environmentally relevant drug/chemical libraries (Knudsen et al., 2017).

We present a novel microphysiological model (MPM) that recapitulates developmental epithelial-mesenchymal organization and is suited for chemical screening. To model embryonic facial growth processes *in vitro*, a layer of oral epithelium is overlaid on mesenchymal 3-dimensional (3D) microtissues that are supported by an extracellular matrix (ECM). We show that cellular organization and gradients of SHH-driven signaling of orofacial development are recapitulated in this model and that it is well-equipped to screen for chemicals that modulate various distinct targets across the Shh signaling pathway. This microphysiological system provides a novel approach for identifying environmental influences that contribute to OFC susceptibility and a tractable foundation to examine complex gene-environment interaction.

MATERIALS AND METHODS

Chemicals/Reagents

SHH-N peptide (R&D Systems) and SAG (CAS #2095432-58-7, Selleckchem) were used to exogenously induce Shh pathway activity. The potent Smoothened inhibitors cyclopamine (CAS #4449-51-8) and vismodegib (CAS #879085-55-9) were purchased from LC Laboratories. Additional Shh pathway disruptors assessed include U18666A (CAS #3039-71-2, Tocris), RU-SKI 43 (CAS # 1782573-67-4, Tocris), the anti-SHH monoclonal neutralizing 5E1 antibody (Developmental Studies Hybridoma Bank at the University of Iowa), piperonyl butoxide (CAS #51-03-6, Toronto Research Chemicals), and GANT61 (CAS # 500579-04-4, Tocris). The negative control compound benzo[a]pyrene was purchased from Sigma-Aldrich (CAS #50-32-8). All chemicals were dissolved in DMSO or water.

Maintenance and Engineering of Cell Lines

The embryonic murine mesenchymal cell line 3T3 Shh-Light2, human fetal oral epithelial (GMSM-K), and mouse cranial neural crest mesenchymal (O9-1) cell lines (Gilchrist et al., 2000; Taipale et al., 2000; Ishii et al., 2012) were used as indicated. The Shh-Light2 variant of the 3T3 cell line expresses a *Gli*-driven firefly luciferase reporter enabling real-time evaluation of the SHH-pathway activation (Taipale et al., 2000). We also used two types of GMSM-K cell lines: a *SHH*-null variant and a variant that stably overexpresses human full-length *SHH* (Fan et al., 2004). In addition, each cell line was engineered for *in situ* visualization; GMSM-K SHH-null cells express RFP and GMSM-K SHH overexpressing cells express GFP. GMSM-K and O9-1 cells were maintained in DMEM with 10% FBS and 1% penicillin-streptomycin and maintained in an incubator at 37°C and 5%

CO2. 3T3 Shh-Light2 cells were similarly maintained in media containing the selection agents G418 (0.4 mg/mL, Invivogen, San Diego, CA) and zeocin (0.15 mg/mL, Invivogen).

Device Design and Construction

Devices were designed and modeled with computer aided design (CAD) modeling software (Solidworks, Dessault Systems, Vélizy-Villacoublay, France). SprutCAM software was used to generate toolpaths, and devices were CNC milled (Tormach Inc., Waunakee, WI, USA) from clear 96-well non-tissue culture-treated plates (Corning Inc., Corning, NY, USA). After milling, each plate was cleaned by sonication for 15 min in 100% isopropyl alcohol. Milled plates were washed with water, dried with compressed air, then heated to 70°C. While plate devices were heating, 0.19 mm thick polystyrene sheets (Goodfellow, Huntingdon, England) were cut just slightly larger than the milled plate devices, sprayed with 70% ethanol, and rinsed with water. Sheets were dried with compressed air and added to the 70°C hot plate. Once the devices and sheets reached temperature, 35 μL of acetonitrile was added to milled bonding ports in the upper left-hand corner of the device to bond the polystyrene sheet to the milled plate. Excess acetonitrile was aspirated from adjacent corners and channels to avoid plate etching. This process was repeated for each of the three remaining corner holes in the milled plate resulting in a bonded seal completely around the device. Bonded devices were cooled at room temperature. Excess polystyrene was trimmed from the outside of the device using a handheld razor blade to complete device construction. Devices were then treated with UV light for 15 min and transferred to a biosafety hood for cell culture. Device design and construction are illustrated in **Figure 2**.

Seeding of Devices

All experimental cultures were seeded and maintained in DMEM supplemented with 1% FBS and 1% penicillin-streptomycin. In luciferase assays, 2 mM VivoGlo luciferin (Promega, Madison, WI, USA) and 25 mM HEPES were included in the culture media. To improve hyaluronic acid attachment to the device, each device well was filled with 3 μL of polyethyleneimine for 10 min. The wells were then aspirated and filled with 3 μL of glutaraldehyde (GA) for 30 min. Following GA treatment, each device well was washed three times with water. Devices were air dried in a biosafety hood before cells were loaded into device wells. While devices were air drying, hyaluronic acid was prepared according to the manufacturer's protocol. Hystem-C, a hyaluronic acid collagen gel solution (Sigma-Aldrich, St. Louis, MO, USA) was mixed 1:1 with a 100,000 mesenchymal/fibroblast cells/μL solution. The hyaluronic acid:cell solution (1.75–3 uL) was added to each device well; therefore, at most 150,000 cells were seeded per well. Microtissues were allowed to polymerize at room temperature for 45 min, then media was added to the top of cultures. One day after mesenchymal seeding, 10 μL of a 4,000 GMSM-K cells/μL solution was loaded into one or both side channels of the well, and, where indicated, 5 μL of cells were also seeded directly on top of the mesenchymal cells to increase signal for screening. 30 min later, wells and channels of the devices were flushed with media to remove unattached cells. A hydraulic head inducing gravity-driven perfusion of the microtissue was created by adding 100–150 μL media to the center well. Perfused media collected in the half moon reservoirs in the bottom well, which were aspirated each day. Media was changed every 1–2 days, and cultures were dosed daily for 3 days or as indicated after seeding.

Animal Studies

This study was conducted in strict accordance with the recommendations in the Guide for the Care and Use of Laboratory Animals of the National Institutes of Health. The protocol was approved by the University of Wisconsin School of Veterinary Medicine Institutional Animal Care and Use Committee (protocol number G005396). C57BL/6J mice were purchased from The Jackson Laboratory and housed under specific pathogen-free conditions in disposable, ventilated cages (Innovive, San Diego, CA, USA). Rooms were maintained at 22 ± 2°C and 30–70% humidity on a 12-h light, 12-h dark cycle. Mice were fed 2,920× Irradiated Harlan Teklad Global Soy Protein-Free Extruded Rodent Diet (Envigo Teklad Global, Indianapolis, IN, USA) until day of plug, when dams received 2,919 Irradiated Teklad Global 19% Protein Extruded Rodent Diet (Envigo Teklad Global). Mice were set up for timed pregnancies as previously described (Heyne et al., 2015b). Scanning electron microscopy and hematoxylin and eosin (H&E) staining were conducted as previously described (Dunty et al., 2002; Heyne et al., 2015a).

In situ Hybridization (ISH)

ISH analysis was performed as previously described (Heyne et al., 2016) using an established high-throughput technique (Abler et al., 2011). Embryos were processed whole or embedded in 4% agarose gel and cut in 50 μm sections using a vibrating microtome. Embryos were imaged using a MicroPublisher 5.0 camera connected to an Olympus SZX-10 stereomicroscope for whole mount imaging or a Nikon Eclipse E600 microscope for imaging sections. ISH riboprobe primer sequences: *Ptch1*-fwd GACGTGAGGACAGAAGATTG and *Ptch1*-rev + **T7 leader CGATGTTAATACGACTCACTATAGGG**AACTGGGCAGCTATGAAG.

Evaluation of Gli-Driven Luciferase

For *in situ* quantification of SHH-induced luciferase activity, culture media included 2 mM VivoGlo luciferin (Promega), which is an injectable *in vivo*-grade substrate that is cleaved by luciferase, producing a luminescent signal. Persistent exposure showed no adverse cytotoxic effect nor reduced luminescent signal in response to SHH ligand (data not shown). Luminescence was measured prior to dosing, as well as after the dosing period to enable normalization to any baseline differences in luminescence across replicates. Luminescence was quantified on a Chemicdoc luminescent imager (BioRad, Hercules, CA, USA) or Pherastar plate reader (BMG, Offenburg, Germany), and magnified images of the SHH-mediated gene expression gradient were enabled by placing a 2X dissecting microscope lens (Leica, Wetzlar, Germany) in the optical path between the camera and the plate. Quantification was performed in ImageLab (Biorad) or ImageJ implemented through Fiji (Schindelin et al., 2012). Cytotoxicity was assessed via multiple means including

microscopic evaluation of epithelia, recovery of luminescent activity after chemical wash-out, or evaluation of Renilla luciferase activity using a dual-luciferase assay (endpoint only, Promega). Doses that induced cytotoxicity were not included in regression analysis.

Histopathology

Microtissues were fixed in 10% formalin for 24 h and a razor was used to remove the bonded thin polystyrene sheet of each device so that a sharp probe could be used to extract the microtissues. Mouse tissues were dissected and fixed in 10% formalin for 24 h. Samples were embedded in paraffin then sectioned at 5 μm. Tissues were stained with H&E to identify the cytoplasm and nuclei of cells, then imaged.

Statistical Analyses

Quantification of SHH-induced bioluminescent signaling was done in ImageLab software (BioRad Inc). For single comparisons, Student's *t*-test was used to identify significant differences in treatment vs. control ($p < 0.05$). For dose-response experiments, data was background subtracted and normalized to the vehicle control (100% activity). A three-parameter non-linear regression curve-fit was generated in Graphpad Prism to determine antagonism/inhibition and IC50 values were determined for each chemical curve fit. Data are representative of at least two independent experiments.

RESULTS

Design and Engineering of a Microplate-Based Microphysiological Model

We sought to create an *in vitro* platform that recapitulates key aspects of epithelial-mesenchymal interaction in development while remaining suitable for drug/chemical screening. The medial nasal process (MNP) and maxillary process (MXP) that form the upper lip and secondary palate, respectively, share morphology as well as intercellular signaling events that orchestrate their development (**Figure 1**). These structures are composed of a dense 3D cranial neural crest-derived mesenchyme covered by an ectoderm-derived epithelium (Ferguson, 1988; Jiang et al., 2006) (**Figure 1A**). The tissue outgrowth and fusion of these structures is driven by a continuous epithelial-mesenchymal interaction that is essential for the growth and fusion required to close the upper lip and palate. Deficient outgrowth and/or subsequent fusion of these tissues results in orofacial clefts of the lip and/or palate. Coordinated expansion of these facial growth centers is driven in part by a gradient of epithelium-secreted SHH ligand that induces pathway activation and drives proliferation in the proximal mesenchyme through *Gli*-driven gene transcription (Lan and Jiang, 2009; Hu et al., 2015; Kurosaka, 2015). Both the tissue architecture and epithelial-mesenchymal signaling informed the development of a microtissue design consisting of a dense 3D mesenchyme with an epithelial layer perpendicular to the imaging plane to study epithelial-mesenchymal interactions (depicted in **Figure 1B**).

Development of Microtissues That Recapitulate Orofacial Organization in a Throughput-Compatible Format

To create biomimetic microtissues in a format that is compatible with drug/chemical screening we designed devices using microfluidic principles and manufactured the devices using CNC micromilling of microtiter plates. Devices were milled directly into polystyrene cell culture plates (20 devices/plate) to maintain throughput compatibility, and a thin sheet (190 um) of optically clear polystyrene was bonded to the bottom of the plate to seal the culture chambers (**Figure 2A**). The devices are manufactured solely from polystyrene to avoid pitfalls of using polydimethylsiloxane (PDMS), which is a common material used for organotypic models and has been previously shown to sequester hydrophobic molecules including many drugs/chemicals (Regehr et al., 2009; Guckenberger et al., 2015). Device design includes a central chamber (**Figure 2B**, left) that is loaded with a hydrogel-ECM/mesenchymal cell suspension to form the body of the microtissue. Surface tension causes the matrix to pin at 200 μm tall × 1 mm wide openings in the bottom of the chamber (phase barrier) instead of flowing out into adjacent flanking microchannels (**Figure 2B**, center). The matrix, once polymerized, forms a portion of the wall of the flanking microchannel. Epithelial cells suspended in media are pipetted into the flanking channels. Laminar flow, with a high linear flow rate through the center of the channel and a low linear flow rate at the edges of the channel, leaves cells coating the matrix while cells remaining in the center of the channel are removed via flow (**Figure 2B**, right). The resulting microtissue consists of a 3D mesenchymal matrix overlaid with epithelial cells perpendicular to the imaging plane. A culture method was developed through many iterations, which resulted in a method whereby a biomimetic mesenchyme was generated by embedding 50,000 cells/μL murine embryonic fibroblast cells (O9-1 or 3T3) in a hyaluronic acid/collagen gel. Hyaluronic acid was used as the microtissue matrix due to its importance in the developing palate (Ferguson, 1988). The microtissues were then overlaid with GMSM-K oral epithelial cells through flanking microchannels to coat the side of the microtissue. To evaluate if the microtissues appear phenotypically similar to the developing orofacial processes *in vivo*, we compared microtissues to the developing lip and palate of embryonic mice at gestational days 11 and 14, respectively. The H&E stains of the murine medial nasal and maxillary processes (**Figure 2C**, left, center respectively) and the organotypic microtissues (**Figure 2C**, right) appeared morphologically similar, where the dense mesenchyme was overlaid with epithelium.

SHH-Induced Gli-Luciferase Enables Exogenous or Endogenous Real-Time *in situ* Quantification

Shh signaling drives the cell proliferation and tissue outgrowth that are critical for orofacial development (Yamada et al., 2005; Kurosaka, 2015; Everson et al., 2017). To enable the real-time evaluation of SHH-driven gene activation, we used a variant

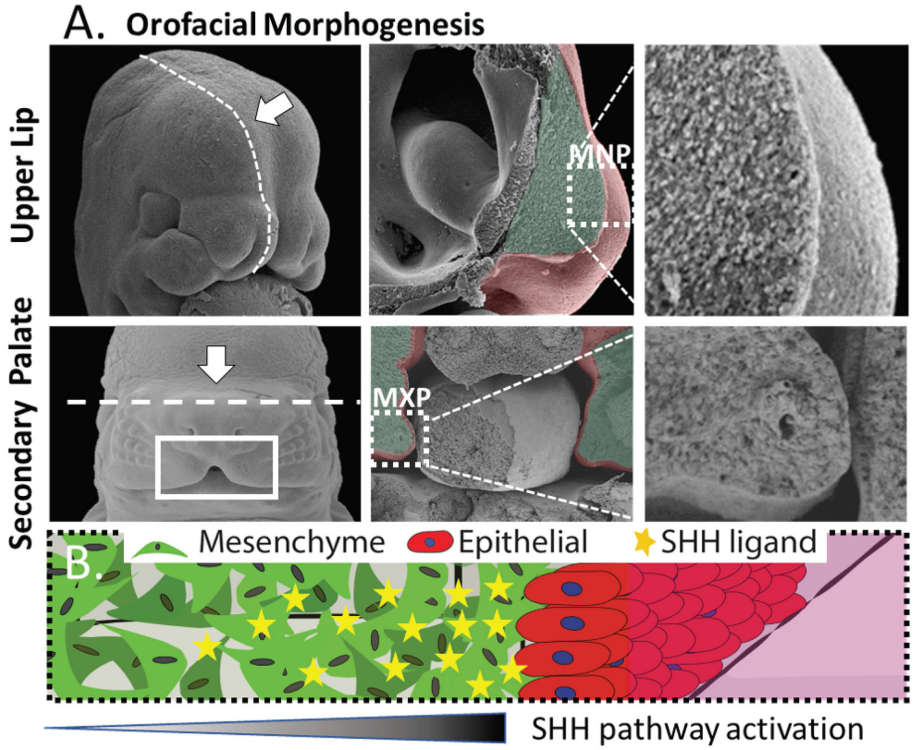

FIGURE 1 | Morphogenesis of the orofacial processes. **(A)** Formation of the upper lip (upper panels) and secondary palate (lower panels) occurs through outgrowth and fusion of embryonic growth centers including the medial nasal process (MNP) and maxillary process (MXP). These tissues consist of a dense 3D mesenchyme covered with ectodermal epithelium. **(B)** Generalized epithelial-mesenchymal tissue architecture of the orofacial processes with high proximal SHH-induced activation.

of the 3T3 cell line that produces a luminescent signal upon Shh pathway activation. By incorporating a live cell-compatible luciferase substrate into the media, we sought to test if SHH-driven Gli transcriptional activity could be identified from both exogenously added and endogenously secreted SHH ligand *in situ* (**Figure 3A**). To incorporate endogenous SHH signaling into the microtissues, we applied a variant of the human fetal oral epithelial GMSM-K cells that stably overexpress GFP and SHH (GMSM-K GFP SHH+ cells). The matrix-embedded 3T3 cells were cultured adjacent to GMSM-K GFP SHH+ cells or RFP-overexpressing GMSM-K cells that are SHH- (GMSM-K RFP cells), then exposed to a vehicle control or 0.8 μg/mL of exogenous SHH. After 72 h, microtissues were evaluated for luminescence. 3T3 cells co-cultured with GMSM-K GFP SHH+ cells exhibited a 19-fold higher ($p < 0.05$, Student's *t*-test) signal of *Gli*-driven luciferase compared to 3T3 cells co-cultured with GMSM-K RFP cells. When the GMSM-K GFP SHH+ co-cultures were exposed to exogenous SHH, there was no significant change in *Gli*-driven luciferase activity. In contrast, the GMSM-K RFP co-cultures exhibited a 14-fold higher ($p < 0.05$, Student's *t*-test) signal of *Gli*-driven luciferase when exposed to exogenous SHH (**Figures 3B,C**). To test dose-responsiveness of the reporter activity, microtissues were exposed to four concentrations of exogenous SHH which produced a concentration-dependent increase in *Gli*-driven luciferase (EC50 = 0.4 μg/mL, non-linear regression curve fit- three parameter) (**Figure 3D**, left panel). Next, microtissues were exposed to the synthetic Smoothened agonist, SAG, which also showed a concentration-dependent increase in luminescence (EC50 = 178nM, on-linear regression curve fit- three parameter) (**Figure 3D**, right panel).

SHH Ligand From the Epithelium Stimulates a Gradient of Pathway Activation in the Mesenchyme

Formation of a gradient of Shh pathway activity is involved in the morphogenesis of many tissues, including the upper lip and palate (Lan and Jiang, 2009; Kurosaka, 2015; Everson et al., 2017) and limbs (Li et al., 2006). To test whether SHH gradients observed during orofacial morphogenesis *in vivo* are recapitulated *in vitro,* microtissues were generated with non-SHH-expressing GMSM-K RFP cells or SHH-expressing GMSM-K GFP SHH+ cells overlaid on one edge of the mesenchyme (one flanking channel) for 48 h (**Figure 4A**). A merged brightfield and fluorescent image of the microtissues is shown in **Figure 4B** indicating RFP and GFP expression in the epithelia. Microtissues were then evaluated for *Gli*-driven luciferase using a luminescence imager and showed a gradient of luciferase activity in the mesenchyme with higher activity proximal to the epithelium (**Figure 4B**). To better compare *in vitro* to *in vivo* gradients, we sought to improve resolution of

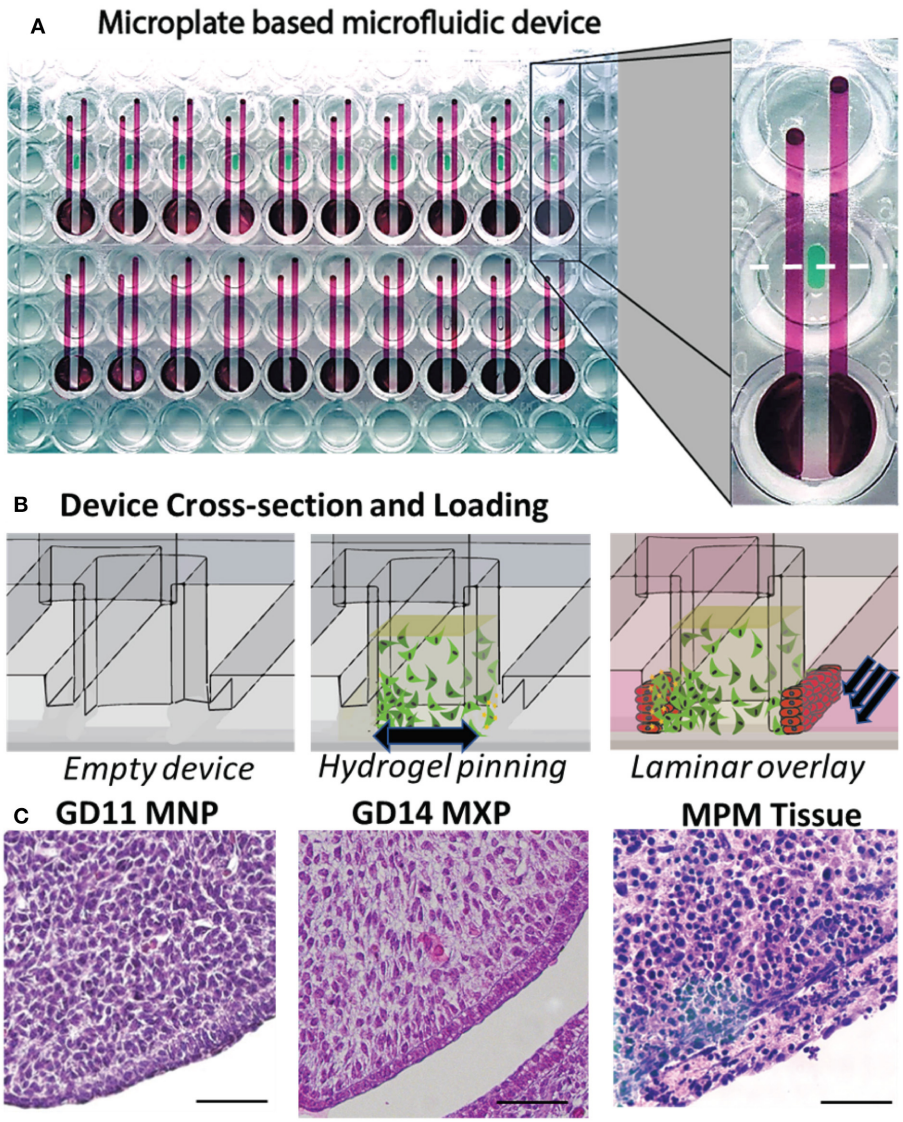

FIGURE 2 | Development of a microplate-based microphysiological culture model. **(A)** Devices incorporate 3 wells of a 96-well plate, where the top and bottom wells are connected through two subsurface microchannels (red) which flank a microtissue well (green) milled into the center well. An array of 20 devices is CNC milled into each plate (bottom view). **(B)** Cross-sectional view of microtissue formation including the empty microtissue well (left panel), addition of the mesenchymal/ECM matrix (center panel), and epithelial overlay (right panel). **(C)** H&E stained formalin-fixed, paraffin-embedded sections of the mouse MNP (left panel) and MXP (center), and O9-1 mesenchymal/GMSM-K epithelial microtissue (right panel), scale bar = 50μm.

the luminescent imaging. In a separate experiment, additional optics were added to the light path in the luminescent imager. Using landmarks of the microfluidic device captured by both the luminescent imager and the microscope, we were able to overlay these images at higher resolution for comparison (**Figure 4C**, right). A photomicrograph of *in situ* hybridization of the SHH-responsive gene *Ptch1* in the MNP of a GD10.25 mouse embryo is provided as an *in vivo* reference (**Figure 4C**, left). Similar to previous studies (Everson et al., 2017), there was a gradient of SHH-responsive gene expression in the mesenchyme that decreased as distance from the epithelium increased (**Figure 4C**).

Sensitivity to Chemical Disruption Across the Shh Signaling Cascade

To test the utility of the platform for screening drug or chemical modulators of the complete Shh signaling cascade, microtissues were exposed to various small molecule inhibitors that target distinct aspects of Shh signal transduction, including epithelial secretion processes (cholesterol modification and palmitoylation), ligand bioavailability, and mesenchymal signal transduction (Smoothened, Gli proteins). **Figure 5A** illustrates the target of each inhibitor. After 3 days of exposure, cultures were evaluated for luminescence (**Figure 5B**). Cytotoxicity,

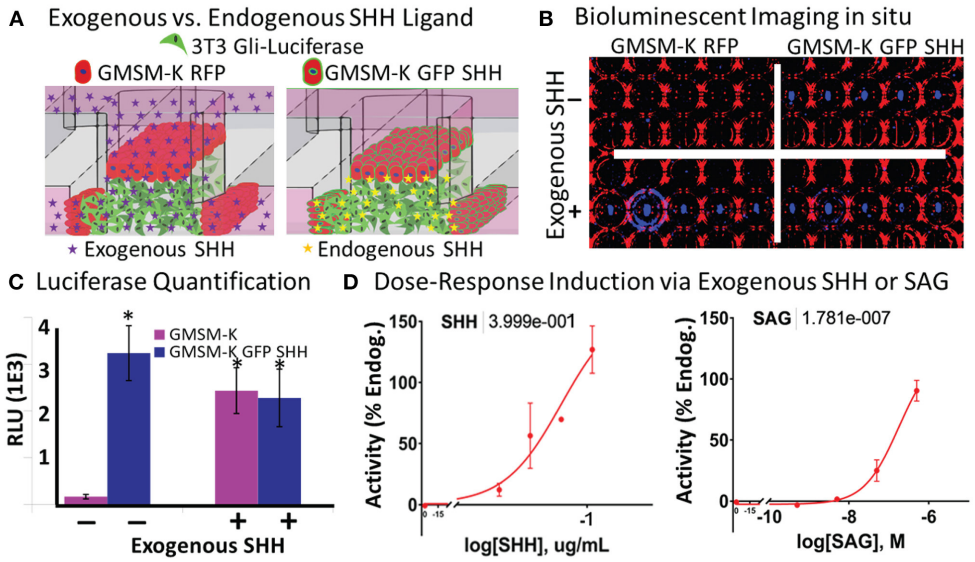

FIGURE 3 | Vital *in situ* quantification of endogenous and exogenous SHH ligand-induced pathway activity. **(A)** Experimental schematic shows incorporation of non-SHH-secreting and SHH-secreting epithelia and exogenously or endogenously derived SHH ligand. **(B)** Brightfield (red) and darkfield (blue) image of bioluminescent signal under different experimental conditions in a single plate. **(C)** Quantification of bioluminescent signal in **(B)** (*$p < 0.05$ vs. GMSM-K without exogenous SHH, Student's *t*-test). **(D)** Dose-response quantification of exogenously added SHH ligand (left) and SAG (right). Non-linear regression curve fit (Graphpad Prism). EC50 values shown above.

monitored by loss of fluorescent signal, washout and luminescent signal recovery, or a lytic cytotoxicity assay, was assessed after dosing, and data from cytotoxic doses were not included in analysis. Inhibitors of SHH posttranslational modification in epithelia affecting SHH secretion include cholesterol (U1886A) and palmitoylation (Ruski-43) inhibitors, which showed IC50 values at 10.1 μM and 11.2 μM, respectively. Importantly, these inhibitors do not exhibit inhibition in a standard 2-dimensional (2D) monoculture assay of 3T3-Gli Luc cells exposed exogenously to SHH ligand (**Supplementary Figure 1**). The anti-SHH monoclonal 5E1 antibody, which binds and neutralizes secreted SHH ligand, also inhibited *Gli*-driven luciferase signaling in the microtissues with an IC50 of 4.9 μM. Reception of SHH ligand and the subsequent signaling cascade that results in Gli activation in mesenchymal cells can also be inhibited by structurally diverse ligands at multiple molecular targets. The Smoothened antagonists piperonyl butoxide, cyclopamine, and vismodegib inhibited luciferase activity with IC50 values of 219, 195, and 12.5 nM, respectively (non-linear regression curve fit- three parameter). The Gli inhibitor GANT61 also inhibited *Gli*-driven luciferase in a dose-dependent manner with an IC50 value of 23.6 μM (non-linear regression curve fit- three parameter). The chemical benzo[a]pyrene, which can induce cleft palate in rodents through a mechanism independent of Shh signaling, showed no concentration-dependent inhibitory activity. As expected, inhibitors of intracellular Shh signal transduction did exhibit inhibition in a standard 2D monoculture assay of 3T3-Gli Luc cells with IC50 values at or above those seen in the microtissues (non-linear regression curve fit- three parameter) (**Supplementary Figure 1**).

DISCUSSION

Here we describe a novel microphysiological culture system that recapitulates key cellular and molecular aspects of developmental Shh paracrine signaling and demonstrate its utility for examining chemical influences that may contribute to birth defects. This elegantly simple microphysiological system mimics both the 3D epithelial-mesenchymal interactions and critical molecular processes of Shh pathway-driven orofacial development, including formation of an *in vivo*-like gradient of pathway activity. Application of a battery of mechanistically diverse chemical inhibitors further demonstrated the sensitivity of the MPM to Shh pathway effectors exhibiting distinct mechanistic targets throughout the inter- and intracellular signal transduction cascade. These observations underscore several important elements of both the developmental fidelity and investigative utility of this microphysiological approach to modeling paracrine signaling in development.

In vitro models are often used to elucidate transduction mechanisms and identify xenobiotic pathway modulators, although common culture systems typically fail to recapitulate the complex intercellular signaling pathways that produce morphogen gradients and involve crosstalk between different cell types (Li et al., 2018). Orofacial morphogenesis requires paracrine signaling involving epithelial secretion of SHH

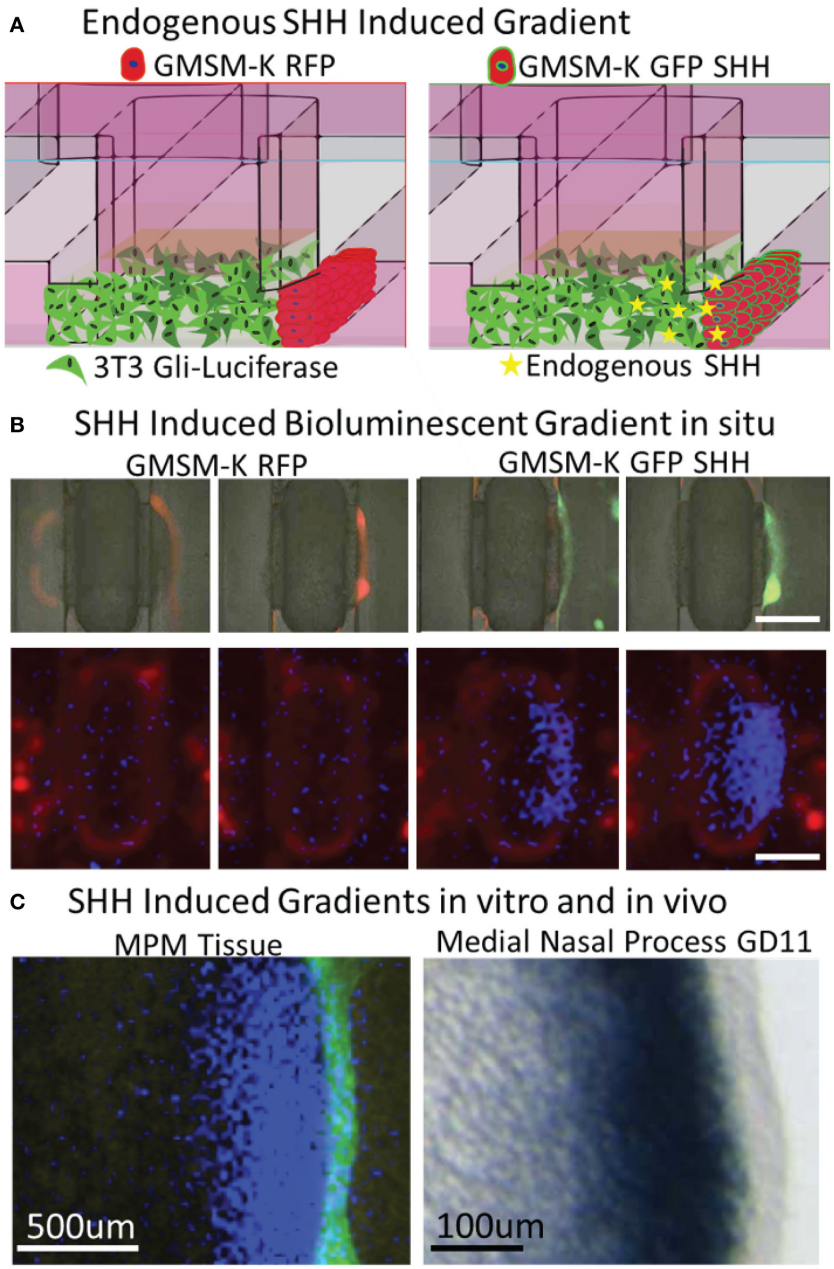

FIGURE 4 | Vital epithelial-mesenchymal SHH gradient *in situ*. **(A)** Experimental schematic shows incorporation of non-SHH-secreting and SHH-secreting epithelia and endogenously produced SHH ligand. **(B)** Brightfield (greyscale) and fluorescent red (530/560 nm) and green (488/515 nm) images indicating GMSM-K overlayed epithelia (upper panels) and bioluminescent signal shows high activity proximal only to SHH secreting epithelia (lower panels), scale bar = 1mm. **(C)** Fluorescent and bioluminescent images taken at higher magnification were integrated to better illustrate gradient (left panel) and compared to ISH staining of SHH-responsive *Ptch1* gene in the medial nasal process of a GD10.25 mouse embryo. Scale bars in luminescent (left) and ISH image (right) are 500 and 100 μm, respectively.

ligand and transport through a 3D matrix of SHH-sensing mesenchyme (Lan and Jiang, 2009; Kurosaka, 2015), a paradigm observed in many developmental contexts. 2D cultures can be designed to incorporate a localized population of SHH producers, but the distribution of secreted ligand has been shown to differ between 2D and 3D cultures (Cederquist et al., 2019). The microphysiological approach described here achieves increased cellular complexity by incorporating epithelium and mesenchyme that are predictably engineered in direct contact facilitating analysis. Biologically active SHH ligand secreted from the epithelium induced pathway activity in the adjacent mesenchyme with maximal induction of downstream Shh target genes occurring nearest the epithelial signaling source, mimicking *in vivo* gene expression gradients. Thus, this MPM,

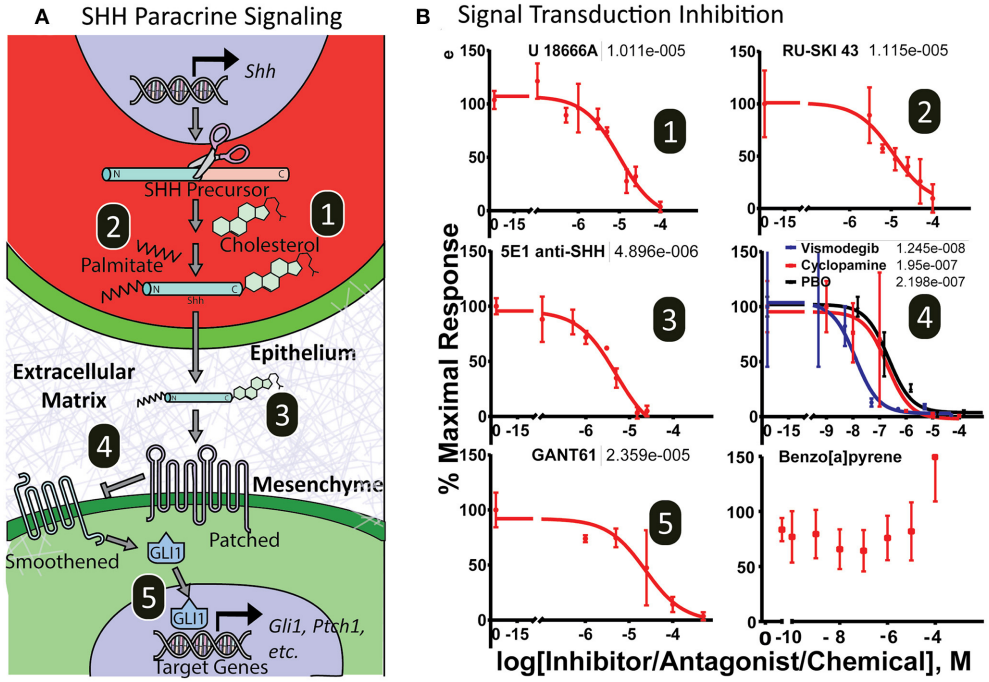

FIGURE 5 | Dose-response curves of SHH pathway inhibitors. **(A)** Illustration of the Sonic hedgehog inter- and intracellular transduction pathway with important molecular targets numbered. **(B)** Microtissues show dose-response inhibition of endogenously derived SHH-induced pathway activity by xenobiotics targeting epithelial secretory SHH ligand cholesterol modification (1) and SHH palmitoylation modification (2); extracellular SHH ligand trafficking (3); and mesenchymal receptor SHH sensing and signal transduction by Patched/Smoothened (4) and Gli-driven transcription (5). The chemical 3-benzo[a]pyrene did not antagonize the pathway. Non-linear regression curve fit (Graphpad Prism). EC50 values shown above.

along with other recently developed 3D *in vitro* organoid models (Cederquist et al., 2019), may aid in our understanding of how concentration gradients are formed and, more specifically, address persistent questions of how secreted SHH ligand is shuttled through extracellular spaces while remaining available to bind transmembrane receptors to initiate signal transduction (Wierbowski et al., 2020). A novel organoid model consisting of human progenitor/stem cells designed to model disruption of palatal fusion, which occurs later in development was also described recently (Belair et al., 2017). Predictably, a follow-up screen did not detect any effects of the SHH antagonist vismodegib on the viability or fusion of their organoid model (Belair et al., 2018). These models can therefore be viewed as complementary and could be employed in parallel to screen for chemical disruption over a greater range of orofacial development.

The Shh pathway illustrates the importance of designing *in vitro* models that recapitulate the complexity of the inter- and intracellular signaling cascades, rather than just a single point of sensitivity. While Smoothened has been given much attention as a molecular target, the Shh pathway is sensitive to small molecule modulation at several steps. For example, distal cholesterol synthesis inhibitors cause palate and limb malformations consistent with Shh pathway disruption (Chevy et al., 2002), but can fail to impact Shh signaling in simpler *in vitro* cultures (**Supplementary Figure 1**). Traditional *in vitro* assays examining Shh pathway activity may involve exogenous treatment of a 2D cell monolayer with pre-modified SHH ligand or cells modified to constitutively drive downstream pathway activation (e.g., *Ptch1* knockout or *Gli* overexpression) (Chen et al., 2002; Lipinski and Bushman, 2010), entirely circumventing upstream intercellular signaling events, such as the modification of SHH ligand by cholesterol. Here, application of mechanistically distinct antagonists demonstrated that Shh signaling in the MPM is sensitive to disruption at multiple points in the inter- and intracellular signaling cascade. Shh pathway activity was potently inhibited by blocking cholesterol trafficking (U18666A), SHH palmitoylation (RU-SKI), receptor binding by inactivating secreted SHH ligand (5E1), inhibiting Smoothened (vismodegib, cyclopamine, piperonyl butoxide), and targeting Gli activation (GANT61). Because our engineered approach to *SHH* expression bypasses endogenous *SHH* transcriptional regulators, this approach is unlikely to capture influences that act further upstream, such as those that have been hypothesized for fetal alcohol exposure (Ahlgren et al., 2002; Hong et al., 2020). However, these results demonstrate that the MPM approach described here offers broader sensitivity to mechanistically distinct pathway effectors than typical *in vitro* approaches.

We sought with this MPM to address a significant limitation of microfluidic devices: technical complexity. Even with the appropriate expertise, the technical aspects of advanced systems can contribute to variability between users or prevent widespread dissemination and use (Paguirigan and Beebe, 2008). Machining devices directly into microplates enabled rapid prototyping

based on operational feedback and provided a familiar user format without introducing new materials into the experiment. Operationally, engineering devices that leverage the physical properties of fluids at the microscale enabled the simple creation of a microtissue ideally suited to quantify the biology of interest without greatly increasing the expertise required for use. Employing a hydraulic head to facilitate perfusion rather than a mechanical pump allowed us to retain a throughput-compatible format, which is a key advantage for conducting chemical screens, and incorporation of live-cell endpoints greatly reduced handling time and enabled us to monitor activity without sacrificing the culture. Furthermore, the use of polystyrene rather than polydimethylsiloxane (PDMS), a common component of microfluidic devices that sequesters hydrophobic molecules (Regehr et al., 2009), makes this device appropriate for screening a diverse set of compounds.

The operational simplicity of this microphysiological device should enable ready use by other groups for a variety of biological applications in toxicology, pharmacology, and regenerative medicine. The MPM's design affords substantial flexibility and even a "plug and play" paradigm with respect to cells and ECMs, allowing it to model specific developmental environments. For example, although we specifically modeled epithelial-mesenchymal Shh signaling in this study, an iteration of this device was recently used instead to model neurovascular development (Kaushik et al., 2020). Particular attention may be given to Shh-associated congenital malformations, including OFCs, holoprosencephaly, and hypospadias, that are often etiologically complex and difficult to model in *in vitro* systems (Murray, 2002; Carmichael et al., 2012; Krauss and Hong, 2016; Beames and Lipinski, 2020). Full integration of gene-editing techniques such as CRISPR into the MPM could open the door to studying these complex etiologies in a biologically faithful system and even allow for "personalized toxicology" by providing a platform to identify environmental factors that preferentially interact with personal/familial mutations. Another emerging strategy for toxicity testing utilizes *in silico* models built from data collected from *in vitro* and *in vivo* models to predict adverse effects associated with toxicant exposures. A computational model to predict the effects of chemicals on the growth and fusion of the palate was recently reported (Hutson et al., 2017), and informing the development and refinement of *in silico* models and conducting secondary screening of molecules identified by *in silico* screening is another logical niche for MPMs like the one described herein.

The development of model systems that are physiologically relevant but also amenable to mechanistic studies and chemical screening is needed to bridge the gap between existing *in vitro* and *in vivo* models (Beames and Lipinski, 2020). Addressing this need, we present the engineering, construction, and implementation of a novel microphysiological culture model of epithelial-mesenchymal interactions as applied to the Shh signaling pathway. We show that embryonic facial growth processes can be biomimetically modeled *in vitro* by culturing an oral ectodermal monolayer over 3D-embedded mesenchymal cells and that the microtissues and expression patterns phenotypically resemble orofacial morphogenesis. The simplicity of this device makes it adaptable with respect to cell types, pathways, and endpoints of interest. The microplate design also makes this platform amenable to throughput screening, while recent advances in gene-editing technology open the door to its use in investigating gene-environment interactions. Leveraging the physiological relevance and high tractability of this approach illustrate its potential value, particularly for investigating biologically and etiologically complex outcomes including human birth defects like orofacial clefts.

DATA AVAILABILITY STATEMENT

The original contributions presented in the study are included in the article/**Supplementary Material**, further inquiries can be directed to the corresponding author.

ETHICS STATEMENT

The animal study was reviewed and approved by University of Wisconsin School of Veterinary Medicine Institutional Animal Care and Use Committee.

AUTHOR CONTRIBUTIONS

BJ devised the device design and construction. BJ, RV, and RL planned the experiments. BJ, RV, and PG conducted the experiments. DF prepared specialized cells/reagents. BJ, RV, MM, TB, and RL wrote the manuscript. BJ and MM drew the figures. DB and RL supervised the research and helped develop the idea. All authors contributed to the article and approved the submitted version.

FUNDING

Research reported in this publication was supported by the National Institute of Environmental Health Sciences of the National Institutes of Health under award numbers K99ES028744, R01ES026819, and T32ES007015, EPA Science to Achieve Results (STAR) grant number 83573701, and the University of Wisconsin Carbone Cancer Center Support Grant P30 CA014520.

SUPPLEMENTARY MATERIAL

The Supplementary Material for this article can be found online at: https://www.frontiersin.org/articles/10.3389/fcell.2021.621442/full#supplementary-material

REFERENCES

Abler, L. L., Mehta, V., Keil, K. P., Joshi, P. S., Flucus, C. L., Hardin, H. A., et al. (2011). A high throughput in situ hybridization method to characterize mRNA expression patterns in the fetal mouse lower urogenital tract. *J. Vis. Exp*. 19:2912. doi: 10.3791/2912

Ahlgren, S. C., Thakur, V., and Bronner-Fraser, M. (2002). Sonic hedgehog rescues cranial neural crest from cell death induced by ethanol exposure. *Proc. Natl. Acad. Sci. U. S. A*. 99, 10476–10481. doi: 10.1073/pnas.162356199

Beames, T. G., and Lipinski, R. J. (2020). Gene-environment interactions: aligning birth defects research with complex etiology. *Development* 147:dev191064. doi: 10.1242/dev.191064

Belair, D. G., Wolf, C. J., Moorefield, S. D., Wood, C., Becker, C., and Abbott, B. D. (2018). A Three-dimensional organoid culture model to assess the influence of chemicals on morphogenetic fusion. *Toxicol. Sci*. 166, 394–408. doi: 10.1093/toxsci/kfy207

Belair, D. G., Wolf, C. J., Wood, C., Ren, H., Grindstaff, R., Padgett, W., et al. (2017). Engineering human cell spheroids to model embryonic tissue fusion *in vitro*. *PLoS ONE* 12:e0184155. doi: 10.1371/journal.pone.0184155

Carmichael, S. L., Shaw, G. M., and Lammer, E. J. (2012). Environmental and genetic contributors to hypospadias: a review of the epidemiologic evidence. *Birth Defects Res. Part A Clin. Mol. Teratol*. 94, 499–510. doi: 10.1002/bdra.23021

Cederquist, G. Y., Asciolla, J. J., Tchieu, J., Walsh, R. M., Cornacchia, D., Resh, M. D., et al. (2019). Specification of positional identity in forebrain organoids. *Nat. Biotechnol*. 37, 436–444. doi: 10.1038/s41587-019-0085-3

Chen, J. K., Taipale, J., Young, K. E., Maiti, T., and Beachy, P. A. (2002). Small molecule modulation of Smoothened activity. *Proc. Natl. Acad. Sci. U. S. A*. 99, 14071–14076. doi: 10.1073/pnas.182542899

Chevy, F., Illien, F., Wolf, C., and Roux, C. (2002). Limb malformations of rat fetuses exposed to a distal inhibitor of cholesterol biosynthesis. *J. Lipid Res*. 43, 1192–1200. doi: 10.1194/jlr.M200082-JLR200

Dunty, W. C. Jr., Zucker, R. M., and Sulik, K. K. (2002). Hindbrain and cranial nerve dysmorphogenesis result from acute maternal ethanol administration. *Dev. Neurosci*. 24, 328–342. doi: 10.1159/000066748

Everson, J. L., Fink, D. M., Yoon, J. W., Leslie, E. J., Kietzman, H. W., Ansen-Wilson, L. J., et al. (2017). Sonic hedgehog regulation of Foxf2 promotes cranial neural crest mesenchyme proliferation and is disrupted in cleft lip morphogenesis. *Development* 144, 2082–2091. doi: 10.1242/dev.149930

Everson, J. L., Sun, M. R., Fink, D. M., Heyne, G. W., Melberg, C. G., Nelson, K. F., et al. (2019). Developmental toxicity assessment of piperonyl butoxide exposure targeting sonic hedgehog signaling and forebrain and face morphogenesis in the mouse: an *in vitro* and *in vivo* study. *Environ. Health Perspect*. 127:107006. doi: 10.1289/EHP5260

Fan, L., Pepicelli, C. V., Dibble, C. C., Catbagan, W., Zarycki, J. L., Laciak, R., et al. (2004). Hedgehog signaling promotes prostate xenograft tumor growth. *Endocrinology* 145, 3961–3970. doi: 10.1210/en.2004-0079

Ferguson, M. W. (1988). Palate development. *Development* 103, 41–60.

Gilchrist, E. P., Moyer, M. P., Shillitoe, E. J., Clare, N., and Murrah, V. A. (2000). Establishment of a human polyclonal oral epithelial cell line. *Oral Surg. Oral Med. Oral Pathol. Oral Radiol. Endod*. 90, 340–347. doi: 10.1067/moe.2000.107360

Graham, J. M. Jr., and Shaw, G. M. (2005). Gene-environment interactions in rare diseases that include common birth defects. *Birth Defects Res. Part A Clin. Mol. Teratol*. 73, 865–867. doi: 10.1002/bdra.20193

Guckenberger, D. J., de Groot, T. E., Wan, A. M., Beebe, D. J., and Young, E. W. K. (2015). Micromilling: a method for ultra-rapid prototyping of plastic microfluidic devices. *Lab Chip* 15, 2364–2378. doi: 10.1039/C5LC00234F

Heyne, G. W., Everson, J. L., Ansen-Wilson, L. J., Melberg, C. G., Fink, D. M., Parins, K. F., et al. (2016). Gli2 gene-environment interactions contribute to the etiological complexity of holoprosencephaly: evidence from a mouse model. *Dis. Model. Mech*. 9, 1307–1315. doi: 10.1242/dmm.026328

Heyne, G. W., Melberg, C. G., Doroodchi, P., Parins, K. F., Kietzman, H. W., Everson, J. L., et al. (2015a). Definition of critical periods for Hedgehog pathway antagonist-induced holoprosencephaly, cleft lip, and cleft palate. *PLoS ONE* 10:e0120517. doi: 10.1371/journal.pone.0120517

Heyne, G. W., Plisch, E. H., Melberg, C. G., Sandgren, E. P., Peter, J. A., and Lipinski, R. J. (2015b). A simple and reliable method for early pregnancy detection in inbred mice. *J. Am. Assoc. Lab. Anim. Sci*. 54, 368–371.

Hong, M., Christ, A., Christa, A., Willnow, T. E., and Krauss, R. S. (2020). Mutation and fetal alcohol converge on Nodal signaling in a mouse model of holoprosencephaly. *Elife* 9: e60351. doi: 10.7554/eLife.60351.sa2

Hu, D., Young, N. M., Li, X., Xu, Y., Hallgrímsson, B., and Marcucio, R. S. (2015). A dynamic Shh expression pattern, regulated by SHH and BMP signaling, coordinates fusion of primordia in the amniote face. *Development* 142, 567–574. doi: 10.1242/dev.114835

Hutson, M. S., Leung, M. C. K., Baker, N. C., Spencer, R. M., and Knudsen, T. B. (2017). Computational model of secondary palate fusion and disruption. *Chem. Res. Toxicol*. 30, 965–979. doi: 10.1021/acs.chemrestox.6b00350

Ishii, M., Arias, A. C., Liu, L., Chen, Y. B., Bronner, M. E., and Maxson, R. E. (2012). A stable cranial neural crest cell line from mouse. *Stem Cells Dev*. 21, 3069–3080. doi: 10.1089/scd.2012.0155

Jeong, J., and McMahon, A. P. (2002). Cholesterol modification of Hedgehog family proteins. *J. Clin. Invest*. 110, 591–596. doi: 10.1172/JCI0216506

Jiang, R., Bush, J. O., and Lidral, A. C. (2006). Development of the upper lip: morphogenetic and molecular mechanisms. *Dev. Dyn*. 235, 1152–1166. doi: 10.1002/dvdy.20646

Juriloff, D. M., and Harris, M. J. (2008). Mouse genetic models of cleft lip with or without cleft palate. *Birth Defects Res. Part A Clin. Mol. Teratol*. 82, 63–77. doi: 10.1002/bdra.20430

Kaushik, G., Gupta, K., Harms, V., Torr, E., Evans, J., Johnson, H. J., et al. (2020). Engineered perineural vascular plexus for modeling developmental toxicity. *Adv. Healthc. Mater*. 9:e2000825. doi: 10.1002/adhm.202000825

Knudsen, T., Klieforth, B., and Slikker, W. (2017). Programming microphysiological systems for children's health protection. *Exp. Biol. Med*. 242, 1586–1592. doi: 10.1177/1535370217717697

Krauss, R. S., and Hong, M. (2016). Gene–environment interactions and the etiology of birth defects. *Curr. Top. Dev. Biol*. 116, 569–580. doi: 10.1016/bs.ctdb.2015.12.010

Kurosaka, H. (2015). The Roles of Hedgehog signaling in upper lip formation. *Biomed Res. Int*. 2015:901041. doi: 10.1155/2015/901041

Lan, Y., and Jiang, R. (2009). Sonic hedgehog signaling regulates reciprocal epithelial-mesenchymal interactions controlling palatal outgrowth. *Development* 136, 1387–1396. doi: 10.1242/dev.028167

Lauth, M., Bergström, A., Shimokawa, T., and Toftgård, R. (2007). Inhibition of GLI-mediated transcription and tumor cell growth by small-molecule antagonists. *Proc. Natl. Acad. Sci. U.S.A*. 104, 8455–8460. doi: 10.1073/pnas.0609699104

Leslie, E. J., and Marazita, M. L. (2013). Genetics of cleft lip and cleft palate. *Am. J. Med. Genet. C Semin. Med. Genet*. 163C, 246–258. doi: 10.1002/ajmg.c.31381

Li, P., Markson, J. S., Wang, S., Chen, S., Vachharajani, V., and Elowitz, M. B. (2018). Morphogen gradient reconstitution reveals Hedgehog pathway design principles. *Science* 360, 543–548. doi: 10.1126/science.aao0645

Li, Y., Zhang, H., Litingtung, Y., and Chiang, C. (2006). Cholesterol modification restricts the spread of Shh gradient in the limb bud. *Proc. Natl. Acad. Sci. U. S. A*. 103, 6548–6553. doi: 10.1073/pnas.0600124103

Lidral, A. C., Moreno, L. M., and Bullard, S. A. (2008). Genetic factors and orofacial clefting. *Semin. Orthod*. 14, 103–114. doi: 10.1053/j.sodo.2008.02.002

Lipinski, R. J., and Bushman, W. (2010). Identification of Hedgehog signaling inhibitors with relevant human exposure by small molecule screening. *Toxicol. In Vitro* 24, 1404–1409. doi: 10.1016/j.tiv.2010.04.011

Lipinski, R. J., Dengler, E., Kiehn, M., Peterson, R. E., and Bushman, W. (2007). Identification and characterization of several dietary alkaloids as weak inhibitors of hedgehog signaling. *Toxicol. Sci*. 100, 456–463. doi: 10.1093/toxsci/kfm222

Lipinski, R. J., Song, C., Sulik, K. K., Everson, J. L., Gipp, J. J., Yan, D., et al. (2010). Cleft lip and palate results from Hedgehog signaling antagonism in the mouse: phenotypic characterization and clinical implications. *Birth Defects Res. Part A Clin. Mol. Teratol*. 88, 232–240. doi: 10.1002/bdra.20656

Murray, J. C. (2002). Gene/environment causes of cleft lip and/or palate. *Clin. Genet*. 61, 248–256. doi: 10.1034/j.1399-0004.2002.610402.x

Paguirigan, A. L., and Beebe, D. J. (2008). Microfluidics meet cell biology: bridging the gap by validation and application of microscale techniques for cell biological assays. *Bioessays* 30, 811–821. doi: 10.1002/bies.20804

Petrova, E., Rios-Esteves, J., Ouerfelli, O., Glickman, J. F., and Resh, M. D. (2013). Inhibitors of Hedgehog acyltransferase block Sonic Hedgehog signaling. *Nat. Chem. Biol.* 9, 247–249. doi: 10.1038/nchembio.1184

Regehr, K., Domenech, M., Koepsel, J., Carver, K., Ellison-Zelski, S., Murphy, W., et al. (2009). Biological implications of polydimethylsiloxane-based microfluidic cell culture. *Lab Chip* 9, 2132–2139. doi: 10.1039/b903043c

Rivera-González, K. S., Beames, T. G., and Lipinski, R. J. (2021). Examining the developmental toxicity of piperonyl butoxide as a Sonic hedgehog pathway inhibitor. *Chemosphere* 264:128414. doi: 10.1016/j.chemosphere.2020.128414

Roessler, E., Du, Y. Z., Mullor, J. L., Casas, E., Allen, W. P., Gillessen-Kaesbach, G., et al. (2003). Loss-of-function mutations in the human GLI2 gene are associated with pituitary anomalies and holoprosencephaly-like features. *Proc. Natl. Acad. Sci. U. S. A.* 100, 13424–13429. doi: 10.1073/pnas.2235734100

Schindelin, J., Arganda-Carreras, I., Frise, E., Kaynig, V., Longair, M., Pietzsch, T., et al. (2012). Fiji: an open-source platform for biological-image analysis. *Nat. Methods* 9, 676–682. doi: 10.1038/nmeth.2019

Taipale, J., Chen, J. K., Cooper, M. K., Wang, B., Mann, R. K., Milenkovic, L., et al. (2000). Effects of oncogenic mutations in Smoothened and Patched can be reversed by cyclopamine. *Nature* 406, 1005–1009. doi: 10.1038/35023008

Vieira, A. R. (2008). Unraveling human cleft lip and palate research. *J. Dent. Res.* 87, 119–125. doi: 10.1177/154405910808700202

Wang, J., Lu, J., Mook, R., Zhang, M., Zhao, S., Barak, L., et al. (2012). The insecticide synergist piperonyl butoxide inhibits Hedgehog signaling: assessing chemical risks. *Toxicol. Sci.* 128, 517–523. doi: 10.1093/toxsci/kfs165

Wierbowski, B. M., Petrov, K., Aravena, L., Gu, G., Xu, Y., and Salic, A. (2020). Hedgehog Pathway activation requires coreceptor-catalyzed, lipid-dependent relay of the Sonic Hedgehog ligand. *Dev. Cell.* 55, 450–467. doi: 10.1016/j.devcel.2020.09.017

Yamada, Y., Nagase, T., Nagase, M., and Koshima, I. (2005). Gene expression changes of sonic hedgehog signaling cascade in a mouse embryonic model of fetal alcohol syndrome. *J. Craniofacial Surg.* 16, 1055–1061. doi: 10.1097/01.scs.0000183470.31202.c9

Conflict of Interest: BJ holds equity in Onexio Biosystems L.L.C. DB holds equity in Bellbrook Labs, L.L.C., Tasso, Inc., Stacks to the Future, L.L.C., Salus Discovery, L.L.C., Lynx Biosciences, Inc., and Onexio Biosystems L.L.C.

The remaining authors declare that the research was conducted in the absence of any commercial or financial relationships that could be construed as a potential conflict of interest.

frontiers in Cell and Developmental Biology

ORIGINAL RESEARCH
published: 09 April 2021
doi: 10.3389/fcell.2021.621482

Genome-Wide Association Study of Non-syndromic Orofacial Clefts in a Multiethnic Sample of Families and Controls Identifies Novel Regions

Nandita Mukhopadhyay[1], Eleanor Feingold[1,2,3], Lina Moreno-Uribe[4], George Wehby[5], Luz Consuelo Valencia-Ramirez[6], Claudia P. Restrepo Muñeton[6], Carmencita Padilla[7], Frederic Deleyiannis[8], Kaare Christensen[9], Fernando A. Poletta[10], Ieda M. Orioli[11,12], Jacqueline T. Hecht[13], Carmen J. Buxó[14], Azeez Butali[15], Wasiu L. Adeyemo[16], Alexandre R. Vieira[1], John R. Shaffer[1,3], Jeffrey C. Murray[17], Seth M. Weinberg[1,3], Elizabeth J. Leslie[18] and Mary L. Marazita[1,3,19]*

[1] Center for Craniofacial and Dental Genetics, Department of Oral Biology, School of Dental Medicine, University of Pittsburgh, Pittsburgh, PA, United States, [2] Department of Biostatistics, Graduate School of Public Health, University of Pittsburgh, Pittsburgh, PA, United States, [3] Department of Human Genetics, Graduate School of Public Health, University of Pittsburgh, Pittsburgh, PA, United States, [4] Department of Orthodontics, The Iowa Institute for Oral Health Research, College of Dentistry, University of Iowa, Iowa City, IA, United States, [5] Department of Health Management and Policy, College of Public Health, University of Iowa, Iowa City, IA, United States, [6] Fundación Clínica Noel, Medellín, Colombia, [7] Department of Pediatrics, College of Medicine, Institute of Human Genetics, National Institutes of Health, University of the Philippines, Manila, Philippines, [8] UCHealth Medical Group, Colorado Springs, CO, United States, [9] Department of Epidemiology, Institute of Public Health, University of Southern Denmark, Odense, Denmark, [10] CEMIC: Center for Medical Education and Clinical Research, Buenos Aires, Argentina, [11] Department of Genetics, Institute of Biology, Federal University of Rio de Janeiro, Rio de Janeiro, Brazil, [12] Instituto Nacional de Genética Médica Populacional INAGEMP, Porto Alegre, Brazil, [13] Department of Pediatrics, University of Texas Health Science Center at Houston, Houston, TX, United States, [14] Dental and Craniofacial Genomics Core, School of Dental Medicine, University of Puerto Rico, San Juan, Puerto Rico, [15] Department of Oral Pathology, Radiology and Medicine, College of Dentistry, Iowa Institute for Oral Health Research, University of Iowa, Iowa City, IA, United States, [16] Department of Oral and Maxillofacial Surgery, College of Medicine, University of Lagos, Lagos, Nigeria, [17] Department of Pediatrics, Carver College of Medicine, University of Iowa, Iowa City, IA, United States, [18] Department of Human Genetics, Emory University, Atlanta, GA, United States, [19] Clinical and Translational Science, School of Medicine, University of Pittsburgh, Pittsburgh, PA, United States*

OPEN ACCESS

Edited by:
Noah Lucas Weisleder, The Ohio State University, United States

Reviewed by:
L. V. K. S. Bhaskar, Guru Ghasidas Vishwavidyalaya, India
Renato Assis Machado, Campinas State University, Brazil

***Correspondence:**
Nandita Mukhopadhyay
nandita@pitt.edu

Specialty section:
This article was submitted to Molecular Medicine, a section of the journal Frontiers in Cell and Developmental Biology

Received: *26 October 2020*
Accepted: *15 March 2021*
Published: *09 April 2021*

Citation:
Mukhopadhyay N, Feingold E, Moreno-Uribe L, Wehby G, Valencia-Ramirez LC, Muñeton CPR, Padilla C, Deleyiannis F, Christensen K, Poletta FA, Orioli IM, Hecht JT, Buxó CJ, Butali A, Adeyemo WL, Vieira AR, Shaffer JR, Murray JC, Weinberg SM, Leslie EJ and Marazita ML (2021) Genome-Wide Association Study of Non-syndromic Orofacial Clefts in a Multiethnic Sample of Families and Controls Identifies Novel Regions. Front. Cell Dev. Biol. 9:621482. doi: 10.3389/fcell.2021.621482

Orofacial clefts (OFCs) are among the most prevalent craniofacial birth defects worldwide and create a significant public health burden. The majority of OFCs are non-syndromic and vary in prevalence by ethnicity. Africans have the lowest prevalence of OFCs (~1/2,500), Asians have the highest prevalence (~1/500), Europeans and Latin Americans lie somewhere in the middle (~1/800 and 1/900, respectively). Thus, ethnicity appears to be a major determinant of the risk of developing OFC. The Pittsburgh Orofacial Clefts Multiethnic study was designed to explore this ethnic variance, comprising a large number of families and individuals (~12,000 individuals) from multiple populations worldwide: US and Europe, Asians, mixed Native American/Caucasians, and Africans. In this current study, we analyzed 2,915 OFC cases, 6,044 unaffected individuals related to the OFC cases, and 2,685 controls with no personal or family history of OFC. Participants were grouped by their ancestry into African, Asian, European, and Central and South American subsets, and genome-wide association run on the combined sample as well as the four ancestry-based groups. We observed 22 associations to cleft lip with or without cleft palate at 18 distinct loci with p-values $<$ 1e-06, including 10 with

genome-wide significance (<5e-08), in the combined sample and within ancestry groups. Three loci - 2p12 (rs62164740, $p = 6.27e-07$), 10q22.2 (rs150952246, $p = 3.14e-07$), and 10q24.32 (rs118107597, $p = 8.21e-07$) are novel. Nine were in or near known OFC loci - *PAX7*, *IRF6*, *FAM49A*, *DCAF4L2*, 8q24.21, *NTN1*, *WNT3-WNT9B*, *TANC2,* and *RHPN2*. The majority of the associations were observed only in the combined sample, European, and Central and South American groups. We investigated whether the observed differences in association strength were (a) purely due to sample sizes, (b) due to systematic allele frequency difference at the population level, or (c) due to the fact certain OFC-causing variants confer different amounts of risk depending on ancestral origin, by comparing effect sizes to observed allele frequencies of the effect allele in our ancestry-based groups. While some of the associations differ due to systematic differences in allele frequencies between groups, others show variation in effect size despite similar frequencies across ancestry groups.

Keywords: multiethnic, GWAS, genetic factors in OFC, genetic heterogeneity, family study

INTRODUCTION

Orofacial clefts are among the most common birth defects in all populations worldwide and pose a significant health burden. Surgical treatment along with ongoing orthodontia, speech and other therapies, are very successful in ameliorating the physical health effects of OFC, but there is still a significant social, emotional, and financial burden for individuals with OFC, their families, and society (Wehby and Cassell, 2010; Nidey et al., 2016). Furthermore, there are disparities in access to such therapies for OFCs (Nidey and Wehby, 2019), similar to other malformations with complex medical and surgical needs. Some studies have suggested a reduced quality of life for individuals with OFCs (Naros et al., 2018), while other studies have identified higher risk to certain types of cancers (Bille et al., 2005; Taioli et al., 2010; Bui et al., 2018). Thus, it is critical to identify etiologic factors leading to OFCs to improve diagnostics, treatments, and outcomes.

OFCs manifest themselves in many forms - cleft lip alone (CL), cleft palate alone (CP), combination of the two (CLP), and vary in their severity. A large proportion of the causal genes involved with syndromic OFCs (i.e., OFCs that are part of other syndromes) are known (OMIM, https://www.omim.org/search/advanced/geneMap). However, the majority of OFC cases - including about 70% of CL with or without CP (CL/P) and 50% of CP alone - are considered non-syndromic, i.e., occurring as the sole defect without any other apparent cognitive or structural abnormalities (Dixon et al., 2011). The genetic causes of non-syndromic OFCs are still largely undiscovered.

There are differences in birth prevalence around the world with respect to OFC, that may be the result of etiological differences among these different populations, both genetic and non-genetic. Populations of Native American and Asian ancestry have the highest prevalence of ∼2 per 1,000 live births, European ancestry populations have an intermediate prevalence of ∼1 per 1,000, and African-ancestry populations have the lowest prevalence, ∼1 per 2,500 (Dixon et al., 2011). Most of the reported GWAS loci are observed within specific ancestry groups, and there are only a few studies that conducted a systematic comparison of genetic differences between populations of different ancestry, largely due to the lack of sufficiently large samples.

In the current study, we expanded this analysis to other loci and additional populations from the Pittsburgh Orofacial Clefts (POFC) study to describe differences in the genetic etiology of OFC across populations of varying ancestral origin. The POFC Multiethnic study is a geographically diverse, family-based study comprising a large number of families and individuals (∼12,000 participants) from multiple populations worldwide including those of European ancestry from the US and Europe, Asians from China and the Philippines, mixed Native American, European and African ancestry from Central and South America, and Africans from Nigeria and Ethiopia. The POFC Multiethnic study sample is therefore a rich resource for examining the genetic heterogeneity across populations. In two previous GWAS studies (Leslie et al., 2016, 2017), a subset of the total POFC participants were analyzed, including 1,319 independent parent-offspring trios, 823 unrelated cases and 1,700 controls. These previous GWASs have focused on unrelated cases and controls, or parent-offspring trios, not fully taking advantage of the fact that OFCs often segregate within families. Here, we include all available participants from simplex and multiplex pedigrees, along with singleton cases and controls for a total sample size of 2,915 affected and 8,729 unaffected individuals. As a result of the increased sample size, our study should provide more power to detect novel OFC loci, while providing stronger evidence for previously reported associations that are common to all OFCs.

MATERIALS AND METHODS

Study Sample

The current study sample consists of 2,915 participants with OFCs, 6,044 unaffected individuals related to the OFC cases, and 2,685 controls with no personal or family history of OFC. The participants were recruited from multiple sites from Asia

(China, India, Philippines, and Turkey), Europe (Spain, Hungary, Denmark), Africa (Nigeria and Ethiopia), and the Americas (Argentina, Colombia, Guatemala, mainland USA, and Puerto Rico). All study sites provided local IRB approval, then the University of Pittsburgh Coordinating Center (Marazita, PD/PI) received approval from the University of Pittsburgh IRB (FWA # 00006790) for the overall project (IRB approval number CR19080127-001). Genotyping was performed at the Center for Inherited Disease Research (CIDR) at Johns Hopkins University, on the Illumina platform on ∼580 K variants. QC was carried out by the CIDR genotyping coordination center at the University of Washington. Genotypes were then imputed using the 1,000 genome project phase three reference panel, at ∼35,000,000 variants of the GrCH37 genome assembly. More details on the POFC Multiethnic study can be found in the Database of Genotypes and Phenotypes (dbGaP; study accession number phs000774.v2.p1) and at the FaceBase resource for craniofacial research under dataset OFC4: Genetics of Orofacial Clefts and Related Phenotypes (URL https://www.facebase.org/id/1-50DT) (Marazita, 2019).

Ancestry of a subset of unrelated participants from the POFC Multiethnic study was determined based on principal components using genotyped variants, which were then projected onto the larger sample. The first three principal components of ancestry correspond well with the broad geographical origin of the POFC participants, except for those from United States, and were used to classify participants as being of African, Asian, European, or Central and South American origin; this same classification was used for group analyses. Participants from the United States were included in African, European, and Central and South American ancestry groups. Participants from Turkey are part of the European ancestry group. A more detailed description of ancestry determination can be found in the previously published GWASs of POFC Multiethnic study participants (Leslie et al., 2016; Marazita, 2019). The first three PCs provide a workable, although not perfect, separation of participants into the four broad ancestry groups within the POFC Multiethnic study sample. Note that the PCs were not used to account for population substructure in the actual association analysis, therefore we did not need to utilize the higher order PCs.

Genome-wide association was run on the combined study sample (**ALL**), as well as the four ancestry-based groups, Africans (**AFR**), Asians (**ASIA**), Europeans (**EUR**), and Central and South Americans (**CSA**). The sample sizes for each ancestry-based group are provided in **Table 1**. **Table 1** contains the median and maximum pedigree sizes, as well as the median and maximum number of affected individuals per pedigree. The AFR group contains mainly singleton CL/P cases and controls, whereas ASIA and EUR have a larger proportion of extended families; the CSA group's pedigree sizes lie somewhere in between.

TABLE 1 | Study sample characteristics.

	AFR	ASIA	EUR	CSA	ALL
Total pedigrees	227	484	1,271	1,433	3,422
CL/P pedigrees	152	320	507	944	1,925
Median CL/P pedigree size	1	1	1	1	3
Maximum CL/P pedigree size	9	34	35	27	35
Unaffected pedigrees	75	164	764	489	1,498
Median unaffected pedigree size	1	1	1	3	1
Maximum unaffected pedigree size	5	4	15	21	21
Total individuals	428	1,691	3,273	4,038	9,447
Total unaffected individuals	274	1,246	2,704	2,988	7,226
Total affected individuals	154	445	569	1,050	2,221
Median number of affected members per CL/P pedigree	1	1	1	1	1
Maximum number of affected per CL/P pedigree	2	5	5	4	5

Phenotype Definition

In our study, we ran GWAS of CL/P on participants from pedigrees in which the OFC-affected members have a cleft lip only (CL), or a cleft lip and a cleft palate (CLP). Pedigrees with members who are affected with a cleft palate only, or a reported history of cleft palate only, were excluded from our analysis. Within these pedigrees, any member with an OFC was considered to be affected for CL/P; unaffected pedigree members from CL/P pedigrees as well as control pedigrees that do not have any history of OFCs were considered to be unaffected for CL/P. The final combined sample (ALL) included 2,221 affected and 7,226 unaffected participants.

Statistical Method

In our study, we selected all available participants from pedigrees ranging from singletons to 35 members in a single pedigree, for conducting case-control association. The program EMMAX (Kang et al., 2010) was used to run the seven GWAS. EMMAX uses a variance component linear mixed model approach to detect association at each variant. The model includes a genetic relationship matrix (GRM) estimated from the observed genotype data to simultaneously correct for both population structure and familial relatedness. Therefore, ancestry PCs are not separately included in the association analysis. This same GRM is also used to estimate the polygenic variance component. Strength of association is then measured using a score test of comparison between the maximum likelihood conditional on observed genotypes at each variant vs. the unconditional maximum likelihood model. Due to the nature of the score test, the reported effect size is not interpretable for a binary phenotype, therefore we do not utilize the effect sizes reported by EMMAX. Instead, another mixed-model association program, GENESIS (Gogarten et al., 2019) was used to calculate approximate effect sizes (betas and standard errors). The same effect allele is used to report effect size and direction consistently across groups, namely the minor allele at each variant as identified in the combined POFC sample.

Filtering of Variants and Identification of Associated Loci

Variants that met genotyping and imputation quality control filters including significant deviation from Hardy-Weinberg equilibrium (HWE *p*-value 1.0e-05 in European controls) were considered for analysis. These were further filtered based on minor allele frequencies; those with MAF of 2% or more within their respective ancestry groups are included in the GWAS. In this study, loci containing variants with association *p*-value < 1.0e-06 were reported as positive associations. The observed minor allele frequencies of reported loci were compared to the respective population frequencies from the gnomAD database (Karczewski et al., 2020) to ensure that minor allele frequencies were not impacted by the imputation (**Supplementary Table 1**). Note that major and minor alleles may be switched between groups, but this impacts only the direction of effect, not the strength of association.

Identification of Novel OFC Loci

We compared significant and suggestive associations from our GWASs to genes and regions that have been identified through genome-wide linkage or association, as well as by candidate gene studies by multiple previous genetic studies of OFCs. Our reference loci consist of the 29 genomic regions listed in the review article by Beaty et al. (2016), combined with loci reported by six recently published GWASs. The six newer GWASs include (1) combined meta-analysis of parent-offspring trio and case-control cohorts from the current POFC multiethnic study sample (Leslie et al., 2016), (2) meta-analysis of the cohorts used in (1) with another OFC sample consisting of European and Asian participants (Leslie et al., 2017), (3) GWAS of cleft lip with cleft palate in Han Chinese samples (Yu et al., 2017), (4) GWAS of cleft lip only and cleft palate only in Han Chinese (Huang et al., 2019), (5) GWAS of cleft lip with or without cleft palate in Dutch and Belgian participants (van Rooij et al., 2019), and (6) GWAS of sub-Saharan African participants from Nigeria, Ghana, Ethiopia, and the Republic of Congo (Butali et al., 2019). Although this study excludes OFC cases affected with cleft palate only, we included those loci that are considered to play a role in the development of cleft palate (without cleft lip), such as *GRHL3*, *BAALC*, *TBK1*, and *ZNF236* in the list of 29 reference loci. CP GWAS *p*-values, if reported by the six recent GWAS studies, are also included in the comparison.

For each comparison, we derived search intervals for detecting overlaps between published/known OFC loci and the associations reported in this current study. For each known OFC gene, GrCH37 base pair positions of start and end transcription sites from the UCSC genome browser were used to measure distance between our locus and the gene. For the 8q24.21 locus, which is a gene desert, we checked whether any of our associated SNPs were located within the 8q24.21 chromosome band. A positive replication is reported where the minimum *p*-value observed within 500 KB on either side of the gene exceeds 1e-05. For comparing published GWAS loci, separate 1 MB search intervals were created around the reported lead variants, and a positive replication noted if any of our selected associations were within 500 KB of these intervals.

Comparison Between Ancestry Groups

For comparing GWASs of ancestry groups, we first compared association results, namely, effect size and direction, and association *p*-value of each lead variant within each ancestry group, as well as variants nearby. However, comparing association outcomes at a single variant is not always feasible, nor advisable, as association outcomes are impacted by differences in variant allele frequencies and LD, which differ by ancestry. We therefore looked at intervals of 500 KB to either side of the lead SNPs, and selected the 30 top associations observed within these intervals within each GWAS. Approximate effect sizes for selected variants were computed using the same effect allele at each variant, which is the minor allele for that variant in ALL. GENESIS (Gogarten et al., 2019) reports the beta coefficient for each SNP in terms of allele dosage. In our analysis, a positive effect size indicates that the effect allele increases risk of CL/P and vice-versa.

We hypothesized that the main reason for difference in association outcomes between ancestry groups is due to the fact that variants are common in one population, but rare in others. If an OFC causing variant is observed with similar frequency in multiple groups, we expect to see elevated association signals in all these groups as well. Although the strength of association indicated by a *p*-value is dependent on sample size and may be reduced in the smaller groups, the magnitude and direction of effect sizes should be similar. If this is not the case, it implies that variant's contribution to the development of OFCs varies depending on the participants' ancestral origin. Thus, we compared the effect size and effect allele frequencies of the top 30 associations observed close to each lead SNP. In order to assess whether allele frequencies are different between groups, we calculated the fixation index F_{ST} for the top 30 associations, using the ancestry-based groups in our ALL sample, and used the 95% percentile of the distribution of F_{ST} as a threshold value to decide whether the effect allele frequencies were similar or different. To compare effect size estimates, we examined whether the point estimate was in the same direction and if the confidence intervals overlapped. We also ran a meta-analysis of the selected variants as a statistical means for measuring whether the effect allele affects CL/P risk similarly across ancestry groups. The meta-analysis procedure reports the *p*-value for Cochrane's Q statistic at each analyzed variant, testing the hypothesis that effect sizes differ across the groups. PLINK (Chang et al., 2015) was used to run meta-analysis and for calculation of Wright's F_{ST} fixation index.

We used these comparisons to categorize each locus into one of three categories:

Category 1: The effect alleles have similar frequencies within the groups, and association *p*-values are estimates are also similar.

Category 2: Effect allele frequency differs across groups, effect size estimates may or may not differ.

Category 3: Allele frequencies are similar between groups, but the effect size estimates differ.

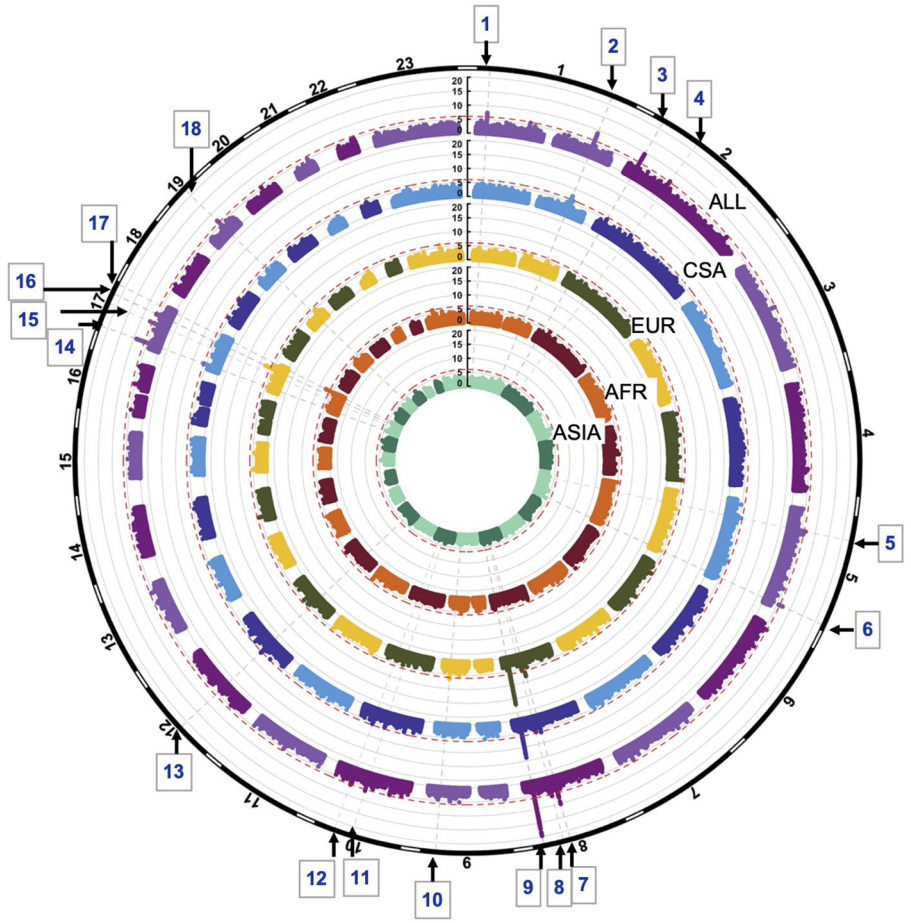

FIGURE 1 | Circular Manhattan plots of ALL, CSA, EUR, AFR and ASIA. Red lines are drawn at the 1e-06 significance level. Loci significant at the 1e-06 significance level are indicated by the gray dotted lines and numbered 1–18. Chromosomes are depicted by the black bands in the outermost circle.

RESULTS

GWASs of the combined sample and the four ancestry-based groups yielded 22 associations with *p*-values < 1e-06, including 10 genome-wide significant associations (i.e., below the Bonferroni threshold of 5e-08) at 18 distinct loci. In some cases, these loci are observed in more than one ancestry-based group (**Figure 1**, **Table 2**). Of the 18 loci, 15 are in or near reported OFC genes and reported associations from the published OFC GWASs listed in **Methods**, and the other three are novel. The novel associations include (i) chromosome 2p12 (rs62164740, *p*-value 6.27E-07); (ii) 10q22.2 (rs150952246, *p*-value 3.14E-07); and (iii) 10q24.32 (rs118107597, *p*-value 8.21E-07). All three showed the strongest association in the combined ALL sample. Four of the 22 associations were observed within a specific ancestry group: these included (i) chromosome 9q33.1 in EUR, rs9408874, *p*-value 2.59E-07; (ii) 12q13.2 in CSA, rs34260065, *p*-value 3.87E-07; (iii) *TANC2* in EUR, rs1588366, *p*-value 1.09E-08; and (iv) 17q25.3 in AFR, rs1975866, *p*-value 3.13E-08. The ASIA subgroup did not yield any association with a significance *p*-value less than our threshold of 1e-06. The strongest associations were seen at the 8q24 locus with *p*-value 2.80E-29 in ALL, as well as exceeding genome-wide significance in EUR and CSA. **Table 2** lists the 18 associations, with the three novel loci are listed in bold. **Figure 1** shows the Manhattan plots of the five GWASs.

Novel Associations and Replication

There were three novel associations that did not correspond to known OFC GWAS loci, including the previously published GWASs of POFC Multiethnic Study participants (Leslie et al., 2016, 2017), GWAS of Europeans (van Rooij et al., 2019), and GWAS of Africans (Butali et al., 2019). Along with the three novel loci, we also investigated four additional associations that were reported in Han Chinese GWASs with significance below the genomewide suggestive threshold of 1e-05 for possible roles in the development of CL/P. Interestingly, the four loci reported in Chinese samples do not show association with the ASIA group in our study, rather they are observed with ancestry groups other than Asians in our current study. These 7 loci are listed in **Table 3** along with the gene nearest the lead SNP. The nearest gene was identified based on gene locations, specifically, transcription start and end positions obtained from the UCSC genome browser. In **Table 3**, we also note whether there are regulatory elements such as super-enhancers involved in craniofacial development,

TABLE 2 | Associations with *p*-values < 1e-06.

Locus	Chromosome band	Lead SNP (effect allele)	Lead SNP position	*P*-value[a]	Effect size, Std. error[b]	Groups with *p* < 1e-06[a]	OFC Gene/prior GWAS
1	1p36.13	rs9439714 (C)	18,976,489	3.27E-08	0.15 ± 0.04	ALL	*PAX7*
2	1q32.2	rs17015217 (A)	209,966,629	1.46E-09	−0.19 ± 0.05	ALL, CSA	*IRF6*
3	2p24.3-24.2	rs6745357 (G)	16,713,395	3.62E-10	0.25 ± 0.03	ALL	*FAM49A*
4	**2p12**	**rs62164740 (A)**	**78,177,488**	**6.27E-07**	**0.25 ± 0.06**	**ALL**	
5	5p13.2-13.1	rs181764204 (T)	38,205,024	2.63E-07	0.54 ± 0.10	ALL	Huang et al., 2019
6	5q35.2-35.1	rs17075892 (T)	172,827,353	6.95E-08	−0.25 ± 0.04	ALL	Butali et al., 2019; Huang et al., 2019
7	8q21.3	rs12543318 (C)	88,868,340	7.45E-11	0.24 ± 0.04	ALL, EUR	*DCAF4L2*
8	8q22.2	rs185266751 (G)	99,712,644	2.49E-07	0.50 ± 0.09	ALL	Huang et al., 2019
9	8q24.21	rs72728755 (A)	129,990,382	2.80E-29	0.48 ± 0.05	ALL, CSA, EUR	8q24
10	9q33.1	rs9408874 (T)	118,279,489	2.59E-07	0.26 ± 0.05	EUR	Huang et al., 2019
11	**10q22.2**	**rs150952246 (C)**	**77,151,597**	**3.14E-07**	**0.37 ± 0.08**	**ALL**	
12	**10q24.32**	**rs118107597 (A)**	**104,283,510**	**8.21E-07**	**0.58 ± 0.12**	**ALL**	
13	12q13.2	rs34260065 (C)	55,540,318	3.87E-07	0.12 ± 0.04	CSA	Huang et al., 2019
14	17p13.1	rs16957821 (G)	8,948,104	9.12E-10	0.25 ± 0.04	ALL	*NTN1*
15	17q21.31-21.32	rs7216951 (T)	44,972,810	1.42E-07	−0.20 ± 0.04	ALL	*WNT3, WNT9B*
16	17q23.2-23.3	rs1588366 (G)	61,076,428	1.09E-08	−0.24 ± 0.05	EUR	*TANC2*
17	17q25.3	rs1975866 (C)	77,267,377	3.13E-08	0.39 ± 0.09	AFR	Huang et al., 2019
18	19q13.11	rs2003950 (A)	33,546,283	1.21E-07	0.21 ± 0.04	ALL	*RHPN2*

Novel loci highlighted in bold; [a]Association p-values from the EMMAX program; [b]Effect size (Beta coefficient) and standard error of effect size from the GENESIS program.

TABLE 3 | Novel loci, closest gene, and contribution to craniofacial development.

Locus	Chrom. band	Groups with *p* < 1e-06	Nearest gene	Regulatory elements for craniofacial development and other roles in OFCs
4	2p12	ALL, CSA	*SNAR-H*	Evidence of methylation during craniofacial development
8	8q22.2	ALL, CSA	*STK3*	Transcription start site, upstream promoter and enhancer region
10	9q33.1	EUR	*LINC00474*	Craniofacial super-enhancer region
11	10q22.2	ALL, CSA	*ZNF503*	Transcription start site and promoter region
12	10q24.32	ALL, CSA	*SUFU*	Promoter, transcription enhancer; *SUFU* is involved in the Hedgehog signaling pathway
13	12q13.2	CSA	*OR9K2*	Craniofacial super-enhancer region; *OSR2* gene 240Kb upstream codes for transcription factor shown to control palatal development Lan et al., 2004; Fu et al., 2017
17	17q25.3	AFR	*RBFOX3*	Craniofacial super-enhancer region; *TIMP2* gene 335Kb connected to increased risk of CL/P Letra et al., 2014

Peak numbers in bold indicate novel loci, other loci showed modest association (p < 1e-04) in GWAS of Chinese (Huang et al., 2019).

or if these regions appear to be expressed in fetal craniofacial tissue, as listed in Epigenomic Atlas of Early Human Craniofacial Development (Wilderman et al., 2018; Justin Cotney, 2020).

Comparison of Associations by Ancestry Group

Consistent with previous studies, we observed that many loci show significant association in one ancestry group, but are well below the suggestive threshold in the others. We wanted to explore the possible explanations for these findings and categorized each locus into one of three categories, which we describe below. We were able to easily categorize some of the associated loci into one of these three groups, while others were not as definitive. **Table 4** lists the category that best fits each associated locus and summarizes the characteristics of top associations at each locus in brief, with respect to their allele frequencies, main SNP effects, and significance of the Q-statistics. The effect sizes are noted as being different if their confidence

TABLE 4 | Comparison of effect allele frequency and effect size of lead SNPs within each locus.

Peak	Locus	Gene	Category	*P*-value of Q statistic	Effect allele frequency	Main SNP effect (Beta) of top SNPs
1	1p36.13	*PAX7*	2	Not significant	Low in ASIA	Smaller in ASIA at several SNPs
2	1q32.2	*IRF6*	2	Not significant	Low in EUR, AFR	Larger in EUR than CSA, ASIA
3	2p24.3-24.2	*FAM49A*	2	Not significant	Effect allele common in all groups	Similar effect size estimates at most SNPs
4	2p12		1	Not significant	Low in ASIA	Larger in ASIA but not statistically different
5	5p13.2-13.1		1+3	$p(Q) < 0.05$ at some SNPs,	Low in EUR, similar in others	Larger in EUR at SNPs with significant $p(Q)$
6	5q35.2-35.1		1	Not significant	Similar across groups	More negative in AFR, but not statistically different
7	8q21.3	*DCAF4L2*	2+3	Highly significant at a few SNPs, $p(Q) < 0.001$	Similar across groups	Smaller in ASIA at SNPs with $p(Q) < 0.001$
8	8q22.2		2	Not significant	Common (15–50%) in CSA, a few variants rare in others (<2%).	Similar across groups
9	8q24.21		1	Not significant	Low in ASIA (2–5%)	Similar across groups
10	9q33.1		3	Significant	Similar across groups	Significantly larger in EUR
11	10q22.2		2	Not significant except a few SNPs with $p(Q) \sim = 0.05$	Rare in AFR (<2%)	Larger in AFR at SNPs at SNPs with $p(Q) \sim = 0.05$
12	10q24.32		1	Not significant	Low in all groups (<2–15%)	Similar across groups
13	12q13.2		3	$p(Q) < 0.05$	Common in all groups (15–45%)	Significantly larger in CSA, larger but not significantly so in AFR
14	17p13.1	*NTN1*	1	Not significant except one, $p(Q) < 0.01$	Common in all groups	Significantly larger in AFR only for SNP with significant $p(Q)$
15	17q21.31-21.32	*WNT3, WNT9B*	1	Not significant	Common in all groups (15–45%)	Similar across groups
16	17q23.2-23.3	*TANC2*	3	Significant, $p(Q) < 0.01$	Low in ASIA (5–15%)	Significantly larger in EUR
17	17q25.3		3	Significant, $p(Q) < 0.001$	Common in all groups (>15%)	Significantly larger in AFR
18	19q13.11	*RHPN2*	2	Not significant	Common in all groups	Similar effect sizes

intervals do not overlap, and allele frequencies are considered to vary across groups if the F_{ST} value falls above 0.065, which is the 95th percentile of the genome-wide distribution of F_{ST} values in ALL. From these results, one can conclude that consistently significant Q statistics within a locus is indicative of a category 3 locus (when allele frequencies are similar), wherein the same variant contributes differently to CL/P risk in populations with different ancestry. The reverse is almost always true where the variant has similar effects irrespective of ancestry, i.e., those located within category 1 loci. Category 2 loci appear to lie somewhere in between.

Category 1

The significance of association appears to be a function of the sample size. In this category, the effect sizes are similar in all four ancestry groups; therefore, larger ancestry groups (e.g., CSA) and/or larger effect allele frequencies will have greater power to detect an association than the smaller ancestry groups (e.g., Asian and African), and/or if the effect allele is rare. We found this to be the case for six loci, which included 2p12, 5q35.1-q35.2, 8q24.21, 10q24.32 (novel locus), 17p13.1 (*NTN1*), and 17q21.31-q21.32 (*WNT3* and *WNT9B*). The Q statistic *p*-value for meta-analysis is not significant at the nominal threshold of 5% at the top associated positions, and F_{ST} values are generally small (0.05 or less). The 8q24.21 locus is a special case where effect allele frequencies of top associated SNPs are much lower in the ASIA group than the others.

Category 2

Association *p*-values differ between groups due to the fact that the allele frequencies are different. Effect size and direction appear to be similar across the subgroups. Six associated loci, 1p36.13 (*PAX7*), 1q32.2 (*IRF6*), 2p24.3-p24.2 (*FAM49A*), 8q22.2, 10q22.2, and 19q13.11 (*RHPN2*) are consistent with this category. The Q statistic is not significant, however, F_{ST} values are on the average high (>0.1).

Category 3

Association *p*-values differ between groups. Effect sizes and direction vary substantially indicating that the same allele increases risk of OFC in certain ancestry groups, but has the opposite effect or has no effect on risk of OFC in others. However, effect allele frequency match across groups. Four associations, 9q33.1, 12q13.2, 17q23.2-q23.3 (*TANC2*), and 17q25.3 are consistent with this category.

Uncertain Category

The 5p13.2-p13.1 locus appears to contain associated SNPs from categories 1 and 3. The effect sizes are not the same for all groups at a few SNPs, however, effect allele frequencies appear to be mostly similar, with F_{ST} values around 0.05. The 8q21.3 (*DCAF4L2*) locus also contains a few loci that belong in category 3, where effect allele frequencies are the same across all groups (F_{ST} <0.05), while effects differ significantly (*p*-value of Q statistic $<$ 1e-03). Other variants conform to category 2, where the effect sizes are statistically similar, but allele frequencies differ.

An example from each of the three categories are shown in **Figures 2–4** below, the 17p13.1 (*NTN1*) locus from category 1, the 1q32.2 (*IRF6*) locus from category 2, and the novel association in AFR at 17q25.3 from category 3. Each figure shows a regional plot of association *p*-values (1st row), effect size and confidence intervals (forest plot in 2nd row left), and allele frequencies of the effect allele in each group (heatmap in 2nd row right). The regional plot spans the top 30 associations observed at that locus, with the top 10 SNPs identified. The forest plots show effect sizes and confidence intervals on the effect sizes (x axis) of the top 10 SNPs (listed on the y-axis) for each group. The Q-statistic *p*-value (precision above 0.001) is noted below each variant in the forest plots. The heatmap shows effect allele frequencies of the top 10 variants for each group (y-axis); the lead variant is highlighted in red within each heatmap. Variants are ordered by base-pair position from top to bottom in each forest plot of effect size, and allele frequency heatmap.

In **Figure 2**, the largest sample, CSA produces the highest association *p*-values, followed by EUR and ASIA, and AFR. The effect sizes are very similar across the groups. The combined ALL sample shows the strongest association, and all four of the ancestry-based groups appear to contribute evidence for association at the 17p13.1 (*NTN1*) locus. This association conforms to the characteristics that describe category 1.

In **Figure 3**, CSA and ASIA show elevated association *p*-values at the 1q32.2 (*IRF6*) locus, and are the major contributors to the significant association observed for the combined ALL sample, whereas EUR and AFR are weakly associated. The variants' effect alleles are common in CSA and ASIA, and rare in the other two samples. The effect sizes are all similar, therefore, it is likely that the heterogeneity observed at this locus is due to difference in allele frequencies. The *IRF6* association conforms to category 2.

In **Figure 4**, at the 17q25.3 locus, the effect alleles are common in all four groups, however, a significant association is observed only in AFR. This is consistent with the small effect sizes observed in all groups except AFR. The 17q25.3 locus conforms is consistent with category 3.

DISCUSSION

The current study extends previously published GWAS studies by using a substantially larger study sample than the previous GWAS study that included unrelated case trios, and singleton cases and controls. The larger sample size allowed us to identify three new potential loci that confer risk of CL/P, however, the addition of participants also contributed to added genetic heterogeneity, that diminished the strength of association in some cases.

One of the striking findings from OFC GWAs to date is the difference in association signals between populations. Although some loci such as 1q32 (IRF6) have been replicated in almost every population, most loci have not replicated between different populations. The lack of replication of associated loci between different populations can be attributed to differences in phenotype, sample size, or differences in allele frequency of the variants themselves. For example, the 8q24 locus is strongly associated in European populations but has not been detected in Asian populations because the risk alleles in Europeans have low

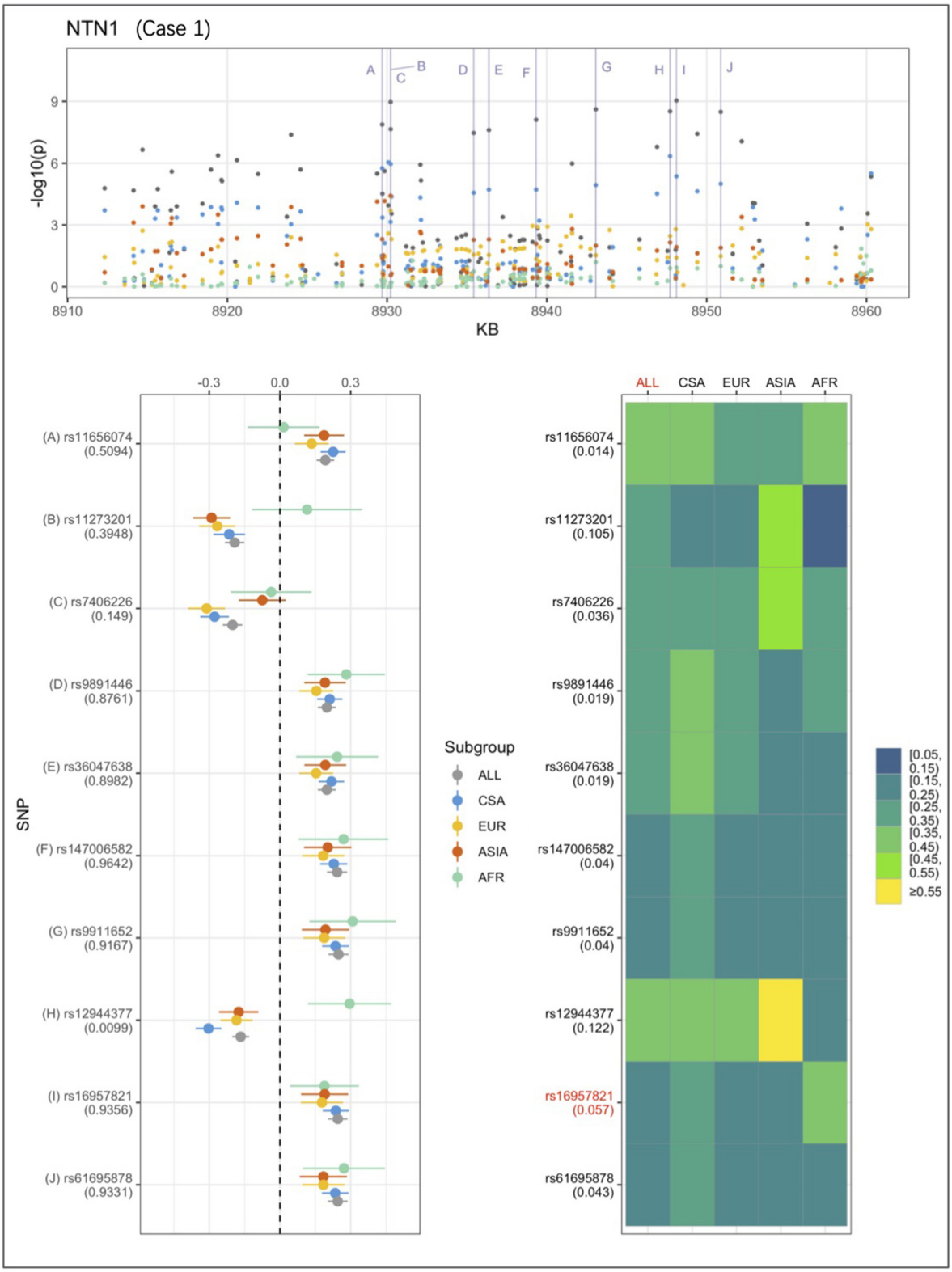

FIGURE 2 | Association peak in 17p13.1 (*NTN1*) consistent with category 1. SNPs are ordered by base-pair position in lower panels; Q-statistic *p*-value noted under each SNP in forest plot of effect size; Wright's F_{ST} value noted under each SNP name in heatmap of effect allele frequencies; lead variant and group with most significant *p*-value shown in red in heatmap.

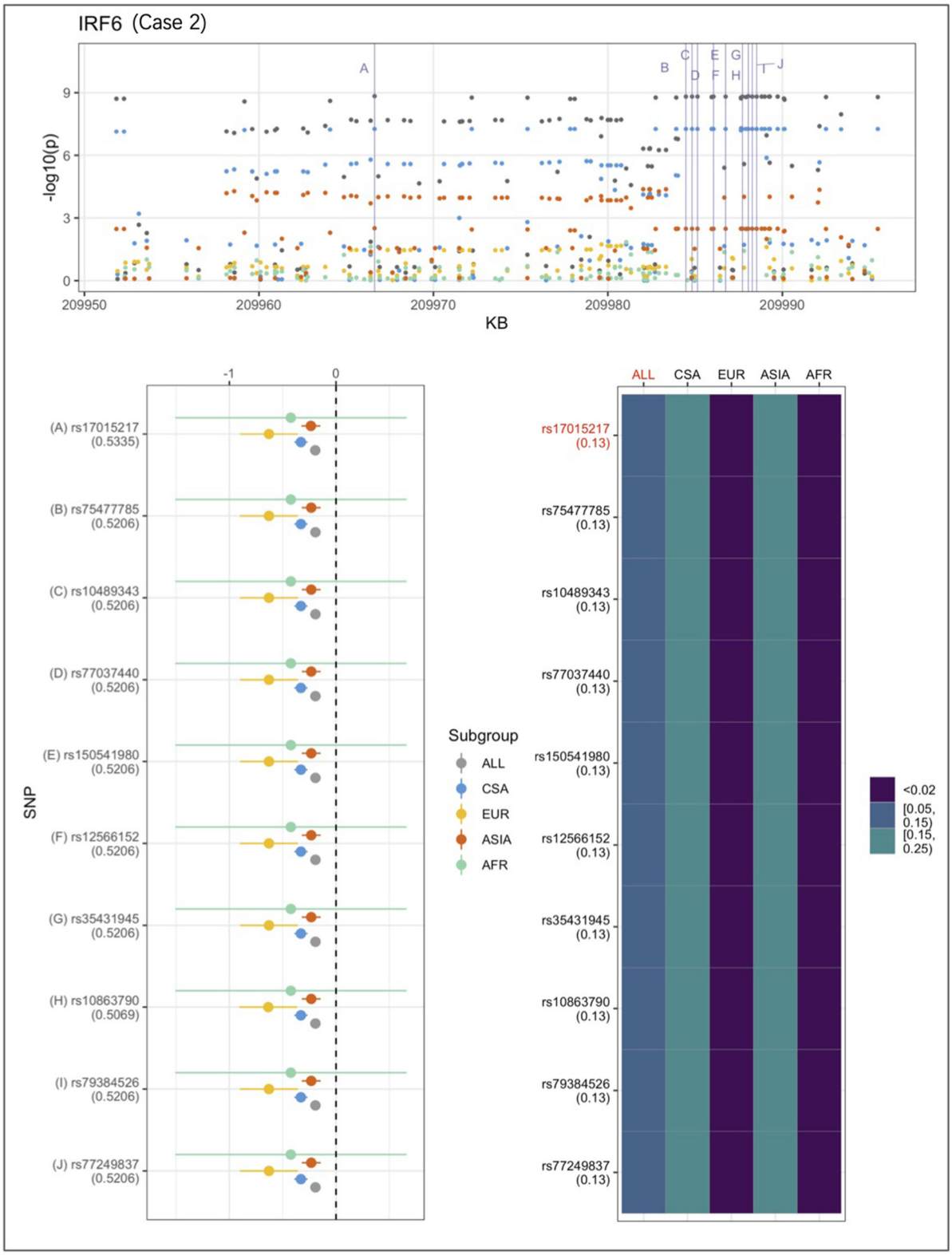

FIGURE 3 | Association peak in 1q32.2 (*IRF6*) consistent with category 2. SNPs are ordered by base-pair position; Q-statistic *p*-value noted under each SNP in forest plot; lead variant and sample with highest *p*-value shown in red in heatmap and F_{ST} values noted under each SNP. The top 10 associated variants fall below our MAF filter in the EUR and ASIA groups.

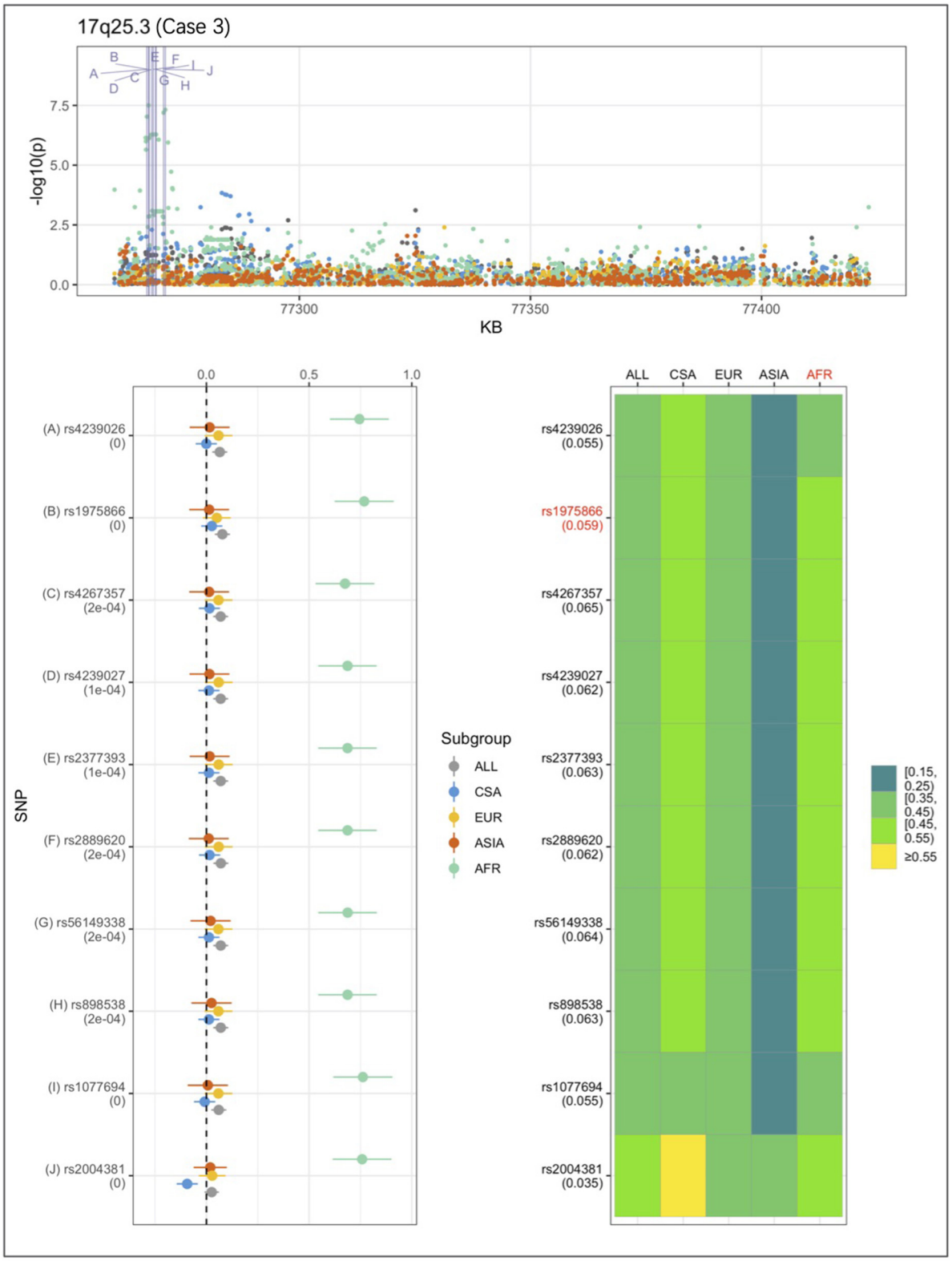

FIGURE 4 | Association peak in 17q25.3 in the AFR group consistent with category 3. SNPs are ordered by base-pair position; Q-statistic *p*-value noted under each SNP in forest plot; lead variant and sample with highest *p*-value shown in red in heatmap, and F_{ST} values noted under each SNP.

frequencies in Asian populations, limiting the power to detect associations (Murray et al., 2012).

In our current study, we explored the genetic heterogeneity of cleft lip with or without cleft palate as a result of difference in ancestry, by running GWASs of CL/P within participants classified into four ancestry groups. As a result, we found that association outcomes differed substantially by ancestry. Our hypothesis was that variants controlling the risk of CL/P differs by ancestry, although these variants are distributed similarly. To test this hypothesis, we compared the main SNP effects of top associations in each locus to their observed allele frequencies. Our comparison showed evidence that some loci confer risk in every population, and the likelihood of observing an association is low in populations where these variants occur at a low frequency.

More importantly, we identified loci at which, the variants produced significantly different association outcomes, even though they were similarly distributed across the ancestry-based groups. It is likely that these loci do not modulate genetic risk of CL/P directly, but through gene-by-gene and gene-by-environment interactions.

An analysis of genetic diversity across the sites within each ancestry group showed that the ASIA and AFR groups are most diverse (median F_{ST} 0.02), indicating more distinct population admixture within those samples, while the EUR and CSA groups show lower diversity (median F_{ST} 0.003 and 0.009, respectively). It is likely that the genetic diversity of the ASIA sample was responsible for the lack of genome-wide significant or even suggestive associations, although the sample size is adequate (445 affected and 1,246 unaffected participants). The ASIA sample is geographically diverse, consisting of participants from China, India, and Philippines. The AFR and CSA groups are also geographically diverse (although CSA has a low F_{ST} genetic diversity coefficient), which could have led to weaker associations; there are only two genome-wide significant associations in CSA, even though this is our largest group consisting of 1,050 affected and 2,988 unaffected participants. In a previous whole genome sequence study that included only the CSA participants from Colombia, we observed a genome-wide significant association in chromosome 21q22.3 (Mukhopadhyay et al., 2020), but no corresponding association is seen either in this current study or the two previous studies that used CSA participants (Leslie et al., 2016, 2017). The variants in the chromosome 21q22.3 in Colombian CL/P trios were observed to have similar allele frequencies across the subpopulations that make up the CSA group, but yielded no significant association when non-Colombian CSA participants were analyzed separately. That locus now appears to fit the characteristics of our current study's category 3 loci.

Another contributing factor to the genetic heterogeneity is due to our phenotype itself. CL/P combines the two cleft subtypes: cleft lip only, and cleft lip with cleft palate. It has been shown by previous studies that the two subtypes are etiologically different (Carlson et al., 2017, 2019). In the POFC multiethnic study sample, the frequency of these two subtypes differ among the sub-populations present, which can further reduce the power to detect association.

The exploration of the genetic differences between cleft subtypes is the focus of our ongoing investigation. This current study on the characterization of ancestry-level differences is an important step toward a more fine-grained and detailed investigation into the genetic heterogeneity of OFCs.

DATA AVAILABILITY STATEMENT

Publicly available datasets were analyzed in this study. This data can be found here: https://www.ncbi.nlm.nih.gov/projects/gap/cgi-bin/study.cgi?study_id=phs000774.v2.p1.

ETHICS STATEMENT

The studies involving human participants were reviewed and approved by University of Pittsburgh IRB. Written informed consent to participate in this study was provided by the participants' legal guardian/next of kin.

AUTHOR CONTRIBUTIONS

NM, EF, EL, and MM were responsible for the study design and manuscript preparation. NM performed the data analysis. LM-U, GW, LV-R, CM, CP, FD, KC, FP, IO, JH, CB, AB, WA, and AV contributed participant data to this study. All the authors reviewed the manuscript.

FUNDING

This work was supported by grants from the National Institutes of Health (NIH) including: R01-DE016148 [MM, SW], X01-HG007485 [MM, EF], U01-DE024425 [MM], R37-DE008559 [JM, MM], R21-DE016930 [MM], R01-DE012472 [MM], R01-DE011931 [JH], U01-DD000295 [GW], R00-DE024571 [CB], R25-MD007607 [CB], S21-MD001830 [CB], U54-MD007587 [CB], K99/R00 DE022378 [AB]. Genotyping and data cleaning were provided via an NIH/NIDCR contract to the Johns Hopkins Center for Inherited Disease Research: HHSN268201200008I. Additional support provided by an intramural grant from the Research Institute of the Children's Hospital of Colorado [FD]; additional operating costs support in the Philippines was provided by the Institute of Human Genetics, National Institutes of Health, University of the Philippines, Manila [CP].

ACKNOWLEDGMENTS

Many thanks to the participant families worldwide, without whom this research would not have been possible. Special thanks to Dr. Eduardo Castilla and Dr. Andrew Czeizel, and to the devoted staff at the many recruitment sites.

SUPPLEMENTARY MATERIAL

The Supplementary Material for this article can be found online at: https://www.frontiersin.org/articles/10.3389/fcell.2021.621482/full#supplementary-material

REFERENCES

Beaty, T. H., Marazita, M. L., and Leslie, E. J. (2016). Genetic factors influencing risk to orofacial clefts: today's challenges and tomorrow's opportunities. *F1000Res* 5:2800. doi: 10.12688/f1000research.9503.1

Bille, C., Winther, J. F., Bautz, A., Murray, J. C., Olsen, J., and Christensen, K. (2005). Cancer risk in persons with oral cleft–a population-based study of 8,093 cases. *Am. J. Epidemiol.* 161, 1047–1055. doi: 10.1093/aje/kwi132

Bui, A. H., Ayub, A., Ahmed, M. K., Taioli, E., and Taub, P. J. (2018). Association between cleft lip and/or cleft palate and family history of cancer: a case-control study. *Ann. Plast. Surg.* 80, 178–181. doi: 10.1097/SAP.0000000000001331

Butali, A., Mossey, P. A., Adeyemo, W. L., Eshete, M. A., Gowans, L. J. J., Busch, T. D., et al. (2019). Genomic analyses in African populations identify novel risk loci for cleft palate. *Hum. Mol. Genet.* 28, 1038–1051. doi: 10.1093/hmg/ddy402

Carlson, J. C., Anand, D., Butali, A., Buxo, C. J., Christensen, K., Deleyiannis, F., et al. (2019). A systematic genetic analysis and visualization of phenotypic heterogeneity among orofacial cleft GWAS signals. *Genet. Epidemiol.* 43, 704–716. doi: 10.1002/gepi.22214

Carlson, J. C., Taub, M. A., Feingold, E., Beaty, T. H., Murray, J. C., Marazita, M. L., et al. (2017). Identifying genetic sources of phenotypic heterogeneity in orofacial clefts by targeted sequencing. *Birth Defects Res.* 109, 1030–1038. doi: 10.1002/bdr2.23605

Chang, C. C., Chow, C. C., Tellier, L. C., Vattikuti, S., Purcell, S. M., and Lee, J. J. (2015). Second-generation PLINK: rising to the challenge of larger and richer datasets. *Gigascience* 4:8. doi: 10.1186/s13742-015-0047-8

Dixon, M. J., Marazita, M. L., Beaty, T. H., and Murray, J. C. (2011). Cleft lip and palate: understanding genetic and environmental influences. *Nat. Rev. Genet.* 12, 167–178. doi: 10.1038/nrg2933

Fu, X., Xu, J., Chaturvedi, P., Liu, H., Jiang, R., and Lan, Y. (2017). Identification of Osr2 transcriptional target genes in palate development. *J. Dent. Res.* 96, 1451–1458. doi: 10.1177/0022034517719749

Gogarten, S., Sofer, T., Chen, H., Yu, C., Brody, J., Thornton, T., et al. (2019). Genetic association testing using the GENESIS R/Bioconductor package. *Bioinformatics* 35, 5346–5348. doi: 10.1093/bioinformatics/btz567

Huang, L., Jia, Z., Shi, Y., Du, Q., Shi, J., Wang, Z., et al. (2019). Genetic factors define CPO and CLO subtypes of nonsyndromicorofacial cleft. *PLoS Genet.* 15:e1008357. doi: 10.1371/journal.pgen.1008357

Justin Cotney, A. W. (2020). *Epigenomic Atlas of Early Human Craniofacial Development*. Bethesda, MD: FaceBase Consortium.

Kang, H. M., Sul, J. H., Service, S. K., Zaitlen, N. A., Kong, S. Y., Freimer, N. B., et al. (2010). Variance component model to account for sample structure in genome-wide association studies. *Nat. Genet.* 42, 348–354. doi: 10.1038/ng.548

Karczewski, K. J., Francioli, L. C., Tiao, G., Cummings, B. B., Alföldi, J., Wang, Q., et al. (2020). The mutational constraint spectrum quantified from variation in 141,456 humans. *Nature* 581, 434–443. doi: 10.1038/s41586-020-2308-7

Lan, Y., Ovitt, C. E., Cho, E. S., Maltby, K. M., Wang, Q., and Jiang, R. (2004). Odd-skipped related 2 (Osr2) encodes a key intrinsic regulator of secondary palate growth and morphogenesis. *Development* 131, 3207–3216. doi: 10.1242/dev.01175

Leslie, E. J., Carlson, J. C., Shaffer, J. R., Butali, A., Buxo, C. J., Castilla, E. E., et al. (2017). Genome-wide meta-analyses of nonsyndromic orofacial clefts identify novel associations between FOXE1 and all orofacial clefts, and TP63 and cleft lip with or without cleft palate. *Hum. Genet.* 136, 275–286. doi: 10.1007/s00439-016-1754-7

Leslie, E. J., Carlson, J. C., Shaffer, J. R., Feingold, E., Wehby, G., Laurie, C. A., et al. (2016). A multi-ethnic genome-wide association study identifies novel loci for non-syndromic cleft lip with or without cleft palate on 2p24.2, 17q23 and 19q13. *Hum. Mol. Genet.* 25, 2862–2872. doi: 10.1093/hmg/ddw104

Letra, A., Zhao, M., Silva, R. M., Vieira, A. R., and Hecht, J. T. (2014). Functional significance of MMP3 and TIMP2 polymorphisms in cleft lip/palate. *J. Dent. Res.* 93, 651–656. doi: 10.1177/0022034514534444

Marazita, M. L. (2019). *OFC4: Genetics of Orofacial Clefts and Related Phenotypes*. Bethesda, MD: FaceBase Consortium.

Mukhopadhyay, N., Bishop, M., Mortillo, M., Chopra, P., Hetmanski, J. B., Taub, M. A., et al. (2020). Whole genome sequencing of orofacial cleft trios from the Gabriella Miller Kids First Pediatric Research Consortium identifies a new locus on chromosome 21. *Hum. Genet.* 139, 215–226. doi: 10.1007/s00439-019-02099-1

Murray, T., Taub, M. A., Ruczinski, I., Scott, A. F., Hetmanski, J. B., Schwender, H., et al. (2012). Examining markers in 8q24 to explain differences in evidence for association with cleft lip with/without cleft palate between Asians and Europeans. *Genet. Epidemiol.* 36, 392–399. doi: 10.1002/gepi.21633

Naros, A., Brocks, A., Kluba, S., Reinert, S., and Krimmel, M. (2018). Health-related quality of life in cleft lip and/or palate patients - a cross-sectional study from preschool age until adolescence. *J. Craniomaxillofac. Surg.* 46, 1758–1763. doi: 10.1016/j.jcms.2018.07.004

Nidey, N., Moreno Uribe, L. M., Marazita, M. M., and Wehby, G. L. (2016). Psychosocial well-being of parents of children with oral clefts. *Child Care Health Dev.* 42, 42–50. doi: 10.1111/cch.12276

Nidey, N., and Wehby, G. (2019). Barriers to health care for children with orofacial clefts: a systematic literature review and recommendations for research priorities. *Oral Health Dental Stud.* 2:2.

Taioli, E., Ragin, C., Robertson, L., Linkov, F., Thurman, N. E., and Vieira, A. R. (2010). Cleft lip and palate in family members of cancer survivors. *Cancer Invest.* 28, 958–962. doi: 10.3109/07357907.2010.483510

van Rooij, I. A., Ludwig, K. U., Welzenbach, J., Ishorst, N., Thonissen, M., Galesloot, T. E., et al. (2019). Non-syndromic cleft lip with or without cleft palate: genome-wide association study in europeans identifies a suggestive risk locus at 16p12.1 and supports SH3PXD2A as a clefting susceptibility gene. *Genes* 10:1023. doi: 10.3390/genes10121023

Wehby, G. L., and Cassell, C. H. (2010). The impact of orofacial clefts on quality of life and healthcare use and costs. *Oral Dis.* 16, 3–10. doi: 10.1111/j.1601-0825.2009.01588.x

Wilderman, A., VanOudenhove, J., Kron, J., Noonan, J. P., and Cotney, J. (2018). High-resolution epigenomic atlas of human embryonic craniofacial development. *Cell Rep.* 23, 1581–1597. doi: 10.1016/j.celrep.2018.03.12

Yu, Y., Zuo, X., He, M., Gao, J., Fu, Y., Qin, C., et al. (2017). Genome-wide analyses of non-syndromic cleft lip with palate identify 14 novel loci and genetic heterogeneity. *Nat. Commun.* 8:14364. doi: 10.1038/ncomms14364

Conflict of Interest: The authors declare that the research was conducted in the absence of any commercial or financial relationships that could be construed as a potential conflict of interest.

frontiers in Cell and Developmental Biology

ORIGINAL RESEARCH
published: 16 April 2021
doi: 10.3389/fcell.2021.621018

Detecting Gene-Environment Interaction for Maternal Exposures Using Case-Parent Trios Ascertained Through a Case With Non-Syndromic Orofacial Cleft

Wanying Zhang[1†], Sowmya Venkataraghavan[1†], Jacqueline B. Hetmanski[1], Elizabeth J. Leslie[2], Mary L. Marazita[3,4], Eleanor Feingold[4], Seth M. Weinberg[3,4], Ingo Ruczinski[5], Margaret A. Taub[5], Alan F. Scott[6], Debashree Ray[1] and Terri H. Beaty[1]**

[1] Department of Epidemiology, School of Public Health, Johns Hopkins University, Baltimore, MD, United States, [2] Department of Human Genetics, School of Medicine, Emory University, Atlanta, GA, United States, [3] Center for Craniofacial and Dental Genetics, Department of Oral and Craniofacial Sciences, School of Dental Medicine and Clinical and Translational Science, School of Medicine, University of Pittsburgh, Pittsburgh, PA, United States, [4] Department of Human Genetics, Graduate School of Public Health, University of Pittsburgh, Pittsburgh, PA, United States, [5] Department of Biostatistics, School of Public Health, Johns Hopkins University, Baltimore, MD, United States, [6] Department of Genetic Medicine, School of Medicine, Johns Hopkins University, Baltimore, MD, United States

Two large studies of case–parent trios ascertained through a proband with a non-syndromic orofacial cleft (OFC, which includes cleft lip and palate, cleft lip alone, or cleft palate alone) were used to test for possible gene–environment (G × E) interaction between genome-wide markers (both observed and imputed) and self-reported maternal exposure to smoking, alcohol consumption, and multivitamin supplementation during pregnancy. The parent studies were as follows: GENEVA, which included 1,939 case–parent trios recruited largely through treatment centers in Europe, the United States, and Asia, and 1,443 case–parent trios from the Pittsburgh Orofacial Cleft Study (POFC) also ascertained through a proband with an OFC including three major racial/ethnic groups (European, Asian, and Latin American). Exposure rates to these environmental risk factors (maternal smoking, alcohol consumption, and multivitamin supplementation) varied across studies and among racial/ethnic groups, creating substantial differences in power to detect G × E interaction, but the trio design should minimize spurious results due to population stratification. The GENEVA and POFC studies were analyzed separately, and a meta-analysis was conducted across both studies to test for G × E interaction using the 2 df test of gene and G × E interaction and the 1 df test for G × E interaction alone. The 2 df test confirmed effects for several recognized risk genes, suggesting modest G × E effects. This analysis did reveal suggestive evidence for G × Vitamin interaction for *CASP9* on 1p36 located about 3 Mb from *PAX7*, a recognized risk gene. Several regions gave suggestive evidence of G × E interaction in the 1 df test. For example, for G × Smoking interaction, the

OPEN ACCESS

Edited by:
Ricardo D. Coletta, University of Campinas, Brazil

Reviewed by:
Michele Rubini, University of Ferrara, Italy
Renato Assis Machado, University of Campinas, Brazil

***Correspondence:**
Debashree Ray
dray@jhu.edu
Terri H. Beaty
tbeaty1@jhu.edu

† These authors have contributed equally to this work and share first authorship

Specialty section:
This article was submitted to Molecular Medicine, a section of the journal Frontiers in Cell and Developmental Biology

Received: *24 October 2020*
Accepted: *15 March 2021*
Published: *16 April 2021*

Citation:
Zhang W, Venkataraghavan S, Hetmanski JB, Leslie EJ, Marazita ML, Feingold E, Weinberg SM, Ruczinski I, Taub MA, Scott AF, Ray D and Beaty TH (2021) Detecting Gene-Environment Interaction for Maternal Exposures Using Case-Parent Trios Ascertained Through a Case With Non-Syndromic Orofacial Cleft. Front. Cell Dev. Biol. 9:621018. doi: 10.3389/fcell.2021.621018

1 df test suggested markers in *MUSK* on 9q31.3 from meta-analysis. Markers near *SLCO3A1* also showed suggestive evidence in the 1 df test for G × Alcohol interaction, and rs41117 near *RETREG1* (a.k.a. *FAM134B*) also gave suggestive significance in the meta-analysis of the 1 df test for G × Vitamin interaction. While it remains quite difficult to obtain definitive evidence for G × E interaction in genome-wide studies, perhaps due to small effect sizes of individual genes combined with low exposure rates, this analysis of two large case–parent trio studies argues for considering possible G × E interaction in any comprehensive study of complex and heterogeneous disorders such as OFC.

Keywords: orofacial clefts, oral clefts, gene-environment interaction, case-parent trio design, genome-wide association study, maternal smoking, maternal vitamin supplementation

INTRODUCTION

Orofacial clefts (OFCs) are the most common craniofacial malformations in humans, affecting approximately one per 1,000 live births (Mai et al., 2014). OFCs are commonly categorized into two anatomically and embryologically distinct entities: cleft lip with or without cleft palate (CL/P) and cleft palate alone (CP) (Jiang et al., 2006). Among all infants born with an OFC, 70% of CL/P cases and 50% of CP cases occur as isolated, non-syndromic malformations (Shi et al., 2008). Non-syndromic CL/P occurs more frequently in males than females (2:1) whereas non-syndromic CP occurs more often in females (Mossey et al., 2009). Substantial variation in birth prevalence rates of non-syndromic CL/P has been reported across populations: Asian populations have higher birth prevalence rates compared to those of European descent (Dixon et al., 2011) and African populations have the lowest birth prevalence rates (Mossey et al., 2009). Compared to CL/P, non-syndromic CP shows less variability in birth prevalence rates across populations (Genisca et al., 2009; Beaty et al., 2011). Due to the high overall birth prevalence rate and the large financial, medical, and emotional burden of treatment required by children with an OFC, understanding the etiology of OFCs is an important public health goal.

Genome-wide association studies (GWAS) using both case–control (Birnbaum et al., 2009; Mangold et al., 2010) and case–parent trio designs (Beaty et al., 2010, 2011, 2013; Leslie et al., 2016a) have identified multiple genetic risk factors for OFCs. There have been multiple GWAS for CL/P (Birnbaum et al., 2009; Grant et al., 2009; Beaty et al., 2010; Mangold et al., 2010; Camargo et al., 2012; Sun et al., 2015; Wolf et al., 2015; Leslie et al., 2016a; Yu et al., 2017; Butali et al., 2019; Huang et al., 2019), two genome-wide meta-analysis of CL/P (Ludwig et al., 2012; Leslie et al., 2017), and four GWAS of CP (Beaty et al., 2011; Leslie et al., 2016b; Butali et al., 2019; He et al., 2020). These studies have revealed a complex genetic architecture controlling risk to OFCs. More than 40 different genes or regions have yielded genome-wide significant associations with risk to CL/P from multiple populations, while one gene (*GRHL3*) has been clearly identified as associated with risk to CP [largely limited to populations of European ancestry (Leslie et al., 2016b)]. A recent case–control study of Han Chinese CP cases and controls also identified the region on chromosome 15q24.3 as associated with risk of CP (He et al., 2020). Of these recognized risk genes achieving genome-wide significance, four regions (*IRF6* on 1q32-41, the gene desert on 8q24, markers on 10q25.3 and on 17q22) can explain about a quarter of the estimated heritability in risk to CL/P based on twin and family studies (Beaty et al., 2016; Lupo et al., 2019), which has been estimated to be around 90% for both CL/P and CP based on twin registry data in European populations (Grosen et al., 2011). Thus, additional genetic risk factors likely remain to be identified.

In addition to a strong genetic component to risk for OFCs, several environmental risk factors contribute to its etiology. For example, maternal smoking (Honein et al., 2014), passive exposure to cigarette smoke (Kummet et al., 2016), and binge alcohol consumption (Romitti et al., 2007) have been reported to significantly increase risk of OFCs, while multivitamin supplementation appears to play a protective role (Johnson and Little, 2008). Whenever there is some effect of an environmental risk factor, it is important to test for potential gene–environment (G × E) interaction, where the joint risk of exposure and a genetic risk factor may become more important than predicted by the respective marginal effects of the gene or the exposure. While it is quite difficult to prove the existence of G × E interaction based on statistical evidence alone (Aschard, 2016), there are some examples of possible G × E interactions relevant to OFCs. For example, variants in the *GRID2* and *ELAVL2* genes showed evidence of G × E interaction with maternal smoking in influencing the risk of CL/P among mothers of European ancestry (Beaty et al., 2013). A Brazilian sample of case–parent trios yielded suggestive evidence for G × E interaction between a marker in *RAD51*, a DNA repair gene, and risk of CL/P (Machado et al., 2016). Moreover, variants in *SMC2* on chromosome 9 appeared to increase the risk of CP in the presence of maternal drinking, while variants in *BAALC* on chromosome 8 appeared to reduce risk of CP in the presence of multivitamin supplementation (Beaty et al., 2011). Although it has been widely acknowledged OFCs result from a complex interplay of genetic and environmental risk factors, specific evidence for G × E interaction remains tentative at best.

In this paper, we used a trio-based design to explore possible G × E interaction effects using two large multi-ethnic studies of case–parent trios: the Gene, Environment Association (GENEVA) consortium and case–parent trios drawn from the Pittsburgh Orofacial Cleft (POFC) study. Both studies have genome-wide marker data available and additional markers were

imputed against the same reference panel (1000G phase 3 v5). The case–parent trio design provides a unique advantage when analyzing samples from distinct populations for a relatively rare disorder. Unlike a cohort study with randomly ascertained individuals or the more conventional case–control study design, the case–parent trio design is robust to spurious signals arising from population stratification (a form of confounding due to differences in marker allele frequencies and disease risk across genetically distinct sub-populations), which can occur whenever samples from multiple populations are combined. We used the genotypic transmission disequilibrium test (gTDT) to test for possible G × E interactions considering three common maternal exposures (maternal smoking, maternal alcohol consumption, and maternal vitamin supplementation in the 3 months before conception through the first trimester).

MATERIALS AND METHODS

GENEVA Study Samples

The samples in the GENEVA consortium include case–parent trios from multiple populations combined in a GWAS of non-syndromic OFC. Case–parent trios were recruited largely through surgical treatment centers by multiple investigators from Europe (Norway), the United States (Iowa, Maryland, Pennsylvania, and Utah) and Asia (People's Republic of China, Taiwan, South Korea, Singapore, and the Philippines) (Beaty et al., 2010, 2011; Leslie et al., 2017). Phenotypes (e.g., type of cleft), sex, race, as well as common environmental risk factors [e.g., maternal smoking, environmental tobacco smoke (ETS), multivitamin supplementation, and alcohol consumption during the periconceptual period] were obtained through direct maternal interview (Beaty et al., 2010, 2011). The research protocol was approved by the Institutional Review Boards (IRBs) at the Johns Hopkins Bloomberg School of Public Health and at each participating recruitment site. Written informed consent was obtained from both parents, and assent from the case was solicited whenever the child was old enough to understand the purpose of the study. Originally, 412 individuals from POFC were included in GENEVA (Leslie et al., 2016a) and these duplicated samples were subsequently removed from the GENEVA samples used here, so these GENEVA and POFC trios represent independent, non-overlapping case–parent trios from three major racial/ethnic groups (European, Asian, and Latin American).

POFC Study Samples

The POFC study included case–parent trios ascertained through a proband with an isolated CL/P or CP from multiple populations and a large number of OFC cases and ethnically matched controls from some of these same populations (Leslie et al., 2016a, 2017). However, in this analysis, only unrelated case–parent trios from POFC were used. The distribution of trios by cleft subtype (CL/P and CP) and racial/ethnic groups from both studies is given in **Table 1**.

Similar to the GENEVA study, the three environmental risk factors (e.g., maternal smoking, multivitamin supplementation, and alcohol consumption during the 3 months before conception and for each trimester of pregnancy) were obtained through direct maternal interview. Exposure to ETS, however, was not available in the POFC data. The research protocol was approved by the IRBs at the University of Pittsburgh and all participating institutions, and informed consent was obtained from all participants.

Genotyping and Imputation

In the GENEVA study, DNA was genotyped at the Center for Inherited Disease Research[1] on the Illumina Human610 Quadv1_B array, which includes 589,945 SNPs through the NHGRI GENEVA program and submitted to dbGaP ([2]accession number phs000094.v2.p1). To take advantage of more efficient imputation tools and larger reference panels, we re-imputed genotypes on the GENEVA dataset using the Michigan Imputation Server (Das et al., 2016) after dropping very low frequency SNPs (i.e., those with minor allele frequency or MAF < 0.01) and phasing haplotypes from the observed genotypes using SHAPEIT (Delaneau et al., 2011) while considering family structure (Taub et al., 2012). This imputation tool provides an efficient computation with comparable accuracy to traditional imputation tools (e.g., IMPUTE2). The reference panel was "1000G phase 3 v5" as used on POFC data. For quality control purposes, all genotyped SNPs with missingness $> 5\%$, Mendelian error rate $> 5\%$, those having a MAF $< 5\%$, as well as SNPs showing deviation from Hardy-Weinberg equilibrium (HWE) at $p < 10^{-4}$ among parents were dropped, following the procedures used with POFC (Carlson et al., 2017; Leslie et al., 2017). All imputed SNPs were filtered to exclude any with an $R^2 < 0.3$ with BCFtools-v1.9[3]. Additionally, individuals with low-quality DNA, individuals with SNP missingness $> 10\%$, and individuals duplicated across the POFC and GENEVA datasets were removed. Only complete trios were kept for the final analysis. The final GENEVA dataset contained 6,762,077 SNPs (including both observed and imputed SNPs with MAF $> 5\%$ among parents) for 1,939 complete case–parent trios (including 1,126 Asian and 778 European trios).

The case–parent trios from the POFC study were genotyped for 539,473 SNPs using the Illumina HumanCore + Exome array (available through dbGAP accession number phs000774.v2.p1), and similar quality control filtering was used to remove rare and poor-quality SNPs. Genomic coordinates were given in human genome build 37 (hg19). Genotype data were pre-phased with SHAPEIT taking family structure into account (Taub et al., 2012) and then imputed with IMPUTE2 using the 1000 Genomes Phase 3 reference panel as described previously (Leslie et al., 2016a). Incomplete trios, trios with parents from different racial/ethnic groups and ethnic groups with insufficient sample sizes for effective imputation were dropped from the analyses. The final POFC trio dataset analyzed here contained 6,350,243 SNPs (including both observed and imputed SNPs with MAF $> 5\%$

[1]CIDR.jhmi.edu

[2]www.ncbi.nlm.nih.gov/gap

[3]https://samtools.github.io/bcftools

TABLE 1 | Number of case–parent trios in the GENEVA and the POFC studies stratified by type of cleft (CL/P and CP) and racial/ethnic group (European, Asian, and Latin American).

			All CL/P	Euro. CL/P	Asian CL/P	All CP	Euro. CP	Asian CP	Latin Am. CL/P	Latin Am. CP
GENEVA Study										
Trios before individual filtering [1]			1591	668	895	466	215	237		
Trios after individual filtering [2]			1487	575	891	452	203	235		
Exposure	Environ. tobacco smoke	Trios [3]	1254	454	784	403	158	232		
		Exposed trios	370 (30%)	64 (14%)	300 (38%)	116 (29%)	22 (14%)	94 (41%)		
	Maternal Smoking	Trios [3]	1485	573	891	452	203	235		
		Exposed trios	208 (14%)	179 (31%)	26 (3%)	65 (14%)	57 (28%)	7 (3%)		
	Multivitamin	Trios [3]	1258	486	752	397	180	205		
		Exposed trios	430 (34%)	287 (59%)	131 (17%)	170 (43%)	111 (62%)	49 (24%)		
	Alcohol	Trios [3]	1474	573	880	449	202	233		
		Exposed trios	249 (17%)	227 (40%)	19 (2%)	94 (21%)	83 (41%)	9 (4%)		
POFC Study										
Trios before individual filtering [1]			1319	406	284	165	93	38	601	29
Trios after individual filtering [2]			1284	403	284	159	93	38	597	28
Exposure	Environ. tobacco smoke	Trios								
		Exposed trios								
	Maternal Smoking	Trios [3]	953	339	127	120	81	13	487	26
		Exposed trios	155 (16%)	70 (21%)	8 (6%)	18 (15%)	15 (19%)	1 (8%)	77 (16%)	2 (8%)
	Multivitamin	Trios [3]	770	249	127	94	74	14	394	6
		Exposed trios	565 (73%)	208 (84%)	100 (79%)	71 (76%)	55 (74%)	13 (93%)	257 (65%)	3 (50%)
	Alcohol	Trio [3]	860	249	127	115	76	13	484	26
		Exposed trios	195 (23%)	91 (37%)	10 (8%)	29 (25%)	18 (24%)	2 (15%)	94 (19%)	9 (35%)

[1]*Number of complete trios in the original GENEVA/POFC dataset.*
[2]*Number of complete trios after quality control.*
[3]*Number of complete trios after excluding those with missing information on maternal exposure.*

among parents) for 1,443 complete case–parent trios (including 322 Asian, 625 Latin American, and 496 European trios).

Statistical Analysis

Because larger sample sizes are required to detect G × E interaction effects compared to the marginal effects of genes alone (Aschard, 2016), here we deliberately combined case–parent trios from all recruitment sites within each study and pooled both of the major subgroups of OFC (i.e., CL/P and CP) to maximize sample size. Our goal in pooling is not to identify G × E effects specific to one cleft subgroup but to identify G × E effects present in one or both subgroups. Thus, findings of G × E effects in our "all OFC" group should be interpreted as such. It is worth noting that pooling CL/P and CP trios increases the chance of missing signals when true interaction effects exist only in one cleft subgroup (i.e., increased false negatives or reduced power) but does *not* result in spurious findings (i.e., unchanged false positives or controlled type I error). However, reduced power due to genetic heterogeneity is counter-balanced by improved power due to increased sample size when genetic sharing between CL/P and CP exists (Leslie et al., 2017; Carlson et al., 2019; Ray et al., 2020).

For our G × E interaction analyses, we considered three self-reported maternal exposures: maternal smoking, alcohol consumption, and multivitamin supplementation. Note that ETS was not available in both GENEVA and POFC, and hence not studied in this analysis. We used the gTDT in the R *trio* package (Schwender et al., 2014) for this case–parent trio study to test the null hypothesis of independence between each common SNP and no interaction with these environmental risk factors. Closed-form solutions were used to estimate the regression coefficients and their respective standard errors under a conditional logistic regression model for different genetic models (recessive, dominant, or additive) while allowing efficient implementation on a genome-wide scale (Schwender et al., 2012). The *trio* package (v3.20.0[4]) was used on common SNPs in the combined set of all OFC trios from GENEVA and POFC separately. For a common bi-allelic marker, a conditional logistic model can be used to test the null hypothesis of independence between each common SNP and disease (or equivalently, the composite null hypothesis of no linkage *or* no association between a SNP and an unobserved causal variant). In this article, we assume an additive genetic model and consider the conditional logistic model that models the association between each common SNP and its interaction with a maternal exposure and OFC:

$$P\left(Y_0 = 1 \,\middle|\, \{\textstyle\sum_{l=0}^{3} Y_l = 1\},\ \{G_0, G_1, G_2, G_3\}, E\right) = \frac{e^{\beta_G * G_0 + \beta_{GE} * G_0 * E}}{\sum_{l=0}^{3} e^{\beta_G * G_l + \beta_{GE} * G_l * E}}$$

where Y_0 is the disease status of the child (taking the value 1 for the observed child in a case–parent trio study); Y_l is the disease status of the lth pseudo-control (taking value 0 for all pseudo-controls, $l = 1, 2, 3$); G_0 is the genotype of the child (case) at the marker coded additively as 0, 1, or 2; G_l is the genotype of the lth pseudo-control at this same marker; and E is a binary environmental variable denoting presence/absence of a maternal exposure during pregnancy. Basically, G_1, G_2, and G_3 represent possible SNP genotypes the observed case did not inherit from the parents. We first performed a 2 df χ^2 test of the null hypothesis $H_0 : \beta_G = 0,\ \beta_{GE} = 0$ to identify markers with either a main effect, or a G × E interaction effect, or both. To focus exclusively on G × E interaction between a marker and a maternal exposure, we conducted a 1 df χ^2 test of the null hypothesis $H_0^{(GE)} : \beta_{GE} = 0$ within each dataset.

Finally, we conducted a combined analysis of the GENEVA and the POFC studies using inverse-variance weighted fixed effect meta-analysis. The closed form solutions of the coefficients and their standard errors from the gTDT model discussed above enable computationally efficient genome-wide meta-analysis across both studies. In particular, for the 1 df G × E interaction test, if $\widehat{\beta}_{GE,1}$ and $\widehat{\beta}_{GE,2}$ represent the G × E coefficient estimates from the two studies, and $\widehat{SE}_{GE,1}$ and $\widehat{SE}_{GE,2}$ are their respective estimated standard errors (all of which are output from the *trio* package), then the overall meta-analyzed estimates are $\widehat{\beta}_{GE} = \frac{\sum_{i=1,2} \widehat{\beta}_{GE,i}\omega_i}{\sum_{i=1,2}\omega_i}$ and $\widehat{SE}_{GE} = \sqrt{\frac{1}{\sum_{i=1,2}\omega_i}}$, where $\omega_i = \frac{1}{\widehat{SE}^2_{GE,i}}$ for $i = 1, 2$. We calculated these meta-analyzed estimates $\widehat{\beta}_{GE}$ and $\widehat{SE}_{GE}$ using the R package *meta* (v4.13.0) (Balduzzi et al., 2019) and applied a 1 df χ^2 test of the null hypothesis $H_0^{(GE)} : \beta_{GE} = 0$ for each marker and three maternal exposures (smoking, alcohol consumption, and multivitamin supplementation). To account for multiple comparisons in this genome-wide analysis, we used the conventional threshold of 5×10^{-8} to declare genome-wide significance but also investigated SNPs yielding only suggestive evidence of G × E interaction effects ($p < 10^{-6}$). For the 2 df G × E interaction test, we meta-analyzed using the approach described in Manning et al. (2011). Specifically, we implemented the 2 df χ^2 test of $H_0 : \beta_G = 0,\ \beta_{GE} = 0$ by jointly meta-analyzing estimates $\widehat{\beta}_{G,1}$, $\widehat{\beta}_{GE,1}$, $\widehat{\beta}_{G,2}$, $\widehat{\beta}_{GE,2}$, $\widehat{SE}_{G,1}$, $\widehat{SE}_{GE,1}$, $\widehat{SE}_{G,2}$, and $\widehat{SE}_{GE,2}$ across these two studies using 6,761,961 SNPs including those present in both datasets and those unique to one dataset if the allele calls and position were consistent. Our R code for this 2 df joint meta-analysis of main and interaction effects can be found at https://github.com/RayDebashree/GxE.

Manhattan plots and QQ plots were created for each analysis to show signals and to check for potential bias in the test statistic, respectively (Taub et al., 2012). The genomic inflation factors (λ) were calculated using the "estlambda" function with the "median" option from the GenABEL R package v1.8-0 (Aulchenko et al., 2007). SNPs achieving significance from the gTDT analyses were annotated with an online tool SNPnexus[5] (Dayem Ullah et al., 2012) to identify potentially important genes. Regional association plots generated using LocusZoom[6] (Pruim et al., 2010) were used to examine

[4]https://bioconductor.org/packages/release/bioc/html/trio.html

[5]https://snp-nexus.org

[6]http://locuszoom.org/

detailed evidence of association for each region achieving or approaching genome-wide significance under an additive model in the combined meta-analysis. For these LocusZoom plots, we used genome build hg19 with no specified linkage disequilibrium (LD) reference panel due to the multi-ethnic nature of these two datasets.

RESULTS

Meta-Analysis of G and G × E Interaction Effects in the 2 df Test

It has been suggested the 2 df joint test for gene (G) and G × E interaction could provide more power to detect genes influencing risk to complex and heterogeneous diseases when there is any possibility of G × E interaction (Kraft et al., 2007). **Figure 1** shows the Manhattan plot from a meta-analysis across both studies of this joint 2 df test for all three available exposures for all OFC case–parent trios (corresponding QQ plots for this 2 df test are shown in **Supplementary Figure 1**). Clearly, the multiple recognized risk genes/regions yielding strong evidence of linkage and association for CL/P dominate the statistical results shown in **Figure 1**. These different peaks represent recognized risk genes for CL/P (e.g., *PAX7* on 1p36, *ABCA4* on 1p22, *IRF6* on 1q32, *DCAF4L2* on 8q21, the 8q24 gene desert region, *VAX1* on 10q25.3, *NTN1* on 17p13.1, and *MAFB* on 20q12). This meta-analysis does show recognized risk genes for OFCs are not obscured in this 2 df joint test of G and G × E interaction.

There are some differences among these results from meta-analysis across the three exposures considered (i.e., across panels A–C in **Figure 1**), and their differences must arise from the estimated G × E interaction parameter (β_{GE}). For example, the signal for SNPs near *PAX7* on 1p36 almost achieved genome-wide significance for the joint test of G and G × Smoking (**Figure 1A**) where the top SNP (rs7541797) gave $p = 5.5 \times 10^{-8}$ in the 2 df test, but was less significant when G and G × Alcohol ($p = 3.4 \times 10^{-6}$) and when G and G × Vitamin ($p = 8.6 \times 10^{-6}$) were analyzed in this joint test (**Figures 1B,C**). In fact, this peak on 1p36 was joined by a second peak 3.2 Mb telomeric of *PAX7* that encompassed *CASP9* in the 2 df test for G and G × Vitamin interaction, sufficient physical distance to result in very weak LD between top SNPs in these two genes (all $r^2 < 0.1$). Specifically, SNP rs4646022 yielded suggestive significance for G and G × Vitamin interaction in this 2 df test ($p = 3.1 \times 10^{-7}$). **Figure 2** shows the region of 1p36 encompassing *CASP9* and *PAX7* for the 2 df joint test of G and G × E interaction for each of the three maternal exposures. **Figures 2A,B** show a clear peak near *PAX7* and virtually no signal in the region of *CASP9* (n.b. the peak SNP from the 2 df test for G and G × Smoking interaction is noted by the red dot, while the blue dot represents SNP rs4646022). **Figure 2C** where G and G × Vitamin interaction was considered, however, shows considerable support against the null hypothesis for both genes although multiple genes are located within this region around *CASP9*.

Meta-Analysis of the 1 df Test for Maternal Smoking Interaction

To focus explicitly on tests of G × E interaction, we used the 1 df test for H_0:$\beta_{GE} = 0$ over all SNPs (observed and imputed) in a similar meta-analysis over both the GENEVA and the POFC studies (**Figure 3A** with the corresponding QQ plot in **Supplementary Figure 2A**). While no SNPs achieved formal genome-wide significance in this meta-analysis, several genes did yield suggestive evidence (with $p < 10^{-6}$) of possible G × Smoking interaction and may warrant further exploration. **Table 2** lists the most significant SNPs (and their nearest genes) for each region showing suggestive evidence in the meta-analysis, noting which allele was the effect allele, along with its corresponding estimated relative risk (RR) of G × E interaction, 95% confidence interval (CI), *p* value, and frequency in each racial/ethnic group. **Figure 4** shows the RR estimates and their 95% CI for each of these top SNPs from the meta-analysis and from stratified analyses based on CL/P and CP groups separately. There is consistency in the estimated effect sizes and directions within each stratum, and as expected, the 95% CIs are always larger for the CP group due to their smaller sample size.

A polymorphic insertion/deletion (indel) at position 191,830,067 on 3q28-q29 near *FGF12* and an intronic SNP rs2186801 in the 9q31.3 region containing the *MUSK* (muscle associated receptor tyrosine kinase) gene both gave such suggestive evidence when testing for G × Smoking interaction. The top signal near *FGF12* is questionable, however, because nearby SNPs did not show any supporting evidence of linkage and association (see **Figure 5A**), and this polymorphic indel was only imputed in the GENEVA study with somewhat reduced quality ($R^2 = 0.84$). As indels are intrinsically more difficult to call, extreme caution should be used when interpreting suggestive evidence of possible G × Smoking interaction. Also, the frequency of the allele associated with any effect on risk showed considerable variability across racial/ethnic groups (**Table 2**). The peak on 9q31.3 is, however, more interesting where several SNPs in and near *MUSK* gave suggestive evidence. **Figure 5B** shows greater resolution for this region where multiple SNPs yielded suggestive evidence of G × Smoking interaction, and the peak SNP (rs2186801) had $p = 1.68 \times 10^{-7}$, with the G allele having an apparent protective effect on risk (**Table 2**). This imputed SNP was highly polymorphic in all racial/ethnic groups in these two datasets.

Meta-Analysis of the 1 df Test for Maternal Alcohol Consumption

Meta-analysis over the GENEVA and the POFC studies was conducted using the 1 df test for G × Alcohol interaction for all observed and imputed SNPs (**Figure 3B** with the corresponding QQ plot shown in **Supplementary Figure 2B**). Only 2 SNPs (imputed SNPs rs8031462 and rs4777824) near *SLCO3A1* on 15q26 achieved suggestive evidence of linkage and association ($p = 4.0 \times 10^{-7}$ and $p = 7.2 \times 10^{-7}$, respectively, with the former listed in **Table 2**). **Figure 5C** shows this peak region at greater resolution where multiple SNPs yielded nominal evidence of G × Alcohol interaction.

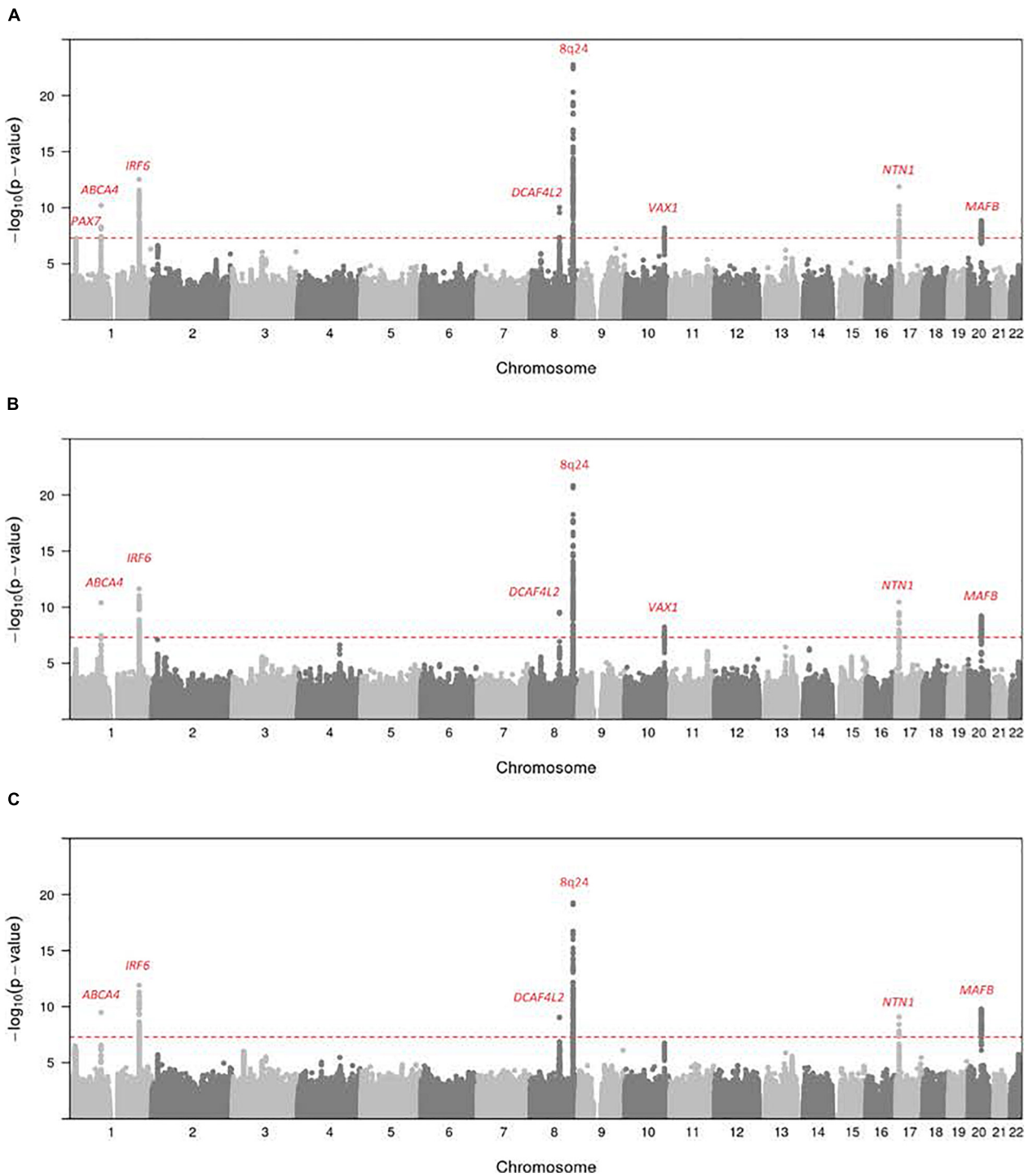

FIGURE 1 | Meta-analysis of the 2 df joint test for G and G × E interaction on all OFC case–parent trios across both the GENEVA and POFC studies. Numerous genes/regions show strong evidence of influencing risk to OFC largely through the main gene effect (β_G) with very subtle differences that could be attributed to G × E interaction effect (β_{GE}). Most of these strong signals represent recognized risk genes for CL/P. **(A)** Meta-analysis of 2 df test for G and G × Smoking interaction. **(B)** Meta-analysis of the 2 df test for G and G × Alcohol interaction. **(C)** Meta-analysis of the 2 df test for G and G × Vitamin interaction. The red dashed line represents the conventional threshold for genome-wide significance (5×10^{-8}).

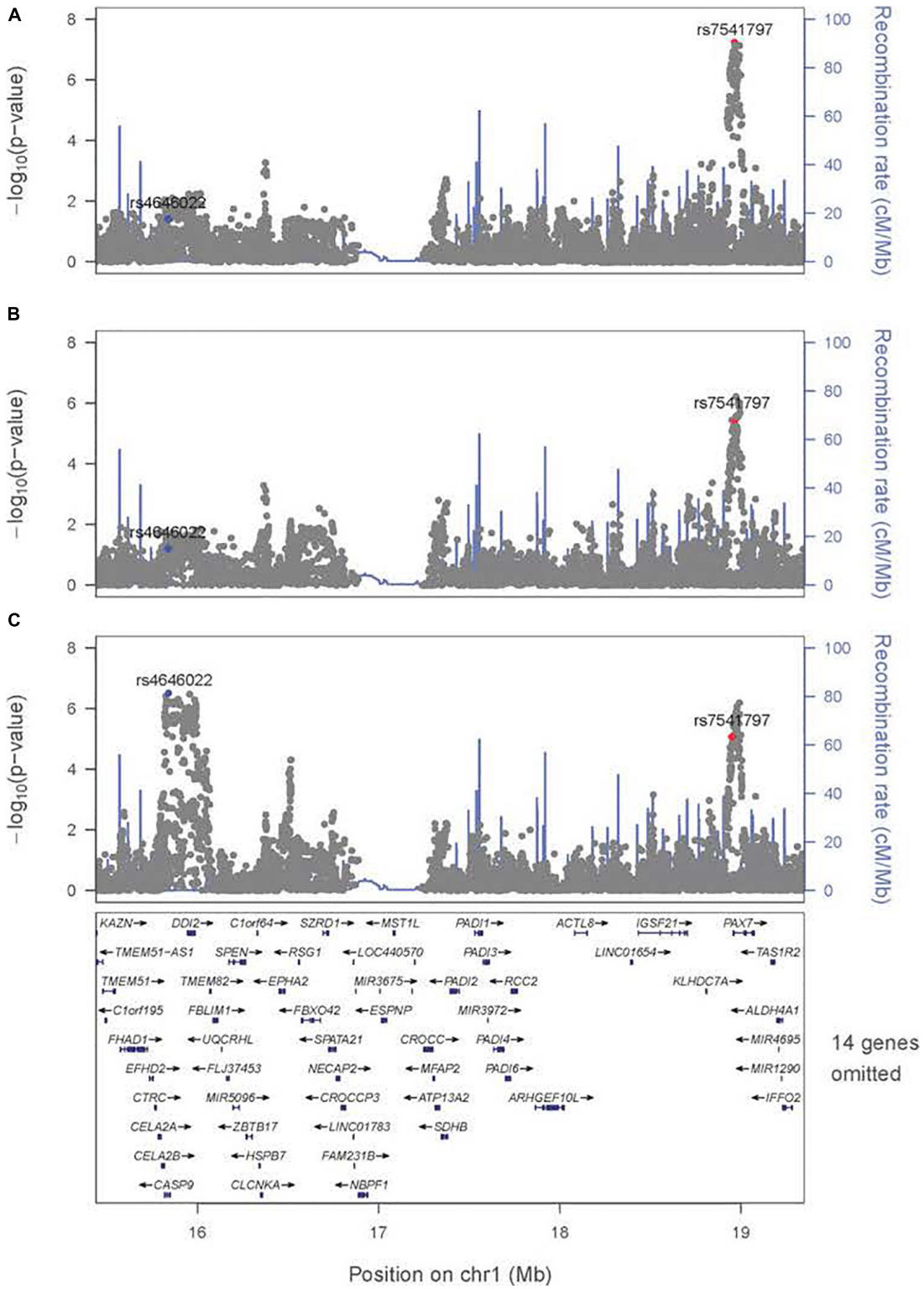

FIGURE 2 | Significance of the 2 df test considering G and G × E interaction for the region on 1p36 encompassing *CASP9* and *PAX7*. Regional association plot for the 2 df test for **(A)** G and G × Smoking interaction, **(B)** G and G × Alcohol interaction, and **(C)** G and G × Vitamin interaction. The most significant SNP (rs4646022) in the 1 df test for G × Vitamin interaction is denoted in blue; the most significant SNP (rs7541797) in the 2 df test for G and G × Smoking interaction is denoted in red.

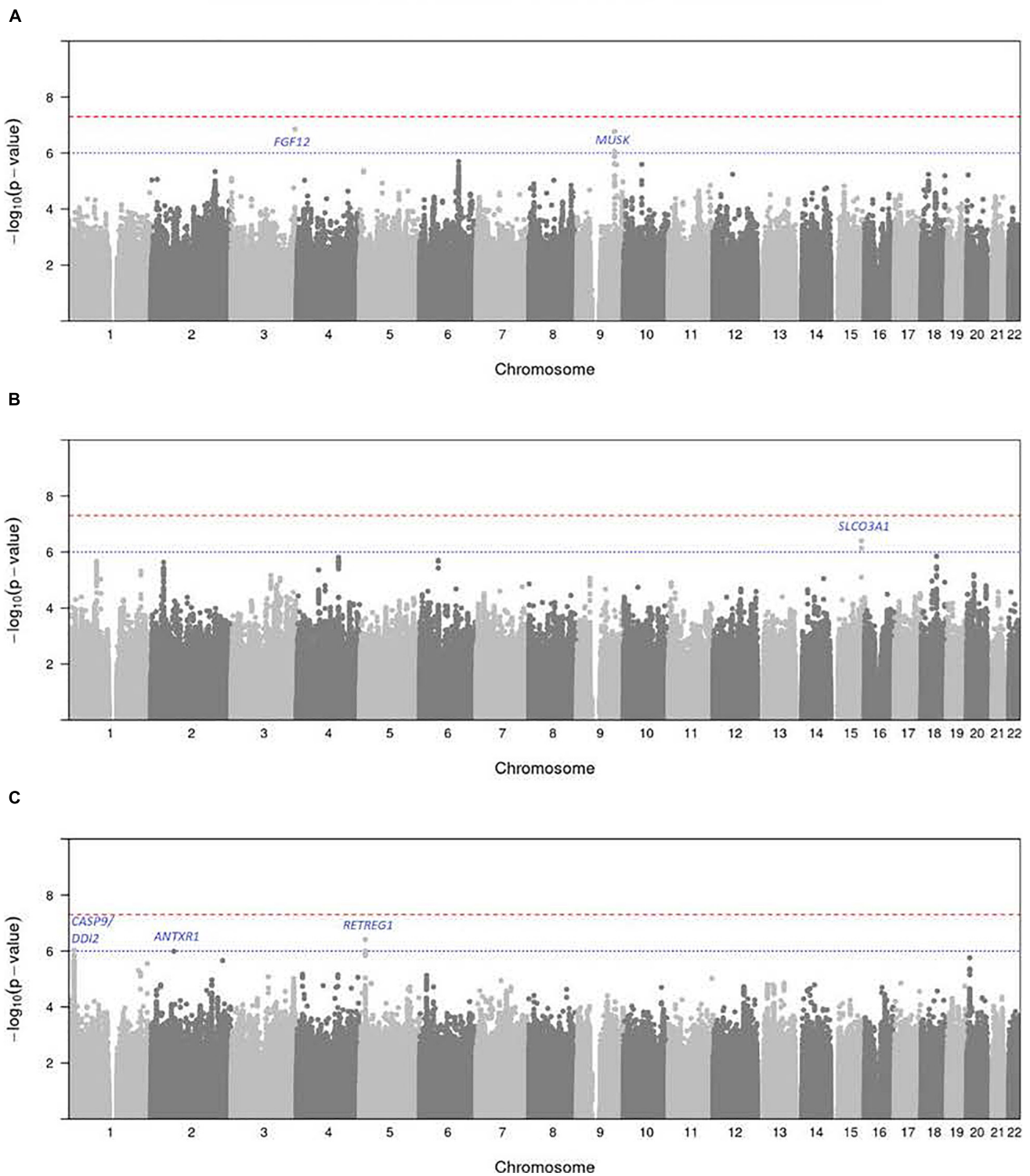

FIGURE 3 | Manhattan plots for the 1 df test for G × E interaction from meta-analysis over both GENEVA and POFC studies for **(A)** maternal smoking, **(B)** maternal alcohol consumption, and **(C)** maternal multivitamin supplementation. The red dashed line represents conventional critical value for genome-wide significance (5×10^{-8}) and the blue dotted line represents a less stringent threshold (10^{-6}) for "suggestive" evidence of G × E interaction.

TABLE 2 | Markers exceeding the threshold for "suggestive" evidence ($p < 10^{-6}$) in the 1 df test for G × E interaction from meta-analysis over GENEVA and POFC case–parent trios for all OFC.

Chr	Position	rs ID	Nearest Gene	Relative Risk [95% CI]	*p* value	Effect Allele Frequency		
						Euro.	Asian	Latin Am.
G × Smoking interaction 1 df test in meta-analysis								
3	191830067	–	*FGF12*	0.379 [0.264, 0.544]	1.37×10^{-7}	0.24	0.05	–
9	113523091	rs2186801: C:G^	*MUSK*	0.494 [0.379, 0.643]	1.68×10^{-7}	0.20	0.33	0.41
G × Alcohol interaction 1 df test in meta-analysis								
15	92737555	rs8031462: T:C^	*SLCO3A1*	1.804 [1.436, 2.267]	3.99×10^{-7}	0.48	0.17	0.42
G × Vitamin interaction 1 df test in meta-analysis								
1	15839112	rs4646022: G:A^	*CASP9*	1.807 [1.427, 2.288]	9.06×10^{-7}	0.23	0.08	0.18
5	16509183	rs41117: A:G^	*RETREG1*	1.585 [1.327, 1.894]	3.87×10^{-7}	0.39	0.63	0.41

^*Effect allele.*

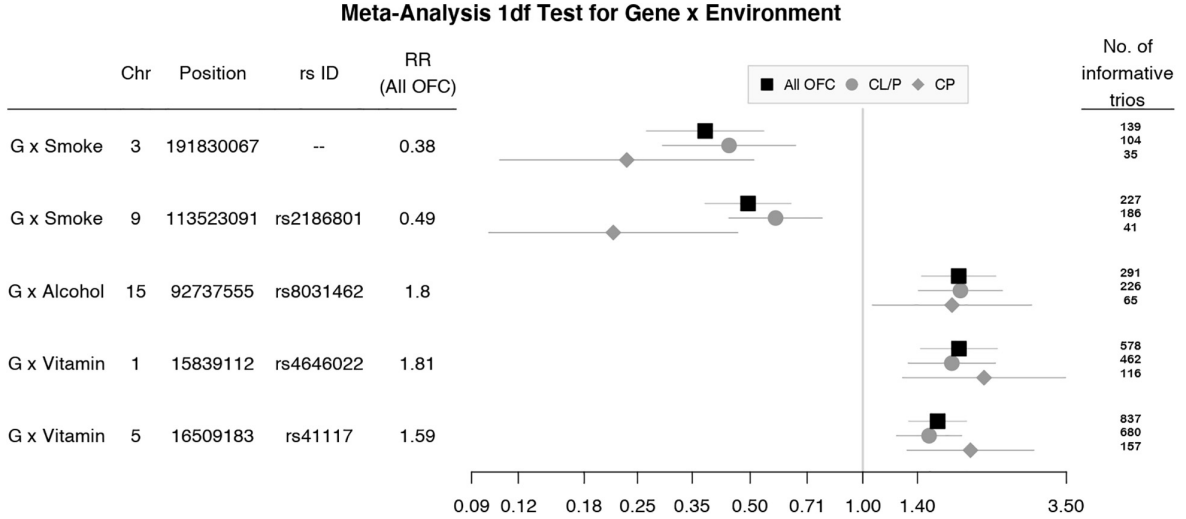

FIGURE 4 | Estimated relative risks (RR) and 95% CI for SNPs listed in **Table 2** from the 1 df test of G × E interaction in meta-analysis of all OFC trios (black squares) and stratified analysis of CL/P (gray circles) and CP trios (gray diamonds).

Meta-Analysis of the 1 df Test for Maternal Vitamin Supplementation

Meta-analysis was conducted on all OFC case–parent trios using the 1 df test for G × Vitamin interaction (**Figure 3C** with corresponding QQ plot shown in **Supplementary Figure 2C**). As seen with the 2 df test discussed above, the suggestive peak seen on 1p36 reflected SNPs near the *CASP9* gene in the meta-analysis of this 1 df test (with the same SNP rs4646022 mentioned above yielding $p = 9.06 \times 10^{-7}$ in this 1 df test for G × Vitamin interaction). **Figure 5D** shows this evidence of linkage and association around rs4646022 in greater detail and reveals a broad region of statistical signal against the null hypothesis of no G × Vitamin interaction. While many genes fall in this region, the *CASP9* gene is of interest because it has been previously associated with risk of OFC (Holzinger et al., 2017).

Also, one imputed SNP (r68079474) in *ANTXR1* on 2p13.3 approached (but did not exceed) the threshold for "suggestive" significance ($p = 1.02 \times 10^{-6}$) in this 1 df test for G × Vitamin interaction (see **Supplementary Figure 3**). Caution must be used in interpreting this observation, however, because this variant had a low frequency in all racial/ethnic groups (0.08 among parents of European ancestry, 0.04 among parents of Asian ancestry, and 0.12 among Latin American parents).

Another imputed SNP rs41117 located near *RETREG1* (a.k.a. *FAM134B*) on 5p15.1 also achieved suggestive evidence for G × Vitamin interaction in this 1 df test. **Figure 5E** shows the suggestive evidence of linkage and association around rs41117 in greater detail and **Table 2** lists its estimated effect sizes and allele frequencies in each of the major racial/ethnic groups. This imputed SNP was highly polymorphic in all groups.

DISCUSSION

While it is widely accepted that both genes and environmental risk factors influence risk to OFC, it is quite difficult to formally test for statistical interaction between the two (Aschard, 2016). Statistical interaction is defined as an observable deviation (either

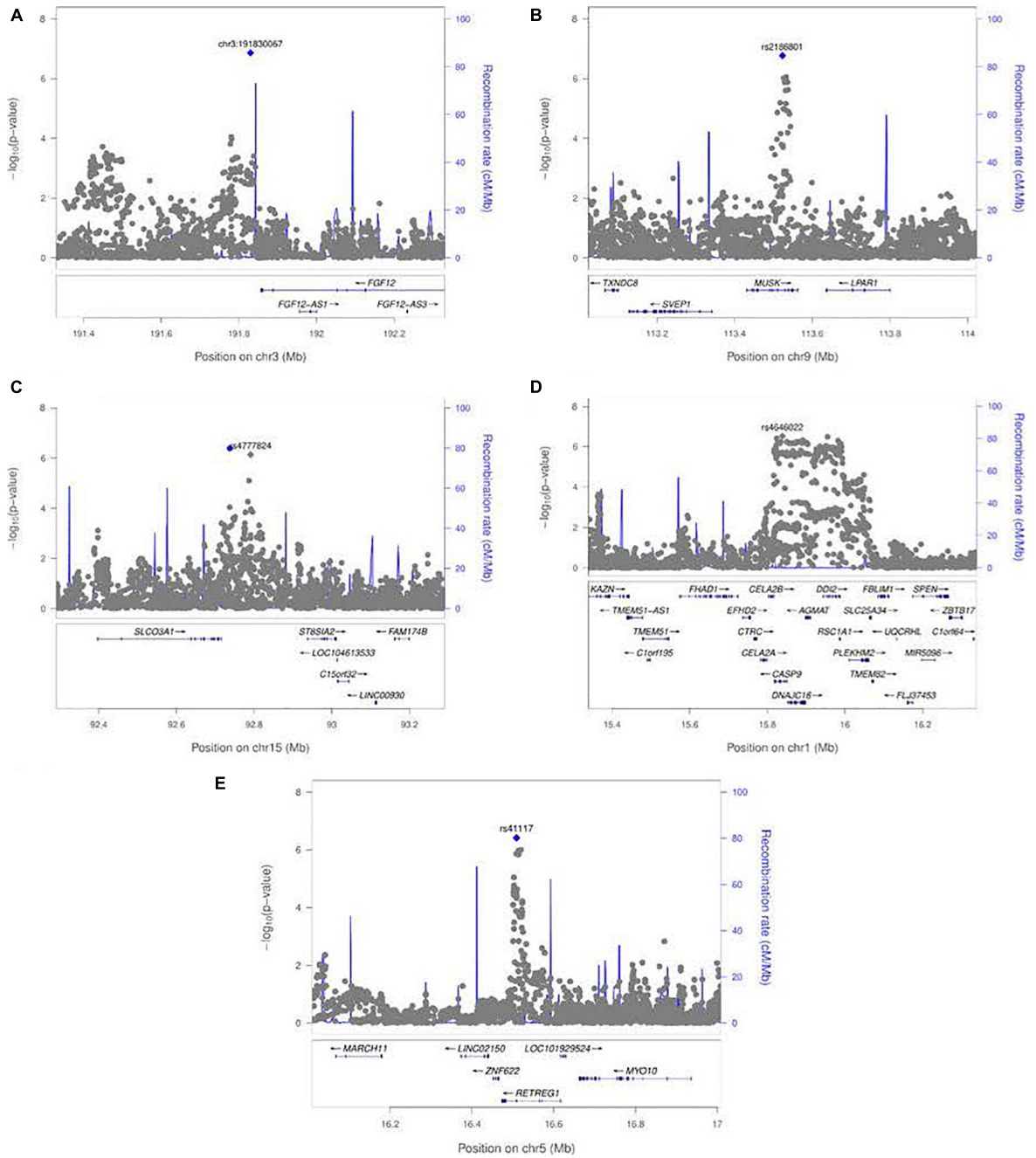

FIGURE 5 | LocusZoom plots for the 1 df test of G × E interaction between maternal exposures and SNPs near their respective peak signals from meta-analysis over both GENEVA and POFC studies. **(A)** Peak on chr. 3 near *FGF12* from the test for G × Smoking interaction shown in **Figure 3A**. **(B)** Peak on chr. 9 near *MUSK* from the test for G × Smoking interaction shown in **Figure 3A**. **(C)** Peak on chr. 15 near *SLCO3A1* from the test for G × Alcohol interaction shown in **Figure 3B**. **(D)** Peak on chr. 1 near *CASP9* for G × Vitamin interaction shown in **Figure 3C**. **(E)** Peak on chr. 5 near *RETREG1* from the test for G × Vitamin interaction shown in **Figure 3C**.

increasing or decreasing risk) from the predicted joint effect of a gene and an environmental risk factor based on their respective estimated marginal effects. Detecting G × E interaction requires larger sample sizes than necessary to estimate their respective main effects (perhaps more than is feasible to accumulate for low prevalence diseases), especially when the measure of exposure to the environmental risk factor is crude and imprecise, e.g., a simple binary classification of exposed vs. unexposed. Here, we have tried to maximize sample size by considering two large family-based studies of OFC each recruiting case–parent trios from multiple populations and pooling CL/P and CP into an all OFC group. Our findings of G × E effects in this manuscript

should be interpreted as G × E signals that may be present in one or both cleft subgroups.

This strategy to maximize sample size by pooling together all OFC subtypes carries its own risks due to the documented genetic heterogeneity between CL/P and CP; chiefly multiple different genes have been shown to influence risk for CL/P, but there are fewer recognized genetic risk factors for CP. Historically, these two subgroups of OFC have been thought to have distinct etiologies based on developmental and epidemiologic patterns. Recently, some studies reported evidence of shared genetic risk for variants in *IRF6*, *GRHL3*, and *ARHGAP29* regions (Schutte et al., 1993; Beaty et al., 2010; Liu et al., 2017a,b). Leslie et al. (2017) found that variants near *FOXE1* influenced risk of both CL/P and CP in GWAS from both the GENEVA and the POFC studies but including additional case–control subjects from POFC. There is some evidence that markers can show association with risk to CL/P and CP in opposite directions. For instance, markers near *NOG* on 17q22 have shown weak evidence of decreased risk for one OFC subgroup and increased risk for the other (Moreno Uribe et al., 2017; Carlson et al., 2019). In a parallel study, our group has explored genetic overlap between OFC subtypes using a new statistical approach, PLACO (Ray and Chatterjee, 2020). In that study, we not only found loci in/near recognized OFC genes and some novel genes exerting shared risk but also identified some genetic regions with apparently opposite effects on risk to CL/P and CP (Ray et al., 2020).

Furthermore, when we pool samples from multiple racial/ethnic groups, different populations will vary in the statistical support for different genes (due to variation in allele frequencies and underlying patterns of LD), but also just due to different exposure rates. If sub-populations differ in both their allele frequencies and their exposure rates (i.e., if the two are correlated in the combined sample), an estimation approach can be used to estimate mean exposure rates within distinct sub-populations, which may protect from spurious results in tests for G × E interaction (Shin et al., 2012). However, if the overall exposure rate is simply too low in one or more sub-populations, there will be little statistical power to estimate or test for G × E interaction, and the results from any analysis of combined samples will be dominated by those sub-populations with higher exposure rates. It would be difficult to predict specific circumstances under which countervailing effects on risk could enhance or negate evidence for marginal effects of individual genetic risk factors and their potential G × E interaction effects.

The 2 df test from the meta-analysis of all OFC case–parent trios revealed many recognized risk genes for CL/P, the predominant form of OFC in this study. Confirmed risk genes include the following: *PAX7* (1p36.13), *ABCA4* (1q22), *IRF6* (1q32.2), *DCAF4L2* (8q21.3), 8q.24 (gene desert), *VAX1* (10q25.2), *NTN1* (17p13.1), and *MAFB* (20q12). This is reassuring and argues that testing for possible G × E interaction will not conceal genetic risk factors when they do exist. Also, G × E interaction may not be an overwhelming risk factor for OFC controlled by these well-recognized risk genes.

The region on 1p36.13 includes the well-recognized risk gene *PAX7* but interestingly when G × Vitamin interaction was included in the conditional logistic model for the gTDT, a rather distinct suggestive peak becomes apparent a short physical distance from *PAX7* (see **Figure 2C**). While this peak encompasses many genes, *CASP9* (caspase 9) is of particular interest because it was previously identified as a potential risk gene for OFC based on a sequencing study of members of multiplex cleft families from Syria (Holzinger et al., 2017). In this study, a rare, non-synonymous variant in *CASP9* (predicted to be pathogenic) occurred in three homozygous family members with an OFC as well as other affected relatives who were heterozygous. *CASP9* is directly involved in an apoptotic signaling pathway shown to result in a facial cleft phenotype in mouse models (D'Amelio et al., 2010). A more recent sequencing study of Chinese cases with a neural tube defect (NTD) found more rare harmful variants in *CASP9* compared to matched controls and documented lower expression of this gene in cell culture when exposed to low folate levels (Liu et al., 2018). A recent whole exome sequencing study of two multiplex families with folate-resistant NTD showed variants in the intrinsic apoptotic pathway genes, *CASP9* and *APAF1*. These rare variants were loss-of-function changes occurring as compound heterozygous (Spellicy et al., 2018) and were approximately 1 Kb away from the rare variant reported in the multiplex cleft family (Holzinger et al., 2017). While both NTDs and OFCs are considered "mid-line birth defects" and studies have shown supplementation with folate and multivitamins can reduce risk to both (Wilson et al., 2015), it remains unknown if the same genes influence risk to both perhaps through G × E interaction.

When we focused on the 1 df test for evidence of G × E interaction alone, no markers achieved genome-wide significance, but several gave "suggestive" evidence and some of these are worthy of further consideration. Several SNPs in and near *MUSK* (muscle associated receptor tyrosine kinase) on 9p31.3 showed well-defined evidence against the null hypothesis (**Figure 5B**). The highly polymorphic SNP rs2186801 gave $p = 1.68 \times 10^{-7}$ with its G allele having an apparent protective effect on risk (**Table 2**). Mutations in *MUSK* are responsible for an autosomal recessive form of congenital myasthenic syndrome and a recessive form of fetal akinesia deformation sequence (FADS), providing support for its involvement in fetal development.

Two imputed SNPs (rs8031462 and rs4777824) near *SLCO3A1* (solute carrier organic anion transporter family member 3A1) on 15q26 yielded suggestive evidence G × Alcohol interaction (**Figure 5C**). The solute-carrier gene (SLC) superfamily encodes membrane-bound transporters and includes 55 gene families having at least 362 putatively functional protein-coding genes (He et al., 2009). These genes play an important role in transporting inorganic cations/anions (as well as vitamins) in and out of cells. There is suggestive evidence that *SLCO3A1* may be associated with nicotine dependence (Wang et al., 2012) and blood pressure through interaction with smoking (Montasser et al., 2009).

RETREG1 (reticulophagy regulator 1; a.k.a. *FAM134B*) on 5p15.1 is a *cis*-Golgi transmembrane protein, and mutations in this gene lead to the production of an impaired gene product, which is unable to act as an autophagy receptor and leads to hereditary sensory and autonomic neuropathy in humans

(HSAN IIB; OMIM 613135). This gene can also act as a tumor suppressor in colorectal adenocarcinoma and an oncogene in esophageal squamous cell carcinoma, and loss-of-function mutations can control viral replication (Islam et al., 2018).

This meta-analysis illustrates some of the strengths and challenges of searching for evidence of G × E interaction for complex and heterogeneous disorders such as OFC. Large sample sizes are needed, which inevitably result in both genetic heterogeneity and variation in exposure frequencies across subgroups. While combining the two anatomical forms of OFCs (CL/P and CP) together is unusual, it is reassuring that the estimated effect sizes in **Figure 4** were always quite similar and showed the same direction of effect for those markers giving suggestive evidence of G × E interaction, although of course the 95% CIs were larger for the smaller CP group compared to the larger CL/P group. Ideally, we would like to have precise biomarkers of exposure (e.g., maternal cotinine measured during early pregnancy) rather than crude self-reported "yes/no" measures. In future studies, epigenetic markers may prove useful to confirm exposure, but validated epigenetic markers for early *in utero* exposures are not currently available. Even in large samples such as the two used here, statistical power may be limited, and statistical evidence may not achieve conventional genome-wide thresholds. Still in this manuscript, we have presented suggestive findings that may warrant further investigation to fully understand the etiology of OFC.

DATA AVAILABILITY STATEMENT

The datasets analyzed for this study can be found in dbGaP at (www.ncbi.nlm.nih.gov/gap) through dbGaP accession number phs000094.vl.pl (GENEVA) and accession number phs000774.v2.p1 (POFC), respectively.

ETHICS STATEMENT

The studies involving human participants were reviewed and approved by the Institutional Review Boards (IRB) of each participating site, both domestic and foreign. For the GENEVA study, IRB at the Johns Hopkins Bloomberg School of Public Health and at each participating recruitment site aooroved. The research protocol for the POFC was approved by the IRB at the University of Pittsburgh and all participating institutions. Informed consent was obtained from all participants. Written informed consent to participate in this study was provided by the participants' legal guardian/next of kin for minor children.

AUTHOR CONTRIBUTIONS

WZ did the re-imputation of the GENEVA genome-wide markers and conducted the statistical analyses of this dataset. SV ran the analyses of POFC data and the meta-analysis, summarized the findings, and generated the visualizations. JH managed the GENEVA dataset and directed quality control after imputation. MM, EF, SMW, and EL conducted data acquisition and analysis for the POFC. TB, JH, AS, IR, and MT conducted data acquisition and analysis for GENEVA. DR, MT, and IR designed and executed the statistical analysis. TB, DR, and WZ wrote the manuscript with input from JH, SV, MT, MM, IR, and AS. All authors contributed to the article and approved the submitted version.

FUNDING

This work was supported for the study entitled "International Consortium to Identify Genes and Interactions Controlling Oral Clefts" was provided by several previous grants from the National Institute of Dental and Craniofacial Research (NIDCR). Data and samples were drawn from several studies awarded to members of this consortium. Funding to support original data collection, previous genotyping, and analysis came from several sources to individual investigators. Funding for individual investigators include the following: R21-DE-013707 and R0l-DE-014581 (TB); R03-DE-027121 (TB, MT); R37-DE-08559 and PS0-DE-016215 (Murray, MM) and the Iowa Comprehensive Program to Investigate Craniofacial and Dental Anomalies (Murray); R0l-DE-09886 (MM); R0l-DE-012472 (MM); R0l-DE-014677 (MM); R0l-DE-016148 (MM), R03-DE-029254 (DR); R21-DE-016930 (MM); and R0l-DE-013939 (AS). Parts of this research were supported in part by the Intramural Research Program of the NIH, National Institute of Environmental Health Sciences (Wilcox, Lie). Additional recruitment was supported by the Smile Train Foundation for recruitment in China (Jabs, TB, Shi) and a grant from the Korean government (Jee). The genome-wide association study, also known as the Cleft Consortium, is part of the Gene Environment Association Studies (GENEVA) program of the *trans*-NIH Genes, Environment and Health Initiative (GEi) supported by U0l-DE-018993. Genotyping services were provided by the Center for Inherited Disease Research (CIDR). CIDR is fully funded through a federal contract from the National Institutes of Health (NIH) to The Johns Hopkins University, contract number HHSN268200782096C. Funds for genotyping were provided by the NIDCR through CIDR's NIH contract. Assistance with genotype cleaning, as well as with general study coordination, was provided by the GENEVA Coordinating Center (U0l-HG-004446) and by the National Center for Biotechnology Information (NCBI).

ACKNOWLEDGMENTS

We sincerely thank all the patients and families at each recruitment site for participating in this study, and we gratefully acknowledge the invaluable assistance of clinical, field, and laboratory staff who contributed to this effort over the years.

SUPPLEMENTARY MATERIAL

The Supplementary Material for this article can be found online at: https://www.frontiersin.org/articles/10.3389/fcell.2021.621018/full#supplementary-material

REFERENCES

Aschard, H. (2016). A perspective on interaction effects in genetic association studies. *Genet. Epidemiol.* 40, 678–688. doi: 10.1002/gepi.21989

Aulchenko, Y. S., Ripke, S., Isaacs, A., and van Duijn, C. M. (2007). GenABEL: an R library for genome-wide association analysis. *Bioinformatics* 23, 1294–1296. doi: 10.1093/bioinformatics/btm108

Balduzzi, S., Rucker, G., and Schwarzer, G. (2019). How to perform a meta-analysis with R: a practical tutorial. *Evid. Based Ment. Health* 22, 153–160. doi: 10.1136/ebmental-2019-300117

Beaty, T. H., Marazita, M. L., and Leslie, E. J. (2016). Genetic factors influencing risk to orofacial clefts: today's challenges and tomorrow's opportunities. *F1000Research* 5:2800. doi: 10.12688/f1000research.9503.1

Beaty, T. H., Murray, J. C., Marazita, M. L., Munger, R. G., Ruczinski, I., Hetmanski, J. B., et al. (2010). A genome-wide association study of cleft lip with and without cleft palate identifies risk variants near MAFB and ABCA4. *Nat. Genet.* 42, 525–529. doi: 10.1038/ng.580

Beaty, T. H., Ruczinski, I., Murray, J. C., Marazita, M. L., Munger, R. G., Hetmanski, J. B., et al. (2011). Evidence for gene-environment interaction in a genome wide study of nonsyndromic cleft palate. *Genet. Epidemiol.* 35, 469–478. doi: 10.1002/gepi.20595

Beaty, T. H., Taub, M. A., Scott, A. F., Murray, J. C., Marazita, M. L., Schwender, H., et al. (2013). Confirming genes influencing risk to cleft lip with/without cleft palate in a case-parent trio study. *Hum. Genet.* 132, 771–781. doi: 10.1007/s00439-013-1283-6

Birnbaum, S., Ludwig, K. U., Reutter, H., Herms, S., Steffens, M., Rubini, M., et al. (2009). Key susceptibility locus for nonsyndromic cleft lip with or without cleft palate on chromosome 8q24. *Nat. Genet.* 41, 473–477. doi: 10.1038/ng.333

Butali, A., Mossey, P. A., Adeyemo, W. L., Eshete, M. A., Gowans, L. J. J., Busch, T. D., et al. (2019). Genomic analyses in African populations identify novel risk loci for cleft palate. *Hum. Mol. Genet.* 28, 1038–1051. doi: 10.1093/hmg/ddy402

Camargo, M., Rivera, D., Moreno, L., Lidral, A. C., Harper, U., Jones, M., et al. (2012). GWAS reveals new recessive loci associated with non-syndromic facial clefting. *Eur. J. Med. Genet.* 55, 510–514. doi: 10.1016/j.ejmg.2012.06.005

Carlson, J. C., Anand, D., Butali, A., Buxo, C. J., Christensen, K., Deleyiannis, F., et al. (2019). A systematic genetic analysis and visualization of phenotypic heterogeneity among orofacial cleft GWAS signals. *Genet. Epidemiol.* 43, 704–716. doi: 10.1002/gepi.22214

Carlson, J. C., Taub, M. A., Feingold, E., Beaty, T. H., Murray, J. C., Marazita, M. L., et al. (2017). Identifying genetic sources of phenotypic heterogeneity in orofacial clefts by targeted sequencing. *Birth Defects Res.* 109, 1030–1038. doi: 10.1002/bdr2.23605

D'Amelio, M., Cavallucci, V., and Cecconi, F. (2010). Neuronal caspase-3 signaling: not only cell death. *Cell Death Differ.* 17, 1104–1114. doi: 10.1038/cdd.2009.180

Das, S., Forer, L., Schonherr, S., Sidore, C., Locke, A. E., Kwong, A., et al. (2016). Next-generation genotype imputation service and methods. *Nat. Genet.* 48, 1284–1287. doi: 10.1038/ng.3656

Dayem Ullah, A. Z., Lemoine, N. R., and Chelala, C. (2012). SNPnexus: a web server for functional annotation of novel and publicly known genetic variants (2012 update). *Nucleic Acids Res.* 40, W65–W70. doi: 10.1093/nar/gks364

Delaneau, O., Marchini, J., and Zagury, J. F. (2011). A linear complexity phasing method for thousands of genomes. *Nat. Methods* 9, 179–181. doi: 10.1038/nmeth.1785

Dixon, M. J., Marazita, M. L., Beaty, T. H., and Murray, J. C. (2011). Cleft lip and palate: understanding genetic and environmental influences. *Nat. Rev. Genet.* 12, 167–178. doi: 10.1038/nrg2933

Genisca, A. E., Frias, J. L., Broussard, C. S., Honein, M. A., Lammer, E. J., Moore, C. A., et al. (2009). Orofacial clefts in the National Birth Defects Prevention Study, 1997-2004. *Am. J. Med. Genet. A* 149A, 1149–1158. doi: 10.1002/ajmg.a.32854

Grant, S. F., Wang, K., Zhang, H., Glaberson, W., Annaiah, K., Kim, C. E., et al. (2009). A genome-wide association study identifies a locus for nonsyndromic cleft lip with or without cleft palate on 8q24. *J. Pediatr.* 155, 909–913. doi: 10.1016/j.jpeds.2009.06.020

Grosen, D., Bille, C., Petersen, I., Skytthe, A., Hjelmborg, J., Pedersen, J. K., et al. (2011). Risk of oral clefts in twins. *Epidemiology* 22, 313–319. doi: 10.1097/EDE.0b013e3182125f9c

He, L., Vasiliou, K., and Nebert, D. W. (2009). Analysis and update of the human solute carrier (SLC) gene superfamily. *Hum. Genomics* 3, 195–206. doi: 10.1186/1479-7364-3-2-195

He, M., Zuo, X., Liu, H., Wang, W., Zhang, Y., Fu, Y., et al. (2020). Genome-wide analyses identify a novel risk locus for nonsyndromic cleft palate. *J. Dent. Res.* 99, 1461–1468. doi: 10.1177/0022034520943867

Holzinger, E. R., Li, Q., Parker, M. M., Hetmanski, J. B., Marazita, M. L., Mangold, E., et al. (2017). Analysis of sequence data to identify potential risk variants for oral clefts in multiplex families. *Mol. Genet. Genomic Med.* 5, 570–579. doi: 10.1002/mgg3.320

Honein, M. A., Devine, O., Grosse, S. D., and Reefhuis, J. (2014). Prevention of orofacial clefts caused by smoking: implications of the Surgeon General's report. *Birth Defects Res. A Clin. Mol. Teratol.* 100, 822–825. doi: 10.1002/bdra.23274

Huang, L., Jia, Z., Shi, Y., Du, Q., Shi, J., Wang, Z., et al. (2019). Genetic factors define CPO and CLO subtypes of nonsyndromicorofacial cleft. *PLoS Genet.* 15:e1008357. doi: 10.1371/journal.pgen.1008357

Islam, F., Gopalan, V., and Lam, A. K. (2018). RETREG1 (FAM134B): a new player in human diseases: 15 years after the discovery in cancer. *J. Cell Physiol.* 233, 4479–4489. doi: 10.1002/jcp.26384

Jiang, R., Bush, J. O., and Lidral, A. C. (2006). Development of the upper lip: morphogenetic andmolecular mechanisms. *Dev. Dyn.* 235, 1152–1166. doi: 10.1002/dvdy.20646

Johnson, C. Y., and Little, J. (2008). Folate intake, markers of folate status and oral clefts: is the evidence converging? *Int. J. Epidemiol.* 37, 1041–1058. doi: 10.1093/ije/dyn098

Kraft, P., Yen, Y. C., Stram, D. O., Morrison, J., and Gauderman, W. J. (2007). Exploiting gene-environment interaction to detect genetic associations. *Hum. Heredity.* 63, 111–119. doi: 10.1159/000099183

Kummet, C. M., Moreno, L. M., Wilcox, A. J., Romitti, P. A., DeRoo, L. A., Munger, R. G., et al. (2016). Passive smoke exposure as a risk factor for oral clefts-a large international population-based study. *Am. J. Epidemiol.* 183, 834–841. doi: 10.1093/aje/kwv279

Leslie, E. J., Carlson, J. C., Shaffer, J. R., Butali, A., Buxo, C. J., Castilla, E. E., et al. (2017). Genome-wide meta-analyses of nonsyndromic orofacial clefts identify novel associations between FOXE1 and all orofacial clefts, and TP63 and cleft lip with or without cleft palate. *Hum. Genet.* 136, 275–286. doi: 10.1007/s00439-016-1754-7

Leslie, E. J., Carlson, J. C., Shaffer, J. R., Feingold, E., Wehby, G., Laurie, C. A., et al. (2016a). A multi-ethnic genome-wide association study identifies novel loci for non-syndromic cleft lip with or without cleft palate on 2p24.2, 17q23 and 19q13. *Hum. Mol. Genet.* 25, 2862–2872. doi: 10.1093/hmg/ddw104

Leslie, E. J., Liu, H., Carlson, J. C., Shaffer, J. R., Feingold, E., Wehby, G., et al. (2016b). A genome-wide association study of nonsyndromic cleft palate identifies an etiologic missense variant in GRHL3. *Am. J. Hum. Genet.* 98, 744–754. doi: 10.1016/j.ajhg.2016.02.014

Liu, H., Busch, T., Eliason, S., Anand, D., Bullard, S., Gowans, L. J. J., et al. (2017a). Exome sequencing provides additional evidence for the involvement of ARHGAP29 in Mendelian orofacial clefting and extends the phenotypic spectrum to isolated cleft palate. *Birth Defects Res.* 109, 27–37. doi: 10.1002/bdra.23596

Liu, H., Leslie, E. J., Carlson, J. C., Beaty, T. H., Marazita, M. L., Lidral, A. C., et al. (2017b). Identification of common non-coding variants at 1p22 that are functional for non-syndromic orofacial clefting. *Nat. Commun.* 8:14759. doi: 10.1038/ncomms14759

Liu, X. Z., Zhang, Q., Jiang, Q., Bai, B. L., Du, X. J., Wang, F., et al. (2018). Genetic screening and functional analysis of CASP9 mutations in a Chinese cohort with neural tube defects. *CNS Neurosci. Ther.* 24, 394–403. doi: 10.1111/cns.12797

Ludwig, K. U., Mangold, E., Herms, S., Nowak, S., Reutter, H., Paul, A., et al. (2012). Genome- wide meta-analyses of nonsyndromic cleft lip with or without cleft palate identify six new risk loci. *Nat. Genet.* 44, 968–971. doi: 10.1038/ng.2360

Lupo, P. J., Mitchell, L. E., and Jenkins, M. M. (2019). Genome-wide association studies of structural birth defects: a review and commentary. *Birth Defects Res.* 111, 1329–1342. doi: 10.1002/bdr2.1606

Machado, R. A., Moreira, H. S. B., de Aquino, S. N., Martelli-Junior, H., de Almeida Reis, S. R., Persuhn, D. C., et al. (2016). Interactions between RAD51 rs1801321 and maternal cigarette smoking as risk factor for nonsyndromic cleft lip with or without cleft palate. *Am. J. Med. Genet. A* 170A, 536–539. doi: 10.1002/ajmg.a.37281

Mai, C. T., Cassell, C. H., Meyer, R. E., Isenburg, J., Canfield, M. A., Rickard, R., et al. (2014). Birth defects data from population-based birth defects surveillance programs in the United States, 2007 to 2011: highlighting orofacial clefts. *Birth Defects Res. A Clin. Mol. Teratol.* 100, 895–904. doi: 10.1002/bdra.23329

Mangold, E., Ludwig, K. U., Birnbaum, S., Baluardo, C., Ferrian, M., Herms, S., et al. (2010). Genome-wide association study identifies two susceptibility loci for nonsyndromic cleft lip with or without cleft palate. *Nat. Genet.* 42, 24–26. doi: 10.1038/ng.506

Manning, A. K., LaValley, M., Liu, C. T., Rice, K., An, P., Liu, Y., et al. (2011). Meta-analysis of gene-environment interaction: joint estimation of SNP and SNP x environment regression coefficients. *Genet. Epidemiol.* 35, 11–18. doi: 10.1002/gepi.20546

Montasser, M. E., Shimmin, L. C., Hanis, C. L., Boerwinkle, E., and Hixson, J. E. (2009). Gene by smoking interaction in hypertension: identification of a major quantitative trait locus on chromosome 15q for systolic blood pressure in Mexican-Americans. *J. Hypertens.* 27, 491–501. doi: 10.1097/hjh.0b013e32831ef54f

Moreno Uribe, L. M., Fomina, T., Munger, R. G., Romitti, P. A., Jenkins, M. M., Gjessing, H. K., et al. (2017). A population-based study of effects of genetic loci on orofacial clefts. *J. Dent. Res.* 96, 1322–1329. doi: 10.1177/0022034517716914

Mossey, P. A., Little, J., Munger, R. G., Dixon, M. J., and Shaw, W. C. (2009). Cleft lip and palate. *Lancet* 374, 1773–1785. doi: 10.1016/S0140-6736(09)60695-4

Pruim, R. J., Welch, R. P., Sanna, S., Teslovich, T. M., Chines, P. S., Gliedt, T. P., et al. (2010). LocusZoom: regional visualization of genome-wide association scan results. *Bioinformatics* 26, 2336–2337. doi: 10.1093/bioinformatics/btq419

Ray, D., and Chatterjee, N. (2020). A powerful method for pleiotropic analysis under composite null hypothesis identifies novel shared loci between type 2 diabetes and prostate cancer. *PLoS Genet.* 16:e1009218. doi: 10.11371/journal.pgen.1009218

Ray, D., Venkataraghavan, S., Zhang, W., Leslie, E. J., Hetmanski, J. B., Marazita, M. L., et al. (2020). Pleiotropy method identifies genetic overlap between orofacial clefts at multiple loci from GWAS of multi-ethnic trios. *MedRxiv* [Preprint]. doi: 10.1101/2020.11.132023654

Romitti, P. A., Sun, L., Honein, M. A., Reefhuis, J., Correa, A., and Rasmussen, S. A. (2007). Maternal periconceptional alcohol consumption and risk of orofacial clefts. *Am. J. Epidemiol.* 166, 775–785. doi: 10.1093/aje/kwm146

Schutte, B. C., Saal, H. M., Goudy, S., and Leslie, E. (1993). "IRF6-Related Disorders," in *GeneReviews((R))*, eds M. P. Adam, H. H. Ardinger, R. A. Pagon, S. E. Wallace, L. J. H. Bean, K. Stephens, et al. (Seattle, WA: Springer).

Schwender, H., Li, Q., Neumann, C., Taub, M. A., Younkin, S. G., Berger, P., et al. (2014). Detecting disease variants in case-parent trio studies using the bioconductor software package trio. *Genet. Epidemiol.* 38, 516–522. doi: 10.1002/gepi.21836

Schwender, H., Taub, M. A., Beaty, T. H., Marazita, M. L., and Ruczinski, I. (2012). Rapid testing of SNPs and gene-environment interactions in case-parent trio data based on exact analytic parameter estimation. *Biometrics* 68, 766–773. doi: 10.1111/j.1541-0420.2011.01713.x

Shi, M., Wehby, G. L., and Murray, J. C. (2008). Review on genetic variants and maternal smoking in the etiology of oral clefts and other birth defects. *Birth Defects Res. C Embryo. Today* 84, 16–29. doi: 10.1002/bdrc.20117

Shin, J. H., Infante-Rivard, C., Graham, J., and McNeney, B. (2012). Adjusting for spurious gene-by-environment interaction using case-parent triads. *Stat. Appl. Genet. Mol. Biol.* 11. doi: 10.2202/1544-6115.1714

Spellicy, C. J., Norris, J., Bend, R., Bupp, C., Mester, P., Reynolds, T., et al. (2018). Key apoptotic genes APAF1 and CASP9 implicated in recurrent folate-resistant neural tube defects. *Eur. J. Hum. Genet.* 26, 420–427. doi: 10.1038/s41431-017-0025-y

Sun, Y., Huang, Y., Yin, A., Pan, Y., Wang, Y., Wang, C., et al. (2015). Genome-wide association study identifies a new susceptibility locus for cleft lip with or without a cleft palate. *Nat. Commun.* 6:6414. doi: 10.1038/ncomms7414

Taub, M. A., Schwender, H., Beaty, T. H., Louis, T. A., and Ruczinski, I. (2012). Incorporating genotype uncertainties into the genotypic TDT for main effects and gene-environment interactions. *Genet. Epidemiol.* 36, 225–234. doi: 10.1002/gepi.21615

Wang, K. S., Liu, X., Zhang, Q., and Zeng, M. (2012). ANAPC1 and SLCO3A1 are associated with nicotine dependence: meta-analysis of genome-wide association studies. *Drug Alcohol Depend.* 124, 325–332. doi: 10.1016/j.drugalcdep.2012.02.003

Wilson, R. D., Genetics, C., Wilson, R. D., Audibert, F., Brock, J. A., Carroll, J., et al. (2015). Pre-conception folic acid and multivitamin supplementation for the primary and secondary prevention of neural tube defects and other folic acid-sensitive congenital anomalies. *J. Obstet. Gynaecol. Can.* 37, 534–552. doi: 10.1016/s1701-2163(15)30230-9

Wolf, Z. T., Brand, H. A., Shaffer, J. R., Leslie, E. J., Arzi, B., Willet, C. E., et al. (2015). Genome-wide association studies in dogs and humans identify ADAMTS20 as a risk variant for cleft lip and palate. *PLoS Genet.* 11:e1005059. doi: 10.1371/journal.pgen.1005059

Yu, Y., Zuo, X., He, M., Gao, J., Fu, Y., Qin, C., et al. (2017). Genome-wide analyses of non-syndromic cleft lip with palate identify 14 novel loci and genetic heterogeneity. *Nat. Commun.* 8:14364. doi: 10.1038/ncomms14364

Conflict of Interest: The authors declare that the research was conducted in the absence of any commercial or financial relationships that could be construed as a potential conflict of interest.

frontiers in Cell and Developmental Biology

REVIEW
published: 20 May 2021
doi: 10.3389/fcell.2021.644410

Diabetes, Oxidative Stress, and DNA Damage Modulate Cranial Neural Crest Cell Development and the Phenotype Variability of Craniofacial Disorders

Sharien Fitriasari[1] *and Paul A. Trainor*[1,2]*

[1] Stowers Institute for Medical Research, Kansas City, MO, United States, [2] Department of Anatomy and Cell Biology, University of Kansas Medical Center, Kansas City, KS, United States

Craniofacial malformations are among the most common birth defects in humans and they often have significant detrimental functional, aesthetic, and social consequences. To date, more than 700 distinct craniofacial disorders have been described. However, the genetic, environmental, and developmental origins of most of these conditions remain to be determined. This gap in our knowledge is hampered in part by the tremendous phenotypic diversity evident in craniofacial syndromes but is also due to our limited understanding of the signals and mechanisms governing normal craniofacial development and variation. The principles of Mendelian inheritance have uncovered the etiology of relatively few complex craniofacial traits and consequently, the variability of craniofacial syndromes and phenotypes both within families and between families is often attributed to variable gene expression and incomplete penetrance. However, it is becoming increasingly apparent that phenotypic variation is often the result of combinatorial genetic and non-genetic factors. Major non-genetic factors include environmental effectors such as pregestational maternal diabetes, which is well-known to increase the risk of craniofacial birth defects. The hyperglycemia characteristic of diabetes causes oxidative stress which in turn can result in genotoxic stress, DNA damage, metabolic alterations, and subsequently perturbed embryogenesis. In this review we explore the importance of gene-environment associations involving diabetes, oxidative stress, and DNA damage during cranial neural crest cell development, which may underpin the phenotypic variability observed in specific craniofacial syndromes.

Keywords: diabetes, ROS, DNA damage, neural crest cell, craniofacial development

OPEN ACCESS

Edited by:
Sebastian Dworkin, La Trobe University, Australia

Reviewed by:
Guang Wang, Jinan University, China
Regie Santos-Cortez, University of Colorado, United States

***Correspondence:**
Paul A. Trainor
pat@stowers.org

Specialty section:
This article was submitted to Molecular Medicine, a section of the journal Frontiers in Cell and Developmental Biology

Received: *21 December 2020*
Accepted: *21 April 2021*
Published: *20 May 2021*

Citation:
Fitriasari S and Trainor PA (2021) Diabetes, Oxidative Stress, and DNA Damage Modulate Cranial Neural Crest Cell Development and the Phenotype Variability of Craniofacial Disorders. Front. Cell Dev. Biol. 9:644410. doi: 10.3389/fcell.2021.644410

INTRODUCTION

The vertebrate head and face comprise a complex assemblage of specialized tissues including the viscerocranium, chondrocranium and neurocranium, the central and peripheral nervous systems, and all of the major sense organs (Trainor, 2013). The anatomical complexity of the craniofacial complex coupled with the initiation of its development during early embryogenesis renders the head and face prone to malformation. In fact, of the 1% of all live births that present with a

minor or major anomaly, about one-third affect the head and face (Gorlin et al., 1990). To date, more than 700 distinct craniofacial disorders have been identified and phenotypically described (Carey, 1992), and orofacial clefts (1:1,000) and craniosynostosis (1:2,500) represent two of the most common craniofacial birth defects. These disorders are characterized by a wide spectrum of anomalies with varying degrees of severity, and no phenotypes or syndromes are identical in all affected individuals. In fact, many affected individuals with extremely mild phenotypes go undiagnosed or are only diagnosed retrospectively upon the birth of a severely affected sibling or progeny (Trainor et al., 2009). Additionally, craniofacial anomalies can occur sporadically without a familial history of mutation, indicating that genetic background, environmental factors, and stochastic events can influence the etiology and pathogenesis of craniofacial disorders (Jones et al., 1975; Trainor et al., 2009; Bartzela et al., 2017). Therefore, a thorough understanding of the events controlling normal craniofacial morphogenesis is central to improving diagnosis and care for patients.

Craniofacial malformations typically arise due to defects in cranial neural crest cell formation, migration, or differentiation and are collectively termed "neurocristopathies." Distinct and diverse phenotypes manifest depending on which phase of cNCC development is disrupted (Trainor, 2010; Watt and Trainor, 2014). Although variable gene expression and incomplete penetrance contribute to phenotypic variability, the impact of combinatorial genetic and non-genetic factors in craniofacial malformations is increasingly being recognized. A growing body of evidence demonstrates that neural crest cells are particularly sensitive to environmental influences such as diabetes and oxidative stress. Maternal diabetes is associated with an increased risk of birth defects (Kucera, 1971; Casson et al., 1997; Hawthorne et al., 1997; Von Kries et al., 1997; Mills, 2010) and may account for half of all perinatal deaths (Greene, 2001). In fact, women with pre-gestational diabetes have children with birth defects three to five times more frequently than women without diabetes (Greene, 2001). Oxidative stress-inducing teratogens, such as alcohol (Sulik et al., 1988), retinoic acid (Williams and Bohnsack, 2019), and nicotine (Zhao and Reece, 2005; Schneider et al., 2010), can also increase the likelihood of embryos born with craniofacial anomalies. Persistent oxidative stress can impinge on neural crest cell development through distinct mechanisms such as DNA damage, p53 activation and autophagy (Wang et al., 2015; Sakai et al., 2016; Han et al., 2019; Cao et al., 2020). Consistent with this idea, DNA damage and genome instability are associated with an increased incidence of cleft lip and/or palate (Kobayashi et al., 2013). Furthermore, mutations in DNA damage repair genes can result in craniofacial malformations, highlighting the importance of maintaining genome stability during normal craniofacial morphogenesis (Wong et al., 2003; Seeman et al., 2004; Altmann and Gennery, 2016; Sakai et al., 2016; Kitami et al., 2018; Boone et al., 2019; Yamaguchi et al., 2021). This led us to postulate that exogenous stressors, particularly oxidative stress and DNA damage, can worsen the damage caused by a particular neural crest cell disruptive mutation, thus exacerbating its phenotypic outcome. In this review, we provide a brief overview of cranial neural crest cell development and the effects of diabetes and oxidative stress on craniofacial morphogenesis. We will also discuss potential mechanisms for oxidative stress-induced DNA damage in modulating the phenotypic variability associated with craniofacial disorders.

NEURAL CREST CELL AND CRANIOFACIAL DEVELOPMENT

Underpinning the complex morphogenesis of head and facial development is a population of cells called neural crest cells (NCC). Considered a vertebrate-specific cell type, NCC are transiently generated during the neurulation phase of embryogenesis which corresponds to about 3–4 weeks of human development. Specified in the neural ectoderm along nearly the entire length of the embryo, NCC undergo an epithelial-to-mesenchymal transition (EMT), which facilitates their delamination and migration throughout the primitive head. Cranial NCC give rise to the chondrocytes and osteoblasts of cartilage and bone, the fibroblasts of connective tissue, the odontoblasts in teeth, the sensory neurons and glia in the peripheral nervous system, and the pigment cells in the skin (Le Douarin and Kalcheim, 1999; Bronner and LeDouarin, 2012). Ultimately, there is barely a tissue or organ throughout the entire body that does not receive a contribution from NCC. Given this remarkable differentiation capacity, NCC have been described as the fourth primary germ layer (Hall, 1999). The specification of neural crest cell progenitors is thought to occur during gastrulation in the neural plate border (Trainor and Krumlauf, 2001, 2002; García-Castro et al., 2002; Basch et al., 2006; Prasad et al., 2020). This territory is defined as the junction between the neural ectoderm and the surface ectoderm and in chick embryos is demarcated by the expression of *Pax7* (Basch et al., 2006). During neurulation, the two halves of the neural ectoderm or neural plate elevate, converge and fuse to form a neural tube, which is the precursor of the central nervous system (**Figure 1A**). At the same time, neural crest cells are induced to form in the dorsolateral aspect of the neural plate in response to signals from the surrounding ectoderm, mesoderm, and endoderm. Considerable evidence has shown that signaling cascades mediated by BMP (Bone Morphogenetic Protein), FGF (fibroblast growth factor), and Wnt (Wingless/Int) play central roles in neural crest induction, although the importance and spatiotemporal regulation of these individual signaling pathways varies depending on the species (Bae and Saint-Jeannet, 2014). The potential reasons for, and significance of, these species-specific differences have been previously discussed (Barriga et al., 2015).

Irrespective of which signaling pathways are involved, the formation of NCC involves tremendous cytoskeletal changes. During EMT, adjoining neuroepithelial cells lose their intracellular tight junctions, adherens junctions, and apicobasal polarity, and acquire focal adhesions, become polarized and migratory (Taneyhill and Padmanabhan, 2014). These changes in cell adhesion are mediated in part by a "Cadherin switch" in which E-cadherin expression is downregulated in concert with N-cadherin upregulation (Hatta and Takeichi, 1986;

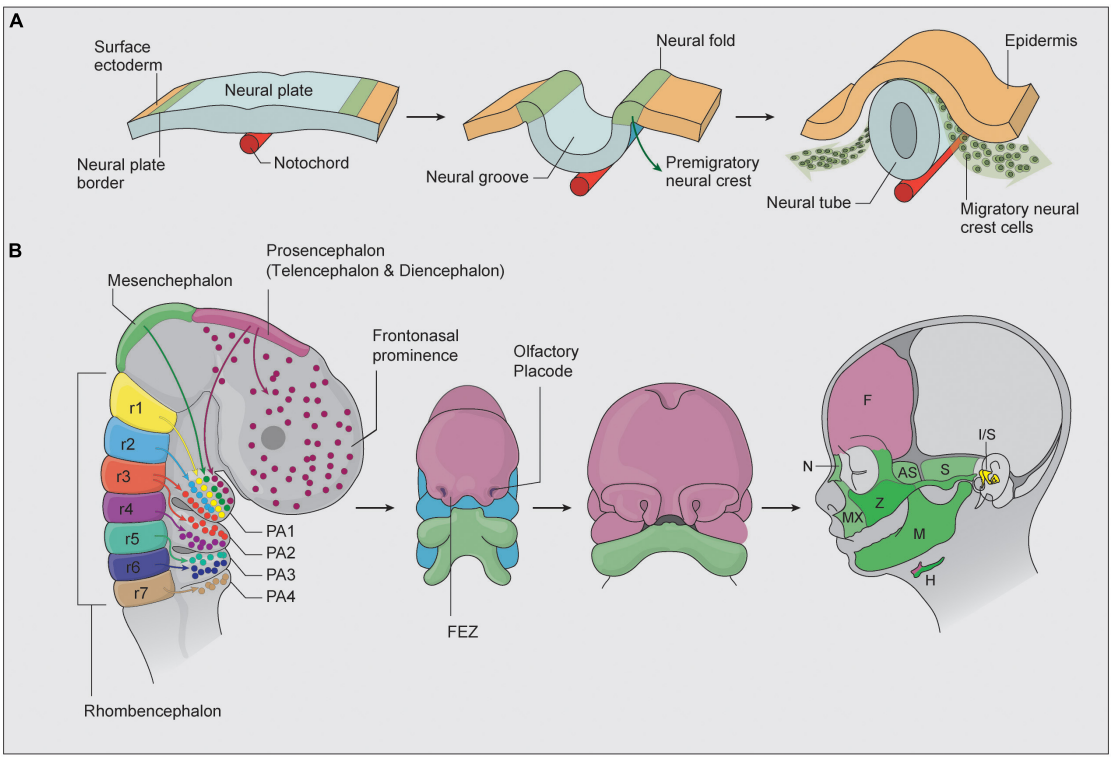

FIGURE 1 | (A) NCC are initially specified within the neural plate border. As the two halves of the neural plate elevate to form a neural tube, NCC are induced and undergo EMT, after which they migrate and colonize the frontonasal prominences, first, second, third, and fourth pharyngeal arches (adapted from Simões-Costa and Bronner, 2015). **(B)** Cranial NCC patterns of migration and differentiation into the bone and cartilage of the head and face. During embryogenesis, the brain is specified into prosencephalon (diencephalon and telencephalon), mesencephalon, and rhombencephalon regions. The colors highlight regions of the developing face that correspond to NCC populations of different axial origins. The facial prominence and pharyngeal arches then undergo complex morphogenesis to form the structures of the face. AS, alisphenoid bone, F, frontal bone, FEZ, frontonasal ectodermal zone, FNP, frontonasal prominence, H, hyoid bone, I/S, incus and stapes, M, mandible, MX, maxilla, N, nasal bone, PA, pharyngeal arches, r, rhombencephalon, S, squamosal, Z, zygomatic bone.

Coles et al., 2007). A number of transcription factors including members of the Snail, Zeb and Twist protein families play critical roles in NCC EMT (Nieto et al., 1994; Van De Putte et al., 2003; Coles et al., 2007; Mayor and Theveneau, 2012) in part through directly repressing the transcriptional activity and function of E-cadherin (Cano et al., 2000). However, again there are species-specific differences in the absolute requirement and functions of these transcription factors in NCC EMT (Barriga et al., 2015). Nonetheless, the induction, EMT, delamination, migration, and differentiation of NCC depends on integrated gene regulatory networks in which many genes and signaling pathways exhibit reiterative functions.

Neural crest cells arise progressively in an anterior-posterior manner along nearly the entire neuroaxis of the embryo and are classified into cranial, cardiac, trunk, vagal, and sacral NCC axial populations. Of particular relevance in this review are the cranial NCC, which generate most of the craniofacial skeleton in vertebrates. Cranial NCC delaminate from the diencephalon (posterior forebrain), mesencephalon (midbrain), and rhombencephalon (hindbrain) and give rise to the majority of the bone, cartilage and connective tissue of the head and face (**Figure 1B**) (Achilleos and Trainor, 2015). The most anterior cranial NCC migrate collectively and populate the frontonasal and periocular regions, where they contribute to the nasal and frontal bones, the meninges underlying the calvarial bones and most of the suture mesenchyme separating the skull bones. The posterior cranial NCC migrate in discrete segregated streams and populate the pharyngeal arches (Osumi-Yamashita et al., 1994; Tam and Trainor, 1994; Trainor and Tam, 1995; Trainor et al., 2002), where they differentiate into the upper and lower jaw, middle ear, and skeletal structures in the neck (**Figure 1B**; Chai et al., 2000; Kulesa et al., 2010). Cranial NCC exhibit varying degrees of unipotency, bipotency and multipotency and are capable of differentiating into neurons and glia of the peripheral nervous system, as well as osteochondroprogenitors (Baroffio et al., 1991; Le Douarin et al., 2004; Dupin et al., 2010; Baggiolini et al., 2015). Migrating neural crest cells express *Sox10* and *Foxd3*, and the activity of these factors persist in cranial NCC destined for neuroglial differentiation, but are switched off in osteochondroprogenitors (Bhatt et al., 2013). Conversely, *Sox9*, a master regulator of chondrogenesis is expressed in cranial NCC destined for cartilage and bone differentiation but is switched off in neuroglia progenitors (Trainor and Krumlauf, 2001; Dash and Trainor, 2020).

Several mechanisms may account for the ability of NCC to differentiate into diverse cell types and tissues. If the fate of NCC was predetermined at the time of induction, NCC would comprise a heterogeneous mixture of unipotent progenitor cells, with each giving rise to a singular distinct cell type. Their differentiation would therefore be primarily dependent upon intrinsic signals (Bhatt et al., 2013). However as noted above, NCC exhibit varying degrees of cell fate potency, and therefore depend upon a combination of intrinsically expressed factors in concert with extrinsic signals emanating from the tissues they contact during their migration to undergo their proper spatiotemporal patterns of differentiation (Trainor and Krumlauf, 2001; Trainor, 2003, 2013; Trainor et al., 2003; Crane and Trainor, 2006). These key principles of NCC heterogeneity, potency, and plasticity which were determined through classic embryology, lineage tracing, and transplantation studies have been further substantiated by more recent genetic and molecular analyses such as single cell RNA-sequencing (Morrison et al., 2017; Shang et al., 2018; Soldatov et al., 2019). The remarkable lineage potential of NCC, combined with a limited capacity for self-renewal that persists even into adult life, has raised the potential for NCC to be used in regenerative medicine (Crane and Trainor, 2006; Achilleos and Trainor, 2012; Shang et al., 2018).

Synonymous with the "new head" hypothesis (Gans and Northcutt, 1983), cranial NCC carry species-specific programming information that is integral to craniofacial development, evolution, variation, and disease (Noden, 1983; Trainor and Krumlauf, 2001; Schneider and Helms, 2003; Trainor, 2003; Trainor et al., 2003; Noden and Trainor, 2005). Proper craniofacial development therefore requires that an embryo generates and maintains a sufficient number of NCC that proliferate, survive, migrate, and differentiate in the correct spatiotemporal manner. Perturbation of any one of these phases of NCC development can lead to variable craniofacial malformations. A growing body of evidence suggests that NCC are particularly sensitive to exogenous environmental stressors such as diabetes, oxidative stress, and DNA damage (Sakai and Trainor, 2016; Sakai et al., 2016; Kitami et al., 2018; Yamaguchi et al., 2021). We postulate that the interactions between these exogenous stressors and genetic risk factors for individual craniofacial malformations compromise NCC viability, thus contributing to the phenotypic variation observed in many craniofacial syndromes. To illustrate this concept, we discuss craniofacial syndromes with well recognized broad phenotypic variation that are known to be influenced by diabetes, oxidative stress, and DNA damage.

GENE-ENVIRONMENT INTERACTIONS INFLUENCE PHENOTYPE VARIABILITY IN DIFFERENT CRANIOFACIAL DISORDERS

Treacher Collins Syndrome

Treacher Collins syndrome (TCS, OMIM number 154500) is a prime example of the considerable phenotypic variability characteristic of congenital craniofacial disorders. Extensive inter- and intra-familial variation is a striking feature of the condition (Dixon et al., 1994; Marres et al., 1995; Jones et al., 2008). TCS is characterized by anomalies of the head and face, including hypoplasia of the facial bones, especially the mandible and zygomatic complex, which may result in dental malocclusion. The palate is often high-arched or cleft (Poswillo, 1975). Other clinical features of TCS include alterations in the shape, size, and position of the external ears, which are frequently associated with atresia of the external auditory canals and anomalies of the middle ear ossicles (Edwards et al., 1996). In the most extreme cases of TCS, the constellation of craniofacial anomalies can result in a compromised airway leading to perinatal death (Edwards et al., 1996). In contrast, some individuals can be so mildly affected that it is difficult to establish an unequivocal diagnosis. It is therefore not uncommon for mildly affected TCS patients to be diagnosed retrospectively, after the birth of a more severely affected child or sibling.

TCS occurs with an estimated incidence of 1 in 50,000 live births (Carey, 1992; Twigg and Wilkie, 2015) and is caused primarily by mutations in the *TCOF1* gene. However, TCS is also associated with mutations in *POLR1B*, *POLR1C* and *POLR1D*. With respect to *TCOF1* the mode of inheritance is autosomal dominant, although very rare cases of autosomal recessive mutations have been observed (Dixon et al., 1996; Edwards et al., 1997). For *POLR1B*, all mutations to date appear to be autosomal dominant, whereas for *POLR1C* they are autosomal recessive (Dauwerse et al., 2011; Ghesh et al., 2019; Sanchez et al., 2020). In contrast, both autosomal dominant and recessive mutations in *POLR1D* have been reported in association with TCS (Dauwerse et al., 2011).

Hundreds of family-specific mutations including deletions, insertions, splice site, missense, and nonsense mutations have been identified in the *TCOF1* gene (databases.lovd.nl/shared/genes/TCOF1). However, irrespective of the position of the mutation, or the type of mutation, or whether the mutation is maternally or paternally inherited, these factors apparently have no impact on the severity of the TCS condition, and there does not appear to be any significant sex-based difference in the effect of a mutation on male vs. female offspring. Although the penetrance of genetic mutations underlying TCS is high, approximately 60% of cases arise randomly or spontaneously as a result of a *de novo* mutation in a family without a history of the disorder. The high degree of variability in which individuals with TCS are affected, together with the high rate of *de novo* mutations and the absence of a strong genotype-phenotype correlation, renders the provision of genetic counseling complicated, particularly where the diagnosis of an affected child's parents is equivocal (Trainor et al., 2009).

TCOF1 encodes the nucleolar phosphoprotein Treacle, which together with Upstream Binding Factor (UBF) stimulates transcription of ribosomal DNA by RNA Polymerase I (Valdez et al., 2004). POLR1B is a catalytic core subunit of RNA Polymerase I, whereas POLR1C and POLR1D comprise core subunits of RNA Polymerases I and III. Each of these factors play essential roles in rDNA transcription, which is the first step and a rate limiting step in ribosome biogenesis. Ribosome biogenesis

is the process of making ribosomes, the ribonucleoprotein machines that translate mRNA into protein, thus synthesizing proteins within all cells. Since ribosomes underpin protein production, their synthesis consumes a cell's metabolic capacity, and ribosome biogenesis is therefore tightly integrated with and regulates many cellular processes including proliferation, survival, growth, and differentiation. Interestingly, deficiencies in rDNA transcription and ribosome biogenesis result in the activation and stabilization of p53 and ultimately cell death (Rubbi and Milner, 2003). Loss-of-function mouse and zebrafish models of *TCOF1*, *POLR1B*, *POLR1C* or *POLR1D* homologs exhibit extensive p53 dependent neuroepithelium and neural crest cell apoptosis, which presages hypoplasia of the craniofacial skeleton, mimicking the characteristic features of TCS in humans (Dixon et al., 2006; Jones et al., 2008; Noack Watt et al., 2016; Sanchez et al., 2020). Furthermore, pharmacological or genetic inhibition of p53-dependent apoptosis prevents TCS in animal models (Jones et al., 2008; Noack Watt et al., 2016). TCS is therefore primarily associated with perturbation of rDNA transcription and a subsequent deficiency in the ribosome biogenesis and protein translation necessary for neuroepithelial neural crest cell proliferation and survival (Dixon et al., 2006; Noack Watt et al., 2016).

The p53 inhibition rescue of TCS occurred without restoration of ribosome biogenesis (Jones et al., 2008). This led to the suggestion that Tcof1/Treacle may also perform non-rDNA transcription and ribosome biogenesis associated functions during development. Treacle was subsequently found to directly interact with the MRNM (MDC1-RAD50-NBS1-MRE11) complex (Sakai et al., 2016), which mediates the double-stranded DNA damage response. In support of this observation, two other studies focused on the role of NBS1 in response to DNA damage induced by laser microirradiation in cultured cells, identified TCOF1/Treacle as a direct binding partner of NBS1 (Ciccia et al., 2014; Larsen et al., 2014; Sakai et al., 2016). Collectively, this implied that TCOF1 might play a key role in the response to DNA damage via the MRNM complex. Treacle was subsequently shown to localize to sites of DNA damage and *Tcof1*$^{+/-}$ embryo-derived mouse embryonic fibroblasts (MEFs) exhibited a delay in DNA damage repair (Sakai et al., 2016). Furthermore, p-ATM was observed to be upregulated in *Tcof1*$^{+/-}$ embryos compared to control littermates, and γ-H2AX, p-Chk2 and p53 were activated in the same neuroepithelial cells undergoing apoptosis *in vivo* in *Tcof1*$^{+/-}$ embryos (Sakai et al., 2016). Treacle-dependent NBS1 translocation regulates silencing of RNA polymerase I-dependent rRNA transcription upon DNA damage (Ciccia et al., 2014; Larsen et al., 2014; Sakai et al., 2016), and interestingly in the absence of Treacle, BRCA1 no longer localizes to sites of DNA damage (Sakai et al., 2016). These results provided direct evidence that *TCOF1*/Treacle functions in the DNA damage response and repair pathway *in vivo* (Sakai et al., 2016). Furthermore, it connected deficient DNA damage repair and the p53 dependent apoptotic elimination of cranial NCC in *Tcof1*$^{+/-}$ embryos as a component of the cellular and developmental mechanisms underlying the pathogenesis of TCS.

Neuroepithelial cells including progenitor neural crest cells endogenously generate high levels of reactive oxygen species (ROS) compared to other tissues during embryogenesis (Sakai et al., 2016). Furthermore, exposing wild-type embryos to strong oxidants such as 3-nitropropionic acid or H_2O_2 induces apoptosis specifically in the neuroepithelium and progenitor neural crest cells. Thus, not only do these cells naturally exist in a highly oxidative state, they are also particularly sensitive to exogenous ROS (Sakai and Trainor, 2016; Sakai et al., 2016). Furthermore, mutations in genes critical for responding to and repairing DNA damage, would increase the sensitivity to exogenous ROS as is the case in *Tcof1*$^{+/-}$ embryos (Sakai et al., 2016). Conversely, antioxidant supplementation provided a therapeutic avenue for ameliorating or even preventing ROS induced DNA damage phenotypes. Treating *Tcof1*$^{+/-}$ embryos *in utero* with a strong antioxidant such as N-acetylcysteine is able to clear the ROS, thereby preventing DNA damage, p53 activation and apoptosis. Consequently, about 30% of antioxidant treated *Tcof1*$^{+/-}$ embryos were fully rescued and morphologically indistinguishable from their wild-type littermates (Sakai et al., 2016). Thus, *Tcof1*/Treacle plays an essential role in protecting neuroepithelial and neural crest cells from endogenous and exogenous oxidative stress-induced DNA damage during normal craniofacial development. Consistent with this idea, a SILAC analysis of oxidative stress-mediated proteins in human pneumocytes revealed a potential role for Treacle in oxidant defense (Duan et al., 2010). Given that the *in utero* gestational environment generates and is subjected to dynamic levels of oxidative stress that fluctuate during an individual pregnancy and vary between pregnancies, these results imply that differential levels of oxidative stress contribute to the inter- and intra-familial variability in craniofacial anomalies characteristic of TCS (**Figure 2**).

The inter-and intra-familial phenotypic variability observed in association with TCS in humans can be reproduced experimentally in mice with mutations in *Tcof1* on different genetic backgrounds (Dixon and Dixon, 2004). This illustrates the potential for complex interactions between *Tcof1* and intrinsic background-specific modifier genes, or extrinsic environmental factors, in modulating phenotype variability and severity. In fact, it is tempting to speculate that a combination of endogenous background specific levels of *TCOF1*/Treacle, genetic modifiers and levels of ROS collectively determines TCS phenotypic outcomes.

Holoprosencephaly

A complex genotype-phenotype relationship has also been observed in holoprosencephaly (HPE; OMIM number 236100), which affects approximately 1 in 16,000 live births (Geng and Oliver, 2009). HPE is a structural brain malformation characterized by incomplete or absent division of the forebrain (prosencephalon) into two cerebral hemispheres, which normally occurs by the 5th week of gestation (Golden, 1999; Kruszka and Muenke, 2018). HPE may present as an isolated phenotype (non-syndromic) or as part of a syndrome (syndromic), the most common of which include Trisomy 13 and 22, as well as Smith-Lemli-Opitz syndrome and Hartsfield syndrome (Kruszka and Muenke, 2018). Non-syndromic HPE is commonly associated with pathogenic variants in one of four principal genes including

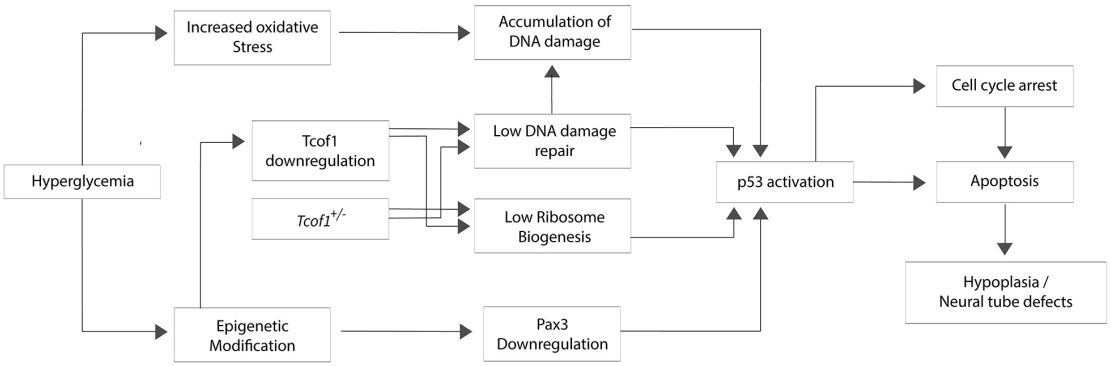

FIGURE 2 | Potential mechanisms for hyperglycemia, oxidative stress, and DNA damage in the pathogenesis of Treacher Collins syndrome. The hyperglycemic environment characteristic of maternal diabetes can lead to oxidative stress and epigenetic modification. Oxidative DNA damage and aberrant *Pax3* silencing lead to p53 activation which induces apoptosis particularly within neuroepithelial cells and neural crest cells, resulting in neural tube defects or hypoplasia of neural crest-derived tissues.

SHH, *ZIC2*, *SIX3*, and *TGIF* (Roessler et al., 1996, 2009; Solomon et al., 2009; Taniguchi et al., 2012). Other genetic loci, such as *GLI2*, *CDON* (also known as *CDO*), *FGF8*, and *DISP1* have also been associated with HPE or HPE-like phenotypes at lower frequency (Roessler et al., 2003, 2009; Bae et al., 2011; Hong et al., 2018).

Similar to *TCOF1* mutations in TCS, the phenotypic consequences of loss-of-functions mutations in these HPE associated loci correlate with a spectrum of facial malformations, ranging from non-lethal microforms such as hypotelorism, midfacial hypoplasia, and a single maxillary incisor, to an extremely severe form characterized by cyclopia and proboscis (Solomon et al., 2010). Depending on the degree of separation between the cerebral hemispheres, HPE is generally classified into four main subtypes: alobar, semilobar, lobar, middle interhemispheric (Solomon et al., 2010), together with a new classification called septopreoptic variant (Hahn et al., 2010). In alobar HPE, the lateral and third ventricles are completely fused, resulting in the absence of midline separation between cerebral hemispheres. Semilobar HPE occurs when the interhemispheric fissure, or the dividing line between left and right side of the brain, is only present posteriorly. In the less severe lobar HPE, the cerebral hemispheres are mostly divided except for the rostral portion of the frontal cortex. Meanwhile, the middle interhemispheric variant of HPE is characterized by the presence of interhemispheric fissure only in the anterior and posterior part of the brain, which results in medial cerebral hemispheres fusion. Lastly, the septopreoptic variant is considered the mildest form of HPE, with fusions only present in the septal and/or preoptic regions of the brain (Petryk et al., 2015). In clinical settings, many patients with HPE fall within the border zone of neighboring subtypes, and thus HPE is postulated to exist as a continuum of phenotypes rather than discrete subtypes (Hahn and Barnes, 2010).

The pathogenesis of HPE is complex and involves both genetic causes and environmental risk factors. HPE occurs due to defective development of the axial midline, which is largely orchestrated by Sonic hedgehog (SHH), BMP, FGF, WNT, Nodal, and retinoic acid signaling pathways (Grinblat and Lipinski, 2019). SHH signaling from the ventral midline is especially crucial for the outgrowth and patterning of developing brain. During embryogenesis, the brain is partitioned into prosencephalon, mesencephalon, and rhombencephalon (**Figure 1B**). While all three regions undergo further compartmentalization, the most relevant region in HPE pathogenesis is the prosencephalon or forebrain, which is further divided anteriorly into the telencephalon and posteriorly into the diencephalon. Unlike TCS, the craniofacial phenotypes associated with HPE do not come primarily from excessive apoptosis within the neural tube but instead are consequences of the molecular reprogramming of SHH signaling activity (Cordero et al., 2004; Richbourg et al., 2020). Nonetheless, apoptosis within cranial NCC due to aberrant Shh signaling can add to the severity of HPE (Cordero et al., 2004).

SHH plays a key role in coordinating dorsoventral polarity of the forebrain by establishing ventral identity in the neural tube during early embryogenesis (Ericson et al., 1995). Hedgehog (HH) proteins undergo lipid modifications and are anchored to the membrane of the producing cells prior to secretion. After being released from the cell membrane by Dispatched (DISP1), HH then binds to its receptor PTCH, which subsequently relieves the inhibition of SMO facilitating signaling through the GLI protein family (Burke et al., 1999; Ruiz and Altaba, 1999; Denef et al., 2000). Other HH-binding proteins, such as BOC, CDO, and GAS1 may act as co-receptors to enhance SHH signaling activity (Tenzen et al., 2006; Allen et al., 2007). Considering the central role that SHH signaling plays during midfacial development, it is perhaps unsurprising that mutations in *SHH* loci are the most common genetic cause of HPE in humans (Roessler et al., 2018). However, individuals with *SHH* mutations display incomplete penetrance, with only about 37% of carriers actually developing HPE (Roessler et al., 1996). Similarly, mutations in other *SHH*-related genes such as *GLI2* and *ZIC2* lead to HPE with variable severity. This indicates that haploinsufficiency for the respective genes alone is insufficient to elicit the full spectrum of HPE phenotypes (Petryk et al., 2015).

The variable severity of HPE may be associated with the time at which HH signaling is disrupted (Cohen, 2006), or a dose-dependent decrease in signaling activity. In 1908, anatomist Harris Wilder postulated the "Morphology of Cosmobia" where he speculated that a spectrum of symmetrical anomalies of the face was due to "*some modification in the germ itself, leading the organisms to develop in accordance with laws as definite and natural, though not as usual, as those governing normal development*" (Wilder, 1908). This spectrum of facial anomalies in effect corresponds to a gradient of Shh signaling activity, where elimination or a significant reduction in Shh signaling leads to cyclopia, a severe form of HPE characterized by a single median eye and proboscis, while in contrast, increased Shh signaling can result in facial duplication (Wilder, 1908; **Figure 3**). In support of this idea, work in chick embryos has shown that varying the level of Shh signaling affects the induction and spatial organization of the frontonasal ectodermal zone (FEZ) (Cordero et al., 2004), and alters dorsoventral patterning of the forebrain (Brugmann et al., 2010), each of which results in significant changes in facial appearance.

Animal models provide evidence for a functional threshold level of Shh signaling below which HPE phenotypes are always severe. In mice, homozygous mutation of *Shh* results in cyclopia and proboscis, leading to embryonic lethality, whereas *Shh* heterozygous mice are morphologically normal (Chiang et al., 1996). Genetic background also has a major effect on the penetrance of HPE phenotypes in mice. For instance, a homozygous mutation of *Cdo* on a 129S6/SvEvTac background results in mild facial microforms of HPE, whereas on a C57BL/6NTac background results in phenotypes similar to semilobar HPE (Chiang et al., 1996). Other intrinsic signaling pathways affecting the level of *Shh* expression may also contribute to HPE phenotypic variation. For example, mutations of *Tgif*, which maintains the balance between Shh and its antagonist Gli3 (Taniguchi et al., 2012), result in a more severe HPE phenotype when coupled with *Shh* haploinsufficiency compared to phenotypes from individual mutations alone (Chiang et al., 1996). Tgif protein can bind to a retinoic acid response element (RARE) in Cyp26a1, which plays a critical role in anterior-posterior patterning of the forebrain through the degradation of retinoic acid (Gongal and Waskiewicz, 2008). Sub-teratogenic doses of retinoic acid, which are often prescribed to treat skin conditions, thereby sensitize embryos to *Tgif* mutations (Bartholin et al., 2006). This supports the notion of a Shh threshold, where any additional stress, be it from genetic factors or the environment, can lower *Shh* expression below the level at which HPE always manifests (Bartholin et al., 2006).

Major environmental risk factors implicated in human HPE include maternal diabetes and ethanol exposure, which converge on SHH signaling. Around 1–2% of infants born from diabetic mothers develop HPE and women with gestational diabetes have twice the risk for HPE compared to control mothers (Petryk et al., 2015). Maternal hyperglycemia can disrupt the oxidant-antioxidant balance in the embryos and increase oxidative stress, increasing the severity of HPE (Zhao and Reece, 2005; **Figure 3**). Similarly, ethanol exposure impairs *Shh* expression and causes defects in midline development. Ethanol activates PKA, a negative regulator of Shh signaling, in the anterior prechordal mesendoderm during midline specification, and subsequently induces apoptosis (Lepage et al., 1995; Pan and Rubin, 1995; Hammerschmidt et al., 1996; Ahlgren and Bronner-Fraser, 1999; Aoto et al., 2008). Both ethanol-induced cranial neural crest cell death and associated craniofacial growth defects can be rescued by exogenous Shh, suggesting that craniofacial anomalies

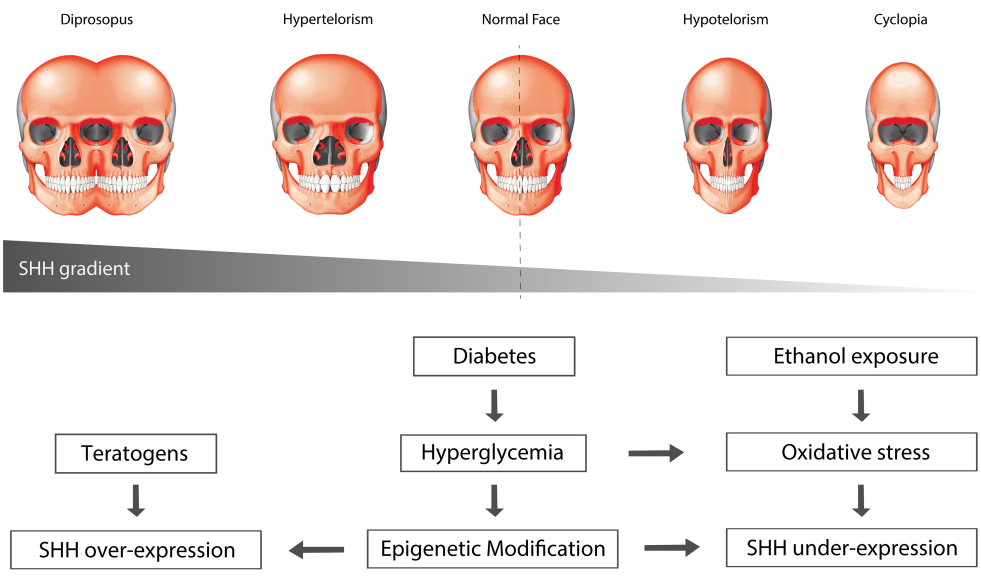

FIGURE 3 | Environmental factors can affect SHH signaling. Oxidative stress and epigenetic modification can alter the levels of SHH signaling. Over-activation of SHH results in widening of the midline, leading to phenotypes such as hypertelorism and diprosopus, or facial duplication. Conversely, suppression of SHH signaling results in narrowing of the midline, leading to hypotelorism and cyclopia, phenotypes that are commonly associated with holoprosencephaly.

resulting from fetal alcohol exposure are caused at least partially by loss of Shh and its effects on neural crest cell survival (Ahlgren et al., 2002). In addition, dietary antioxidant supplementation can prevent the abolition of *Shh* expression as well as apoptosis in a dose-dependent manner. This indicates that oxidative stress can downregulate Shh expression and may contribute to the phenotypic variability observed in *SHH* heterozygous patients (Aoto et al., 2008). More recently, ethanol was shown to synergize directly with *Cdo* mutations to suppress *Shh* expression and elicit severe HPE on a 129S6 background, which would otherwise only exhibit a mild phenotype (Hong and Krauss, 2017). Interestingly, antioxidant treatment did not alter the frequency or severity of HPE phenotypes in these mice despite normalization of ROS levels. These conflicting results suggest that ethanol's teratogenicity may occur via multiple mechanisms depending on the genetic background and developmental context.

With respect to the HPE continuum, a functional ceiling is likely to exist where Shh signaling above a certain level can induce replication stress and DNA damage. Consistent with this idea, overexpression of the Shh co-receptor gene *BOC* results in elevated Shh-induced replication stress and DNA damage, which increases the incidence of *Ptch* loss-of-heterozygosity, leading to constitutive activation of Shh signaling (Mille et al., 2014). It is well-known that *Ptch* gain-of-function can cause HPE due to ventralization of the neural tube and incorrect specification of the forebrain (Goodrich et al., 1999; Mullor and Guerrero, 2000), however, it has yet to be determined whether rescuing DNA damage can ameliorate the effect of Shh over-activation in this case. Aside from replication stress, mutations resulting in excessive Shh signaling lead directly to increased proliferation of neural crest cells, which can manifest as hypertelorism and frontonasal dysplasia (Mille et al., 2014). Furthermore, mouse embryos derived from dams with streptozotocin-induced diabetes exhibit expanded *Shh* expression in the ventral telencephalon, which leads to a phenotype similar to the middle interhemispheric variant of HPE (Brugmann et al., 2010). Taken together, the variable expressivity of similar HPE gene mutations can be attributed to co-morbid genetic interactors and environmental modifiers.

DIABETES, OXIDATIVE STRESS AND DNA DAMAGE AFFECT CRANIOFACIAL DEVELOPMENT AND MODULATE PHENOTYPE VARIBILITY IN CRANIOFACIAL SYNDROMES

Hyperglycemia in Diabetic Pregnancy Alters Cellular Metabolism and Increases Oxidative Stress

Maternal diabetes involves systemic metabolic changes which can affect virtually any organ system, but the craniofacial, central nervous system and cardiovascular structures are primarily affected (Becerra et al., 1990). These diabetic pregnancy-induced malformations, collectively termed diabetic embryopathy, are thought to arise due to defects in neurulation and neural crest cell development during the early stages of organogenesis, which corresponds to approximately the first 8 weeks of human gestation (Mills et al., 1979; Li et al., 2005; Fetita et al., 2006; Loeken, 2006). The prevalence for women with either type 1 or type 2 diabetes to be at high risk for giving birth to babies with diabetic embryopathy (Towner et al., 1995), suggests a fundamental causal role for hyperglycemia and increased glucose uptake to the embryo via glucose transporters (Loeken, 2020).

Excessive glucose metabolism increases oxidative phosphorylation (OXPHOS) and the production of reactive oxygen species (ROS), which induces a state of oxidative stress if not balanced by increased antioxidant capacity (Wentzel and Eriksson, 2011; Kim et al., 2017; Loeken, 2020). Intracellular ROS such as superoxide (O_2^-) is primarily produced via the oxidation of NADPH or by the partial reduction of oxygen during aerobic respiration in mitochondria. Superoxide can be converted into hydrogen peroxide (H_2O_2) by superoxide dismutases, which then either oxidizes cysteine residues on proteins or becomes converted to H_2O by cellular antioxidant proteins such as catalase, glutathione peroxidase or peroxiredoxins. If high levels of H_2O_2 levels go unchecked, hydroxyl radicals (OH^-) will form and this can result in molecular, cellular, and tissue damage during embryogenesis (Jones and Sies, 2015). However, increased oxidant status is complex, involving a combination of increased superoxide production as well as impaired free radical scavenging, although the pathways responsible for increased oxidant status have not been completely elucidated. Interestingly, early embryonic development is especially vulnerable to oxidative stress due to the lack of free radical scavenging enzymes activity (El-hage and Singh, 1990). In fact, premigratory and migratory NCC appear to be particularly at risk of free radical damage since they are deficient in superoxide dismutase and catalase activity, which are necessary for the normal inactivation of superoxide, hydrogen peroxide and hydroxyl radicals (Davis et al., 1990; Chen and Sulik, 1996). This is consistent with the neuroepithelium from which NCC originate, existing in a highly oxidative state and being particularly sensitive to exogenous oxidative stress (Sakai et al., 2016), thus indicating that cranial NCC possess lower tolerance to the detrimental effect of increased ROS.

High glucose metabolism in NCC may be attributable to their rapid proliferation and motile nature, reminiscent of the Warburg effect in cancer metastasis (Warburg, 1956). Actively dividing cells favor glucose metabolism through aerobic glycolysis to produce biomass. In contrast, terminally differentiated cells rely on OXPHOS to generate energy more efficiently from glucose (Warburg, 1956). Cellular glucose metabolism thus alternates between aerobic glycolysis and OXPHOS depending on the stage of development. During EMT, neural crest cells undergo similar cytoskeletal and molecular changes observed in metastatic tumor cells where aerobic glycolysis is increased to serve the anabolic demand of proliferation. Enhanced aerobic glycolysis promotes the Yap/Tead pathway that is necessary for cell delamination during EMT (Bhattacharya et al., 2020). Conversely, the decay of glycolytic activity and increased OXPHOS correlate with the

loss of mesenchymal motility (Warburg, 1956), suggesting that hyperglycemia may accelerate the differentiation of neural crest-derived tissues through preferential switching to OXPHOS. Additionally, hyperglycemia-induced oxidative stress leads to the oxidation of cholesterol, lipids, and proteins, which have been proposed to contribute to the pathology of Smith-Lemli-Opitz syndrome (Richards et al., 2006) and thus may add to the phenotypic variability of HPE. Since proper Shh gradient formation is dependent upon cholesterol modification, oxidation of cholesterol can directly impact Shh signaling and impair neural tube patterning (Guerrero and Chiang, 2007; Porter and Herman, 2011). More studies are still needed to understand whether untimely switching to OXPHOS and increased cholesterol oxidation contribute to increased risk of craniofacial malformation or variation in craniofacial development. However, it is clear that improper fluctuations of glucose metabolism in diabetic embryopathy can adversely affect NCC EMT and migration as well as neural tube patterning, resulting in craniofacial malformations.

Hyperglycemia-Induced Oxidative Stress Leads to Epigenetic Modifications and Altered Gene Expression

One of the negative effects of excess ROS is that it can disrupt key signaling events during cellular differentiation, resulting in structural abnormalities (Kemp et al., 2008). In fact, many developmental genes exhibit specific sensitivities to hyperglycemic conditions and changes in the cellular redox state (Fetita et al., 2006; Wu et al., 2012). This may be due in part to the presence of binding sites for transcription factors involved in response to oxidative stress in their promoters (Pavlinkova et al., 2009). These genes which were identified under the conditions of maternal diabetes, and in the absence of genetic alterations, are therefore subject to gene-environment interactions in their response to the intrauterine environment of a diabetic pregnancy. Further evidence indicates that environmental factors can perturb gene regulation, which may affect gene dosage variability in individuals from different genetic backgrounds (Phelan et al., 1997). For instance, both diabetes and oxidative stress can impair Shh signaling by increasing or reducing Shh expression, which leads to defects in neural tube patterning (Pavlinkova et al., 2009). Furthermore, maternal diabetes increases the overall variability of gene expression levels in embryos, including deregulation of genes involved in Wnt, Hedgehog, and Notch signaling (Salbaum and Kappen, 2010). Additionally, diabetes-induced oxidative stress results in reduced expression of *Pax3*, which plays a major role in neuroepithelial development (Pavlinkova et al., 2009; Salbaum and Kappen, 2010). *Pax3* loss-of-function results in aberrant p53 activation, neuroepithelium and neural crest cell apoptosis, and consequently neural tube defects (Liao et al., 2004; Aoto et al., 2008) as well as malformation of structures derived from neural crest cells (Loeken, 2006; Wu et al., 2012).

Epigenetic factors, such as DNA methylation and histone modification, may also contribute to this variability through gene silencing or aberrant activation. In fact, hyperglycemia and oxidative stress were shown to trigger chromatin modifications via histone and DNA methylation. Mouse neural stem cells derived from the embryos of diabetic mothers exhibit increased global histone H3K9 trimethylation and DNA methylation, as well as decreased histone H3K9 acetylation which leads to altered miRNA expression (Shyamasundar et al., 2013; Ramya et al., 2017). Alteration of miRNA activity can impair autophagy and lead to neural tube defects such as exencephaly (Xu et al., 2013; Wang et al., 2017). The same phenomena were also observed in human neural progenitor cells in which high glucose modifies the DNA methylation pattern of neurodevelopment-associated genes, hence affecting their activity (Kandilya et al., 2020). These findings suggest that hyperglycemia can interact with genetic loci by influencing the activities of histone-modifying and DNA methyltransferase enzymes. Indeed, increased activity of DNA methyltransferase 3b (*Dnmt3b*) in mouse embryos and embryonic stem cells (mESC) of diabetic mothers result in decreased methylation of *Pax3* CpG island, which leads to silencing of *Pax3* (Wei and Loeken, 2014). More importantly, *Tcof1* and *Cdo* were shown to be deregulated in hyperglycemic embryos (Salbaum and Kappen, 2010), indicating that maternal diabetes may exacerbate TCS and HPE phenotypes by directly lowering *Tcof1* and *Cdo* expression even further. It has yet to be determined what epigenetic modification occurs within *Tcof1* and *Cdo* CpG islands, however, hyperglycemia-induced epigenetic modifications potentially underlie gene expression variability in $Tcof1^{+/-}$ or $Cdo^{-/-}$ mutant mice on different genetic background, which may correlate with phenotypic variability in TCS and HPE.

A Potential Role for DNA Damage in Craniofacial Development

The rapid and sustained proliferation of premigratory and migratory NCC results in naturally high levels of ROS, which if left unchecked can lead to genotoxic stress in the form of DNA damage (Sakai and Trainor, 2016; Sakai et al., 2016). Newborns from mothers with diabetes exhibit elevated levels of 8-OHdG, which is a widely used marker for oxidative nucleotide damage (Gelaleti et al., 2015; Castilla-Peon et al., 2019), and suggests that hyperglycemia can induce DNA damage. In support of this idea, analysis of neurulation-stage mouse embryos showed that hyperglycemia increases the DNA damage marker p-H2AX, which can be suppressed by overexpression of antioxidant SOD1 both *in vitro* and *in vivo*. This indicates that the hyperglycemic environment triggers DNA damage and the DNA damage response (DDR) pathway through oxidative stress (Dong et al., 2015).

NCC-derived tissues seem to be particularly sensitive to DNA damage accumulation due to the lower antioxidant capacity and higher level of ROS in the neuroepithelium and progenitor NCC. Global treatment of mouse embryos with the mitochondrial inhibitor 3-nitropropionic acid induces ROS over-production, resulting in elevated levels of DNA damage specifically within the neuroepithelium (Sakai and Trainor, 2016; Sakai et al., 2016). Although ubiquitously expressed and central to cell survival, the localized endogenous spatiotemporal generation of ROS could render the effects of mutations in DDR genes more significant in

NCC-derived tissues compared to other tissues. This is evident from the phenotypes of mutations in *BRCA1*, *MRE11*, *RAD50* and *NBS1* in humans and in mouse models. Mutations affecting the *MRE11-RAD50-NBS1* (*MRN*) protein complex are known to cause craniofacial anomalies (Chrzanowska et al., 2001; Fernet et al., 2005; Waltes et al., 2009). The MRN complex functions as a DNA damage sensor by recognizing and binding to the broken ends of DNA (Assenmacher and Hopfner, 2004; Paull and Lee, 2005; Stracker and Petrini, 2011) and thus regulates initial and sustained responses to DNA damage. Hypomorphic mutations in *NBS1* are associated with Nijmegen breakage syndrome (NBS), which is characterized by distinct facial features including a small lower jaw (Chrzanowska et al., 2012). Similarly, mutations in *MRE11* have also been shown to underlie craniofacial anomalies such as a small lower jaw, together with microcephaly as part of the rare Ataxia Telangiectasia-like disorder (Matsumoto et al., 2011). Developmentally, these phenotypes are thought to arise in part through extensive neuroepithelial apoptosis (Kobayashi et al., 2004; McKinnon, 2012), and consistent with these observations in humans, neural stem cell-specific conditional deletion of *Nbs1* and *Mre11* in mouse embryos results in microcephaly (Frappart et al., 2005).

Further support for the importance of DNA damage repair in neural crest cell and craniofacial development can be found in *BRCA1*, a tumor suppressor and a key player in the DNA damage response through its central role in homologous recombination (Frappart et al., 2005). *BRCA1* dysregulation is associated with non-syndromic cleft lip and palate, which is one of the most common human craniofacial defects (Kobayashi et al., 2013). Knockout of *Brca1* in mouse embryos results in extensive neuroepithelial cell apoptosis during the early stages of craniofacial development (Gowen et al., 1996; Hakem et al., 1996; Liu et al., 1996). Conditional deletion of *Brca1* in NCC in mouse embryos manifests in hypoplastic jaws, cleft palate, and microcephaly. NCC-derived osteogenic progenitors exhibited increased levels of γ-H2AX and p53 activation, which subsequently led to their apoptosis, resulting in cranioskeletal hypoplasia. Interestingly, the loss of *Brca1* did not affect osteogenic differentiation, indicating that Brca1-mediated DNA damage repair is critically required for osteoprogenitor survival during craniofacial development (Kitami et al., 2018; Yamaguchi et al., 2021).

These findings illustrate the importance of maintaining genome integrity during NCC development and help to account for why disruptions in a central process such as the DNA damage response can result in tissue-specific developmental defects. Given that the neuroepithelium exists naturally in a highly oxidative state, which lowers its threshold for oxidative stress-induced p53 activation compared to other tissues (Sakai et al., 2016), suppressing p53 function should in theory offer an avenue for the prevention of some craniofacial malformations. Indeed, both pharmacological and genetic inhibition of p53 function can decrease neuroepithelial apoptosis and rescue animal models of TCS (Jones et al., 2008), open neural tube defects (Pani et al., 2002), and HPE (Billington et al., 2011). Preventing p53 activation through maintenance of proper physiological levels of ROS can therefore help avoid the detrimental effects of DNA damage. In support of this idea, NAC antioxidant supplementation ameliorated the TCS phenotype in *Tcof1*$^{+/-}$ mouse embryos via the diminishment of γ-H2AX, p-Chk2, and p53 (Sakai et al., 2016). Similarly, several studies have shown that administration of antioxidants, particularly vitamins C or E, or overexpression of superoxide dismutase reduce the incidence of developmental defects in experimental models of intrauterine diabetes and hyperglycemia (Aoto et al., 2008). Taken together, these data reveal the importance of redox homeostasis for proper developmental signaling and cell viability. Redox homeostasis is maintained through a fine balance between oxidants and antioxidants and when an imbalance occurs prolonged oxidative stress can induce genotoxic stress in the form of DNA strand breaks. Maternal diabetes, smoking and alcohol consumption during pregnancy are all factors known to increase maternal ROS levels, which can be damaging to the genomic DNA of embryos (Ornoy, 2007). Thus in the absence of key pathways for detoxifying ROS or DNA damage repair, persistent hyperglycemia-induced oxidative stress can have embryopathic consequences (Wells et al., 2010) or exacerbate the phenotypic severity caused by a particular genetic mutation (**Figure 4**). Although the full extent of oxidative stress-induced DNA damage remains to be elucidated, multiple studies have indicated that insufficient DNA damage repair capacity, particularly within premigratory and migratory neural crest cells, can lead to craniofacial malformations (Ornoy, 2007). More importantly, this suggests that oxidative stress-induced DNA damage can underpin gene-environment interactions and influence the variable phenotypic severity observed in many craniofacial disorders and syndromes.

CONCLUDING REMARKS AND FUTURE PERSPECTIVES

The anatomical complexity of the craniofacial complex coupled with the initiation of its development during early embryogenesis renders the head and face prone to malformation. One of the biggest clinical challenges in craniofacial biology is the frequent lack of accurate genotype-phenotype correlation. This illustrates the need for more detailed quantitative phenotyping to accurately capture the full spectrum of variation for an individual craniofacial syndrome, but it also implies that both genetic and environmental factors contribute to the etiology and pathogeneses of craniofacial anomalies. One of the biggest risk factors for increased severity in craniofacial disorders is maternal diabetes (Ewart-Toland et al., 2000; Chappell et al., 2009). Hyperglycemia, which is the hallmark of diabetes, disrupts cellular metabolism, induces over-production of reactive oxygen species (ROS), and dysregulates genes involved in craniofacial development. We postulate that the detrimental effect of any candidate mutation causing a craniofacial anomaly will be amplified by oxidative stress-induced DNA damage in the neuroepithelium and NCC (**Figure 4**). TCS is a prime example of this synergistic interaction. Haploinsufficiency of *Tcof1* not only disrupts rDNA transcription and ribosome biogenesis, which activates p53 thereby diminishing NCC proliferation

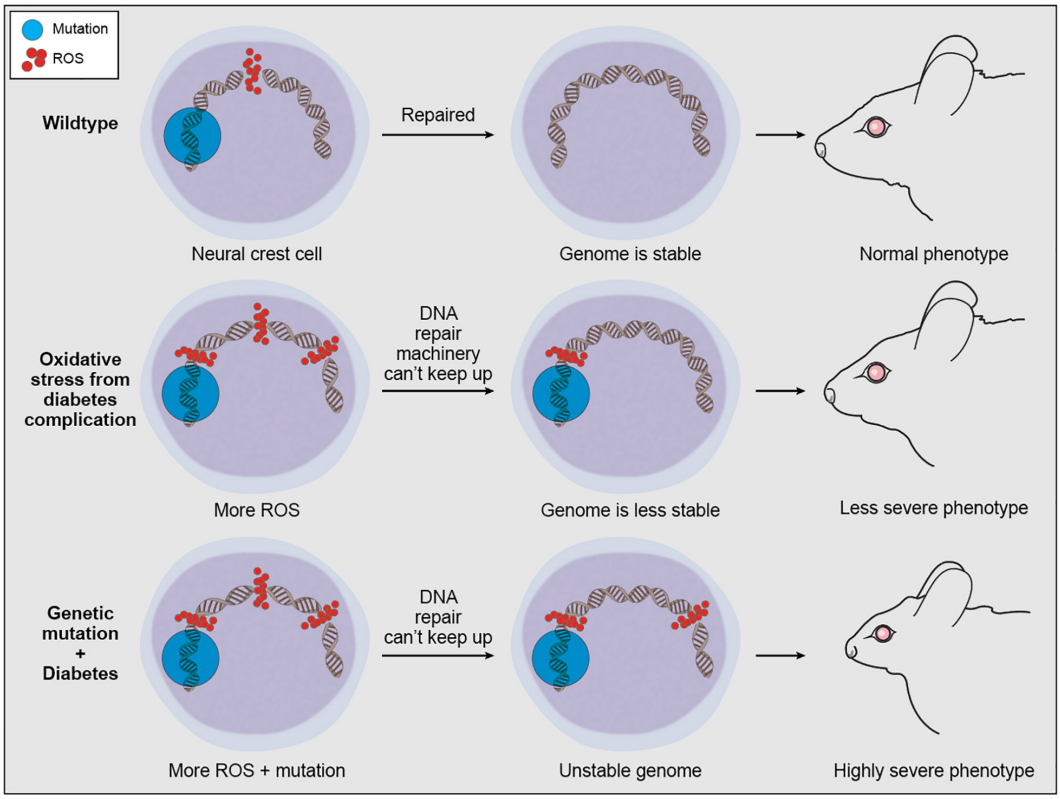

FIGURE 4 | Proposed mechanism of oxidative stress contribution to phenotypic variability in craniofacial anomalies. ROS is a natural byproduct of cellular metabolism which can be scavenged by antioxidant enzymes, and ROS-induced DNA damage within normal levels can be repaired by the DDR machinery. However, continuous exogenous or environmental oxidative stress can overwhelm antioxidant enzymes and DDR capacity, leaving some ROS-induced DNA damage unrepaired. This unrepaired DNA damage can compound the detrimental effects of genetic mutations associated with craniofacial malformations.

and survival, but haploinsufficiency of *Tcof1* also perturbs the DNA damage response and affects the ability of *Tcof1*$^{+/-}$ embryos to survive under endogenously high levels of oxidation (Dixon et al., 2006; Jones et al., 2008; Sakai et al., 2016). This demonstrates that DNA damage-inducing stress in the gestational environment, such as in the case of maternal diabetes and alcohol exposure, or modifier mutations in DNA damage response and repair genes could therefore affect phenotypic variability and compound TCS severity.

Although the complete mechanisms underpinning the teratogenic effects of maternal diabetes during pregnancy on development are not yet fully understood, it is clear that diabetes-induced oxidative stress, and oxidative stress-induced DNA damage, impacts neuroepithelial and neural crest cell survival and patterning, resulting in significant craniofacial dysmorphogenesis (Aoto et al., 2008). Optimizing maternal metabolic control in the first trimester of gestation during which neurulation and neural crest cell formation and migration occur is therefore critical for protecting newborns against oxidative damage and to ensure normal craniofacial morphogenesis. Suppression of p53-dependent apoptosis appears to be key in preventing many craniofacial anomalies by ensuring survival of neural crest cells throughout development. Although promising, inhibition of p53 poses an unacceptably high risk due to its role as a tumor suppressor. Thus, circumventing p53 activation by maintaining the correct physiological levels of oxidation is a potential avenue for preventing or reducing the severity of craniofacial anomalies. It is important to note however, that lowering ROS too far can pose a cytostatic risk where neural crest cells may not fully grow or differentiate, as well as increase the risk for immunosuppression within the embryo. It is also important to keep in mind that the nature of gene interactions with oxidative stress may differ according to their temporal, spatial, and biochemical context. To date, antioxidant supplementation has only been performed successfully in animal models of craniofacial disorders. Further investigation is needed to elucidate the appropriate dosage, time of administration, and side effects of antioxidant treatment as a viable means for preventing craniofacial anomalies in a clinical setting. Nonetheless, new studies should more extensively investigate the diagnostic and therapeutic value of various oxidative stress biomarkers and antioxidants to reduce oxidative tissue injury to developing newborns. Since phenotypes are frequently affected by gene-environment interactions, examining Quantitative Trait Loci using genetically diverse backgrounds under different environmental conditions may be beneficial for identifying such interactions. Using genome wide association studies (GWAS) to

identify gene-environment interaction can also be advantageous for identifying high-risk subjects and improving the diagnosis of complex craniofacial diseases.

AUTHOR CONTRIBUTIONS

SF and PT co-drafted, edited, and revised this review article. Both authors contributed to the article and approved the submitted version.

FUNDING

Research in the Trainor Laboratory is supported by the Stowers Institute for Medical Research.

ACKNOWLEDGMENTS

We would like to thank Mark Miller for his help in illustrating **Figures 1**, **3**, and **4**.

REFERENCES

Achilleos, A., and Trainor, P. A. (2012). Neural crest stem cells: discovery, properties and potential for therapy. *Cell Res.* 22, 288–304. doi: 10.1038/cr.2012.11

Achilleos, A., and Trainor, P. A. (2015). Mouse models of rare craniofacial disorders. *Curr. Top. Dev. Biol.* 115, 413–458. doi: 10.1016/bs.ctdb.2015.07.011

Ahlgren, S. C., and Bronner-Fraser, M. (1999). Inhibition of sonic hedgehog signaling in vivo results in craniofacial neural crest cell death. *Curr. Biol.* 9, 1304–1314. doi: 10.1016/s0960-9822(00)80052-4

Ahlgren, S. C., Thakur, V., and Bronner-Fraser, M. (2002). Sonic hedgehog rescues cranial neural crest from cell death induced by ethanol exposure. *Proc. Natl. Acad. Sci.U.S.A.* 99, 10476–10481. doi: 10.1073/pnas.162356199

Allen, B. L., Tenzen, T., and McMahon, A. P. (2007). The Hedgehog-binding proteins Gas1 and Cdo cooperate to positively regulate Shh signaling during mouse development. *Genes Dev.* 21, 1244–1257. doi: 10.1101/gad.1543607

Altmann, T., and Gennery, A. R. (2016). DNA ligase IV syndrome; a review. *Orphanet J. Rare Dis.* 11:137.

Aoto, K., Shikata, Y., Higashiyama, D., Shiota, K., and Motoyama, J. (2008). Fetal ethanol exposure activates protein kinase A and impairs Shh expression in prechordal mesendoderm cells in the pathogenesis of holoprosencephaly. *Birth Defects Res. A Clin. Mol. Teratol.* 82, 224–231. doi: 10.1002/bdra.20447

Assenmacher, N., and Hopfner, K. P. (2004). MRE11/RAD50/NBS1: complex activities. *Chromosoma* 113, 157–166.

Bae, C. J., and Saint-Jeannet, J. P. (2014). " Induction and specification of neural crest cells: extracellular signals and transcriptional switches," in *Neural Crest Cells: Evolution, Development and Disease*, ed. P. Trainor (Amsterdam: Elsevier Inc), 27–49. doi: 10.1016/b978-0-12-401730-6.00002-8

Bae, G. U., Domené, S., Roessler, E., Schachter, K., Kang, J. S., Muenke, M., et al. (2011). Mutations in CDON, encoding a hedgehog receptor, result in holoprosencephaly and defective interactions with other hedgehog receptors. *Am. J. Hum. Genet.* 89, 231–240. doi: 10.1016/j.ajhg.2011.07.001

Baggiolini, A., Varum, S., Mateos, J. M., Bettosini, D., John, N., Bonalli, M., et al. (2015). Premigratory and migratory neural crest cells are multipotent in vivo. *Cell Stem Cell* 16, 314–322. doi: 10.1016/j.stem.2015.02.017

Baroffio, A., Dupin, E., and Le Douarin, N. M. (1991). Common precursors for neural and mesectodermal derivatives in the cephalic neural crest. *Development* 112, 301–305.

Barriga, E. H., Trainor, P. A., Bronner, M., and Mayor, R. (2015). Animal models for studying neural crest development: is the mouse different? *Development* 142, 1555–1560. doi: 10.1242/dev.121590

Bartholin, L., Powers, S. E., Melhuish, T. A., Lasse, S., Weinstein, M., and Wotton, D. (2006). TGIF inhibits retinoid signaling. *Mol. Cell. Biol.* 26, 990–1001. doi: 10.1128/mcb.26.3.990-1001.2006

Bartzela, T. N., Carels, C., and Maltha, J. C. (2017). Update on 13 syndromes affecting craniofacial and dental structures. *Front. Physiol.* 8:1038. doi: 10.3389/fphys.2017.01038

Basch, M. L., Bronner-Fraser, M., and García-Castro, M. I. (2006). Specification of the neural crest occurs during gastrulation and requires Pax7. *Nature* 441, 218–222. doi: 10.1038/nature04684

Becerra, J. E., Khoury, M. J., Cordero, J. F., and Erickson, J. D. (1990). Diabetes mellitus during pregnancy and the risks for the specific birth defects: a population-based case-control study. *Pediatrics* 85, 1–9.

Bhatt, S., Diaz, R., and Trainor, P. A. (2013). Signals and switches in mammalian neural crest cell differentiation. *Cold Spring Harb. Perspect. Biol.* 5:a008326. doi: 10.1101/cshperspect.a008326

Bhattacharya, D., Azambuja, A. P., and Simoes-Costa, M. (2020). Metabolic reprogramming promotes neural crest migration via Yap/Tead signaling. *Dev. Cell* 53, 199–211.e6.

Billington, C. J., Ng, B., Forsman, C., Schmidt, B., Bagchi, A., Symer, D. E., et al. (2011). The molecular and cellular basis of variable craniofacial phenotypes and their genetic rescue in twisted gastrulation mutant mice. *Dev. Biol.* 355, 21–31. doi: 10.1016/j.ydbio.2011.04.026

Boone, A. T. S., Chinn, I. K., Alaez-Versón, C., Yamazaki-Nakashimada, M. A., Carrillo-Sánchez, K., García-Cruz, M. L. H., et al. (2019). Failing to make ends meet: the broad clinical spectrum of DNA ligase IV deficiency. case series and review of the literature. *Front. Pediatr.* 6:426. doi: 10.3389/fped.2018.00426

Bronner, M. E., and LeDouarin, N. M. (2012). Development and evolution of the neural crest: an overview. *Dev. Biol.* 366, 2–9. doi: 10.1016/j.ydbio.2011.12.042

Brugmann, S. A., Allen, N. C., James, A. W., Mekonnen, Z., Madan, E., and Helms, J. A. (2010). A primary cilia-dependent etiology for midline facial disorders. *Hum. Mol. Genet.* 19, 1577–1592. doi: 10.1093/hmg/ddq030

Burke, R., Nellen, D., Bellotto, M., Hafen, E., Senti, K. A., Dickson, B. J., et al. (1999). Dispatched, a novel sterol-sensing domain protein dedicated to the release of cholesterol-modified hedgehog from signaling cells. *Cell* 99, 803–815. doi: 10.1016/s0092-8674(00)81677-3

Cano, A., Pérez-Moreno, M. A., Rodrigo, I., Locascio, A., Blanco, M. J., Del Barrio, M. G., et al. (2000). The transcription factor snail controls epithelial-mesenchymal transitions by repressing E-cadherin expression. *Nat. Cell Biol.* 2, 76–83. doi: 10.1038/35000025

Cao, S., Shen, W. B., Reece, E. A., and Yang, P. (2020). Deficiency of the oxidative stress–responsive kinase p70S6K1 restores autophagy and ameliorates neural tube defects in diabetic embryopathy. *Am. J. Obstet. Gynecol.* 223, 753.e1–753.e14.

Carey, J. C. (1992). Syndromes of the head and neck. Robert J. Gorlin, M. Michael Cohen Jr., and L. Stefan Levin.New York: Oxford University Press, 1990, 977 pp. *Am. J. Med. Genet.* 42:144. doi: 10.1002/ajmg.1320420133

Casson, I. F., Clarke, C. A., Howard, C. V., McKendrick, O., Pennycook, S., Pharoah, P. O. D., et al. (1997). Outcomes of pregnancy in insulin dependent diabetic women: results of a five year population cohort study. *Br. Med. J.* 315, 275–278. doi: 10.1136/bmj.315.7103.275

Castilla-Peon, M. F., Medina Bravo, P. G., Sánchez-Urbina, R., Gallardo-Montoya, J. M., Soriano-López, L. C., and Coronel Cruz, F. M. (2019). Diabetes and obesity during pregnancy are associated with oxidative stress genotoxicity in newborns. *J. Perinatal Med.* 47, 347–353. doi: 10.1515/jpm-2018-0201

Chai, Y., Jiang, X., Ito, Y., Bringas, P., Han, J., Rowitch, D. H., et al. (2000). Fate of the mammalian cranial neural crest during tooth and mandibular morphogenesis. *Development* 127, 1671–1679.

Chappell, J. H., Wang, X. D., and Loeken, M. R. (2009). Diabetes and apoptosis: neural crest cells and neural tube. *Apoptosis* 14, 1472–1483. doi: 10.1007/s10495-009-0338-6

Chen, S. Y., and Sulik, K. K. (1996). Free radicals and ethanol-induced cytotoxicity in neural crest cells. *Alcohol. Clin. Exp. Res.* 20, 1071–1076. doi: 10.1111/j.1530-0277.1996.tb01948.x

Chiang, C., Litingtung, Y., Lee, E., Young, K. E., Corden, J. L., Westphal, H., et al. (1996). Cyclopia and defective axial patterning in mice lacking Sonic hedgehog gene function. *Nature* 383, 407–413. doi: 10.1038/383407a0

Chrzanowska, K. H., Gregorek, H., Dembowska-Baginska, B., Kalina, M. A., and Digweed, M. (2012). Nijmegen breakage syndrome (NBS). *Orphanet J. Rare Dis.* 7:13.

Chrzanowska, K. H., Stumm, M., Bekiesiska-Figatowska, M., Varon, R., Biaecka, M., Gregorek, H., et al. (2001). Atypical clinical picture of the Nijmegen breakage syndrome associated with developmental abnormalities of the brain. *J. Med. Genet.* 38:E3.

Ciccia, A., Huang, J. W., Izhar, L., Sowa, M. E., Harper, J. W., and Elledge, S. J. (2014). Treacher Collins syndrome TCOF1 protein cooperates with NBS1 in the DNA damage response. *Proc. Natl. Acad. Sci.U.S.A.* 111, 18631–18636. doi: 10.1073/pnas.1422488112

Cohen, M. M. (2006). Holoprosencephaly: clinical, anatomic, and molecular dimensions. *Birth Defects Res. A Clin. Mol. Teratol.* 76, 658–673. doi: 10.1002/bdra.20295

Coles, E. G., Taneyhill, L. A., and Bronner-Fraser, M. (2007). A critical role for Cadherin6B in regulating avian neural crest emigration. *Dev. Biol.* 312, 533–544. doi: 10.1016/j.ydbio.2007.09.056

Cordero, D., Marcucio, R., Hu, D., Gaffield, W., Tapadia, M., and Helms, J. A. (2004). Temporal perturbations in sonic hedgehog signaling elicit the spectrum of holoprosencephaly phenotypes. *J. Clin. Investig.* 114, 485–494. doi: 10.1172/jci200419596

Crane, J. F., and Trainor, P. A. (2006). Neural crest stem and progenitor cells. *Annu. Rev. Cell Dev. Biol.* 22, 267–286.

Dash, S., and Trainor, P. A. (2020). The development, patterning and evolution of neural crest cell differentiation into cartilage and bone. *Bone* 137:115409. doi: 10.1016/j.bone.2020.115409

Dauwerse, J. G., Dixon, J., Seland, S., Ruivenkamp, C. A. L., Van Haeringen, A., Hoefsloot, L. H., et al. (2011). Mutations in genes encoding subunits of RNA polymerases i and III cause treacher collins syndrome. *Nat. Genet.* 43, 20–22. doi: 10.1038/ng.724

Davis, W. L., Crawford, L. A., Cooper, O. J., Farmer, G. R., Thomas, D. L., and Freeman, B. L. (1990). Ethanol induces the generation of reactive free radicals by neural crest cells in vitro. *J. Craniofac. Genet. Dev. Biol.* 10, 277–293.

Denef, N., Neubüser, D., Perez, L., and Cohen, S. M. (2000). Hedgehog induces opposite changes in turnover and subcellular localization of patched and smoothened. *Cell* 102, 521–531. doi: 10.1016/s0092-8674(00)00056-8

Dixon, J., and Dixon, M. J. (2004). Genetic Background has a major effect on the penetrance and severity of craniofacial defects in mice heterozygous for the gene encoding the nucleolar protein treacle. *Dev. Dyn.* 229, 907–914. doi: 10.1002/dvdy.20004

Dixon, J., Edwards, S. J., Gladwin, A. J., Dixon, M. J., Loftus, S. K., Bonner, C. A., et al. (1996). Positional cloning of a gene involved in the pathogenesis of treacher collins syndrome. *Nat. Genet.* 12, 130–136. doi: 10.1038/ng0296-130

Dixon, J., Jones, N. C., Sandell, L. L., Jayasinghe, S. M., Crane, J., Rey, J. P., et al. (2006). Tcof1/Treacle is required for neural crest cell formation and proliferation deficiencies that cause craniofacial abnormalities. *Proc. Natl. Acad. Sci.U.S.A.* 103, 13403–13408. doi: 10.1073/pnas.0603730103

Dixon, M. J., Marres, H. A. M., Edwards, S. J., Dixon, J., and Cremers, C. W. R. J. (1994). Treacher collins syndrome: correlation between clinical and genetic linkage studies. *Clin. Dysmorphol.* 3, 96–103.

Dong, D., Yu, J., Wu, Y., Fu, N., Villela, N. A., and Yang, P. (2015). Maternal diabetes triggers DNA damage and DNA damage response in neurulation stage embryos through oxidative stress. *Biochem. Biophys. Res. Commun.* 467, 407–412. doi: 10.1016/j.bbrc.2015.09.137

Duan, X., Kelsen, S. G., Clarkson, A. B., Ji, R., and Merali, S. (2010). SILAC analysis of oxidative stress-mediated proteins in human pneumocytes: new role for treacle. *Proteomics* 10, 2165–2174. doi: 10.1002/pmic.201000020

Dupin, E., Calloni, G. W., and Le Douarin, N. M. (2010). The cephalic neural crest of amniote vertebrates is composed of a large majority of precursors endowed with neural, melanocytic, chondrogenic and osteogenic potentialities. *Cell Cycle* 9, 238–249. doi: 10.4161/cc.9.2.10491

Edwards, S. J., Fowlie, A., Cust, M. P., Liu, D. T., Young, I. D., and Dixon, M. J. (1996). Prenatal diagnosis in treacher collins syndrome using combined linkage analysis and ultrasound imaging. *J. Med. Genet.* 33, 603–606. doi: 10.1136/jmg.33.7.603

Edwards, S. J., Gladwin, A. J., and Dixon, M. J. (1997). The mutational spectrum in treacher collins syndrome reveals a predominance of mutations that create a premature-termination codon. *Am. J. Hum. Genet.* 60, 515–524.

El-hage, S., and Singh, S. M. (1990). Temporal expression of genes encoding free radical–metabolizing enzymes is associated with higher mRNA levels during in utero development in mice. *Dev. Genet.* 11, 149–159. doi: 10.1002/dvg.1020110205

Ericson, J., Muhr, J., Jessell, T. M., and Edlund, T. (1995). Sonic hedgehog: a common signal for ventral patterning along the rostrocaudal axis of the neural tube. *Int. J. Dev. Biol.* 39, 809–816.

Ewart-Toland, A., Yankowitz, J., Winder, A., Imagire, R., Cox, V. A., Aylsworth, A. S., et al. (2000). Oculoauriculovertebral abnormalities in children of diabetic mothers. *Am. J. Med. Genet.* 90, 303–309. doi: 10.1002/(sici)1096-8628(20000214)90:4<303::aid-ajmg8>3.0.co;2-q

Fernet, M., Gribaa, M., Salih, M. A. M., Seidahmed, M. Z., Hall, J., and Koenig, M. (2005). Identification and functional consequences of a novel MRE11 mutation affecting 10 Saudi Arabian patients with the ataxia telangiectasia-like disorder. *Hum. Mol. Genet.* 14, 307–318. doi: 10.1093/hmg/ddi027

Fetita, L. S., Sobngwi, E., Serradas, P., Calvo, F., and Gautier, J. F. (2006). Consequences of fetal exposure to maternal diabetes in offspring. *J. Clin. Endocrinol. Metab.* 91, 3718–3724. doi: 10.1210/jc.2006-0624

Frappart, P. O., Tong, W. M., Demuth, I., Radovanovic, I., Herceg, Z., Aguzzi, A., et al. (2005). An essential function for NBS1 in the prevention of ataxia and cerebellar defects. *Nat. Med.* 11, 538–544. doi: 10.1038/nm1228

Gans, C., and Northcutt, R. G. (1983). Neural crest and the origin of vertebrates: a new head. *Science* 220, 268–273. doi: 10.1126/science.220.4594.268

García-Castro, M. I., Marcelle, C., and Bronner-Fraser, M. (2002). Ectodermal Wnt function as a neural crest inducer. *Science* 297, 848–851.

Gelaleti, R. B., Damasceno, D. C., Salvadori, D. M. F., Marcondes, J. P. C., Lima, P. H. O., Morceli, G., et al. (2015). IRS-1 gene polymorphism and DNA damage in pregnant women with diabetes or mild gestational hyperglycemia. *Diabetol. Metab. Syndr.* 7:30.

Geng, X., and Oliver, G. (2009). Pathogenesis of holoprosencephaly. *J. Clin. Invest.* 119, 1403–1413. doi: 10.1172/jci38937

Ghesh, L., Vincent, M., Delemazure, A., Boyer, J., Corre, P., Perez, F., et al. (2019). Autosomal recessive treacher collins syndrome due to *POLR1C* mutations: report of a new family and review of the literature. *Am. J. Med. Genet. A* 179, 1390–1394.

Golden, J. A. (1999). Towards a greater understanding of the pathogenesis of holoprosencephaly. *Brain Dev.* 21, 513–521. doi: 10.1016/s0387-7604(99)00067-4

Gongal, P. A., and Waskiewicz, A. J. (2008). Zebrafish model of holoprosencephaly demonstrates a key role for TGIF in regulating retinoic acid metabolism. *Hum. Mol. Genet.* 17, 525–538. doi: 10.1093/hmg/ddm328

Goodrich, L. V., Jung, D., Higgins, K. M., and Scott, M. P. (1999). Overexpression of ptc1 inhibits induction of Shh target genes and prevents normal patterning in the neural tube. *Dev. Biol.* 211, 323–334. doi: 10.1006/dbio.1999.9311

Gorlin, R. J., Cohen, M. M. Jr., and Hennekam, R. C. M. (1990). *Syndromes of the Head and Neck*. Oxford: Oxford University Press.

Gowen, L. C., Johnson, B. L., Latour, A. M., Sulik, K. K., and Koller, B. H. (1996). Brca1 deficiency results in early embryonic lethality characterized by neuroepithelial abnormalities. *Nat. Genet.* 12, 191–194. doi: 10.1038/ng0296-191

Greene, M. F. (2001). Diabetic embryopathy 2001: moving beyond the'diabetic milieu'. *Teratology* 63, 116–118.

Grinblat, Y., and Lipinski, R. J. (2019). A forebrain undivided: unleashing model organisms to solve the mysteries of holoprosencephaly. *Dev. Dyn.* 248, 626–633. doi: 10.1002/dvdy.41

Guerrero, I., and Chiang, C. (2007). A conserved mechanism of hedgehog gradient formation by lipid modifications. *Trends Cell Biol.* 17, 1–5. doi: 10.1016/j.tcb.2006.11.002

Hahn, J. S., Barnes, P. D., Clegg, N. J., and Stashinko, E. E. (2010). Septopreoptic holoprosencephaly: a mild subtype associated with midline craniofacial anomalies. *Am. J. Neuroradiol.* 31, 1596–1601. doi: 10.3174/ajnr.a2123

Hahn, J. S., and Barnes, P. D. (2010). Neuroimaging advances in holoprosencephaly: refining the spectrum of the midline malformation. *Am. J. Med. Genet. Pt. C Semin. Med. Genet.* 154C, 120–132. doi: 10.1002/ajmg.c.30238

Hakem, R., De La Pompa, J. L., Sirard, C., Mo, R., Woo, M., Hakem, A., et al. (1996). The tumor suppressor gene Brca1 is required for embryonic cellular

proliferation in the mouse. *Cell* 85, 1009–1023. doi: 10.1016/s0092-8674(00)81302-1

Hall, B. K. (1999). *The Neural Crest in Development and Evolution*. New York, NY: Springer Science.

Hammerschmidt, M., Bitgood, M. J., and McMahon, A. P. (1996). Protein kinase A is a common negative regulator of Hedgehog signaling in the vertebrate embryo. *Genes Dev.* 10, 647–658. doi: 10.1101/gad.10.6.647

Han, D., Schomacher, L., Schüle, K. M., Mallick, M., Musheev, M. U., Karaulanov, E., et al. (2019). NEIL1 and NEIL2 DNA glycosylases protect neural crest development against mitochondrial oxidative stress. *ELife* 8:e49044.

Hatta, K., and Takeichi, M. (1986). Expression of N-cadherin adhesion molecules associated with early morphogenetic events in chick development. *Nature* 320, 447–449. doi: 10.1038/320447a0

Hawthorne, G., Robson, S., Ryall, E. A., Sen, D., Roberts, S. H., and Ward Platt, M. P. (1997). Prospective population based survey of outcome of pregnancy in diabetic women: results of the northern diabetic pregnancy audit, 1994. *Br. Med. J.* 315, 279–281. doi: 10.1136/bmj.315.7103.279

Hong, M., and Krauss, R. S. (2017). Ethanol itself is a holoprosencephaly-inducing teratogen. *PLoS One* 12:e0176440. doi: 10.1371/journal.pone.0176440

Hong, S., Hu, P., Roessler, E., Hu, T., and Muenke, M. (2018). Loss-of-function mutations in FGF8 can be independent risk factors for holoprosencephaly. *Hum. Mol. Genet.* 27, 1989–1998. doi: 10.1093/hmg/ddy106

Jones, D. P., and Sies, H. (2015). The redox code. *Antioxid. Redox Signal.* 23, 734–746. doi: 10.1089/ars.2015.6247

Jones, K. L., Smith, D. W., Harvey, M. A. S., Hall, B. D., and Quan, L. (1975). Older paternal age and fresh gene mutation: data on additional disorders. *J. Pediatr.* 86, 84–88. doi: 10.1016/s0022-3476(75)80709-8

Jones, N. C., Lynn, M. L., Gaudenz, K., Sakai, D., Aoto, K., Rey, J. P., et al. (2008). Prevention of the neurocristopathy treacher collins syndrome through inhibition of p53 function. *Nat. Med.* 14, 125–133. doi: 10.1038/nm1725

Kandilya, D., Shyamasundar, S., Singh, D. K., Banik, A., Hande, M. P., Stünkel, W., et al. (2020). High glucose alters the DNA methylation pattern of neurodevelopment associated genes in human neural progenitor cells in vitro. *Sci. Rep.* 10:15676.

Kemp, M., Go, Y. M., and Jones, D. P. (2008). Nonequilibrium thermodynamics of thiol/disulfide redox systems: a perspective on redox systems biology. *Free Radic. Biol. Med.* 44, 921–937. doi: 10.1016/j.freeradbiomed.2007.11.008

Kim, G., Cao, L., Reece, E. A., and Zhao, Z. (2017). Impact of protein O-GlcNAcylation on neural tube malformation in diabetic embryopathy. *Sci. Rep.* 7:11107.

Kitami, K., Kitami, M., Kaku, M., Wang, B., and Komatsu, Y. (2018). BRCA1 and BRCA2 tumor suppressors in neural crest cells are essential for craniofacial bone development. *PLoS Genet.* 14:e1007340. doi: 10.1371/journal.pgen.1007340

Kobayashi, G. S., Alvizi, L., Sunaga, D. Y., Francis-West, P., Kuta, A., Almada, B. V. P., et al. (2013). Susceptibility to DNA damage as a molecular mechanism for non-syndromic cleft lip and palate. *PLoS One* 8:e65677. doi: 10.1371/journal.pone.0065677

Kobayashi, J., Antoccia, A., Tauchi, H., Matsuura, S., and Komatsu, K. (2004). NBS1 and its functional role in the DNA damage response. *DNA Repair* 3, 855–861. doi: 10.1016/j.dnarep.2004.03.023

Kruszka, P., and Muenke, M. (2018). Syndromes associated with holoprosencephaly. *Am. J. Med. Genet. Semin. Med. Genet.* 178, 229–237. doi: 10.1002/ajmg.c.31620

Kucera, J. (1971). Rate and type of congenital anomalies among offspring of diabetic women. *J. Reprod. Med.* 7, 73–82.

Kulesa, P. M., Bailey, C. M., Kasemeier-Kulesa, J. C., and McLennan, R. (2010). Cranial neural crest migration: new rules for an old road. *Dev. Biol.* 344, 543–554. doi: 10.1016/j.ydbio.2010.04.010

Larsen, D. H., Hari, F., Clapperton, J. A., Gwerder, M., Gutsche, K., Altmeyer, M., et al. (2014). The NBS1-treacle complex controls ribosomal RNA transcription in response to DNA damage. *Nat. Cell Biol.* 16, 792–803. doi: 10.1038/ncb3007

Le Douarin, N. M., Creuzet, S., Couly, G., and Dupin, E. (2004). Neural crest cell plasticity and its limits. *Development* 131, 4637–4650. doi: 10.1242/dev.01350

Le Douarin, N., and Kalcheim, C. (1999). *The Neural Crest*. Cambridge: Cambridge University Press.

Lepage, T., Cohen, S. M., Diaz-Benjumea, F. J., and Parkhurst, S. M. (1995). Signal transduction by cAMP-dependent protein kinase A in Drosophila limb patterning. *Nature* 373, 711–715. doi: 10.1038/373711a0

Li, R., Chase, M., Jung, S.-K., Smith, P. J. S., and Loeken, M. R. (2005). Hypoxic stress in diabetic pregnancy contributes to impaired embryo gene expression and defective development by inducing oxidative stress. *Am. J. Physiol. Endocrinol. Metab.* 289, 591–599.

Liao, D. M., Ng, Y. K., Tay, S. S. W., Ling, E. A., and Dheen, S. T. (2004). Altered gene expression with abnormal patterning of the telencephalon in embryos of diabetic albino swiss mice. *Diabetologia* 47, 523–531. doi: 10.1007/s00125-004-1351-5

Liu, C. Y., Flesken-Nikitin, A., Li, S., Zeng, Y., and Lee, W. H. (1996). Inactivation of the mouse Brca1 gene leads to failure in the morphogenesis of the egg cylinder in early postimplantation development. *Genes Dev.* 10, 1835–1843. doi: 10.1101/gad.10.14.1835

Loeken, M. R. (2006). Advances in understanding the molecular causes of diabetes-induced birth defects. *J. Soc. Gynecol. Investig.* 13, 2–10. doi: 10.1016/j.jsgi.2005.09.007

Loeken, M. R. (2020). Mechanisms of congenital malformations in pregnancies with pre-existing diabetes. *Curr. Diab. Rep.* 20:54.

Marres, H. A. M., Cremers, W. R. J., Dixon, M. J., Huygen, P. L. M., and Joosten, F. B. M. (1995). The treacher collins syndrome: a clinical, radiological, and genetic linkage study on two pedigrees. *Arch. Otolaryngol. Head Neck Surg.* 121, 509–514. doi: 10.1001/archotol.1995.01890050009002

Matsumoto, Y., Miyamoto, T., Sakamoto, H., Izumi, H., Nakazawa, Y., Ogi, T., et al. (2011). Two unrelated patients with MRE11A mutations and Nijmegen breakage syndrome-like severe microcephaly. *DNA Repair* 10, 314–321. doi: 10.1016/j.dnarep.2010.12.002

Mayor, R., and Theveneau, E. (2012). The neural crest. *Development* 140, 2247–2251.

McKinnon, P. J. (2012). ATM and the molecular pathogenesis of ataxia telangiectasia. *Annu. Rev. Pathol.* 7, 303–321. doi: 10.1146/annurev-pathol-011811-132509

Mille, F., Tamayo-Orrego, L., Lévesque, M., Remke, M., Korshunov, A., Cardin, J., et al. (2014). The Shh receptor Boc promotes progression of early medulloblastoma to advanced tumors. *Dev. Cell* 31, 34–47. doi: 10.1016/j.devcel.2014.08.010

Mills, J. L. (2010). Malformations in infants of diabetic mothers. teratology 25:385-94. 1982. *Birth Defects Res. A Clin. Mol. Teratol.* 88, 769–778. doi: 10.1002/bdra.20757

Mills, J. L., Baker, L., and Goldman, A. S. (1979). Malformations in infants of diabetic mothers occur before the seventh gestational week. Implications for treatment. *Diabetes* 28, 292–293. doi: 10.2337/diabetes.28.4.292

Morrison, J. A., McLennan, R., Wolfe, L. A., Gogol, M. M., Meier, S., McKinney, M. C., et al. (2017). Single-cell transcriptome analysis of avian neural crest migration reveals signatures of invasion and molecular transitions. *ELife* 6:e28415.

Mullor, J. L., and Guerrero, I. (2000). A gain-of-function mutant of patched dissects different responses to the Hedgehog gradient. *Dev. Biol.* 228, 211–224. doi: 10.1006/dbio.2000.9862

Nieto, M. A., Sargent, M. G., Wilkinson, D. G., and Cooke, J. (1994). Control of cell behavior during vertebrate development by Slug, a zinc finger gene. *Science* 264, 835–839. doi: 10.1126/science.7513443

Noack Watt, K. E., Achilleos, A., Neben, C. L., Merrill, A. E., and Trainor, P. A. (2016). The roles of RNA polymerase I and III subunits Polr1c and Polr1d in craniofacial development and in zebrafish models of treacher collins syndrome. *PLoS Genet.* 12:e1006187. 10.1371/journal.pgen.1006187

Noden, D. M. (1983). The role of the neural crest in patterning of avian cranial skeletal, connective, and muscle tissues. *Dev. Biol.* 96, 144–165. doi: 10.1016/0012-1606(83)90318-4

Noden, D. M., and Trainor, P. A. (2005). Relations and interactions between cranial mesoderm and neural crest populations. *J. Anat.* 207, 575–601. doi: 10.1111/j.1469-7580.2005.00473.x

Ornoy, A. (2007). Embryonic oxidative stress as a mechanism of teratogenesis with special emphasis on diabetic embryopathy. *Reprod. Toxicol.* 24, 31–41. doi: 10.1016/j.reprotox.2007.04.004

Osumi-Yamashita, N., Ninomiya, Y., Doi, H., and Eto, K. (1994). The contribution of both forebrain and midbrain crest cells to the mesenchyme in the frontonasal mass of mouse embryos. *Dev. Biol.* 164, 409–419. doi: 10.1006/dbio.1994.1211

Pan, D., and Rubin, G. M. (1995). cAMP-dependent protein kinase and hedgehog act antagonistically in regulating decapentaplegic transcription in drosophila imaginal discs. *Cell* 80, 543–552. doi: 10.1016/0092-8674(95)90508-1

Pani, L., Horal, M., and Loeken, M. R. (2002). Rescue of neural tube defects in Pax-3-deficient embryos by p53 loss of function: implications for Pax-3-dependent development and tumorigenesis. *Genes Dev.* 16, 676–680. doi: 10.1101/gad.969302

Paull, T. T., and Lee, J. H. (2005). The Mre11/Rad50/Nbs1 complex and its role as a DNA double-strand break sensor for ATM. *Cell Cycle* 4, 737–740. doi: 10.4161/cc.4.6.1715

Pavlinkova, G., Michael, J. M., and Kappen, C. (2009). Maternal diabetes alters transcriptional programs in the developing embryo. *BMC Genomics* 10:274. doi: 10.1186/1471-2164-10-274

Petryk, A., Graf, D., and Marcucio, R. (2015). Holoprosencephaly: signaling interactions between the brain and the face, the environment and the genes, and the phenotypic variability in animal models and humans. *Wiley Interdiscip. Rev. Dev. Biol.* 4, 17–32. doi: 10.1002/wdev.161

Phelan, S. A., Ito, M., and Loeken, M. R. (1997). Neural tube defects in embryos of diabetic mice: role of the Pax-3 gene and apoptosis. *Diabetes* 46, 1189–1197. doi: 10.2337/diabetes.46.7.1189

Porter, F. D., and Herman, G. E. (2011). Malformation syndromes caused by disorders of cholesterol synthesis. *J. Lipid Res.* 52, 6–34. doi: 10.1194/jlr.r009548

Poswillo, D. (1975). Causal mechanisms of craniofacial deformity. *Br. Med. Bull.* 31, 101–106. doi: 10.1093/oxfordjournals.bmb.a071260

Prasad, M. S., Uribe-Querol, E., Marquez, J., Vadasz, S., Yardley, N., Shelar, P. B., et al. (2020). Blastula stage specification of avian neural crest. *Dev. Biol.* 458, 64–74. doi: 10.1016/j.ydbio.2019.10.007

Ramya, S., Shyamasundar, S., Bay, B. H., and Dheen, S. T. (2017). Maternal diabetes alters expression of MicroRNAs that regulate genes critical for neural tube development. *Front. Mol. Neurosci.* 10:237. doi: 10.3389/fnmol.2017.00237

Richards, M. J., Nagel, B. A., and Fliesler, S. J. (2006). Lipid hydroperoxide formation in the retina: correlation with retinal degeneration and light damage in a rat model of Smith-Lemli-Opitz syndrome. *Exp. Eye Res.* 82, 538–541. doi: 10.1016/j.exer.2005.08.016

Richbourg, H. A., Hu, D. P., Xu, Y., Barczak, A. J., and Marcucio, R. S. (2020). miR-199 family contributes to regulation of sonic hedgehog expression during craniofacial development. *Dev. Dyn.* 249, 1062–1076. doi: 10.1002/dvdy.191

Roessler, E., Belloni, E., Gaudenz, K., Jay, P., Berta, P., Scherer, S. W., et al. (1996). Mutations in the human sonic hedgehog gene cause holoprosencephaly. *Nat. Genet.* 14, 357–360. doi: 10.1038/ng1196-357

Roessler, E., Du, Y. Z., Mullor, J. L., Casas, E., Allen, W. P., Gillessen-Kaesbach, G., et al. (2003). Loss-of-function mutations in the human GLI2 gene are associated with pituitary anomalies and holoprosencephaly-like features. *Proc. Natl. Acad. Sci.U.S.A.* 100, 13424–13429. doi: 10.1073/pnas.2235734100

Roessler, E., Hu, P., Marino, J., Hong, S., Hart, R., Berger, S., et al. (2018). Common genetic causes of holoprosencephaly are limited to a small set of evolutionarily conserved driver genes of midline development coordinated by TGF-β, hedgehog, and FGF signaling. *Hum. Mutat.* 39, 1416–1427. doi: 10.1002/humu.23590

Roessler, E., Lacbawan, F., Dubourg, C., Paulussen, A., Herbergs, J., Hehr, U., et al. (2009). The full spectrum of holoprosencephaly-associated mutations within the ZIC2 gene in humans predicts loss-of-function as the predominant disease mechanism. *Hum. Mutat.* 30, E541–E554.

Rubbi, C. P., and Milner, J. (2003). Disruption of the nucleolus mediates stabilization of p53 in response to DNA damage and other stresses. *EMBO J.* 22, 6068–6077. doi: 10.1093/emboj/cdg579

Ruiz, I., and Altaba, A. (1999). Gli proteins and hedgehog signaling: development and cancer. *Trends Genet.* 15, 418–425. doi: 10.1016/s0168-9525(99)01840-5

Sakai, D., and Trainor, P. A. (2016). Face off against ROS: Tcof1/Treacle safeguards neuroepithelial cells and progenitor neural crest cells from oxidative stress during craniofacial development. *Dev. Growth Differ.* 58, 577–585. doi: 10.1111/dgd.12305

Sakai, D., Dixon, J., Achilleos, A., Dixon, M., and Trainor, P. A. (2016). Prevention of treacher collins syndrome craniofacial anomalies in mouse models via maternal antioxidant supplementation. *Nat. Commun.* 7:10328.

Salbaum, J. M., and Kappen, C. (2010). Neural tube defect genes and maternal diabetes during pregnancy. *Birth Defects Res. A Clin. Mol. Teratol.* 88, 601–611. doi: 10.1002/bdra.20680

Sanchez, E., Laplace-Builhé, B., Mau-Them, F. T., Richard, E., Goldenberg, A., Toler, T. L., et al. (2020). POLR1B and neural crest cell anomalies in treacher collins syndrome type 4. *Genet. Med.* 22, 547–556. doi: 10.1038/s41436-019-0669-9

Schneider, R. A., and Helms, J. A. (2003). The cellular and molecular origins of beak morphology. *Science* 299, 565–568. doi: 10.1126/science.1077827

Schneider, T., Bizarro, L., Asherson, P. J. E., and Stolerman, I. P. (2010). Gestational exposure to nicotine in drinking water: teratogenic effects and methodological issues. *Behav. Pharmacol.* 21, 206–216. doi: 10.1097/fbp.0b013e32833a5bb5

Seeman, P., Gebertová, K., Paděrová, K., Sperling, K., and Seemanová, E. (2004). Nijmegen breakage syndrome in 13% of age-matched Czech children with primary microcephaly. *Pediatric Neurol.* 30, 195–200. doi: 10.1016/j.pediatrneurol.2003.07.003

Shang, Z., Chen, D., Wang, Q., Wang, S., Deng, Q., Wu, L., et al. (2018). Single-cell RNA-seq reveals dynamic transcriptome profiling in human early neural differentiation. *GigaScience* 7:giy117.

Shyamasundar, S., Jadhav, S. P., Bay, B. H., Tay, S. S. W., Kumar, S. D., Rangasamy, D., et al. (2013). Analysis of epigenetic factors in mouse embryonic neural stem cells exposed to hyperglycemia. *PLoS One* 8:e65945. doi: 10.1371/journal.pone.0065945

Simões-Costa, M., and Bronner, M. E. (2015). Establishing neural crest identity: a gene regulatory recipe. *Development* 142, 242–257. doi: 10.1242/dev.105445

Soldatov, R., Kaucka, M., Kastriti, M. E., Petersen, J., Chontorotzea, T., Englmaier, L., et al. (2019). Spatiotemporal structure of cell fate decisions in murine neural crest. *Science* 364, 971–984.

Solomon, B. D., Lacbawan, F., Jain, M., Domene, S., Roessler, E., Moore, C., et al. (2009). A novel six3 mutation segregates with holoprosencephaly in a large family. *Am. J. Med. Genet. A* 149, 919–925. doi: 10.1002/ajmg.a.32813

Solomon, B. D., Mercier, S., Vélez, J. I., Pineda-Alvarez, D. E., Wyllie, A., Zhou, N., et al. (2010). Analysis of genotype-phenotype correlations in human holoprosencephaly. *Am. J. Med. Genet. C Semin. Med. Genet.* 154C, 133–141. doi: 10.1002/ajmg.c.30240

Stracker, T. H., and Petrini, J. H. J. (2011). The MRE11 complex: starting from the ends. *Nat. Rev. Mol. Cell Biol.* 12, 90–103. doi: 10.1038/nrm3047

Sulik, K. K., Cook, C. S., and Webster, W. S. (1988). Teratogens and craniofacial malformations: relationships to cell death. *Development* 103, 213–232.

Tam, P. P. L., and Trainor, P. A. (1994). Specification and segmentation of the paraxial mesoderm. *Anat. Embryol.* 189, 275–305.

Taneyhill, L. A., and Padmanabhan, R. (2014). "The cell biology of neural crest cell delamination and EMT," in *Neural Crest Cells: Evolution, Development and Disease*, ed. P. Trainor (Amsterdam: Elsevier Inc), 51–72. doi: 10.1016/b978-0-12-401730-6.00003-x

Taniguchi, K., Anderson, A. E., Sutherland, A. E., and Wotton, D. (2012). Loss of tgif function causes holoprosencephaly by disrupting the Shh signaling pathway. *PLoS Genet.* 8:e1002524. doi: 10.1371/journal.pgen.1002524

Tenzen, T., Allen, B. L., Cole, F., Kang, J. S., Krauss, R. S., and McMahon, A. P. (2006). The cell surface membrane proteins Cdo and Boc are components and targets of the hedgehog signaling pathway and feedback network in mice. *Dev. Cell* 10, 647–656. doi: 10.1016/j.devcel.2006.04.004

Towner, D., Kjos, S. L., Leung, B., Montoro, M. M., Xiang, A., Mestman, J. H., et al. (1995). Congenital malformations in pregnancies complicated by NIDDM: increased risk from poor maternal metabolic control but not from exposure to sulfonylurea drugs. *Diab. Care* 18, 1446–1451. doi: 10.2337/diacare.18.11.1446

Trainor, P. A. (2003). Making headway: the roles of Hox genes and neural crest cells in craniofacial development. *ScientificWorldJournal* 3, 240–264. doi: 10.1100/tsw.2003.11

Trainor, P. A. (2010). Craniofacial birth defects: the role of neural crest cells in the etiology and pathogenesis of Treacher Collins syndrome and the potential for prevention. *Am. J. Med. Genet. A* 152A, 2984–2994. doi: 10.1002/ajmg.a.33454

Trainor, P. A. (2013). "Molecular blueprint for craniofacial morphogenesis and development," in *Stem Cells in Craniofacial Development and Regeneration*, eds I. Thesleff and G. T. J. Huang (Hoboken, NJ: John Wiley & Sons, Inc), 1–29. doi: 10.1002/9781118498026.ch1

Trainor, P. A., and Krumlauf, R. (2001). Hox genes, neural crest cells and branchial arch patterning. *Curr. Opin. Cell Biol.* 13, 698–705. doi: 10.1016/s0955-0674(00)00273-8

Trainor, P. A., and Krumlauf, R. (2002). Riding the crest of the Wnt signaling wave. *Science* 297, 781–783. doi: 10.1126/science.1075454

Trainor, P. A., and Tam, P. P. L. (1995). Cranial paraxial mesoderm and neural crest cells of the mouse embryo: co-distribution in the craniofacial mesenchyme but distinct segregation in branchial arches. *Development* 121, 2569–2582.

Trainor, P. A., Dixon, J., and Dixon, M. J. (2009). Treacher collins syndrome: etiology, pathogenesis and prevention. *Eur. J. Hum. Genet.* 17, 275–283. doi: 10.1038/ejhg.2008.221

Trainor, P. A., Melton, K. R., and Manzanares, M. (2003). Origins and plasticity of neural crest cells and their roles in jaw and craniofacial evolution. *Int. J. Dev. Biol.* 47, 541–553.

Trainor, P. A., Sobieszczuk, D., Wilkinson, D., and Krumlauf, R. (2002). Signalling between the hindbrain and paraxial tissues dictates neural crest migration pathways. *Development* 129, 433–442.

Twigg, S. R. F., and Wilkie, A. O. M. (2015). New insights into craniofacial malformations. *Hum. Mol. Genet.* 24, R50–R59.

Valdez, B. C., Henning, D., So, R. B., Dixon, J., and Dixon, M. J. (2004). The treacher collins syndrome (TCOF1) gene product is involved in ribosomal DNA gene transcription by interacting with upstream binding factor. *Proc. Natl. Acad. Sci.U.S.A.* 101, 10709–10714. doi: 10.1073/pnas.0402492101

Van De Putte, T., Maruhashi, M., Francis, A., Nelles, L., Kondoh, H., Huylebroeck, D., et al. (2003). Mice lacking Zfhx1b, the gene that codes for Smad-interacting protein-1, reveal a role for multiple neural crest cell defects in the etiology of hirschsprung disease-mental retardation syndrome. *Am. J. Hum. Genet.* 72, 465–470. doi: 10.1086/346092

Von Kries, R., Kimmerle, R., Schmidt, J. E., Hachmeister, A., Böhm, O., and Wolf, H. G. (1997). Pregnancy outcomes in mothers with pregestational diabetes: a population-based study in North Rhine (Germany) from 1988 to 1993. *Eur. J. Pediatr.* 156, 963–967. doi: 10.1007/s004310050752

Waltes, R., Kalb, R., Gatei, M., Kijas, A. W., Stumm, M., Sobeck, A., et al. (2009). Human RAD50 deficiency in a nijmegen breakage syndrome-like disorder. *Am. J. Hum. Genet.* 84, 605–616. doi: 10.1016/j.ajhg.2009.04.010

Wang, F., Xu, C., Reece, E. A., Li, X., Wu, Y., Harman, C., et al. (2017). Protein kinase C-alpha suppresses autophagy and induces neural tube defects via miR-129-2 in diabetic pregnancy. *Nat. Commun.* 8:15182.

Wang, X. Y., Li, S., Wang, G., Ma, Z. L., Chuai, M., Cao, L., et al. (2015). High glucose environment inhibits cranial neural crest survival by activating excessive autophagy in the chick embryo. *Sci. Rep.* 5:18321.

Warburg, O. (1956). On the origin of cancer cells. *Science* 123, 309–314.

Watt, K. E. N., and Trainor, P. A. (2014). "Neurocristopathies. the etiology and pathogenesis of disorders arising from defects in neural crest cell development," in *Neural Crest Cells: Evolution, Development and Disease*, ed. P. Trainor (Amsterdam: Elsevier Inc), 361–394. doi: 10.1016/b978-0-12-401730-6.00018-1

Wei, D., and Loeken, M. R. (2014). Increased DNA methyltransferase 3b (dnmt3b)-mediated CpG island methylation stimulated by oxidative stress inhibits expression of a gene required for neural tube and neural crest development in diabetic pregnancy. *Diabetes* 63, 3512–3522. doi: 10.2337/db14-0231

Wells, P. G., McCallum, G. P., Lam, K. C. H., Henderson, J. T., and Ondovcik, S. L. (2010). Oxidative DNA damage and repair in teratogenesis and neurodevelopmental deficits. *Birth Defects Res. C Embryo Today* 90, 103–109. doi: 10.1002/bdrc.20177

Wentzel, P., and Eriksson, U. J. (2011). Altered gene expression in rat cranial neural crest cells exposed to a teratogenic glucose concentration in vitro-paradoxical downregulation of antioxidative defense genes. *Birth Defects Res. B Dev. Reprod. Toxicol.* 92, 487–497. doi: 10.1002/bdrb.20321

Wilder, H. H. (1908). The morphology of cosmobia; speculations concerning the significnace of certain types of monsters. *Am. J. Anat.* 8, 355–440. doi: 10.1002/aja.1000080113

Williams, A. L., and Bohnsack, B. L. (2019). What's retinoic acid got to do with it? Retinoic acid regulation of the neural crest in craniofacial and ocular development. *Genesis* 57:e23308. doi: 10.1002/dvg.23308

Wong, J. C. Y., Alon, N., Mckerlie, C., Huang, J. R., Meyn, M. S., and Buchwald, M. (2003). Targeted disruption of exons 1 to 6 of the fanconi anemia group A gene leads to growth retardation, strain-specific microphthalmia, meiotic defects and primordial germ cell hypoplasia. *Hum. Mol. Genet.* 12, 2063–2076. doi: 10.1093/hmg/ddg219

Wu, Y., Viana, M., Thirumangalathu, S., and Loeken, M. R. (2012). AMP-activated protein kinase mediates effects of oxidative stress on embryo gene expression in a mouse model of diabetic embryopathy. *Diabetologia* 55, 245–254. doi: 10.1007/s00125-011-2326-y

Xu, C., Li, X., Wang, F., Weng, H., and Yang, P. (2013). Trehalose prevents neural tube defects by correcting maternal diabetes-suppressed autophagy and neurogenesis. *Am. J. Physiol. Endocrinol. Metab.* 305, E667–E678.

Yamaguchi, H., Kitami, K., Wu, X., He, L., Wang, J., Wang, B., et al. (2021). Alterations of DNA damage response causes cleft palate. *Front. Physiol.* 12:649492. doi: 10.3389/fphys.2021.649492

Zhao, Z., and Reece, E. A. (2005). Nicotine-induced embryonic malformations mediated by apoptosis from increasing intracellular calcium and oxidative stress. *Birth Defects Res. B Dev. Reprod. Toxicol.* 74, 383–391. doi: 10.1002/bdrb.20052

Zhao, Z., and Reece, E. A. (2013). New concepts in diabetic embryopathy. *Clin. Lab. Med.* 33, 207–233. doi: 10.1016/j.cll.2013.03.017

Conflict of Interest: The authors declare that the research was conducted in the absence of any commercial or financial relationships that could be construed as a potential conflict of interest.

frontiers in Cell and Developmental Biology

ORIGINAL RESEARCH
published: 26 May 2021
doi: 10.3389/fcell.2021.621249

Using Sensitivity Analysis to Develop a Validated Computational Model of Post-operative Calvarial Growth in Sagittal Craniosynostosis

*Connor Cross[1], Roman H. Khonsari[2], Leila Galiay[2], Giovanna Patermoster[3], David Johnson[4], Yiannis Ventikos[1] and Mehran Moazen[1]**

[1] Department of Mechanical Engineering, University College London, London, United Kingdom, [2] Service de Chirurgie Maxillo-Faciale et Plastique, Assistance Publique des Hôpitaux de Paris, Paris, France, [3] Department of Neurosurgery, Craniofacial 16 Surgery Unit, Necker–Enfants Malades University Hospital, Assistance Publique–Hôpitaux de 17 Paris, Université de Paris, Paris, France, [4] Oxford Craniofacial Unit, Oxford University Hospital, NHS Foundation Trust, Oxford, United Kingdom

Craniosynostosis is the premature fusion of one or more sutures across the calvaria, resulting in morphological and health complications that require invasive corrective surgery. Finite element (FE) method is a powerful tool that can aid with preoperative planning and post-operative predictions of craniosynostosis outcomes. However, input factors can influence the prediction of skull growth and the pressure on the growing brain using this approach. Therefore, the aim of this study was to carry out a series of sensitivity studies to understand the effect of various input parameters on predicting the skull morphology of a sagittal synostosis patient post-operatively. Preoperative CT images of a 4-month old patient were used to develop a 3D model of the skull, in which calvarial bones, sutures, cerebrospinal fluid (CSF), and brain were segmented. Calvarial reconstructive surgery was virtually modeled and two intracranial content scenarios labeled "CSF present" and "CSF absent," were then developed. FE method was used to predict the calvarial morphology up to 76 months of age with intracranial volume-bone contact parameters being established across the models. Sensitivity tests with regards to the choice of material properties, methods of simulating bone formation and the rate of bone formation across the sutures were undertaken. Results were compared to the *in vivo* data from the same patient. Sensitivity tests to the choice of various material properties highlighted that the defined elastic modulus for the craniotomies appears to have the greatest influence on the predicted overall skull morphology. The bone formation modeling approach across the sutures/craniotomies had a considerable impact on the level of contact pressure across the brain with minimum impact on the overall predicated morphology of the skull. Including the effect of CSF (based on the approach adopted here) displayed only a slight reduction in brain pressure outcomes. The sensitivity tests performed in this study set the foundation for future comparative studies using FE method to compare outcomes of different reconstruction techniques for the management of craniosynostosis.

Keywords: craniosynostosis, cerebrospinal fluid, finite element, calvarial growth, sagittal synostosis, biomechanics

OPEN ACCESS

Edited by:
Karen Liu,
King's College London,
United Kingdom

Reviewed by:
Jordi Marcé-Nogué,
University of Rovira i Virgili, Spain
Junning Chen,
University of Exeter, United Kingdom

****Correspondence:***
Mehran Moazen
m.moazen@ucl.ac.uk

Specialty section:
This article was submitted to Molecular Medicine, a section of the journal Frontiers in Cell and Developmental Biology

Received: *25 October 2020*
Accepted: *21 April 2021*
Published: *26 May 2021*

Citation:
Cross C, Khonsari RH, Galiay L, Patermoster G, Johnson D, Ventikos Y and Moazen M (2021) Using Sensitivity Analysis to Develop a Validated Computational Model of Post-operative Calvarial Growth in Sagittal Craniosynostosis. Front. Cell Dev. Biol. 9:621249. doi: 10.3389/fcell.2021.621249

INTRODUCTION

The cranium consists of several bones that are connected via cranial joints or sutures. Sutures facilitate the birth and accommodate the radial expansion of the brain during infancy (Anatole and Dekaban, 1977; Morriss-Kay and Wilkie, 2005; Lieberman, 2011; Richtsmeier and Flaherty, 2013; Jin et al., 2016; Adigun and Al-Dhahir, 2017; Hegazy and Hegazy, 2018). Early fusion of the sutures is a medical condition called craniosynostosis with the most common form of this condition being the early fusion of the sagittal suture i.e., occurring in ca. 3 per 10,000 live births (Morriss-Kay and Wilkie, 2005; Cunningham and Heike, 2007; Johnson and Wilkie, 2011; Cornelissen et al., 2016; Kalantar-Hormozi et al., 2019). The condition results in limited expansion of the skull perpendicular to the fused suture, leading to compensatory anteroposterior growth. In addition, raised intracranial pressure may cause cognitive impairment and visual loss (Gault et al., 1992; Lo and Chen, 1999). Various calvarial reconstructions to alleviate and correct these abnormalities have existed since the late nineteenth century (Lane, 1892; Lauritzen et al., 2006; Rocco et al., 2012; Simpson et al., 2015; Mathijssen, 2015; Microvic et al., 2016) with their various cognitive and morphological outcomes debated and compared to optimize the management of this condition (Hashim et al., 2014; Isaac et al., 2018; Magge et al., 2019).

Finite element (FE) method is a powerful computational tool that has been widely used in the field of biomechanics for the design and development of various structures and systems. The same technique has huge potentials to optimize the management of various form of craniosynostosis (e.g., You et al., 2010; Wolański et al., 2013; Malde et al., 2019; Dolack et al., 2020). Several recent studies have developed validated computational model of calvarial growth in rodent (Lee et al., 2017; Marghoub et al., 2018), and human infant models (Libby et al., 2017; Weickenmeier et al., 2017) as well as predicting follow up results in treated sagittal craniosynostosis patients (Malde et al., 2020). However, few studies have carried out detail investigations to understand the sensitivity of these models to the choice of their input parameters (Barbelto-Andres et al., 2020). Such sensitivity studies are crucial to advance our understanding of the limitations of FE models as well as achieving more accurate predictions of the skull growth using this method.

The aim of this study was to carry out a series of sensitivity studies to understand the effect of various input parameters on predicting the skull morphology of a sagittal synostosis patient post-operatively. Therefore, a preoperative patient-specific finite element model was developed. The post-operative skull morphology and the level of contact pressure at the intracranial volume (ICV)-bone interface were quantified and compared across a number of sensitivity tests.

MATERIALS AND METHODS

Patient Computed Tomography Data

Computed tomography (CT) images of a sagittal craniosynostosis patient were retrieved from the Hôpital—Necker Enfants—Malades Cranio-facial Surgery Unit (Paris, France) at a resolution of 0.625 × 0.625 mm. Full ethical consent from the center and the patients' guardians was granted for the purposes of this study. Preoperative and immediate post-operative images were taken at 4 months of age and 6 days after the operation, respectively. Long term follow up CT images were taken at 76 months of age (i.e., 72 months after the operation). Anatomical 3D segmentation of the preoperative CT data was performed in Avizo image processing software (Thermo Fisher Scientific, Mass, United States). The follow up data at 76 months was used for morphological validation. 3D reconstructions of all CT data are highlighted in **Figure 1A** at each time point.

Model Development

Segmentation of the calvarial bone, sutures, and the ICV was undertaken. The segmentation consisted of four components: (1) Calvarial bone (frontal, parietal, occipital, temporal, and craniofacial bones); (2) Sutures (metopic, squamosal, coronal, lambdoid, anterior fontanelle, frontozygomatic and zygomaticotemporal); (3) cerebrospinal fluid (CSF) and (4) the brain (frontal lobe, temporal lobe, parietal lobe, occipital lobe and cerebellum). Bone was segmented automatically based on grayscale values while other tissues were segmented manually. The mandible was removed from the segmentation as the primary focus was on calvarial growth.

The *in vivo* surgical craniotomies (i.e., Renier's "H" technique) were also replicated across the calvaria (Rocco et al., 2012) and confirmed by the surgical team (i.e., Roman H. Khonsari and Giovanna Patermoster). A 3–4-cm wide rectangular cut was performed across the parietal, posterior of the coronal and anterior of the lambdoid sutures. The fused suture was removed and divided into two square portions. These were then reinserted to aid with long term calvarial healing. Two wedges extending from craniotomy-squamosal were created on each side of the parietal bone to assist with post-operative skull widening and anteroposterior shortening.

The ICV was modeled under two conditions (**Figures 1B,C**):

> Model I: CSF present consisted of a uniform 2–3 mm thick material layer defined as CSF between the cranial bones and the brain. Due to the resolution of the CT images, accurate *in vivo* representation of the CSF could not be achieved. Therefore, the aforementioned thickness was used based on previous studies (see e.g., Lam et al., 2001; Clouchoux et al., 2012).
>
> Model II: CSF absent defined the total ICV as the brain for comparison. Model II was used as the baseline approach for our sensitivity studies. Following segmentation, the surface model of the skull was transformed into a meshed solid geometry in Avizo that was then imported into a finite element package.

Finite Element Analysis

Both models were imported into ANSYS finite element software (Canonsburg, United States) as solid meshed models. A quadratic tetrahedral mesh consisting of 3,100,000 elements across the skull and 900,000 elements across the CSF-brain was chosen after a mesh convergence analysis (i.e., several models were

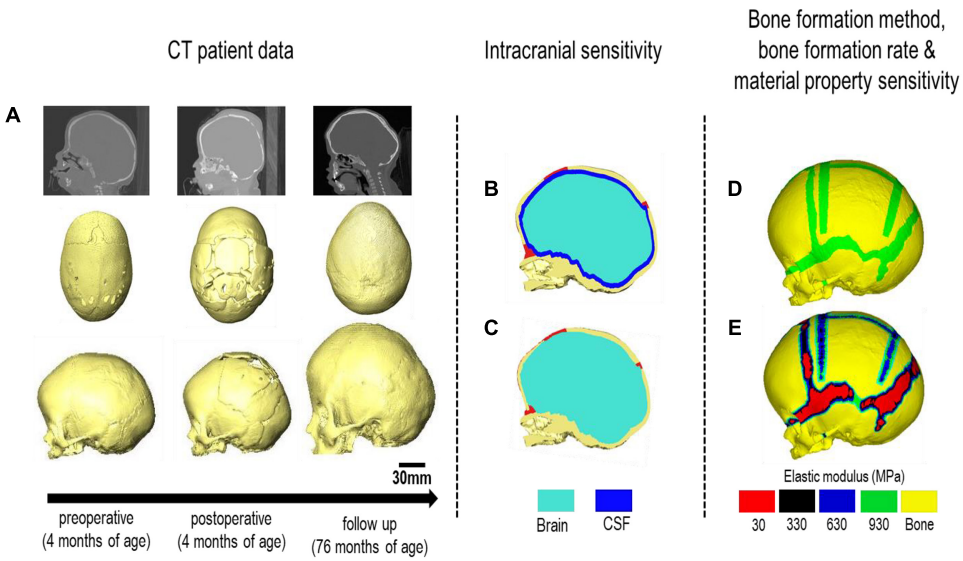

FIGURE 1 | Workflow of the study. CT images of the patient are obtained at various treatment stages. **(A)** The preoperative CT is used for image processing and 3D reconstruction. Two intracranial volume models **(B,C)** were then compared under differing bone formation methods **(D,E)**.

imported from Avizo to ANSYS in this respect). Correction of element intersection and poor aspect ratios was performed prior to importation. All material properties were defined as linear isotropic. For both models, the cranial bones, sutures and craniotomies were initially assigned a baseline elastic modulus of 3,000, 30, and 30 MPa, respectively (McPherson and Kriewall, 1980; Moazen et al., 2015—these were altered later—see sensitivity tests section). The brain (intracranial volume) elastic modulus was defined as 100 MPa (Libby et al., 2017) and the CSF elastic modulus was defined as 40 MPa. The Poisson's ratio of the cranial bones, sutures and craniotomies was assumed to be 0.3. The Poisson's ratio of CSF was assumed to be 0.48. Note, since the exact values/distribution of CSF pressure across the skull are not still clear, and modeling the CSF as fluid was beyond the scope of this study, we decided to model the impact of CSF on the prediction of calvarial growth and ICV surface pressures using solid elements.

Boundary Conditions and Modeling of the Growth

A surface-to-surface penalty-based contact was established between the ICV and inner-calvarial interface for both models. These interfaces were initially in contact, after which normal and tangential friction behavior during calvarial growth was granted. A friction coefficient of 0.1, a penetration tolerance of 0.5, and a normal penalty stiffness of 600 N/mm was used at all interfaces where contact was defined. These values were chosen based on our previous sensitivity tests (Malde et al., 2020). A "bonded" interface behavior was enforced between bone, suture, craniotomies and CSF surfaces though out all simulations, i.e., allowing no relative motion at the aforementioned interfaces.

Nodal constraints in all degrees of freedom were placed around the foramen magnum and along the nasion to avoid rigid displacement during skull growth. The radial expansion of the brain/ICV was modeled using thermal analogy as described in detail elsewhere (see Libby et al., 2017; Marghoub et al., 2018, 2019; Malde et al., 2020). To summaries, a linear isotropic expansion was applied to the brain/ICV, where the pre-operative ICV (measured at 659 ml) was expanded to follow up ICV at 76 months of age (measured at 1,245 ml) in six intervals. The estimated age of each interval was calculated by measuring these new volumes (Sgouros et al., 1999). Two methods of bone formation were undertaken here:

Scenario I: applies a bone formation across the sutures/craniotomies as described in Marghoub et al. (2019) and here termed "gradual bone formation" (**Figure 1D**). Here, the suture and craniotomy elements within a specified radius from the adjacent bone were selected, at a rate of 0.1 mm for the sutures and 0.8 mm for the craniotomies for every month of volume growth (Mitchell et al., 2011; Thenier-Villa et al., 2018; Riahinezhad et al., 2019). To monitor for the level of strain in the selected elements, all elements with a hydrostatic strain (i.e., summation of all principal strains divided by three) within 0–50% were used. Scenario I was the baseline approach throughout the study.

Scenario II: here termed as "bulk bone formation" increased the bulk elastic modulus of the sutures/craniotomy as appose to simulating bone forming from the bone edge (**Figure 1E**). This method is computationally less expensive, i.e., solves faster but perhaps not as physiologically representative as the "gradual bone formation." Further details are described by Malde et al. (2020).

Sensitivity Tests

The baseline values as detailed above were changed using Model II under bone formation scenario I. **Table 1** details respective sensitivity studies and their independent values, i.e., to the choice of material properties and rate of bone formation.

Material Properties

Three sensitivity analyses were performed to the changes in material properties.

Test 1–Bone Sensitivity: the elastic modulus of the bone was reduced from 3,000 to 421 MPa based on the previous study of Coats and Margulies (2006).

Test 2–Craniotomy Sensitivity: the elastic modulus of the craniotomies were reduced from 30 MPa to 3 kPa, i.e., two extremes that can capture wide range of tissues that can be present in these defects (see e.g., Leong and Morgan, 2008).

Test 3–Brain Sensitivity: the initial value of 100 MPa was reduced to 3 kPa based on nanoindentation studies performed on brain tissues (see e.g., Gefen et al., 2003).

Bone Formation Rate

This test further expanded on scenario II's approach by altering the rate of bone formation across various sutures. This was carried out into two additional tests.

Test 4–Increased Formation Rate: here, we increased the original suture formation radius from 0.1 to 0.2 mm across all the sutures.

Test 5–Metopic and Anterior Fontanelle Closure: here, the complexity of test 4 was increased further. The bone formation rate across the metopic and anterior fontanelle was increased (i.e., 0.6 mm for each month) to replicate the early closure of these sutures. The metopic and the anterior fontanelle progressively closing from 4 months of age until closure is evident by 24 months (Pindrik et al., 2014; Teager et al., 2018). The rate specified for the bone formation across the craniotomy remained unchanged for both scenarios as specified in section "Boundary Conditions and Modeling of the Growth."

Bone Formation Method and Effects of CSF

A comparison of both bone formation scenarios under both models was also undertaken to understand the effects our established CSF and various formation scenarios have on calvarial morphology and contact pressure outcomes across the ICV.

Analysis

All simulations were subject to morphological comparison against the 76 months of age follow up CT data (see section "Patient Computed Tomography Data") through a cross-sectional comparison and dimensional measurement of the length (from glabella to opisthocranion), width (between the left and right euryons) and height (from basion to bregma). All measurement and landmark placements were performed manually. The cephalic index (CI) was also calculated by multiplying the width against the height and dividing by 100. Bone formation rates were compared at various time points to establish the predicted sutures time of closure. A cross-sectional comparison and the level of contact pressure across the ICV was analyzed for both bone formation scenarios (Scenario I vs. II) under both models (Model I vs. II). Overall regional pressure across the ICV was measured to quantify areas of higher pressure.

RESULTS

Material Properties

There was a close match between all considered FE simulations (Test 1, 2, and 3) and the follow up CT skull morphology at 76 months of age (**Figure 2**). Minimal differences were observed across all material property sensitivities considered here, in terms of skull length, width and height measurements (**Figure 2** and **Table 2**). Skull width and height measurements were lower than the follow up data while there was a close match between skull length measurement. Cephalic indexes of all considered sensitivity tests with respect to the changes in the material properties were in the range of 79.04–79.67 vs. the follow up CI of 86.62 (**Table 2**).

Bone Formation Rate

Figure 3 compares the various bone formation rates (Baseline vs. Test 4 vs. 5) as detailed in section Sensitivity Tests. All outcomes predict the closure of the craniotomy by 12 months of age. The coronal suture displays complete closure between 36 and 76 months. The metopic, lambdoid, and squamosal regions remain marginally open, with various regions displaying closure. The anterior fontanelle remains open during the entirety of the growth cycle. Test 4 displays a near-complete closure of all sutures by 36 months of age, disregarding the anterior fontanelle which, similarly to the baseline comparison, remains open for the duration. All other sutures were found to have closed by the final 76 months of age interval. Test 5 displays an accelerated closure of the anterior fontanelle and metopic suture compared to the previous outcomes, which completely closes between 12 and 36 months of age. A close morphological match was seen against the follow up CT across all tests as seen in **Figure 2**.

Bone Formation Method and Effects of CSF

Figure 4 represents the state of the various bone formation approaches at various ages. **Figure 5** highlights the cross-sectional comparison of these bone formation approaches and the effects of CSF against follow up data with numerical measurements summarized in **Table 3**. Biparietal under-prediction and anterior over-prediction was observed in all outcomes. Model I approach (i.e., CSF present) does not appear to have any major implications to morphological outcomes when compared to Model II's approach (i.e., CSF absent). Interestingly, despite the changes in modeling and formation

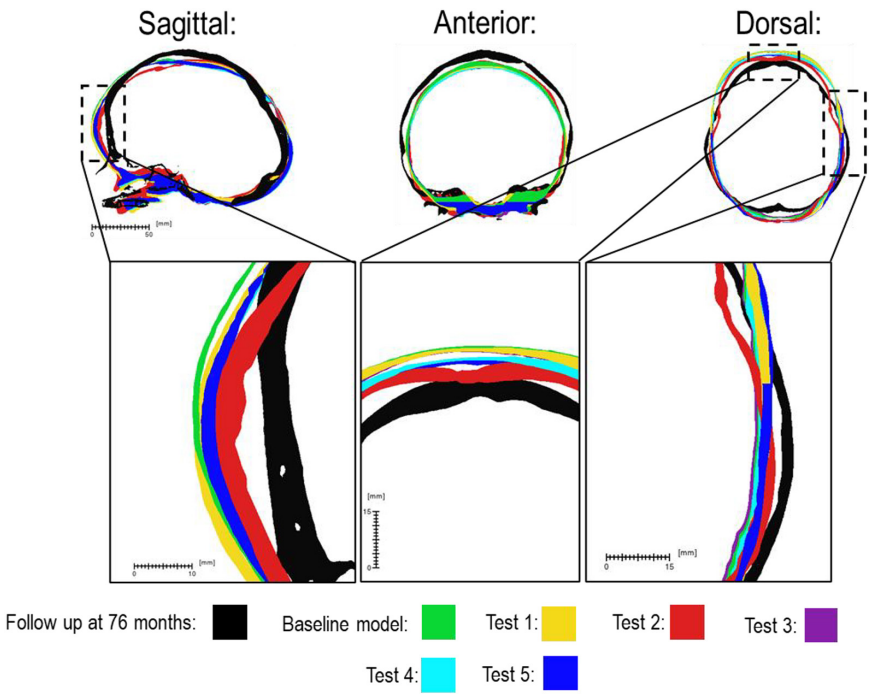

FIGURE 2 | Material property and bone formation rate sensitivity cross-sections vs. follow up at 76 months of age. Dashed boxes indicate enhanced regions of interest.

method, there was no greatly varying impact on morphological outcomes, with all scenarios matching close to follow up data. This is further supported in the numerical measurements, where the length, width and height show an average of 159.9 mm, 129.7 mm and 129.1 mm, respectively. Cephalic index measurements ranged between 79.16 and 83.28 vs. follow up CI of 86.62 (**Table 3**).

Contact pressure mapping across the ICV surface is displayed in **Figure 6**, with the minimum, maximum and average pressure across each lobe region shown in **Table 4**. Incorporating CSF

TABLE 1 | Material property and bone formation rate sensitivity summary.

	Bone E (MPa), υ	Suture E (MPa), υ	Brain E (MPa), υ	Craniotomy E (MPa), υ	Suture formation rate (mm/month)
Baseline model	3,000, 0.3	30, 0.3	100, 0.48	30, 0.3	0.1
Test 1	421, 0.22	NA	NA	NA	NA
Test 2	NA	NA	NA	0.003, 0.3	NA
Test 3	NA	NA	0.003, 0.48	NA	NA
Test 4	NA	NA	NA	NA	0.2
Test 5	NA	NA	NA	NA	0.2 and 0.6 for suture and metopic/anterior fontanelle, respectively. Closure by 24 months.

"E" refers to elastic modulus, "υ" refers to Poisson's ratio and "NA" indicates no change from the Baseline model values.

TABLE 2 | Material property and bone formation rate sensitivity measurements.

	Length (mm)	Width (mm)	Height (mm)	Cephalic index
Baseline model	166.58	131.87	132.93	79.16
Test 1	166.9	132.97	132.43	79.67
Test 2	165.92	129.91	128	78.29
Test 3	166.52	131.62	132.87	79.04
Test 4	168.07	130.52	131.8	77.65
Test 5	169.56	131.3	131.57	77.43
Follow up at 76 months	166.17	143.94	137.23	86.62

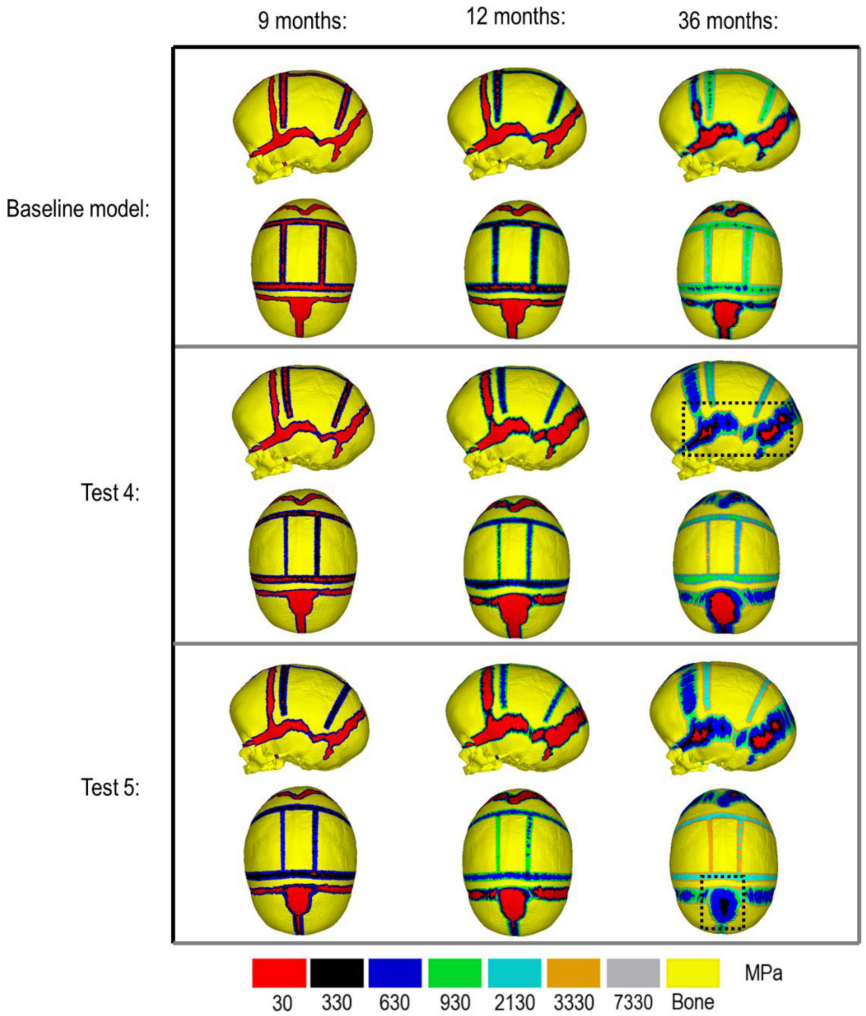

FIGURE 3 | Bone formation rate sensitivity at various stages, sagittal and dorsal views.

TABLE 3 | Summary of various Cerebrospinal fluid (CSF) model under each respective bone formation method.

Bone formation method:	Model	Length (mm)	Width (mm)	Height (mm)	Cephalic index
Scenario I	Model I	160.97	129.46	122.18	80.42
	Model II	166.58	131.87	132.93	79.16
Scenario II	Model I	155.86	129.81	128.31	83.28
	Model II	160.95	132.52	132.96	82.52
Follow up at 76 months		166.17	143.94	137.23	86.62

appears to only slightly reduce the average pressure across all regions. This is further supported by numerical outcomes, where the mean values do not vary more than 1 MPa between all scenarios. The chosen method of bone formation appears to have a greater role in contact pressure outcomes than the intracranial content chosen, where the average pressure across all lobes doubles, with the frontal and occipital lobe displaying the greatest difference (4.21–4.33 MPa and 4.49–4.52 MPa, respectively). A change that is also evident across the represented contact pressure maps.

DISCUSSION

There is a growing body of computational studies based on finite element method that are using this approach to optimize the clinical management of craniosynostosis. To the best of our knowledge, a few studies have carried out detailed sensitivity analysis to the choice of input parameters on the outcome of these models. In this study we investigated the impact of several key parameters on the outcome of a FE model, predicting calvarial growth in a patient-specific sagittal synostosis case. The identified

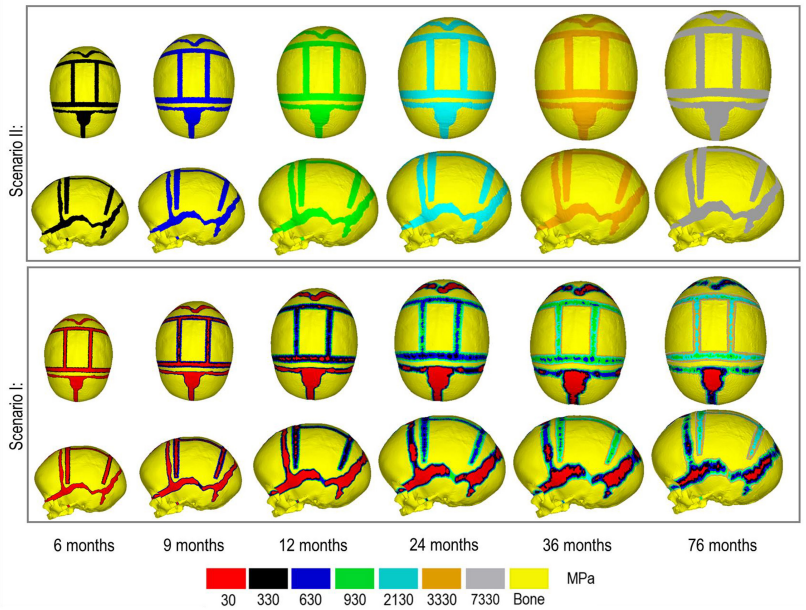

FIGURE 4 | Bone formation methods under scenario I **(bottom)** and scenario II **(top)** during calvarial growth, sagittal and dorsal views (1:1 scale).

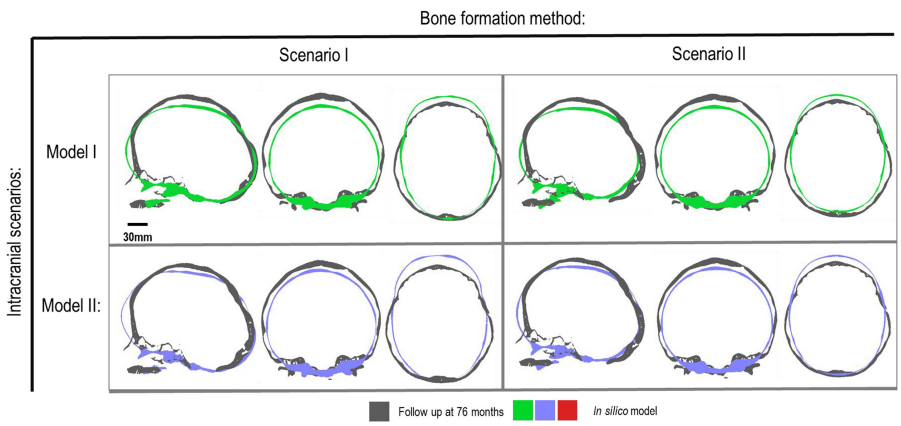

FIGURE 5 | Cross-section analysis of intracranial scenarios (Model I and II) against both bone formation methods (Scenario I and II) at 76 months of age. Showing sagittal, anterior and dorsal planes.

parameters were changes in limited scenarios, based on what is perceived to be a reasonable estimate of their *in vivo* values based on the data in the literature, rather than a wide range of values for each parameter. Our results highlighted that pending the output parameter of interest (i.e., overall skull morphology after surgery or impact of surgical technique on the ICV pressure) the choice of input parameters can have a limited to major impact on the outcomes.

Considering the material property sensitivity tests performed here, our measurements showed the choice of craniotomies elastic modulus has the largest reduction on length (165.9 mm), width (129.9 mm) and height (128 mm) out of all the analyzed parameters (**Table 2**). Clinically craniotomies are gaps with "no material" present at these gaps post-operatively unless a medical device such as plates or springs are used. In the modeling approach implemented here, craniotomies were virtually assumed to be a "material" with low elastic modulus (i.e., low resistance to the applied forces). This approach allows us to model bone formation across the craniotomies that occur post-operatively. While a relatively low baseline elastic modulus was used in the initial models (i.e., 30 MPa similar to the suture properties and 100 times lower than the bone), our cross-sectional results highlight that the predicted skull morphology can be highly sensitive to this choice (**Figure 2**; red outline). This can be explained by the fact that the large displacements occur during the brain/ICV radial expansion across the craniotomies. Clinically (i) considering the operation modeled in this study, this closely replicates the purpose of

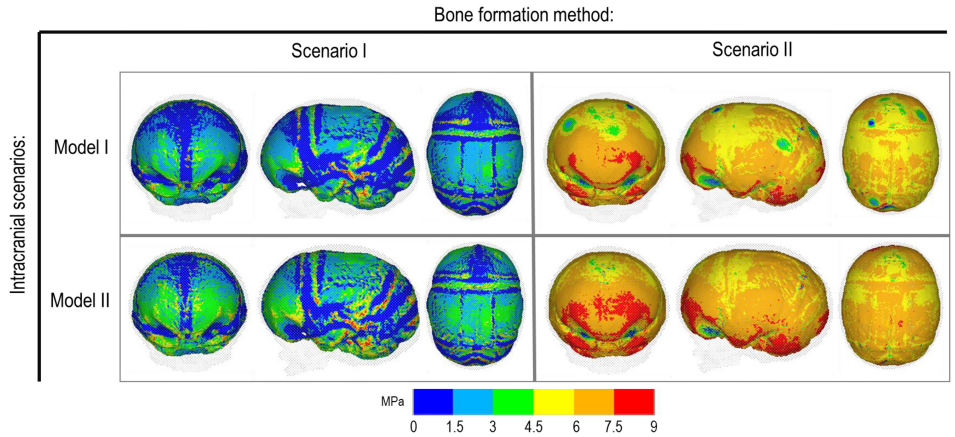

FIGURE 6 | ICV pressure map at 76 months of age. Showing the dorsal, sagittal and anterior views.

these bitemporal craniotomies, which aims to increase the displacement of the bone mediolaterally while reducing anterior-posterior length (Rocco et al., 2012); (ii) this highlights that perhaps the number, position and orientation of craniotomies all contribute to the overall long term morphological outcomes of the surgery and variations observed.

During the natural development and following the surgical operation on craniosynostotic skulls, radial expansion of the skull occur hand in hand with bone formation across the sutures and craniotomies (Richtsmeier and Flaherty, 2013). We recently described a validated finite element-based approach to model the aforementioned phenomena in mice (Marghoub et al., 2019). In the present study for the first time, we applied the same methodologies to model the calvarial growth following calvarial reconstruction. A key unknown in translating our methodology from mouse to human was the rate of bone formation in the human, hence, the sensitivity tests to this choice were performed in this study. Our results highlighted that this parameter does not have a major impact on the overall predicted morphology of the skull (see **Figure 2** for light and dark blue outlines). Gradually increasing the elastic modulus of the whole sutures/craniotomies sections under scenario II (i.e., "bulk bone formation") also led to a close match between the overall predicted morphology of the skull and the *in vivo* data (see **Figure 5** and also Malde et al., 2020). However, the rate of bone formation (Test 4 and 5) has an impact on the predicted pattern and timing (age) of sutures and craniotomies closure (see **Figure 3** e.g., for highlighted dash lines across the anterior fontanels). Studies observing calvarial CT imaging and measurements observe that the majority of the sutures close between 30 and 40 months of age while small gaps might be present at most of the sutures except the metopic throughout life (Opperman, 2000; Lottering et al., 2016). In fact, the metopic and anterior fontanelle are suggested to fuse as early as 9 months of age (Hugh et al., 2001; Boran et al., 2018). Due to the lack of regular CT data for the patient considered here (that clinically is unethical to perform), detail validation of our predictions is challenging while overall it appears that regardless of the rate of bone formation the overall pattern of suture closures is similar to the *in vivo* data. With regards to the craniotomies, all comparisons present a complete closure by 9 months post-operative (12 months of age). This appears to match well with reported *in vivo* literature (e.g., Thenier-Villa et al., 2018). An important consideration when varying surgical techniques in which calvarial healing may prolong, which has been found to vary between different age groups and surgical methods (Hassanein et al., 2011; Thenier-Villa et al., 2018).

An alternative approach to the gradual bone formation approach described above is the "bulk bone formation." The latter is computationally far less expensive and can model the changes in the overall stiffness of the sutures and craniotomies during the development or after surgery. This approach was used in our recent patient-specific modeling of calvarial growth (Malde et al., 2020). Our results here show that both methodologies can reasonably predict the overall morphology of the skull, however, these approaches lead to different levels of contact pressure across the brain/ICV. The gradual bone formation approach (i.e., scenario I) led to a lower level of contact pressure across the brain/ICV in comparison to the "bulk bone formation" (i.e., Scenario II) approach (see **Figure 6** and **Table 4**). Another important parameter that can alter the predicted patterns of contact pressure across the brain is the CSF. CSF was modeled here using solid elements with low elastic modulus (see **Supplementary Data** for sensitivity tests to the impact of CSF elastic modulus on the contact pressure on the ICV). *In vivo*, CSF is obviously a fluid that plays a crucial role in nutrient transfusion across the brain with varied pressure during the development (see e.g., Moazen et al., 2016). Modeling the fluid-solid interaction at this interface was beyond the scope of this work. Yet, the sensitivity analysis performed here, considering its limitations, highlighted that CSF perhaps plays a smaller role on the level of contact pressure across the brain compared to the methods of bone formation during the calvarial growth/healing. Obviously, *in vivo* obstruction of CSF can lead to raised intracranial pressure with potential impacts on the brain that given the approach that was implemented here can be predicted by investigating the level of strain across

TABLE 4 | Summary of intracranial contact pressure outcomes across each region of interest.

Bone formation method:	Model	Frontal lobe			Parietal lobe			Temporal lobe			Occipital lobe			Cerebellum		
		Min	Max	Mean	Min	Max	Mean	Min	Max	Mean	Min	Max	Mean	Min	Max	Mean
Scenario I	Model I	0	17.36	1.65	0	20.82	2.19	0	20.61	1.83	0	22.94	1.45	0	17.49	2.17
	Model II	0	15.40	2.29	0	18.62	2.68	0	22.63	2.33	0	16.95	1.87	0	20.46	2.86
Scenario II	Model I	0	8.83	5.98	0	10.97	5.69	0	18.55	5.66	0	11.37	5.94	0	11.61	6.64
	Model II	0	18.58	6.41	0	23.28	6.08	0	20.82	6.06	0	31.57	6.39	0	31.98	6.88

Values are in MPa.

the modeled CSF elements. Nonetheless, it may prove highly informative to investigate the contact pressures across different surgical techniques for the management of craniosynostosis and to correlate such results to the cognitive data (e.g., Chieffo et al., 2010; Hashim et al., 2014; Bellew and Chumas, 2015) to optimize management of craniosynostosis.

Perhaps the key limitations of the FE models and sensitivity tests described here are that: (1) the pattern of contact pressures on the brain/ICV was not validated and despite the efforts put into this work on including the effect of CSF further studies are required to advance our understanding of the *in vivo* level of loading at this interface; (2) the pattern of tissue differentiation across the sutures/craniotomies were not validated as such studies in human can be challenging. Nonetheless, given our previous studies in mice (e.g., Moazen et al., 2015), these predictions could be within the range of *in vivo* data; (3) bone was modeled as linear elastic homogenous material despite wide literature highlighting its anisotropy, variation in density, elastic modulus and mineral heterogeneity (e.g., Renders et al., 2008). Nonetheless given that at early stages of development and following calvarial reconstructions major deformations occur at the sutures and craniotomies perhaps this assumption could be acceptable or at least based on our results here it seems to have a minimal impact on predictions of calvarial growth in the age range and considering the treatment that was modeled here; (4) there are still differences between the predicted morphology at 76 month and the *in vivo* data (see differences between the outlines shown in **Figures 2**, **5**) that can be e.g., due to manual deformation of the bones during the surgery that were not modeled in this study or the fact that our current modeling approach does not model facial growth that occur hand in hand with calvarial growth. Nonetheless, given the large deformation that the model has predicted i.e., about 72 months of growth considering all its limitations we think this a valuable model and approach that can be used in optimizing treatment of craniosysnotosis while advancing the methodologies implemented here.

In summary, the present study highlights how variations in material property, intracranial content, bone formation methods, and various bone formation rates may affect outcomes in predicting sagittal craniosynostosis correction. The discussed factors provided in this study lays the foundation to simulate various surgical reconstructions and observing their outcomes in correcting sagittal craniosynostosis.

DATA AVAILABILITY STATEMENT

The raw data supporting the conclusions of this article will be made available by the authors, without undue reservation.

ETHICS STATEMENT

The studies involving human participants were reviewed and approved by the Necker–Enfants Malades University Hospital in Paris study No. 2018RK18. Written informed consent to participate in this study was provided by the participants' legal guardian/next of kin.

AUTHOR CONTRIBUTIONS

CC performed the simulations and prepared the results. RK, LG, GP, and DJ provided the clinical case and advised on the clinical aspects of the study. MM, DJ, YV, RK, and GP designed the study. All authors contributed to the analysis of the data and preparation of the manuscript.

FUNDING

This work was supported by the Rosetrees Trust (A1899).

ACKNOWLEDGMENTS

We thank the reviewers for their insightful comments on the earlier version of this manuscript.

SUPPLEMENTARY MATERIAL

The Supplementary Material for this article can be found online at: https://www.frontiersin.org/articles/10.3389/fcell.2021.621249/full#supplementary-material

Supplementary Figure 1 | CSF elastic modulus sensitivity, contact pressure across the brain/ICV.

REFERENCES

Adigun, O., and Al-Dhahir, M. (2017). *Anatomy, Head and Neck, Cerebrospinal Fluid*. Treasure Island, FL: StatPearls Publishing

Anatole, S., and Dekaban, M. (1977). Tables of cranial and orbital measurements, cranial volume, and derived indexes in males and females from 7 days to 20 years of age. *Ann. Neurol.* 2, 485–491. doi: 10.1002/ana.410020607

Barbelto-Andres, J., Bonfill, N., Marce Nogue, J., Bernal, V., and Gonzalez, P. N. (2020). Modeling the effect of brain growth on cranial bones using finite-element analysis and geometric morphometrics. *Surg. Radiol. Anat.* 42, 741–748.

Bellew, M., and Chumas, P. (2015). Long-term development follow-up in children with nonsynodromic craniosynostosis. *J. Neurosurg. Paediatr.* 16, 445–451. doi: 10.3171/2015.3.PEDS14567

Boran, P., Oğuz, F., Furman, A., and Sakarya, S. (2018). Evaluation of fontanel size variation and closure time in children followed up from birth to 24 months. *J. Neurosurg.* 22, 323–329. doi: 10.3171/2018.3.PEDS17675

Chieffo, D., Tamburrini, G., Massimi, L., Giovanni, S. D., Gainsanti, C., Caldarelli, M., et al. (2010). Long-term neuropsychological development in single-suture craniosynostosis treated early. *J. Neurosurg. Paediatr.* 5, 232–237. doi: 10.3171/2009.10.PEDS09231

Clouchoux, C., Guizard, N., Evans, C., Plessis, A., and Limperopoulos, C. (2012). Normative fetal brain growth by quantitative in vivo magnetic resonance imaging. *Am. J. Obstet. Gynecol.* 206, e1–e173. doi: 10.1016/j.ajog.2011.10.002

Coats, B., and Margulies, S. (2006). Material properties of human infant skull and suture at high rates. *J. Neurotrauma* 23, 1222–1232. doi: 10.1089/neu.2006.23.1222

Cornelissen, M., Ottelander, B. D., Rizopoulos, D., van der Hulst, R., Mink van der Molen, A., et al. (2016). Increase of prevalence of craniosynostosis. *J. Craniomaxillofac. Surg.* 44, 1273–1279.

Cunningham, M., and Heike, C. (2007). Evaluation of the infant with an abnormal skull shape. *Curr. Opin. Pediatr.* 19, 645–651. doi: 10.1097/MOP.0b013e3282f1581a

Dolack, M. E., Lee, C., Ru, Y., Marghoub, A., Richtsmeier, J. T., Jabs, E. W., et al. (2020). "Computational morphogenesis of embryonic bone development: past, present, and future," in *Mechanobiology – From Molecular Sensing to Disease*, ed. G. L. Niebur (Amsterdam: Elsevier).

Gault, D., Renier, D., Marchac, D., and Jones, B. M. M. (1992). Intracranial pressure and intracranial volume in children with craniosynostosis. *Plast. Reconstr. Surg.* 90, 377–381. doi: 10.1097/00006534-199209000-00003

Gefen, A., Gefen, N., Zhu, Q., Raghupathi, R., and Margulies, S. (2003). Age-dependent changes in material properties of the brain and braincase of the rat. *J. Neurotrauma* 20, 1163–1177. doi: 10.1089/089771503770802853

Hashim, P., Patel, A., Yang, J., Travieso, R., Terner, J., and Losee, J. (2014). The Effects of whole vault cranioplasty versus strip craniectomy on long-term neuropsychological outcomes in sagittal craniosynostosis. *Plast. Reconstr. Surg.* 134, 491–501. doi: 10.1097/PRS.0000000000000420

Hassanein, A., Couto, R., Nedder, A., Zielins, E., and Greene, A. (2011). Critical-size defect ossification: effect of leporid age in a cranioplasty model. *J. Craniofac. Surg.* 22, 2341–2343. doi: 10.1097/SCS.0b013e318232a71d

Hegazy, A., and Hegazy, M. (2018). Newborns' cranial vault: clinical anatomy and authors' perspective. *Int. J. Hum. Anat.* 1, 21–25. doi: 10.14302/issn.2577-2279.ijha-18-2179

Hugh, V., Jayesh, P., Parker, E., Levine, N., and Francel, P. (2001). The timing of physiologic closure of the metopic suture: a review of 159 patients using reconstructed 3D CT scans of the craniofacial region. *J. Craniofac. Surg.* 12, 527–532. doi: 10.1097/00001665-200111000-00005

Isaac, K., Meara, J., and Proctor, M. (2018). Analysis of clinical outcomes for treatment of sagittal craniosynostosis: a comparison of endoscopic suturectomy and cranial vault remodelling. *J. Neurosurg. Paediatr.* 22, 467–474. doi: 10.3171/2018.5.PEDS1846

Jin, S., Sim, K., and Kim, S. (2016). Development and growth of the normal cranial vault: an embryologic review. *J. Korean Neurosurg. Soc.* 59, 192–196. doi: 10.3340/jkns.2016.59.3.192

Johnson, D., and Wilkie, A. O. M. (2011). Craniosynostosis. *Eur. J. Hum. Genet.* 19, 369–376.

Kalantar-Hormozi, H., Abbaszadeh-Kasbi, A., Sharifi, G., Davai, N., and Kalantar-Hormozi, A. (2019). Incidence of familial craniosynostosis among patients with nonsyndromic craniosynostosis. *J. Craniofac. Surg.* 30, 514–517. doi: 10.1097/scs.0000000000005419

Lam, W., Ai, V., Wong, V., and Leong, L. (2001). Ultrasonographic measurement of subarachnoid space in normal infants and children. *Pediatr. Neurol.* 25, 380–384. doi: 10.1016/s0887-8994(01)00349-6

Lane, L. (1892). Pioneer craniectomy for relief of mental imbecility due to premature sutural closure and microcephalus. *JAMA* 18, 49–50. doi: 10.1001/jama.1892.02411060019001f

Lauritzen, C., Davis, C., Ivarsson, A., Sanger, C., and Hewitt, T. (2006). The evolving role of springs in craniofacial surgery: the first 100 clinical cases. *Plast. Reconstr. Surg.* 121, 545–554. doi: 10.1097/01.prs.0000297638.76602.de

Lee, C., Richtsmeier, J. T., and Kraft, R. H. (2017). A computational analysis of bone formation in the cranial vault using a coupled reaction-diffusion strain model. *J. Mech. Med. Biol.* 17:1750073.

Leong, P. L., and Morgan, E. F. (2008). Measurement of fracture callus material properties via nanoindentation. *Acta Biomater.* 4, 15 69–1575.

Libby, J., Marghoub, A., Johnson, D., Khonsari, R., Fagan, M., and Moazen, M. (2017). Modelling human skull growth: a validated computational model. *J. R. Soc. Interface* 14:20170202. doi: 10.1098/rsif.2017.0202

Lieberman, D. (2011). *Evolution of the Human Head*. London: Harvard University Press.

Lo, L. J., and Chen, Y. R. (1999). Airway obstruction in severe syndromic craniosynostosis. *Ann. Plast. Surg.* 43, 258–264. doi: 10.1097/00000637-199909000-00006

Lottering, N., MacGregor, D., Alston, C., Watson, D., and Gregory, L. (2016). Introducing computed tomography standards for age estimation of modern Australian subadults using postnatal ossification timings of select cranial and cervical sites. *J. Forensic Sci.* 61(Suppl. 1), S39–S52. doi: 10.1111/1556-4029.12956

Magge, S., Bartolozzi, I. V. A., Almeida, N., Tsering, D., Myseros, J., Oluigbo, C., et al. (2019). A comparison of endoscopic strip craniectomy and pi craniectomy for treatment of sagittal craniosynostosis. *J. Neurosurg. Paediatr.* 23, 708–714. doi: 10.3171/2019.1.PEDS18203

Malde, O., Cross, C., Lim, C. L., Marghoub, A., Cunningham, M. L., Hopper, R. A., et al. (2020). Predicting calvarial morphology in sagittal craniosynostosis. *Sci. Rep.* 10:3. doi: 10.1038/s41598-019-55224-5

Malde, O., Libby, J., and Moazen, M. (2019). An overview of modelling craniosynostosis using finite element method. *Mol. Syndromol.* 10, 74–82. doi: 10.1159/000490833

Marghoub, A., Libby, J., Babbs, C., Pauws, E., Fagan, M. J., and Moazen, M. (2018). Predicting calvarial growth in normal and craniosynostotic mice using a computational approach. *J. Anat.* 232, 440–448. doi: 10.1111/joa.12764

Marghoub, A., Libby, J., Babbs, C., Ventikos, Y., Fagan, M. J., and Moazen, M. (2019). Characterizing and modelling bone formation during mouse calvarial development. *Phys. Rev. Lett.* 122:048103. doi: 10.1103/PhysRevLett.122.048103

Mathijssen, I. M. J. (2015). Guideline for care of patients with the diagnoses of craniosynostosis: working group on craniosynostosis. *J. Craniofac. Surg.* 26, 1735–1807.

McPherson, G., and Kriewall, T. (1980). The elastic modulus of fetal cranial bone: a first step towards an understanding of the biomechanics of fetal head molding. *J. Biomech.* 13, 9–16. doi: 10.1016/0021-9290(80)90003-2

Microvic, M., Zivkovic, B., Bascarevic, V., Mijalèiæ, R., and Rasulic, L. (2016). Triple square extended osteotomies for treatment of scaphocephaly (Renier's "H" technique modification). *Neurosurg. Rev.* 39, 115–122. doi: 10.1007/s10143-015-0661-z

Mitchell, L., Kitley, C., Armitage, T., Krasnokutsky, M., and Rooks, V. (2011). Normal sagittal and coronal suture widths by using CT imaging. *Am. J. Neuroradiol.* 32, 1801–1805. doi: 10.3174/ajnr.A2673

Moazen, M., Alazmani, A., Rafferty, K., Liu, Z. J., Gustafson, J., Cunningham, M. L., et al. (2016). Intracranial pressure changes during mouse development. *J. Biomech.* 49, 123–126.

Moazen, M., Peskett, E., Babbs, C., Pauws, E., and Fagan, M. (2015). Mechanical properties of calvarial bones in a mouse model for craniosynostosis. *PLoS One* 10:e0125757. doi: 10.1371/journal.pone.0125757

Morriss-Kay, G., and Wilkie, A. (2005). Growth of the normal skull vault and its alterations in craniosynostosis: insight from human genetics and experimental studies. *J. Anat.* 207, 637–653. doi: 10.1111/j.1469-7580.2005.00475.x

Opperman, L. A. (2000). Cranial sutures as intramembranous bone growth sites. *Dev. Dyn.* 219, 472–485.

Pindrik, J., Ye, X., Ji, B., Pendelton, C., and Ahn, E. (2014). Anterior fontanelle closure and size in full-term children based on head computed tomography. *Clin. Pediatr.* 53, 1149–1157. doi: 10.1177/0009922814538492

Renders, G. A., Mulder, L., Langenbach, G. E., Van Ruijven, L. J., and Van Eijden, T. M. (2008). Biomechanical effect of mineral heterogeneity in trabecular bone. *J. Biomech.* 41, 2793–2798. doi: 10.1016/j.jbiomech.2008.07.009

Riahinezhad, M., Hajizadeh, M., and Farghadani, M. (2019). Normal cranial sutures width in an Iranian infant population. *J. Res. Med. Dental Sci.* 6, 305–309.

Richtsmeier, J. T., and Flaherty, K. (2013). Hand in glove: brain and skull in development and dysmorphogenesis. *Acta Neuropathol.* 125, 469–489.

Rocco, F., Knoll, B., Arnaud, E., Balnot, S., Meyer, P., Cuttarree, H., et al. (2012). Scaphocephaly correction with retrocoronal and prelambdoid craniotomies (Renier's "H" technique). *Childs Nerv. Syst.* 28, 1327–1332. doi: 10.1007/s00381-012-1811-z

Sgouros, S., Goldin, J. H., Hockley, A. D., Wake, M. J. C., and Natarajan, K. (1999). Intracranial volume change in childhood. *J. Neurosurg.* 91, 610–616. doi: 10.3171/jns.1999.91.4.0610

Simpson, A., Wong, A. L., and Bezuhly, M. (2015). Surgical comparison of nonsyndromic sagittal craniosynostosis. Concepts and controversies. *Ann. Plast. Surg.* 78, 103–110. doi: 10.1097/sap.0000000000000713

Teager, S., Constantine, S., Lottering, N., and Anderson, P. (2018). Physiological closure time of the metopic suture in south Australian infants from 3D CT scans. *Childs Nerv. Syst.* 35, 329–335. doi: 10.1007/s00381-018-3957-9

Thenier-Villa, J., Sanromán-Álvarez, P., Miranda-Lloret, P., and Ramirez, M. (2018). Incomplete reossification after craniosynostosis surgery—incidence and analysis of risk factors: a clinical-radiological assessment study. *J. Neurosurg. Pediatr.* 22, 120–127. doi: 10.3171/2018.2.PEDS1771

Weickenmeier, J., Fischer, C., Carter, D., Kuhl, E., and Goriely, A. (2017). Dimensional, geometrical, and physical constraints in skull growth. *Phys. Rev. Lett.* 118:248101.

Wolański, W., Larysz, D., Gzik, M., and Kawlewska, E. (2013). Modeling and biomechanical analysis of craniosynostosis correction with the use of finite element method. *Int. J. Numer. Methods Biomed. Eng.* 29, 916–925. doi: 10.1002/cnm.2506

You, J., Jiang, X., Hu, M., Wang, N., Shen, Z., Li, J., et al. (2010). "The bone slot effect study of pi procedure for craniosynostosis correction plan based on finite element method," in *Proceedings of the 3rd International Conference on Biomedical Engineering and Informatics*, Yantai, 605–608. doi: 10.1109/BMEI.2010.5640019

Conflict of Interest: The authors declare that the research was conducted in the absence of any commercial or financial relationships that could be construed as a potential conflict of interest.

frontiers in Cell and Developmental Biology

ORIGINAL RESEARCH
published: 09 June 2021
doi: 10.3389/fcell.2021.621045

MicroRNA-124-3p Plays a Crucial Role in Cleft Palate Induced by Retinoic Acid

*Hiroki Yoshioka[1,2], Yurie Mikami[1,2], Sai Shankar Ramakrishnan[1,2], Akiko Suzuki[1,2] and Junichi Iwata[1,2,3]**

[1] Department of Diagnostic and Biomedical Sciences, School of Dentistry, The University of Texas Health Science Center at Houston, Houston, TX, United States, [2] Center for Craniofacial Research, The University of Texas Health Science Center at Houston, Houston, TX, United States, [3] MD Anderson Cancer Center UTHealth Graduate School of Biomedical Sciences, Houston, TX, United States

OPEN ACCESS

Edited by:
Sebastian Dworkin,
La Trobe University, Australia

Reviewed by:
Rahul N. Kanadia,
University of Connecticut, United States
Jing Xiao,
Dalian Medical University, China
Jo Huiqing Zhou,
Radboud University Nijmegen, Netherlands
Johannes W. Von den Hoff,
Radboud University Nijmegen Medical Centre, Netherlands

***Correspondence:**
Junichi Iwata
Junichi.Iwata@uth.tmc.edu

Specialty section:
This article was submitted to Molecular Medicine, a section of the journal Frontiers in Cell and Developmental Biology

Received: 24 October 2020
Accepted: 05 May 2021
Published: 09 June 2021

Citation:
Yoshioka H, Mikami Y, Ramakrishnan SS, Suzuki A and Iwata J (2021) MicroRNA-124-3p Plays a Crucial Role in Cleft Palate Induced by Retinoic Acid. Front. Cell Dev. Biol. 9:621045. doi: 10.3389/fcell.2021.621045

Cleft lip with/without cleft palate (CL/P) is one of the most common congenital birth defects, showing the complexity of both genetic and environmental contributions [e.g., maternal exposure to alcohol, cigarette, and retinoic acid (RA)] in humans. Recent studies suggest that epigenetic factors, including microRNAs (miRs), are altered by various environmental factors. In this study, to investigate whether and how miRs are involved in cleft palate (CP) induced by excessive intake of *all-trans* RA (*at*RA), we evaluated top 10 candidate miRs, which were selected through our bioinformatic analyses, in mouse embryonic palatal mesenchymal (MEPM) cells as well as in mouse embryos treated with *at*RA. Among them, overexpression of miR-27a-3p, miR-27b-3p, and miR-124-3p resulted in the significant reduction of cell proliferation in MEPM cells through the downregulation of CP-associated genes. Notably, we found that excessive *at*RA upregulated the expression of miR-124-3p, but not of miR-27a-3p and miR-27b-3p, in both *in vivo* and *in vitro*. Importantly, treatment with a specific inhibitor for miR-124-3p restored decreased cell proliferation through the normalization of target gene expression in *at*RA-treated MEPM cells and *at*RA-exposed mouse embryos, resulting in the rescue of CP in mice. Taken together, our results indicate that *at*RA causes CP through the induction of miR-124-3p in mice.

Keywords: *all-trans* retinoic acid, environmental factor, cleft palate, microRNA, craniofacial development

INTRODUCTION

Cleft lip with/without cleft palate (CL/P) is the second most common congenital birth defect worldwide, with a prevalence of as high as 1 in 700 live births (IPDTOC Working Group, 2011). CL/P impacts on various physiological functions such as swallowing, feeding, speech, and hearing, even after multiple surgical corrections, orthodontic treatment, and speech therapy (Ferguson, 1988); therefore, the quality of life of both patients and their families is strongly diminished (Sischo et al., 2017; Kummer, 2018; De Cuyper et al., 2019). Palate development is regulated

through fine-tuned spatiotemporal gene regulatory networks that control the growth, elevation, and fusion of the palatal shelves through cell migration, proliferation, apoptosis, differentiation, and extracellular matrix secretion and arrangement. Dysregulation of each step of palatogenesis results in a failure in normal palate development and causes cleft palate (CP). Our previous studies showed that at least 223 genes [a total of 198 genes related to cleft palate only (CPO), including cleft in the secondary palate, primary palate, soft palate, and submucous CP, and a total of 45 genes related to cleft lip with cleft palate (CLP), with 20 genes duplicated in CPO and CLP adjusted] in mice and 185 genes (a total of 27 genes related to CPO and a total of 177 genes related to CL/P) in humans are associated with CP (Suzuki et al., 2018a,b, 2019a). Thus, a large number of genes play crucial roles in palate development.

The etiology of CL/P is further complicated with interactions between genetic and environmental factors (Murray, 2002; Beaty et al., 2016; Gonseth et al., 2019). As for environmental factors, maternal exposures to smoking and alcohol consumption are known to be a risk for CL/P (Ericson et al., 1979; Munger et al., 1996; Romitti et al., 1999; Garland et al., 2020). In addition, several chemicals are known to be teratogens that cause CL/P [e.g., dexamethasone, dioxins, and heavy metals (Bove et al., 1995; Buser and Pohl, 2015; Suhl et al., 2018; Pi et al., 2019)]. Malnutrition and mutations in genes related to nutritional metabolic/signaling pathways are also associated with CL/P in humans and animal models. For example, retinoic acid (RA), a metabolite of vitamin A, plays important roles in cell fate determination, cellular patterning, and cell differentiation in development (Rhinn and Dolle, 2012; Roberts, 2020). Excessive RA intake causes CPO in mice (Zhang et al., 2003; Kuriyama et al., 2008; Wang et al., 2019). Mice with deletion in *Cyp26b1*, a key enzyme for RA degradation, cause CPO, micrognathia, truncation of the fore/hind limbs, and ossification defects in calvaria bones (Maclean et al., 2009). In addition, mice with a mutation in retinol dehydrogenase 10, a key enzyme for RA synthesis ($Rdh10^{m366Asp}$ mice), show reduced RA levels and exhibit midline cleft, syndactyly, and a malformed forebrain (Ashique et al., 2012). Mice with dominant negative mutations in retinoic acid receptor alpha ($Rara^{403*}$) and mice with deficiency of both RA receptors alpha and gamma ($Rara^{-/-};Rarg^{-/-}$) exhibit midline cleft (Damm et al., 1993; Lohnes et al., 1994; Mark et al., 1995). Thus, an appropriate amount of RA is crucial for normal embryonic development, with either too much or too low RA levels causing CP in mice. In humans, decreased serum levels of vitamin A and RA binding protein 4 (RBP4), a RA translocator, have been reported in non-syndromic CL/P patients (Zhang et al., 2014). In addition, excessive vitamin A intake is known to be associated with multiple birth defects (Lammer et al., 1985; Martinez-Frias and Salvador, 1990; Werler et al., 1990); however, the minimum teratogenic dose appears to be well above the level consumed by most women through multivitamin and vitamin A supplements during pregnancy (Mills et al., 1997; Skare et al., 2012).

A number of microRNAs (miRs), which are small non-coding RNAs (21–25 nucleotides) that regulate the expression of target genes at the post-transcriptional level (Hudder and Novak, 2008; Hou et al., 2011), play important roles in a wide array of cellular functions during the development of various tissues, including the upper lip and the palate (Shin et al., 2012; Seelan et al., 2014; Warner et al., 2014; Mukhopadhyay et al., 2019). For instance, loss of a miR-processing enzyme, such as DROSHA and DICER, results in craniofacial developmental defects in mice (Zehir et al., 2010; Nie et al., 2011; Schoen et al., 2017), and polymorphisms in *DROSHA* are associated with risk of CL/P in humans (Xu et al., 2018). In addition, mice with a deletion of miR-17-92 cluster, which is located on chromosome 14 in mice and chromosome 13 in humans, exhibit either bilateral or unilateral CLP and delayed endochondral ossification, hypoplastic lung, and cardiac ventricular septal defect (Ventura et al., 2008; de Pontual et al., 2011; Wang et al., 2013). By contrast, overexpression of *miR-17-92* in mouse palatal mesenchymal cells results in increased cell proliferation (Li et al., 2012). Thus, miRs can regulate cellular functions through the regulation of their target's gene expression. Currently, while the importance of miRs in development is well recognized through loss-of-function studies for miRs, it remains largely unknown which miRs are elevated by environmental factors to suppress genes that are crucial for palate development.

Our previous bioinformatic studies showed that 18 miRs are possibly involved in the regulation of CP-associated genes in mice (Suzuki et al., 2018a). Recent studies show that *all-trans* RA (*at*RA) modulates miR expressions in human cancer cell lines (Liu et al., 2018, 2019). However, it is still unclear which miRs are functionally relevant in palate development and whether expression of these miRs is altered by *at*RA exposure. In this study, we investigated the mechanism of how miRs contribute to pathogenesis of CPO induced by excessive *at*RA intake.

MATERIALS AND METHODS

Cell Culture

MEPM cells were isolated from the palatal shelves of E13.5 C57BL/6J mice, as previously described (Iwata et al., 2014). The palatal shelves from one embryo were used for each cell culture, and three independent experiments were conducted using cells from different litters. MEPM cells were maintained under Dulbecco's modified Eagle's medium (DMEM; Sigma Aldrich, St. Louis, MO, United States) supplemented with 10% fetal bovine serum (FBS), penicillin/streptomycin (Sigma Aldrich), 2-mercaptoethanol (Gibco, Waltham, MA, United States), and non-essential amino acids (Sigma Aldrich) at 37°C in a humidified atmosphere with 5% CO_2.

Animals

C57BL/6J mice were obtained from The Jackson Laboratory, Bar Harbor, ME, United States. Pregnant female mice were orally administered 40–70 mg/kg *at*RA (R2625, Sigma-Aldrich) suspended in 10% ethanol and 90% corn oil emulsion at E11.5. Control mice received an equivalent amount of emulsion without *at*RA (0.1 ml/10 g body weight). For the rescue experiments, 50 mg/kg *at*RA was orally administered at E11.5, and then the miR-124-3p inhibitor (Integrated DNA Technologies, Coralville, IA, United States) was intraperitoneally injected at 5 mg/kg at E12.5 and E13.5. The protocol was approved by the Animal Welfare Committee (AWC) and the Institutional Animal Care

and Use Committee (IACUC) of UTHealth (AWC 19-0079). All mice were maintained at the animal facility of UTHealth.

Cell Proliferation Assay

MEPM cells were plated onto 96-well cell culture plates at a density of 5,000 cells per well and treated with a mimic for negative control (4464061), miR-21a-5p (4464066; MC10206), miR-27a-3p (4464066; MC10939), miR-27b-3p (4464066; MC10750), miR-30a-5p (4464066; MC11062), miR-124-3p (4464066; MC10691), miR-141-3p (4464066; MC10860), miR-200a-3p (4464066; MC10991), miR-203-3p (4464066; MC10152), miR-320-3p (4464066; MC11621), and miR-381-3p (4464066; MC10242) [mirVana miRNA mimic (chemically modified double-stranded RNA molecules), ThermoFisher Scientific, Waltham, MA, United States], or an inhibitor for negative control (4464079), miR-27a-3p (4464084; MH10939), miR-27b-3p (4464084; MH10750), and miR-124-3p (4464084; MH10691) [mirVana miRNA inhibitor (chemically modified, single-stranded oligonucleotides with patented secondary structure), Thermo Fisher Scientific], using the Lipofectamine RNAiMAX transfection reagent (Thermo Fisher Scientific), according to the manufacturer's protocol (3 pmol of the mimic or the inhibitor and 0.3 μl of the transfection reagent in 100 μl DMEM per well). Cell proliferation was measured using the Cell Counting Kit 8 (Dojindo Molecular Technologies Inc., Gaithersburg, MD, United States) 24, 48, or 72 h after treatments (n = 6 per group). For the *at*RA exposure experiments, MEPM cells were plated onto 96-well cell culture plates at a density of 5,000 cells per well and treated with 30 μM *at*RA. After 24, 48, or 72 h of treatment, cell numbers were determined as described above.

Bromodeoxyuridine (BrdU) Incorporation Assay

MEPM cells were plated onto 35-mm dishes at a density of 25,000/dish and treated with 30 μM *at*RA or control vehicle (dimethyl sulfoxide). After 24 h, the cells were incubated with 100 μg/ml BrdU (Sigma Aldrich) for 1 h. Incorporated BrdU was stained with a rat monoclonal antibody against BrdU (ab6326; Abcam, Cambridge, MA, United States 1:1,000), as previously described (Iwata et al., 2014). A total of six fields, which were randomly selected from three independent experiments, were used for the quantification of BrdU-positive cells.

Immunoblotting

MEPM cells were plated onto a 60-mm dish at a density of 50,000 cells per dish and treated with either 30 μM *at*RA or vehicle for 72 h, or with each miR mimic or control miR for 48 h. The treated cells were lysed with RIPA buffer (Cell Signaling Technology, Danvers, MA, United States) with a protease inhibitor cocktail (Roche, Indianapolis, IN, United States). The cells were harvested and centrifuged at 21,130 × g for 10 min at 4°C. The supernatant of each sample was collected, and protein concentration was determined using the BCA protein kit (Pierce). Protein samples were applied to Mini-PROTEAN TGX Gels (Bio-Rad, Hercules, CA, United States) and transferred to a polyvinylidene difluoride (PVDF) membrane. A mouse monoclonal antibody against GAPDH (MAB374, Millipore, Burlington, MA, United States, 1:6,000), a rabbit monoclonal antibody against CCND1 (2978, Cell Signaling Technology, 1:1,000), and a rabbit polyclonal antibody against cleaved caspase 3 (9661, Cell Signaling Technology, 1:1,000) were used. Peroxidase-conjugated anti-mouse IgG (7076, Cell Signaling Technology, 1:100,000) and anti-rabbit IgG (7074, Cell Signaling Technology, 1:100,000) were used as secondary antibodies.

Quantitative RT-PCR

MEPM cells were plated onto a 60-mm dish at a density of 40,000 cells per dish. When the cells reached 80% confluence, they were treated with a mimic or an inhibitor for miR-27a-3p, miR-27b-3p, miR-124-3p, or a negative control, at 3 pmol in 6 μl of transfection reagent (Lipofectamine RNAiMAX transfection reagent in 4 ml DMEM per dish). After 24 h of treatment, total RNA was extracted with the QIAshredder and miRNeasy Mini Kit (QIAGEN, Hilden, Germany) according to the manufacturer's instructions. For the *at*RA experiments, the cells were plated onto a 60-mm dish at a density of 50,000 cells per dish and treated with 30 μM *at*RA for 24 h, and total RNA from MEPM cells (n = 6 per group) was isolated as described above. For the animal experiments, palatal shelves were microdissected at E13.5 and E14.5. Total RNA (1 μg) from each sample was reverse-transcribed using iScript Reverse Transcription Supermix for qRT-PCR (Bio-Rad), and the cDNA was amplified with iTaq Universal SYBR Green Supermix (Bio-Rad) using the CFX96 Touch Real-Time PCR Detection system (Bio-Rad). The PCR primers used in this study are listed in **Supplementary Table 1**. The amount of each mRNA was normalized by *Gapdh*. miR expression was measured with Taqman Fast Advanced Master Mix and Taqman Advanced miR cDNA Synthesis Kit (Thermo Fisher Scientific), according to the manufacturer's instructions. Probes for miR-27a-3p (mmu478384_mir), miR-27b-3p (mmu478270_mir), miR-124-3p (mmu480901_mir), and miR-26a-5p (477995_mir) were purchased from Thermo Fisher Scientific.

Histological Analysis

The embryos' heads were collected at E13.5, E14.5, and E18.5 and fixed with 4% paraformaldehyde overnight. After decalcification with 10% ethylenediaminetetraacetic acid-2Na-2H_2O (EDTA), all samples were dehydrated and embedded in paraffin. Paraffin-embedded tissues were sectioned at 4-μm thickness and stained with hematoxylin and eosin (H&E). For immunohistochemistry, paraffin sections were deparaffinized and rehydrated. After antigen retrieval treatment with citrate buffer (pH 6.0) and blocking of endogenous peroxidase with 0.3% hydrogen peroxide in methanol, the sections were incubated with anti-cytokeratin 14 mouse monoclonal antibody (Abcam, ab7800, 1:200 dilution), anti-Ki-67 rabbit monoclonal antibody (Abcam, ab16667, 1:200 dilution), anti-VCAN rabbit polyclonal antibody (Novus Biologicals, Centennial, CO, United States, NBP1-85432, 1:200 dilution), or anti-CDC42 rabbit polyclonal antibody (Proteintech, Rosemont, IL, United States, 10155-1-AP, 1:50 dilution) at 4°C overnight. The sections were then incubated with a secondary antibody, goat anti-rabbit IgG-Alexa Fluor 488 (Thermo Fisher Scientific; A-11008; 1:500 dilution) or goat anti-rabbit IgG (H + L), biotinylated (Vector Laboratories,

Burlingame, CA, United States; BA-1000; 1:500 dilution) for 1 h at room temperature. Sections were counterstained with 4′,6-diamidino-2-phenylindole (DAPI) for nuclear staining for fluorescent imaging and methylene blue for bright field imaging. Azan staining was performed as previously described (Iwata et al., 2013). A total of six fields, which were randomly selected from three independent experiments, were used for the quantification of Ki-67-positive cells. Fluorescence images were obtained using a confocal microscope (Ti-C2, Nikon, Melville, NY, United States), and color images were obtained using a light microscope (BX43, Olympus, Center Valley, PA, United States); $n = 6$ per group in each experiment.

Craniofacial Tissue Explant Culture

Timed-pregnant mice were euthanized at E13.5 and decapitated in PBS. The mandible and tongue were removed from the embryos, and each explant, including the upper half of the head, was placed in a glass tube containing BGJb medium (Gibco, 12591) supplemented with 50% fetal bovine serum, 0.1% ascorbic acid, and antibiotics. The tubes were placed in a rotary apparatus rotating at 50 rpm in an incubator at 37°C and 5% CO_2. After 3 days in culture with/without 30 μM *at*RA, the explants were fixed in 4% PFA and processed.

Flow Cytometry

MEPM cells were plated onto 60-mm dishes at a density of 50,000/dish and treated with 30 μM *at*RA or control vehicle (dimethyl sulfoxide). After 24 h, the cells were harvested by trypsin and washed twice with cold BioLegend's Cell Staining Buffer (BioLegend, San Diego, CA, United States; 420201). Cells were centrifuged at 500 g for 5 min at 4°C. The cell pellets were resuspended with Annexin V Binding Buffer (BioLegend; 422201) at a concentration of 1.5×10^6 cells/ml. Resuspended cells (100 μl) were transferred into a Falcon tube and incubated with 5 μl of Annexin V (BioLegend: 421301) and 10 μl of propidium iodide (BioLegend: 421301) for 15 min at room temperature in the dark. A volume of 400 μl of Annexin V Binding Buffer was added to the Falcon tube, and the samples were analyzed with FACS Aria II (BD Biosciences, San Jose, CA, United States).

Statistical Analysis

All experiments were performed independently three times. All statistical analyses were performed using the SPSS software (version 26.0, IBM, Armonk, NY, United States). The statistical significance of the differences between two groups (control and treated groups) was evaluated using independent *t*-tests. The statistical significance for multiple two groups was evaluated using multiple *t*-tests after Bonferroni correction. An adjusted *p*-value after Bonferroni correction (equivalent to non-adjusted $p < 0.05$) was considered to be statistically significant. For a comparison among multiple groups (e.g., control, treated, and rescued groups) with one factor such as gene or positive cell, a one-way analysis of variance (ANOVA) with Tukey's honest significant difference test was used for assessment. For a comparison among multiple groups (e.g., control, treated, and rescued groups) with multiple factors, a two-way ANOVA with Tukey's honest significant difference test was used for assessment. Cell proliferation assays were analyzed using a two-way ANOVA with Dunnett's (vs. control) or Tukey's (between all groups) honest significant difference test. A $p < 0.05$ was considered to be statistically significant. Data are represented as mean ± standard deviation in the graphs.

RESULTS

Overexpression of miR-27a-3p, miR-27b-3p, and miR-124-3p Inhibits Cell Proliferation in MEPM Cells

To evaluate the effect of overexpression of miRs, which were predicted through our bioinformatic analyses (Suzuki et al., 2018a,b), MEPM cells were treated with each miR mimic (miR-21a-5p, miR-27a-3p, miR-27b-3p, miR-30a-5p, miR-124-3p, miR-141-3p, miR-200a-3p, miR-203-3p, miR-320-3p, and miR-381-3p) and analyzed for their effect on cell proliferation. Among them, miR-27a-3p, miR-27b-3p, miR-30a-5p, and miR-124-3p mimics significantly inhibited cell proliferation in MEPM cells, while the mimic of either miR-21a-5p, miR-141-3p, miR-200a-3p, miR-203-3p, miR-320-3p, or miR-381-3p did not affect cell proliferation (**Figure 1A**). We confirmed that miR-27a-3p, miR-27b-3p, and miR-124-3p mimics did not induce apoptosis (**Figure 1B**). To identify CP-associated genes targeted by either the miR-27a-3p, miR-27b-3p, or miR-124-3p mimic, we conducted quantitative RT-PCR analysis for the predicted target genes (38 CP-associated genes in miR-27a-3p, 37 CP-associated genes in miR-27b-3p, and 55 CP-associated genes in miR-124-3p) in MEPM cells after treatment with each miR mimic (**Supplementary Table 2**). Among them, the expression of four genes (*Bmi1*, *Dicer1*, *Pds5b*, and *Tgfbr3*) in the miR-27a-3p mimic, four genes (*Bmi1*, *Eya1*, *Gab1*, and *Spry2*) in the miR-27b-3p mimic, and nine genes (*Alx1*, *Axin1*, *Fst*, *Hic1*, *Sp8*, *Tm7sf2*, *Tshz1*, *Vcan*, and *Zeb1*) in the miR-124-3p mimic were significantly downregulated in candidate target genes downregulated with treatment of each miR mimic (**Figures 2A–C**). To further evaluate the role of each miR in cell proliferation and gene regulation, we treated MEPM cells with a specific inhibitor for either miR-27a-3p, miR-27b-3p, or miR-124-3p. We found that inhibitors of miR-27a-3p, miR-27b-3p, and miR-124-3p failed to change cell proliferation activity (**Supplementary Figure 1A**). We then performed quantitative RT-PCR analysis for the predicted target genes and found that the expression of 17 genes (*Acvr2a*, *Bmi1*, *Cdc42*, *Chd7*, *Ephb2*, *Eya4*, *Gab1*, *Pax9*, *Pdgfra*, *Prdm16*, *Runx1*, *Six1*, *Sox11*, *Spry1*, *Spry2*, *Tgfbr3*, and *Zeb1*) in the miR-27a-3p inhibitor, 6 genes (*Apaf1*, *Eya4*, *Pds5d*, *Sos1*, *Spry2*, and *Sumo1*) in the miR-27b-3p inhibitor, and 9 genes (*Axin1*, *Cdc42*, *Esrp1*, *Fst*, *Gas1*, *Mmp16*, *Pbx3*, *Vcan*, and *Zeb1*) in the miR-124-3p inhibitor were significantly upregulated in candidate target genes upregulated with treatment of each miR inhibitor (**Supplementary Figures 1B–D**). Therefore, these results suggest that *Bmi1* and *Tgfbr3* in miR-27a-3p, *Spry2* in miR-27b-3p, and *Axin1*, *Fst*, *Vcan*, and *Zeb1* in miR-124-3p were strong candidates regulated by the miRs in a dose-dependent manner.

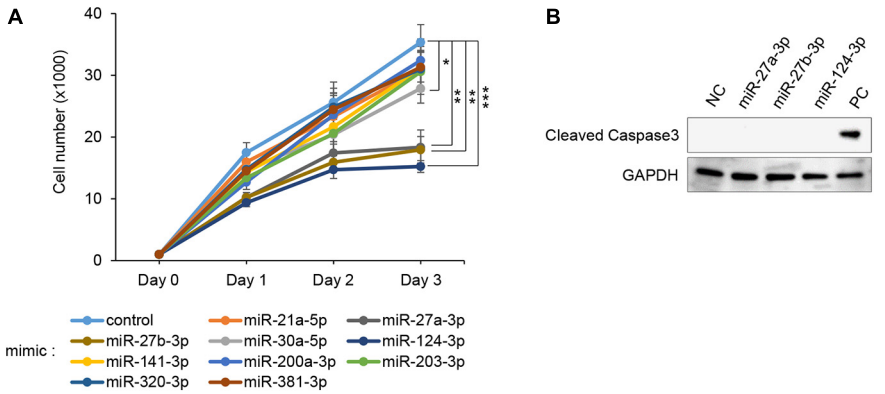

FIGURE 1 | Effect of overexpression of the predicted miRs on cell proliferation in MEPM cells. **(A)** Cell proliferation assays using MEPM cells from E13.5 palatal shelves treated with the indicated miR mimic; control, miR-21a-5p, miR-27a-3p, miR-27b-3p, miR-30a-5p, miR-124-3p, miR-141-3p, miR-200a-3p, miR-203-3p, miR-320, and miR-381-3p mimic. Two-way ANOVA with Dunnett's test ($n = 6$). *$p < 0.05$, **$p < 0.01$, ***$p < 0.001$. Each treatment group was compared with the control. **(B)** Immunoblotting analysis for cleaved caspase 3 in MEPM cells treated with control, miR-27a-3p, miR-27b-3p, or miR-124-3p mimic for 48 h. Intestine was used as a positive control (PC). GAPDH was used as an internal control. Representative images from two independent experiments are shown.

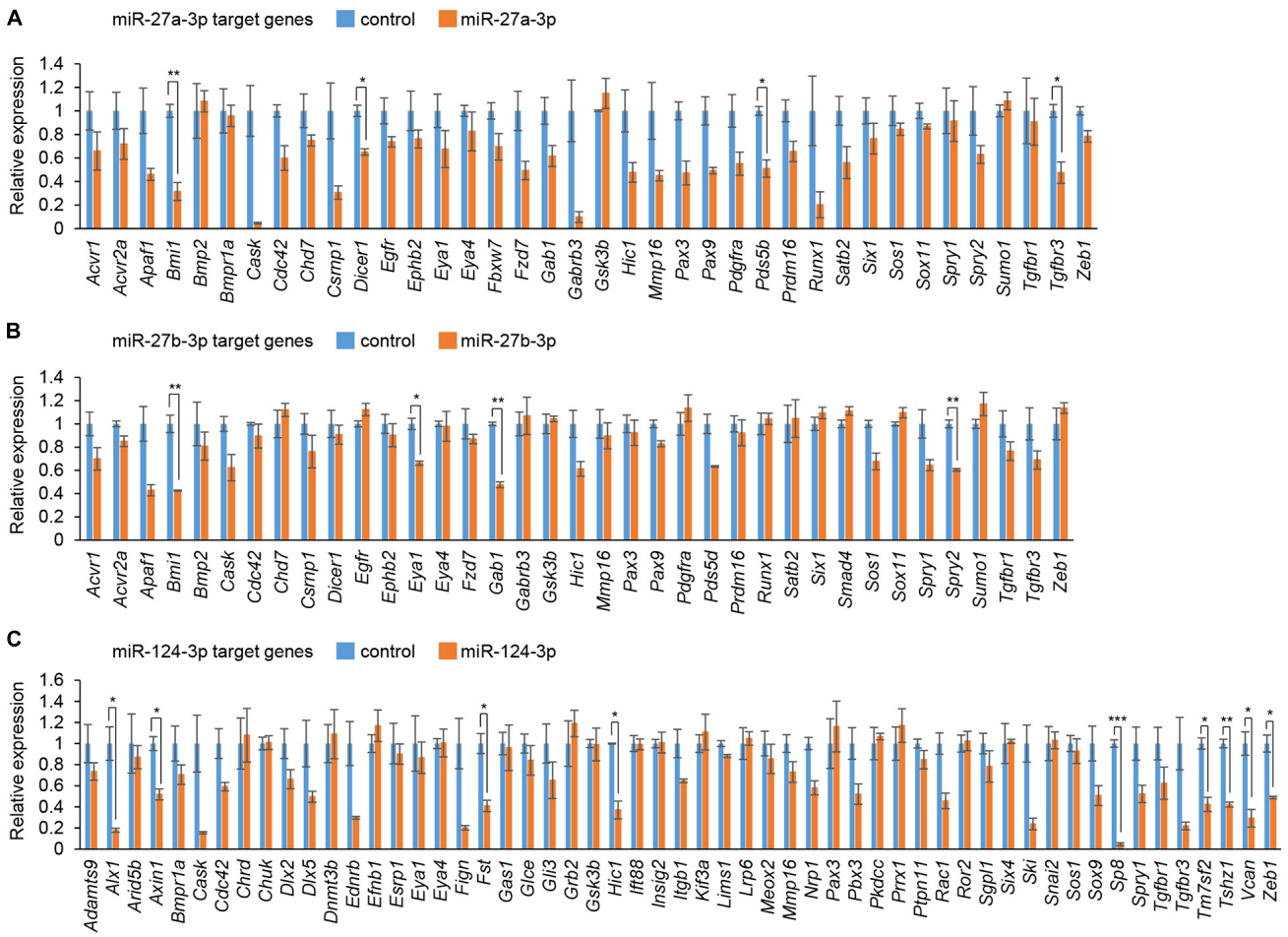

FIGURE 2 | Cleft palate-associated genes suppressed by overexpression of miR-27a-3p, miR-27b-3p, or miR-124-3p in MEPM cells. **(A–C)** Quantitative RT-PCR for the indicated genes after treatment with control or miR-27a-3p mimic **(A)**, control or miR-27b-3p mimic **(B)**, and control or miR-124a-3p mimic **(C)**. Multiple *t*-tests adjusted by Bonferroni ($n = 3$). *Adjusted $p < 0.00132$ in A (38 genes), adjusted $p < 0.00135$ in B (37 genes), adjusted $p < 0.000909$ in C (55 genes), **adjusted $p < 0.000263$ in A (38 genes), adjusted $p < 0.000270$ in B (37 genes), adjusted $p < 0.000182$ in C (55 genes), ***adjusted $p < 0.0000182$ in C (55 genes).

*at*RA Induces miR-124-3p Expression in MEPM Cells

We conducted cell proliferation assays using MEPM cells treated with *at*RA. To determine the *at*RA concentration that affects cell proliferation, the cells were treated with 10 and 30 μM *at*RA. We found that 30 μM *at*RA significantly inhibited cell proliferation in MEPM cells (**Figure 3A** and **Supplementary Figure 2A**). The reduced cell proliferation by *at*RA was confirmed with BrdU incorporation assays (**Figure 3B**) and expression of Cyclin D1 (CCND1), a cell cycle accelerator, in MEPM cells treated with *at*RA (**Figure 3C**). In addition, cleaved caspase 3, an indicator of apoptosis, was undetectable in cells treated and untreated with *at*RA (**Supplementary Figure 2B**). Moreover, flow cytometry analysis showed no significant change in the profile (cell death vs. healthy cells) of cells treated with *at*RA (**Supplementary Figure 2C**). Taken together, these data indicate that *at*RA inhibits the proliferation of MEPM cells. Interestingly, the expression of miR-124-3p was specifically induced by *at*RA treatment (**Figure 3D**); by contrast, expression of miR-27a-3p and miR-27b-3p was not altered by *at*RA treatment. As expected, the miR-124-3p target genes (*Axin1*, *Fst*, *Vcan*, and *Zeb1*) were significantly downregulated with *at*RA treatment (**Figure 3E**). Taken together, these observations suggest that the expression of these genes was downregulated by *at*RA through miR-124-3p. We confirmed that the expression of all the other predicted genes regulated by miR-124-3p (additional 39 genes) was not correlated with the *at*RA condition (**Supplementary Figure 3**). For instance, although three genes (*Bmpr1a*, *Gli3*, and *Snal2*) were significantly downregulated and *Six4* was significantly upregulated under *at*RA treatment, the expression of these genes was not altered with treatment with the miR-124-3p mimic. Therefore, the use of both a mimic and an inhibitor for the identification of genes regulated by miR-124-3p was helpful to identify genes directly regulated by miR-124-3p.

miR-124-3p Inhibitor Partially Rescues Decreased Cell Proliferation in *at*RA-Treated Cells

To evaluate the contribution of miR-124-3p to *at*RA-induced cell proliferation inhibition, we treated MEPM cells with a miR-124-3p inhibitor under *at*RA treatment. The miR-124-3p inhibitor specifically suppressed miR-124-3p expression for treatment at 24 and 48 h (**Supplementary Figures 4A,B**). The miR-124-3p inhibitor could partially rescue reduced cell proliferation (**Figure 4A**). As expected, both the number of BrdU-positive cells and CCND1 expression were normalized with treatment with the miR-124-3p inhibitor (**Figures 4B,C**). In addition, the expression of miR-124-3p target genes (*Fst*, *Vcan*, and *Zeb1*) was partially normalized with the miR-124-3p inhibitor under *at*RA conditions (**Figure 4D**). Taken together, our results

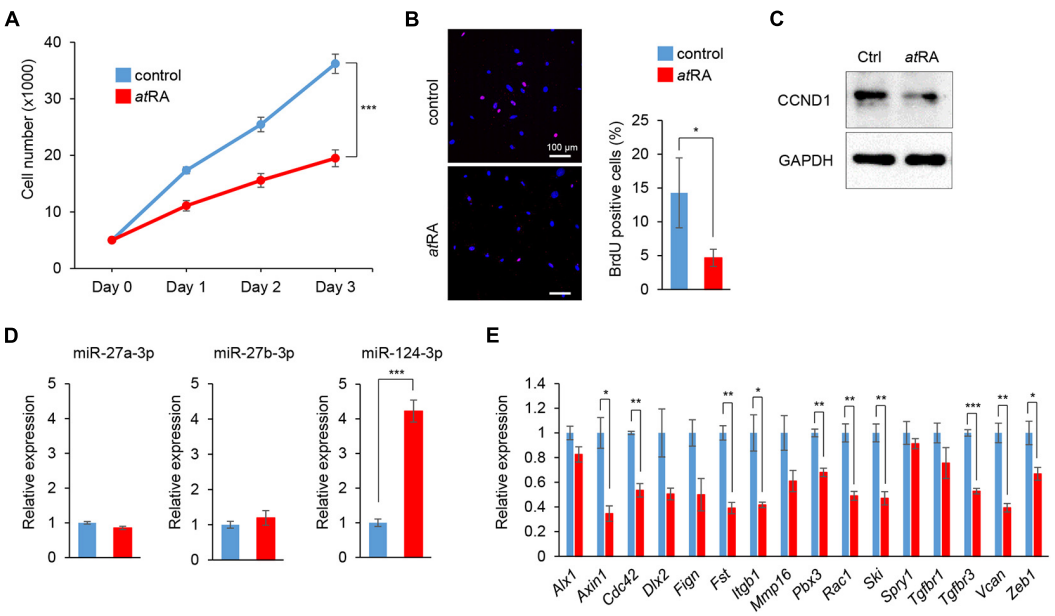

FIGURE 3 | Influence of *at*RA treatment on cell proliferation and gene expression in MEPM cells. **(A)** Cell proliferation assays in MEPM cells treated with 30 μM *at*RA for 24, 48, and 72 h. Two-way ANOVA with Dunnett's test ($n = 6$). ***$p < 0.001$ vs. control. **(B)** BrdU staining (red) in MEPM cells after treatment with 30 μM *at*RA for 72 h. Nuclei were counterstained with DAPI (blue). Representative images from two independent experiments are shown. Graph shows the quantification of BrdU-positive cells. Independent *t*-test. *$p < 0.05$ vs. control. Bars, 50 μm. **(C)** Immunoblotting analysis of CCND1 and GAPDH in MEPM cells treated with 30 μM *at*RA for 72 h. Representative images from two independent experiments are shown. **(C)** Immunoblotting analysis for CCND1 in MEPM cells treated with 30 μM *at*RA for 72 h. GAPDH was used as an internal control. **(D)** Quantitative RT-PCR for miR-27a-3p, miR-27b-3p, or miR-124-3p after treatment with *at*RA for 24 h in MEPM cells. Multiple *t*-tests adjusted by Bonferroni ($n = 3$). ***Adjusted $p < 0.00033$ (three miRs). **(E)** Quantitative RT-PCR for the indicated genes after treatment with *at*RA for 24 h in MEPM cells. Multiple *t*-tests adjusted by Bonferroni ($n = 3$–6). *Adjusted $p < 0.00313$ (16 genes), **adjusted $p < 0.000625$ (16 genes), ***adjusted $p < 0.0000625$ (16 genes) vs. control.

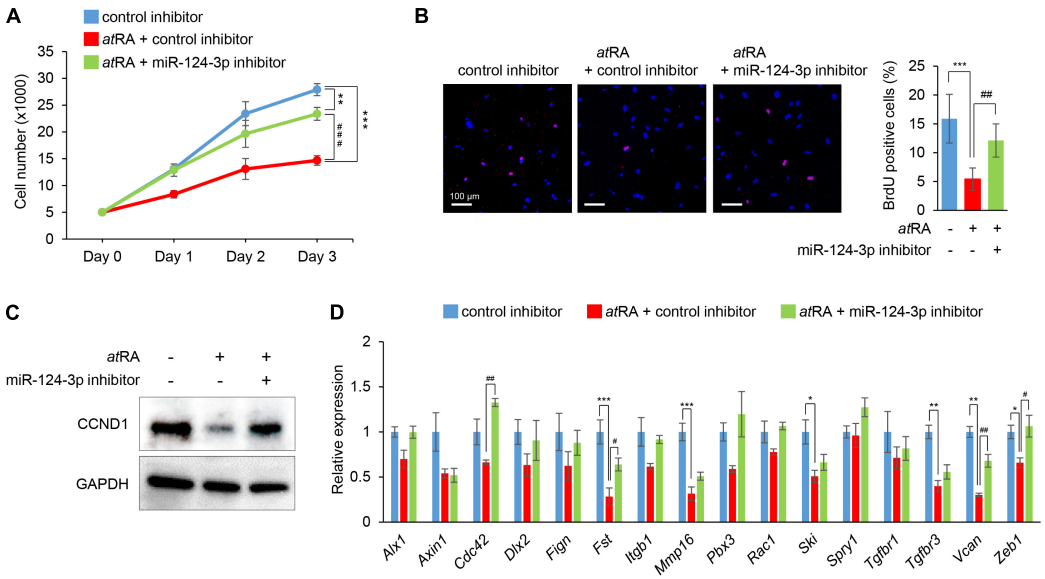

FIGURE 4 | Normalization of *miR-124-3p* expression restores *at*RA-induced cell proliferation defect in MEPM cells. **(A)** Cell proliferation assays in MEPM cells treated with a control or a miR-124-3p inhibitor under the 30 μM *at*RA condition for 0, 24, 48, or 72 h (Days 0–3). Two-way ANOVA with Tukey's honest significant difference test ($n = 6$ per group). $^{**}p < 0.01$, $^{***}p < 0.001$, $^{\#\#\#}p < 0.001$. **(B)** BrdU staining (red) in MEPM cells after treatment with/without a miR-124-3p inhibitor under the 30 μM *at*RA condition for 72 h. Nuclei were counterstained with DAPI (blue). Representative images from two independent experiments are shown. Graph shows the quantification of BrdU-positive cells. One-way ANOVA with Tukey's honest significant difference test. $^{***}p < 0.001$ vs. control inhibitor + vehicle, $^{\#\#}p < 0.01$ vs. control inhibitor + *at*RA. Bars, 50 μm. **(C)** Immunoblotting analysis of CCND1 and GAPDH in MEPM cells treated with 30 μM *at*RA under the effect of a miR-124-3p inhibitor for 72 h. Representative images from two independent experiments are shown. **(D)** Quantitative RT-PCR for the indicated genes in MEPM cells after treatment with *at*RA under the effect of a miR-124-3p inhibitor for 24 h. *Adjusted $p < 0.00313$ (16 genes), **adjusted $p < 0.000625$ (16 genes), and ***adjusted $p < 0.0000625$ (16 genes) vs. control inhibitor + vehicle. $^{\#}$Adjusted $p < 0.00313$ (16 genes), $^{\#\#}$adjusted $p < 0.000625$ (16 genes), and $^{\#\#\#}$adjusted $p < 0.0000625$ (16 genes). Two-way ANOVA with Tukey's honest significant difference test ($n = 3$–6).

indicate that *at*RA inhibits cell proliferation through miR-124-3p expression in MEPM cells.

*at*RA Induces miR-124-3p Expression in the Developing Palate in Mice

The oral administration of *at*RA to pregnant mice is known to induce CP (Abbott et al., 1989; Ross et al., 2000; Wang et al., 2002; Lai et al., 2003; Yao et al., 2011; Havasi et al., 2013; Hu et al., 2013; Hou et al., 2019; Roberts, 2020). However, the amount and timing of *at*RA administration that induces CP may differ in each mouse strain and protocol. Therefore, we tested various doses (40, 50, 60, and 70 mg/kg) of oral *at*RA in C57BL/6J mice. We found that *at*RA administration at 40 mg/kg induced CP with 57% penetrance (12/21 embryos), while more than 50 mg/kg *at*RA induced CP with 100% penetrance (**Table 1**). Therefore, we administered a single dose of 50 mg/kg *at*RA at E11.5 in this study (**Figure 5A**). The palatal shelves of embryos treated with vehicle were normally elevated and fused at E14.5, while the palatal shelves of embryos treated with *at*RA failed to elevate at E14.5, causing CP at E18.5 (**Figure 5B**). To confirm the reduction of cell proliferation in the developing palates of mice treated with *at*RA, we evaluated cell proliferation by Ki-67 immunostaining. As expected, the number of Ki-67-positive cells (i.e., proliferating cells) was significantly reduced in the palatal shelves of *at*RA-treated embryos (**Figure 5C**). Next, we microdissected the palatal shelves at E13.5 and E14.5 from mice treated with either vehicle or *at*RA and measured the miR expression. In the vehicle control group, the expression of miR-27a-3p and miR-27b-3p was not changed between E13.5 and E14.5, while the expression of miR-124-3p at E14.5 was upregulated compared to that of E13.5 (**Figure 5D**). The expression of miR-124-3p was significantly upregulated with *at*RA administration at both E13.5 and E14.5 compared to controls, while the expression of miR-27a-3p and miR-27b-3p was comparable to the controls (**Figure 5D**). Furthermore, quantitative RT-PCR analysis for genes targeted by miR-124-3p confirmed that a total of three genes (*Fst*, *Vcan*, and *Zeb1*) were significantly downregulated in the palatal shelves of mice given *at*RA compared to controls (**Figure 5E**). To confirm that the hypoplastic mandible secondarily caused CP in mice treated with *at*RA, we cultured E13.5 craniofacial explants, which were extracted from the mandible and tongue, with/without *at*RA for 3 days (**Figure 5F**). In controls, the palatal shelves were elevated

TABLE 1 | Incidence of cleft palate (CP) by *at*RA administration at different doses.

*at*RA dose (mg/kg)	Total incidence of CP	Percentage of CP
40	12/21	57%
50	14/14	100%
60	21/21	100%
70	34/34	100%

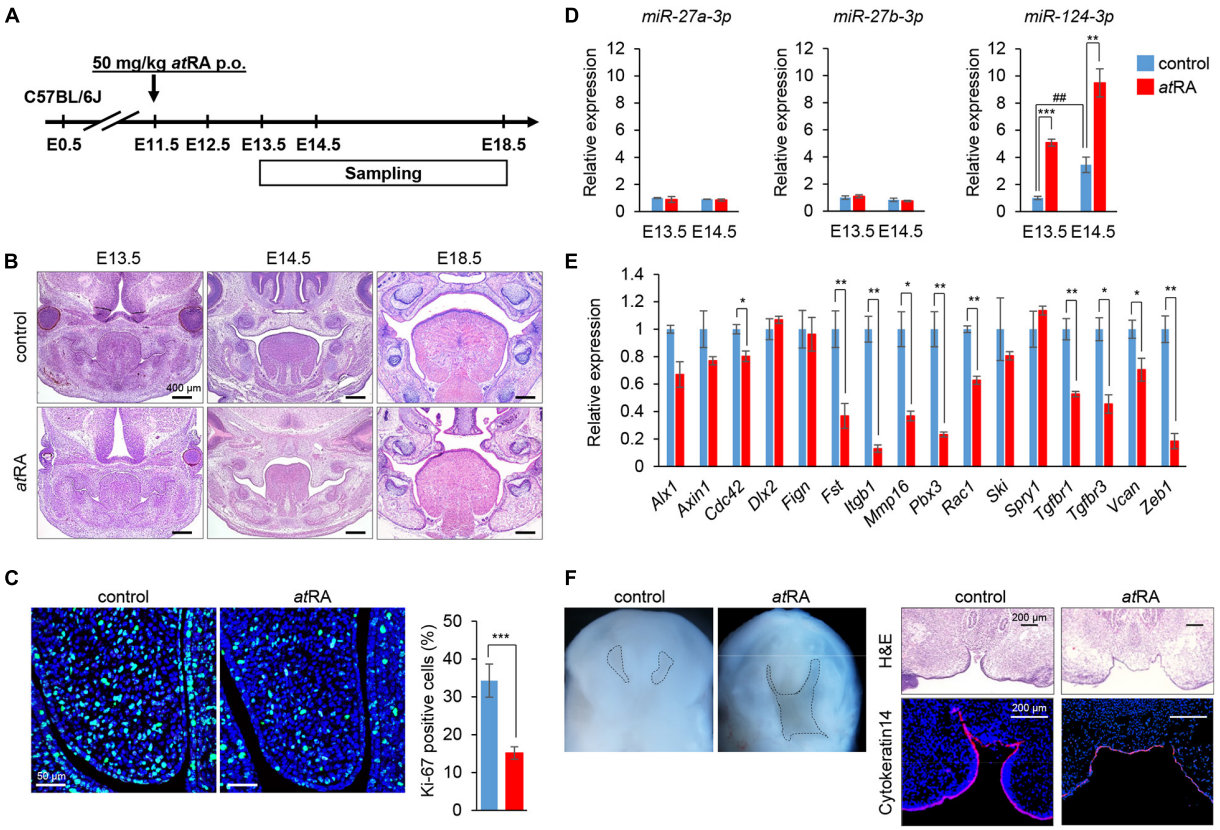

FIGURE 5 | Influence of *at*RA administration on palatal development and gene expression in mice. **(A)** Schematic experimental design. **(B)** H&E staining of face at E13.5, E14.5, and E18.5. Bars, 400 μm. **(C)** Ki-67 staining (green) in the developing palate of E13.5 mice treated with control vehicle or *at*RA (50 mg/kg p.o. at E11.5). Nuclei were counterstained with DAPI (blue). Representative images from two independent experiments are shown. Graph shows the quantification of Ki-67-positive cells. Independent *t*-tests. $^{***}p < 0.001$ vs. control. Bars, 50 μm. **(D)** Quantitative RT-PCR for miR-27a-3p, miR-27b-3p, or miR-124-3p after administration of *at*RA in palatal shelves at E13.5 and E14.5. Two-way ANOVA with Tukey's honest significant difference test ($n = 3$). $^{**}p < 0.01$, $^{***}p < 0.001$ vs. control at each indicated day and $^{\#\#}p < 0.01$ vs. E13.5 control. **(E)** Quantitative RT-PCR for the indicated genes after treatment with *at*RA for 24 h in palatal shelves at E14.5. Multiple *t*-tests adjusted by Bonferroni ($n = 3$–6). *Adjusted $p < 0.00313$ (16 genes), **adjusted $p < 0.000625$ (16 genes) vs. control. **(F)** Intraoral views of heads (left panels) from E13.5 embryos, from which the mandible and tongue were removed and cultured for 3 days with control vehicle or *at*RA ($n = 4$ per group). Dashed lines delineate the palatal shelves. H&E staining and K14 immunostaining (red) (right panels) of coronal sections of 3-day cultured explants with control vehicle or *at*RA. The nuclei were counterstained with DAPI (blue). Bars, 200 μm.

and almost completely fused. By contrast, the explants treated with *at*RA showed a widely opened palate. These results indicate that *at*RA primarily causes CP in mice treated with *at*RA.

Normalization of miR-124-3p Expression Can Rescue CP Induced by *at*RA in Mice

Finally, we attempted to rescue CP induced by *at*RA in mice through treatment with an inhibitor specific for miR-124-3p (**Figure 6A**). The administration of a miR-124-3p inhibitor reduced CP penetrance from 100 to 35% in the *at*RA-induced CPO mouse model (**Figures 6B,C**). The reduced cell proliferation was partially normalized in mice injected with a miR-124-3p inhibitor under *at*RA-treated conditions (**Figure 6D**). Moreover, the expression of *Vcan* and *Zeb1* was partially normalized with a miR-124-3p inhibitor upon *at*RA exposure (**Figure 6E**). To analyze the expression pattern of extracellular matrix (ECM) formation in mice treated with *at*RA, we performed Azan staining for the visualization of overall ECM production and pattern. We did not detect any alteration in ECM patterning. Furthermore, to confirm that there was alteration in the patterning, but not in the level, of expression of the molecules, we conducted immunohistochemical analyses for VCAN and CDC42 in mice treated with *at*RA and confirmed that there was no change in the expression pattern (**Figure 6F**). Taken together, our results indicate that *at*RA induces CPO through the upregulation of miR-124-3p expression in mice.

DISCUSSION

miRs have been implicated in developmental processes and various types of cancers (Mukhopadhyay et al., 2010; Chen et al., 2012), and dysregulation of miR expression has been identified in a variety of human diseases (Mendell and Olson, 2012). Recent studies show that miRs play important roles in craniofacial development (Shin et al., 2012; Seelan et al., 2014; Warner et al.,

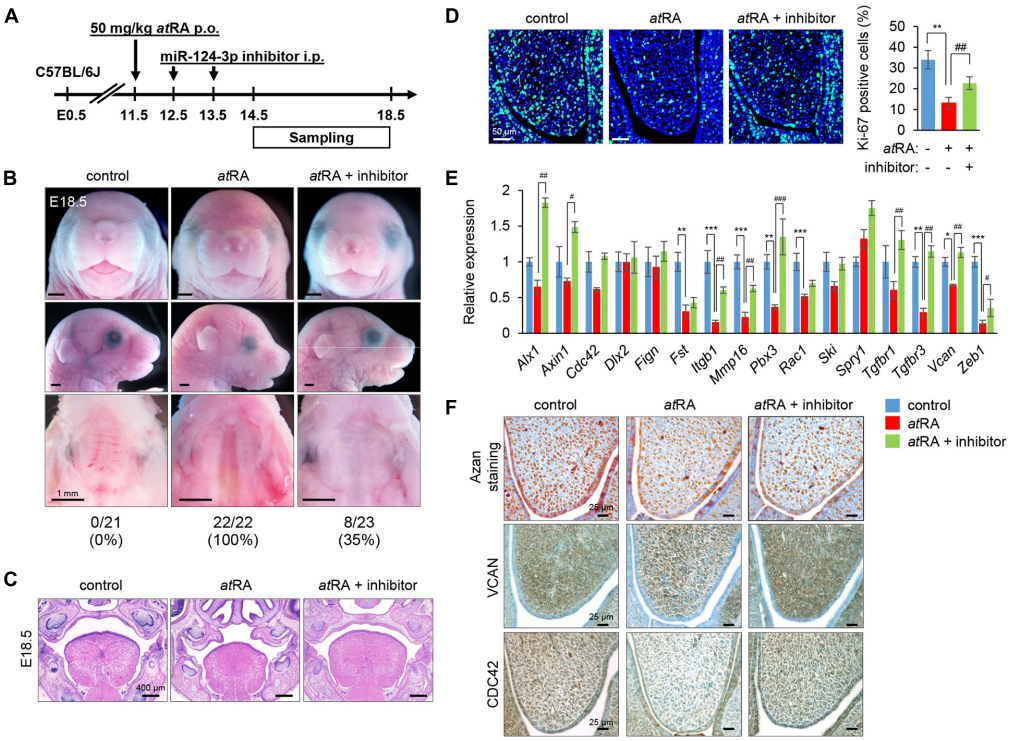

FIGURE 6 | Inhibition of miR-124-3p expression rescues *at*RA-induced CP in mice. **(A)** Schematic experimental design. **(B)** Gross picture of E18.5 C57BL/6J mice treated with control vehicle, *at*RA, or *at*RA + miR-124-3p inhibitor. Bars, 1 mm. **(C)** H&E staining of the face of E18.5 C57BL/6J mice treated with control vehicle, *at*RA, or *at*RA + miR-124-3p inhibitor. Bars, 400 μm. **(D)** Ki-67 staining (green) in the developing palate of E13.5 C57BL/6J mice treated with/without a miR-124-3p inhibitor under *at*RA condition. Nuclei were counterstained with DAPI (blue). Representative images from two independent experiments are shown. Graph shows the quantification of Ki-67 positive cells. One-way ANOVA with Tukey's honest significant difference test. $^{**}p < 0.01$ vs. control. $^{\#\#}p < 0.01$ vs. *at*RA. Bars, 50 μm. **(E)** Quantitative RT-PCR for the indicated genes after treatment with/without a miR-124-3p inhibitor under *at*RA condition in the palatal shelves of E14.5 C57BL/6J mice. Two-way ANOVA with Tukey's honest significant difference test ($n = 3$). *Adjusted $p < 0.00313$ (16 genes), **adjusted $p < 0.000625$ (16 genes), and ***adjusted $p < 0.0000625$ (16 genes) vs. control. $^{\#}$Adjusted $p < 0.00313$ (16 genes), $^{\#\#}$adjusted $p < 0.000625$ (16 genes), and $^{\#\#\#}$adjusted $p < 0.0000625$ (16 genes) vs. *at*RA. **(F)** AZAN staining (upper panels) and immunohistochemical staining for VCAN (middle panels; brown) and CDC42 (bottom panels; brown) in E13.5 C57BL/6J mice treated with control vehicle, *at*RA, or *at*RA + miR-124-3p inhibitor. Bars, 25 μm.

2014; Mukhopadhyay et al., 2019); for example, administration of miR-23b and miR-133 duplex results in facial defects in zebrafish (Ding et al., 2016). A bioinformatic study suggested that miR-199a-5p may be associated with CL/P through the modulation of transforming growth factor (TGF)-α expression (Chen et al., 2018). miR-140-5p overexpression inhibits cell proliferation through the suppression of genes associated with CP, *Fgf9,* and *Pdgfra* in MEPM cells (Li et al., 2020). Mice with a deletion of the miR-17-92 cluster (includes six miRs: miR-17, miR-18a, miR-19a, miR-19b-1, miR-20a, and miR-92a-1) exhibit CP through altered bone morphogenetic protein (BMP) signaling (Wang et al., 2013).

In this study, we found that the overexpression of miR-27a-3p, miR-27b-3p, and miR-124-3p could inhibit cell proliferation through the suppression of genes associated with mouse CP. miR-27 is a small somatic-enriched miR family comprising two paralogous members, miR-27a and miR-27b, in vertebrates (Kozomara and Griffiths-Jones, 2014). In zebrafish, miR-27 is highly expressed in the pharyngeal arches, and knockdown of miR-27 results in a complete loss of pharyngeal cartilage due to downregulated cell proliferation (Kara et al., 2017). miR-27a-3p, a member of the miR-23a/27a/24-2 cluster, is significantly upregulated in laryngeal carcinoma (Tian et al., 2014) and plays important roles in cell proliferation and migration in human gastric and breast cancers (Mertens-Talcott et al., 2007; Zhou et al., 2016). miR-27b-3p, a member of the miR-23b/27b/24-1 cluster, promotes cell proliferation and invasion in breast cancers (Jin et al., 2013), while miR-27b-3p inhibits cell growth and tumor progression in neuroblastoma (Lee et al., 2012), suggesting that miR-27b-3p functions are dependent on cancer types. In addition, a recent study showed that circulating miR-27b might be a potential biomarker for non-alcoholic fatty liver disease (Tan et al., 2014), and another study showed that miR-27b-3p is associated with CP in non-syndromic CL/P (Wang et al., 2017).

miR-124-3p is abundant in the human and mouse brain (Lagos-Quintana et al., 2002; Landgraf et al., 2007). In addition, miR-124-3p acts as a tumor suppressor against breast cancer and hepatocellular carcinoma (Liang et al., 2013; Long et al., 2018). Our previous study showed that the overexpression of miR-124-3p suppresses cell proliferation in primary mouse lip mesenchymal cells (Suzuki et al., 2019b). miR-124-3p regulates cell cycle by targeting integrin subunit beta 1 (ITGB1) in oral

squamous cell carcinoma cells (Hunt et al., 2011), suggesting that miR-124-3p expression might remain at lower levels during normal palate development. Therefore, miR-124-3p may be a potential biomarker and a therapeutic target to prevent and diagnose CP.

In this study, we found that *Bmi1* and *Tgfbr3* in miR-27a-3p, *Spry2* in miR-27b-3p, and *Axin1*, *Fst*, *Vcan*, and *Zeb1* in miR-124-3p were regulated in MEPM cells through both gain-of-function and loss-of-function assays for miR in gene regulation. Because these genes are involved in various signaling pathways, including Wnt/β-catenin, BMP, TGF-β, and epidermal growth factor (EGF) signaling (Iwata et al., 2011; Reynolds et al., 2020), the overexpression of these miRs might lead to the suppression of multiple CP-associated genes through the dysregulation of these signaling pathways. In addition, we found that *at*RA specifically induced miR-124-3p, which suppressed the expression of genes associated with CP. While the expression of some predicted genes (*Dlx2*, *Fign*, *Ski*, *Spry1*, *Tgfbr1*, and *Vcan*) targeted by miR-124-3p was not changed by *atRA* in MEPM cells and mouse palatal shelves, these genes may be regulated by a combination of other miRs or through feedback loops. In addition, since four genes (*Axin1*, *Fst*, *Vcan*, and *Zeb1*) were downregulated in both *miR-124-3p* overexpression and *at*RA treatment conditions, these genes may be closely associated with *at*RA-induced CP in mice. AXIN1 (a WNT signaling negative regulator), FST (a BMP signaling inhibitor), and VCAN (an extracellular matrix) regulate growth factor signaling, which plays crucial roles in embryonic development; therefore, the fine-tuning regulation of the signaling pathways is important for proper embryogenesis. Homeobox gene ZEB1 regulates the epithelial-mesenchymal transition (EMT) in cancer and embryonic development (Schmalhofer et al., 2009; Gheldof et al., 2012); miR-200 family plays a role in EMT by regulating the *ZEB1* expression in the developing palate in mice (Carpinelli et al., 2020).

Our rescue experiments show that a miR-124-3p inhibitor can reduce CP penetrance in the *at*RA-induced CP mouse model. Thus, our study is useful to identify the causative molecular mechanism of CP. However, there are some limitations in this study. First, it is unclear whether any combination of miR inhibitors can achieve better outcomes. In a future study, we will investigate which miRs are the most significantly associated with *at*RA-induced CP. Second, the expression of most genes was tested only by quantitative RT-PCR analysis. A future study may include not only the level but also the patterning of gene expression associated with *at*RA-induced CP. Finally, *at*RA is known to induce tongue abnormalities (Cong et al., 2014), and this study did not exclude the possibility that *at*RA-induced CP was secondarily caused by tongue abnormalities. A future study will test whether or not tongue anomalies due to *at*RA administration cause CP using a tissue explant culture system. Despite these limitations, the understanding of miR dysregulation by *at*RA will shed light on the link between environmental and genetic factors in CP.

DATA AVAILABILITY STATEMENT

The original contributions presented in the study are included in the article/**Supplementary Material**, further inquiries can be directed to the corresponding author/s.

ETHICS STATEMENT

The animal study was reviewed and approved by the Animal Welfare Committee (AWC) and the Institutional Animal Care and Use Committee (IACUC) of UTHealth (AWC19-0079).

AUTHOR CONTRIBUTIONS

AS and JI designed the research. HY, YM, and SR performed the experiments. HY, AS, and JI wrote the manuscript. All authors reviewed the results and approved the final version of the manuscript.

FUNDING

This study was supported by grants from the National Institute of Dental and Craniofacial Research, the NIH (R03DE026208, R03DE026509, R01DE029818, and R01DE026767 to JI), and UTHealth School of Dentistry faculty funding to JI.

SUPPLEMENTARY MATERIAL

The Supplementary Material for this article can be found online at: https://www.frontiersin.org/articles/10.3389/fcell.2021.621045/full#supplementary-material

REFERENCES

Abbott, B. D., Harris, M. W., and Birnbaum, L. S. (1989). Etiology of retinoic acid-induced cleft palate varies with the embryonic stage. *Teratology* 40, 533–553. doi: 10.1002/tera.1420400602

Ashique, A. M., May, S. R., Kane, M. A., Folias, A. E., Phamluong, K., Choe, Y., et al. (2012). Morphological defects in a novel Rdh10 mutant that has reduced retinoic acid biosynthesis and signaling. *Genesis* 50, 415–423. doi: 10.1002/dvg.22002

Beaty, T. H., Marazita, M. L., and Leslie, E. J. (2016). Genetic factors influencing risk to orofacial clefts: today's challenges and tomorrow's opportunities. *F1000Research* 5:2800. doi: 10.12688/f1000research.9503.1

Bove, F. J., Fulcomer, M. C., Klotz, J. B., Esmart, J., Dufficy, E. M., and Savrin, J. E. (1995). Public drinking water contamination and birth outcomes. *Am. J. Epidemiol.* 141, 850–862. doi: 10.1093/oxfordjournals.aje.a117521

Buser, M. C., and Pohl, H. R. (2015). Windows of sensitivity to toxic chemicals in the development of cleft palates. *J. Toxicol. Environ. Health Part B Crit. Rev.* 18, 242–257. doi: 10.1080/10937404.2015.1068719

Carpinelli, M. R., de Vries, M. E., Auden, A., Butt, T., Deng, Z., Partridge, D. D., et al. (2020). Inactivation of Zeb1 in GRHL2-deficient mouse embryos rescues mid-gestation viability and secondary palate closure. *Dis. Models Mech.* 13:dmm042218.

Chen, B., Li, H., Zeng, X., Yang, P., Liu, X., Zhao, X., et al. (2012). Roles of microRNA on cancer cell metabolism. *J. Transl. Med.* 10:228. doi: 10.1186/1479-5876-10-228

Chen, G., Li, M. X., Wang, H. X., Hong, J. W., Shen, J. Y., Wang, Q., et al. (2018). Identification of key genes in cleft lip with or without cleft palate regulated by miR-199a-5p. *Int. J. Pediatr. Otorhinolaryngol.* 111, 128–137. doi: 10.1016/j.ijporl.2018.06.005

Cong, W., Liu, B., Liu, S., Sun, M., Liu, H., Yang, Y., et al. (2014). Implications of the Wnt5a/CaMKII pathway in retinoic acid-induced myogenic tongue abnormalities of developing mice. *Sci. Rep.* 4:6082.

Damm, K., Heyman, R. A., Umesono, K., and Evans, R. M. (1993). Functional inhibition of retinoic acid response by dominant negative retinoic acid receptor mutants. *Proc. Natl. Acad. Sci. U.S.A.* 90, 2989–2993. doi: 10.1073/pnas.90.7.2989

De Cuyper, E., Dochy, F., De Leenheer, E., and Van Hoecke, H. (2019). The impact of cleft lip and/or palate on parental quality of life: a pilot study. *Int. J. Pediatr. Otorhinolaryngol.* 126:109598. doi: 10.1016/j.ijporl.2019.109598

de Pontual, L., Yao, E., Callier, P., Faivre, L., Drouin, V., Cariou, S., et al. (2011). Germline deletion of the miR-17 approximately 92 cluster causes skeletal and growth defects in humans. *Nat. Genet.* 43, 1026–1030. doi: 10.1038/ng.915

Ding, H. L., Hooper, J. E., Batzel, P., Eames, B. F., Postlethwait, J. H., Artinger, K. B., et al. (2016). MicroRNA profiling during craniofacial development: potential roles for Mir23b and Mir133b. *Front. Physiol.* 7:281. doi: 10.3389/fphys.2016.00281

Ericson, A., Kallen, B., and Westerholm, P. (1979). Cigarette smoking as an etiologic factor in cleft lip and palate. *Am. J. Obstetr. Gynecol.* 135, 348–351. doi: 10.1016/0002-9378(79)90703-8

Ferguson, M. W. (1988). Palate development. *Development* 103, 41–60.

Garland, M. A., Sun, B., Zhang, S., Reynolds, K., Ji, Y., and Zhou, C. J. (2020). Role of epigenetics and miRNAs in orofacial clefts. *Birth Defects Res.* 112, 1635–1659. doi: 10.1002/bdr2.1802

Gheldof, A., Hulpiau, P., van Roy, F., De Craene, B., and Berx, G. (2012). Evolutionary functional analysis and molecular regulation of the ZEB transcription factors. *Cell. Mol. Life Sci.: CMLS* 69, 2527–2541. doi: 10.1007/s00018-012-0935-3

Gonseth, S., Shaw, G. M., Roy, R., Segal, M. R., Asrani, K., Rine, J., et al. (2019). Epigenomic profiling of newborns with isolated orofacial clefts reveals widespread DNA methylation changes and implicates metastable epiallele regions in disease risk. *Epigenetics* 14, 198–213. doi: 10.1080/15592294.2019.1581591

Havasi, A., Haegele, J. A., Gall, J. M., Blackmon, S., Ichimura, T., Bonegio, R. G., et al. (2013). Histone acetyl transferase (HAT) HBO1 and JADE1 in epithelial cell regeneration. *Am. J. Pathol.* 182, 152–162. doi: 10.1016/j.ajpath.2012.09.017

Hou, L., Wang, D., and Baccarelli, A. (2011). Environmental chemicals and microRNAs. *Mutation Res.* 714, 105–112. doi: 10.1016/j.mrfmmm.2011.05.004

Hou, L., Zhu, L., Li, H., Jiang, F., Cao, L., Hu, C. Y., et al. (2019). MiR-501-3p forms a feedback loop with FOS, MDFI, and MyoD to regulate C2C12 myogenesis. *Cells* 8:573. doi: 10.3390/cells8060573

Hu, X., Gao, J., Liao, Y., Tang, S., and Lu, F. (2013). Retinoic acid alters the proliferation and survival of the epithelium and mesenchyme and suppresses Wnt/beta-catenin signaling in developing cleft palate. *Cell. Death Dis.* 4:e898. doi: 10.1038/cddis.2013.424

Hudder, A., and Novak, R. F. (2008). miRNAs: effectors of environmental influences on gene expression and disease. *Toxicol. Sci. : Off. J. Soc. Toxicol.* 103, 228–240. doi: 10.1093/toxsci/kfn033

Hunt, S., Jones, A. V., Hinsley, E. E., Whawell, S. A., and Lambert, D. W. (2011). MicroRNA-124 suppresses oral squamous cell carcinoma motility by targeting ITGB1. *FEBS Lett.* 585, 187–192. doi: 10.1016/j.febslet.2010.11.038

IPDTOC Working Group (2011). Prevalence at birth of cleft lip with or without cleft palate: data from the International Perinatal Database of Typical Oral Clefts (IPDTOC). *Cleft Palate-Craniofacial J. : Off. Publ. Am. Cleft Palate-Craniofacial Assoc.* 48, 66–81. doi: 10.1597/09-217

Iwata, J., Parada, C., and Chai, Y. (2011). The mechanism of TGF-beta signaling during palate development. *Oral Dis.* 17, 733–744. doi: 10.1111/j.1601-0825.2011.01806.x

Iwata, J., Suzuki, A., Pelikan, R. C., Ho, T. V., and Chai, Y. (2013). Noncanonical transforming growth factor beta (TGFbeta) signaling in cranial neural crest cells causes tongue muscle developmental defects. *J. Biol. Chem.* 288, 29760–29770. doi: 10.1074/jbc.m113.493551

Iwata, J., Suzuki, A., Pelikan, R. C., Ho, T. V., Sanchez-Lara, P. A., and Chai, Y. (2014). Modulation of lipid metabolic defects rescues cleft palate in Tgfbr2 mutant mice. *Hum. Mol. Genet.* 23, 182–193. doi: 10.1093/hmg/ddt410

Jin, L., Wessely, O., Marcusson, E. G., Ivan, C., Calin, G. A., and Alahari, S. K. (2013). Prooncogenic factors miR-23b and miR-27b are regulated by Her2/Neu, EGF, and TNF-alpha in breast cancer. *Cancer Res.* 73, 2884–2896. doi: 10.1158/0008-5472.can-12-2162

Kara, N., Wei, C., Commanday, A. C., and Patton, J. G. (2017). miR-27 regulates chondrogenesis by suppressing focal adhesion kinase during pharyngeal arch development. *Dev. Biol.* 429, 321–334. doi: 10.1016/j.ydbio.2017.06.013

Kozomara, A., and Griffiths-Jones, S. (2014). miRBase: annotating high confidence microRNAs using deep sequencing data. *Nucleic Acids Res.* 42, D68–D73.

Kummer, A. W. (2018). A Pediatrician's guide to communication disorders secondary to cleft lip/palate. *Pediatr. Clin. North Am.* 65, 31–46. doi: 10.1016/j.pcl.2017.08.019

Kuriyama, M., Udagawa, A., Yoshimoto, S., Ichinose, M., Sato, K., Yamazaki, K., et al. (2008). DNA methylation changes during cleft palate formation induced by retinoic acid in mice. *Cleft Palate-Craniofacial J. : Off. Publ. Am. Cleft Palate-Craniofacial Assoc.* 45, 545–551. doi: 10.1597/07-134.1

Lagos-Quintana, M., Rauhut, R., Yalcin, A., Meyer, J., Lendeckel, W., and Tuschl, T. (2002). Identification of tissue-specific microRNAs from mouse. *Curr. Biol.: CB* 12, 735–739. doi: 10.1016/s0960-9822(02)00809-6

Lai, L., Bohnsack, B. L., Niederreither, K., and Hirschi, K. K. (2003). Retinoic acid regulates endothelial cell proliferation during vasculogenesis. *Development* 130, 6465–6474. doi: 10.1242/dev.00887

Lammer, E. J., Chen, D. T., Hoar, R. M., Agnish, N. D., Benke, P. J., Braun, J. T., et al. (1985). Retinoic acid embryopathy. *New England J. Med.* 313, 837–841.

Landgraf, P., Rusu, M., Sheridan, R., Sewer, A., Iovino, N., Aravin, A., et al. (2007). A mammalian microRNA expression atlas based on small RNA library sequencing. *Cell* 129, 1401–1414.

Lee, J. J., Drakaki, A., Iliopoulos, D., and Struhl, K. (2012). MiR-27b targets PPARgamma to inhibit growth, tumor progression and the inflammatory response in neuroblastoma cells. *Oncogene* 31, 3818–3825. doi: 10.1038/onc.2011.543

Li, A., Jia, P., Mallik, S., Fei, R., Yoshioka, H., Suzuki, A., et al. (2020). Critical microRNAs and regulatory motifs in cleft palate identified by a conserved miRNA-TF-gene network approach in humans and mice. *Briefings Bioinform.* 21, 1465–1478. doi: 10.1093/bib/bbz082

Li, L., Shi, J. Y., Zhu, G. Q., and Shi, B. (2012). MiR-17-92 cluster regulates cell proliferation and collagen synthesis by targeting TGFB pathway in mouse palatal mesenchymal cells. *J. Cell. Biochem.* 113, 1235–1244. doi: 10.1002/jcb.23457

Liang, Y. J., Wang, Q. Y., Zhou, C. X., Yin, Q. Q., He, M., Yu, X. T., et al. (2013). MiR-124 targets Slug to regulate epithelial-mesenchymal transition and metastasis of breast cancer. *Carcinogenesis* 34, 713–722. doi: 10.1093/carcin/bgs383

Liu, D., Zhong, L., Yuan, Z., Yao, J., Zhong, P., Liu, J., et al. (2019). miR-382-5p modulates the ATRA-induced differentiation of acute promyelocytic leukemia by targeting tumor suppressor PTEN. *Cell Signal* 54, 1–9. doi: 10.1016/j.cellsig.2018.11.012

Liu, W., Song, Y., Zhang, C., Gao, P., Huang, B., and Yang, J. (2018). The protective role of all-transretinoic acid (ATRA) against colorectal cancer development is achieved via increasing miR-3666 expression and decreasing E2F7 expression. *Biomed. Pharmacother.* 104, 94–101. doi: 10.1016/j.biopha.2018.05.015

Lohnes, D., Mark, M., Mendelsohn, C., Dolle, P., Dierich, A., Gorry, P., et al. (1994). Function of the retinoic acid receptors (RARs) during development (I). Craniofacial and skeletal abnormalities in RAR double mutants. *Development* 120, 2723–2748. doi: 10.1242/dev.120.10.2723

Long, H. D., Ma, Y. S., Yang, H. Q., Xue, S. B., Liu, J. B., Yu, F., et al. (2018). Reduced hsa-miR-124-3p levels are associated with the poor survival of patients with hepatocellular carcinoma. *Mol. Biol. Rep.* 45, 2615–2623. doi: 10.1007/s11033-018-4431-1

Maclean, G., Dolle, P., and Petkovich, M. (2009). Genetic disruption of CYP26B1 severely affects development of neural crest derived head structures, but does not compromise hindbrain patterning. *Dev. Dynamics : Off. Publ. Am. Assoc. Anatomists* 238, 732–745. doi: 10.1002/dvdy.21878

Mark, M., Lohnes, D., Mendelsohn, C., Dupe, V., Vonesch, J. L., Kastner, P., et al. (1995). Roles of retinoic acid receptors and of Hox genes in the patterning of the teeth and of the jaw skeleton. *Int. J. Dev. Biol.* 39, 111–121.

Martinez-Frias, M. L., and Salvador, J. (1990). Epidemiological aspects of prenatal exposure to high doses of vitamin A in Spain. *Eur. J. Epidemiol.* 6, 118–123. doi: 10.1007/bf00145783

Mendell, J. T., and Olson, E. N. (2012). MicroRNAs in stress signaling and human disease. *Cell* 148, 1172–1187. doi: 10.1016/j.cell.2012.02.005

Mertens-Talcott, S. U., Chintharlapalli, S., Li, X., and Safe, S. (2007). The oncogenic microRNA-27a targets genes that regulate specificity protein transcription factors and the G2-M checkpoint in MDA-MB-231 breast cancer cells. *Cancer Res.* 67, 11001–11011. doi: 10.1158/0008-5472.can-07-2416

Mills, J. L., Simpson, J. L., Cunningham, G. C., Conley, M. R., and Rhoads, G. G. (1997). Vitamin A and birth defects. *Am. J. Obstetr. Gynecol.* 177, 31–36.

Mukhopadhyay, P., Brock, G., Pihur, V., Webb, C., Pisano, M. M., and Greene, R. M. (2010). Developmental microRNA expression profiling of murine embryonic orofacial tissue. *Birth Defects Res. Part A, Clin. Mol. Teratol.* 88, 511–534. doi: 10.1002/bdra.20684

Mukhopadhyay, P., Smolenkova, I., Warner, D., Pisano, M. M., and Greene, R. M. (2019). Spatio-temporal expression and functional analysis of miR-206 in developing orofacial tissue. *MicroRNA* 8, 43–60. doi: 10.2174/2211536607666180801094528

Munger, R. G., Romitti, P. A., Daack-Hirsch, S., Burns, T. L., Murray, J. C., and Hanson, J. (1996). Maternal alcohol use and risk of orofacial cleft birth defects. *Teratology* 54, 27–33. doi: 10.1002/(sici)1096-9926(199607)54:1<27::aid-tera4>3.0.co;2-0

Murray, J. C. (2002). Gene/environment causes of cleft lip and/or palate. *Clin. Genet.* 61, 248–256. doi: 10.1034/j.1399-0004.2002.610402.x

Nie, X., Wang, Q., and Jiao, K. (2011). Dicer activity in neural crest cells is essential for craniofacial organogenesis and pharyngeal arch artery morphogenesis. *Mech. Dev.* 128, 200–207. doi: 10.1016/j.mod.2010.12.002

Pi, X., Jin, L., Li, Z., Liu, J., Zhang, Y., Wang, L., et al. (2019). Association between concentrations of barium and aluminum in placental tissues and risk for orofacial clefts. *Sci. Tot. Environ.* 652, 406–412. doi: 10.1016/j.scitotenv.2018.10.262

Reynolds, K., Zhang, S., Sun, B., Garland, M. A., Ji, Y., and Zhou, C. J. (2020). Genetics and signaling mechanisms of orofacial clefts. *Birth Defects Res.* 112, 1588–1634. doi: 10.1002/bdr2.1754

Rhinn, M., and Dolle, P. (2012). Retinoic acid signalling during development. *Development* 139, 843–858. doi: 10.1242/dev.065938

Roberts, C. (2020). Regulating retinoic acid availability during development and regeneration: the role of the CYP26 enzymes. *J. Dev. Biol.* 8:6. doi: 10.3390/jdb8010006

Romitti, P. A., Lidral, A. C., Munger, R. G., Daack-Hirsch, S., Burns, T. L., and Murray, J. C. (1999). Candidate genes for nonsyndromic cleft lip and palate and maternal cigarette smoking and alcohol consumption: evaluation of genotype-environment interactions from a population-based case-control study of orofacial clefts. *Teratology* 59, 39–50. doi: 10.1002/(sici)1096-9926(199901)59:1<39::aid-tera9>3.0.co;2-7

Ross, S. A., McCaffery, P. J., Drager, U. C., and De Luca, L. M. (2000). Retinoids in embryonal development. *Physiol. Rev.* 80, 1021–1054. doi: 10.1152/physrev.2000.80.3.1021

Schmalhofer, O., Brabletz, S., and Brabletz, T. (2009). E-cadherin, beta-catenin, and ZEB1 in malignant progression of cancer. *Cancer Metastasis Rev.* 28, 151–166. doi: 10.1007/s10555-008-9179-y

Schoen, C., Aschrafi, A., Thonissen, M., Poelmans, G., Von den Hoff, J. W., and Carels, C. E. L. (2017). MicroRNAs in palatogenesis and cleft palate. *Front. Physiol.* 8:165. doi: 10.3389/fphys.2017.00165

Seelan, R. S., Mukhopadhyay, P., Warner, D. R., Appana, S. N., Brock, G. N., Pisano, M. M., et al. (2014). Methylated microRNA genes of the developing murine palate. *MicroRNA* 3, 160–173. doi: 10.2174/2211536604666150131125805

Shin, J. O., Lee, J. M., Cho, K. W., Kwak, S., Kwon, H. J., Lee, M. J., et al. (2012). MiR-200b is involved in Tgf-beta signaling to regulate mammalian palate development. *Histochem. Cell Biol.* 137, 67–78. doi: 10.1007/s00418-011-0876-1

Sischo, L., Wilson-Genderson, M., and Broder, H. L. (2017). Quality-of-life in children with orofacial clefts and caregiver well-being. *J. Dental Res.* 96, 1474–1481. doi: 10.1177/0022034517725707

Skare, O., Jugessur, A., Lie, R. T., Wilcox, A. J., Murray, J. C., Lunde, A., et al. (2012). Application of a novel hybrid study design to explore gene-environment interactions in orofacial clefts. *Ann. Hum. Genet.* 76, 221–236. doi: 10.1111/j.1469-1809.2012.00707.x

Suhl, J., Leonard, S., Weyer, P., Rhoads, A., Siega-Riz, A. M., Renee Anthony, T., et al. (2018). Maternal arsenic exposure and nonsyndromic orofacial clefts. *Birth Defects Res.* 110, 1455–1467. doi: 10.1002/bdr2.1386

Suzuki, A., Abdallah, N., Gajera, M., Jun, G., Jia, P., Zhao, Z., et al. (2018a). Genes and microRNAs associated with mouse cleft palate: a systematic review and bioinformatics analysis. *Mech. Dev.* 150, 21–27. doi: 10.1016/j.mod.2018.02.003

Suzuki, A., Jun, G., Abdallah, N., Gajera, M., and Iwata, J. (2018b). Gene datasets associated with mouse cleft palate. *Data Brief* 18, 655–673. doi: 10.1016/j.dib.2018.03.010

Suzuki, A., Li, A., Gajera, M., Abdallah, N., Zhang, M., Zhao, Z., et al. (2019a). MicroRNA-374a, -4680, and -133b suppress cell proliferation through the regulation of genes associated with human cleft palate in cultured human palate cells. *BMC Med. Genomics* 12:93.

Suzuki, A., Yoshioka, H., Summakia, D., Desai, N. G., Jun, G., Jia, P., et al. (2019b). MicroRNA-124-3p suppresses mouse lip mesenchymal cell proliferation through the regulation of genes associated with cleft lip in the mouse. *BMC Genomics* 20:852. doi: 10.1186/s12864-019-6238-4

Tan, Y., Ge, G., Pan, T., Wen, D., and Gan, J. (2014). A pilot study of serum microRNAs panel as potential biomarkers for diagnosis of nonalcoholic fatty liver disease. *PLoS One* 9:e105192. doi: 10.1371/journal.pone.0105192

Tian, Y., Fu, S., Qiu, G. B., Xu, Z. M., Liu, N., Zhang, X. W., et al. (2014). MicroRNA-27a promotes proliferation and suppresses apoptosis by targeting PLK2 in laryngeal carcinoma. *BMC Cancer* 14:678. doi: 10.1186/1471-2407-14-678

Ventura, A., Young, A. G., Winslow, M. M., Lintault, L., Meissner, A., Erkeland, S. J., et al. (2008). Targeted deletion reveals essential and overlapping functions of the miR-17 through 92 family of miRNA clusters. *Cell* 132, 875–886. doi: 10.1016/j.cell.2008.02.019

Wang, J., Bai, Y., Li, H., Greene, S. B., Klysik, E., Yu, W., et al. (2013). MicroRNA-17-92, a direct Ap-2alpha transcriptional target, modulates T-box factor activity in orofacial clefting. *PLoS Genet.* 9:e1003785. doi: 10.1371/journal.pgen.1003785

Wang, Q., Kurosaka, H., Kikuchi, M., Nakaya, A., Trainor, P. A., and Yamashiro, T. (2019). Perturbed development of cranial neural crest cells in association with reduced sonic hedgehog signaling underlies the pathogenesis of retinoic-acid-induced cleft palate. *Dis. Models Mech.* 12:dmm040279.

Wang, S., Sun, C., Meng, Y., Zhang, B., Wang, X., Su, Y., et al. (2017). A pilot study: Screening target miRNAs in tissue of nonsyndromic cleft lip with or without cleft palate. *Exp. Therapeutic Med.* 13, 2570–2576. doi: 10.3892/etm.2017.4248

Wang, X., Shen, X., Li, X., and Agrawal, C. M. (2002). Age-related changes in the collagen network and toughness of bone. *Bone* 31, 1–7. doi: 10.1016/s8756-3282(01)00697-4

Warner, D. R., Mukhopadhyay, P., Brock, G., Webb, C. L., Michele Pisano, M., and Greene, R. M. (2014). MicroRNA expression profiling of the developing murine upper lip. *Dev. Growth Differ.* 56, 434–447. doi: 10.1111/dgd.12140

Werler, M. M., Lammer, E. J., Rosenberg, L., and Mitchell, A. A. (1990). Maternal vitamin A supplementation in relation to selected birth defects. *Teratology* 42, 497–503. doi: 10.1002/tera.1420420506

Xu, M., Ma, L., Lou, S., Du, Y., Yin, X., Zhang, C., et al. (2018). Genetic variants of microRNA processing genes and risk of non-syndromic orofacial clefts. *Oral Dis.* 24, 422–428. doi: 10.1111/odi.12741

Yao, Z., Chen, D., Wang, A., Ding, X., Liu, Z., Ling, L., et al. (2011). Folic acid rescue of ATRA-induced cleft palate by restoring the TGF-beta signal and inhibiting apoptosis. *J. Oral. Pathol. Med.* 40, 433–439. doi: 10.1111/j.1600-0714.2010.00994.x

Zehir, A., Hua, L. L., Maska, E. L., Morikawa, Y., and Cserjesi, P. (2010). Dicer is required for survival of differentiating neural crest cells. *Dev. Biol.* 340, 459–467. doi: 10.1016/j.ydbio.2010.01.039

Zhang, J., Zhou, S., Zhang, Q., Feng, S., Chen, Y., Zheng, H., et al. (2014). Proteomic analysis of RBP4/vitamin a in children with cleft lip and/or palate. *J. Dent. Res.* 93, 547–552. doi: 10.1177/0022034514530397

Zhang, Y., Mori, T., Iseki, K., Hagino, S., Takaki, H., Takeuchi, M., et al. (2003). Differential expression of decorin and biglycan genes during palatogenesis in normal and retinoic acid-treated mice. *Dev. Dynamics : Off. Publ. Am. Assoc. Anatomists* 226, 618–626. doi: 10.1002/dvdy.10267

Zhou, L., Liang, X., Zhang, L., Yang, L., Nagao, N., Wu, H., et al. (2016). MiR-27a-3p functions as an oncogene in gastric cancer by targeting BTG2. *Oncotarget* 7, 51943–51954. doi: 10.18632/oncotarget.10460

Conflict of Interest: The authors declare that the research was conducted in the absence of any commercial or financial relationships that could be construed as a potential conflict of interest.

frontiers in Cell and Developmental Biology

ORIGINAL RESEARCH
published: 08 July 2021
doi: 10.3389/fcell.2021.638522

Identification of Novel Variants in Cleft Palate-Associated Genes in Brazilian Patients With Non-syndromic Cleft Palate Only

Renato Assis Machado[1,2], Hercílio Martelli-Junior[3,4], Silvia Regina de Almeida Reis[5], Erika Calvano Küchler[6], Rafaela Scariot[7], Lucimara Teixeira das Neves[2,8] and Ricardo D. Coletta[1]*

[1] Department of Oral Diagnosis, School of Dentistry, University of Campinas (FOP), Piracicaba, Brazil, [2] Hospital for Rehabilitation of Craniofacial Anomalies, University of São Paulo, Bauru, Brazil, [3] Stomatology Clinic, School of Dental, State University of Montes Claros, Montes Claros, Brazil, [4] Center for Rehabilitation of Craniofacial Anomalies, School of Dental, UNIFENAS - Universidade José do Rosario Vellano, Alfenas, Brazil, [5] Department of Basic Science, Bahiana School of Medicine and Public Health, Salvador, Brazil, [6] Department of Orthodontics, University of Regensburg, Regensburg, Germany, [7] Department of Oral and Maxillofacial Surgery, School of Health Science, Federal University of Paraná, Curitiba, Brazil, [8] Department of Biological Sciences, Bauru School of Dentistry, University of São Paulo (FOB), Bauru, Brazil

OPEN ACCESS

Edited by:
Mary L. Marazita, University of Pittsburgh, United States

Reviewed by:
Alison L. Reynolds, University College Dublin, Ireland
Julian Little, University of Ottawa, Canada

***Correspondence:**
Renato Assis Machado
renatoassismachado@yahoo.com.br

Specialty section:
This article was submitted to Molecular Medicine, a section of the journal Frontiers in Cell and Developmental Biology

Received: *07 December 2020*
Accepted: *30 April 2021*
Published: *08 July 2021*

Citation:
Machado RA, Martelli-Junior H, Reis SRA, Küchler EC, Scariot R, das Neves LT and Coletta RD (2021) Identification of Novel Variants in Cleft Palate-Associated Genes in Brazilian Patients With Non-syndromic Cleft Palate Only. Front. Cell Dev. Biol. 9:638522. doi: 10.3389/fcell.2021.638522

The identification of genetic risk factors for non-syndromic oral clefts is of great importance for better understanding the biological processes related to this heterogeneous and complex group of diseases. Herein we applied whole-exome sequencing to identify potential variants related to non-syndromic cleft palate only (NSCPO) in the multiethnic Brazilian population. Thirty NSCPO samples and 30 sex- and genetic ancestry-matched healthy controls were pooled (3 pools with 10 samples for each group) and subjected to whole-exome sequencing. After filtering, the functional affects, individually and through interactions, of the selected variants and genes were assessed by bioinformatic analyses. As a group, 399 variants in 216 genes related to palatogenesis/cleft palate, corresponding to 6.43%, were exclusively identified in the NSCPO pools. Among those genes are 99 associated with syndromes displaying cleft palate in their clinical spectrum and 92 previously related to cleft lip palate. The most significantly biological processes and pathways overrepresented in the NSCPO-identified genes were associated with the folic acid metabolism, highlighting the interaction between LDL receptor-related protein 6 (*LRP6*) and 5-methyltetrahydrofolate-homocysteine methyltransferase (*MTR*) that interconnect two large networks. This study yields novel data on characterization of specific variants and complex processes and pathways related to NSCPO, including many variants in genes of the folate/homocysteine pathway, and confirms that variants in genes related to syndromic cleft palate and cleft lip-palate may cause NSCPO.

Keywords: non-syndromic cleft palate only, exome sequence, risk factor, syndrome, oral cleft

INTRODUCTION

Orofacial clefts represent the most common craniofacial malformation in humans with an overall prevalence of approximately 1 per 700 live births, but considerable geographic and ethnic variations exist (Leslie and Marazita, 2013). It may represent the manifestation of a syndrome or as a non-syndromic isolated condition, which corresponds to approximately 70% of all cases (Dixon et al., 2011). Non-syndromic oral clefts (NSOC) comprise two main forms, the cleft lip with or without cleft palate (NSCL ± P) and cleft palate only (NSCPO). Although a multifactorial etiology with a strong genetic component is reported in both NSOC subtypes, many studies have indicated that the genetic factors behind them may be distinct (Mangold et al., 2016; Ludwig et al., 2017). Different genes and chromosomal regions, many identified by genome-wide association studies (GWAS), were described as causal genetic factors for NSCL ± P (Beaty et al., 2016; Yu et al., 2017), but due to lower prevalence, embryological aspects, and recurrence rates, less is known about NSCPO.

To date, five GWAS have been conducted with NSCPO (Beaty et al., 2011; Leslie et al., 2016; Butali et al., 2019; Huang et al., 2019; He et al., 2020). The first studies have identified variants in grainyhead-like transcription factor 3 (*GRHL3*), a gene underlying van der Woude syndrome, the most common genetic syndrome associated with cleft lip and palate, and other few markers that, in interaction with maternal smoking or multivitamin supplementation (gene–environment interactions), were associated with increased odds to NSCPO development (Beaty et al., 2011; Leslie et al., 2016), whereas the most recent GWAS have identified only single-nucleotide polymorphisms (SNPs) in intergenic regions in association with NSCPO (Butali et al., 2019; Huang et al., 2019; He et al., 2020). The study conducted by Butali et al. (2019) has identified the SNP rs80004662 on chromosome 2, near the catenin alpha 2 (*CTNNA2*), as a novel marker for NSCPO in the African population, and the study of Huang et al. (2019) has revealed 11 SNPs in nine loci in genome-wide significance with NSCPO in the Han Chinese population. Four SNPs in a novel locus (15q24.3) were reported in the GWAS conducted by He et al. (2020) with a Han Chinese population of patients with NSCPO. These genetic findings suggest that the effects of polymorphic variants in NSCPO are much less frequent or may be caused by rare variants, which are undetectable in GWAS (Hecht et al., 2002; Koillinen et al., 2005; Ishorst et al., 2018). Moreover, it is possible that specific variants in genes associated with syndromic forms of CPO (SCPO) display a causal effect in the non-syndromic clinical phenotype, and the NSCPO may be the result of genetic factors associated with clefts involving both lip and palate (CLP). A previous study supports this hypothesis; out of 350 genes associated with NSCPO, 177 were also identified in patients with CLP and 28 in patients with SCPO (Funato and Nakamura, 2017).

Whole-exome sequencing (WES) has been applied for the genetic characterization of NSCPO (Bureau et al., 2014; Pengelly et al., 2016; Liu et al., 2017; Hoebel et al., 2017; Basha et al., 2018). The study performed by Liu et al. (2017) has identified a rare variant (p.Ser552Pro) in Rho GTPase activating protein 29 (*ARHGAP29*) in a family spanning NSCPO under the assumption of an autosomal dominant of inheritance. Applying WES in multiple affected NSCPO pedigrees and validation of the potential deleterious variants in a case–control approach, Hoebel et al. (2017) have suggested the participation of acetyl-CoA carboxylase beta (*ACACB*), CREB-binding protein (*CREBBP*), *GRHL3*, MIB E3 ubiquitin protein ligase 1 (*MIB1*), and protein tyrosine phosphatase receptor type S (*PTPRS*) in the etiology of NSCPO. In the study conducted by Basha et al. (2018), the c.819_820dupCC and c.3373C > T mutations in tumor protein P63 (*TP63*) and LDL receptor-related protein 6 (*LRP6*), respectively, were described in two families with NSCPO. On the other hand, the studies conducted by Bureau et al. (2014); Pengelly et al. (2016) have analyzed multiplex families of patients with NSOC, including NSCPO among those affected, which makes more difficult to understand the exact participation of genes identified in the pathogenesis of NSCPO.

Large-scale genetic studies have confirmed the genetic contribution to the etiology of NSCL ± P but have also demonstrated that these defects can result from variation in multiple genes (Carlson et al., 2019). However, much less is known in terms of genetic etiology of NSCPO. Furthermore, most patients included in the genome-wide studies, including GWAS and genomic sequencing, have been of European or Asian ancestry, and the genetic predisposition to NSOC is ethnicity-dependent, e.g., the association of 8q24 is consistently observed in European patients with NSCL ± P, but much less among patients with Asian ancestry or in Brazilians with high African ancestry (do Rego et al., 2015; Wattanawong et al., 2016). In this context, it is quite important to perform large-scale genetic studies in different populations to define common and ethnic-specific risk genes, but the costs of those assays in a large number of participants are still challenging. To genomic sequencing, pool sequencing (mix DNA samples from several patients prior to sequencing) has proved to be an effective alternative to overcome the problems related to costs (Collins et al., 2016; Popp et al., 2017). In the current study, we applied whole-exome pool sequencing to characterize genetic variants related to NSCPO in the multiethnic Brazilian population. This is the first study to perform WES in Brazilian patients with NSCPO, and our findings revealed a large list of novel variants in previously CPO and CLP-associated genes as well in genes not related to oral clefts.

MATERIALS AND METHODS

Study Participants

A total of 30 samples from patients with NSCPO and 30 healthy controls were recruited after approval by the Institutional Review Boards at the Center for Rehabilitation of Craniofacial Anomalies, University of José Rosário Vellano, Alfenas, Minas Gerais, and at the Santo Antonio Hospital, Salvador, Bahia. The patients with NSCPO were carefully investigated by specialist teams of the two Centers for the occurrence of associated abnormalities or syndromes, and only unrelated patients with complete NSCPO, without any other congenital malformation

or mental disability, were included. The control group consisted of unrelated healthy patients, without congenital malformations, mental disorders, or family history of orofacial clefts, living in the same geographic areas. Cases and controls were unrelated newborn infants or young children. **Supplementary Table 1** depicts the main characteristics of the participants of this study, including sex and proportion of genomic ancestry.

Samples and Pooling Strategy

Genomic DNA was isolated from oral mucosa cells, obtained by mouthwash with a 3% sucrose solution or by scraping the buccal mucosa with a swab, using a salting-out protocol (Aidar and Line, 2007). The concentration and quality of DNA samples were assessed by spectrophotometry and agarose gel electrophoresis. Each pool represented 10 samples, and the amount of DNA was adequately balanced to represent each genome equally (**Figure 1**). After mixing the samples, the pools were quantified using the fluorometric method (Qubit®, Thermo Fisher Scientific, Waltham, MA, United States) and normalized to 10 mM Tris–EDTA buffer pH 8.0 at a final concentration of 5 ng/μl. To ensure greater homogeneity, each pool was composed of patients of the same sex (two pools with females and one pool with males for each group) and from the same geographic location. In addition, the genomic ancestry was assessed in each sample with a 40 biallelic short insertion–deletion polymorphism panel, which was previously validated as ancestry informative of the Brazilian population (Messetti et al., 2017), and the averages of contributions from European, African, and Amerindian ancestries among pools were similar (**Supplementary Table 1**).

WES and Bioinformatic Analyses

The pools were enriched in libraries with the Nextera™ DNA sample preparation kit (Illumina, San Diego, CA, United States), and each library was quantified by RT-qPCR using the KAPA Library Quantification Kit (KAPA Biosystems Inc., Wilmington, MA, United States). The libraries were diluted to a concentration of 16 pM and pooled by cBOT (Illumina) using the TruSeq PE cluster v3-cBOT-HS Kit (Illumina). Paired sequencing, with a reading length of 100 bp, was performed on the HiSeq 1000 equipment (Illumina), aiming at covering 18 × /pool. Following the sequencing, the sequences of each pool (FASTQ files) were aligned with the human reference genome RCh38/hg19 through the Burrows–Wheeler aligner program [BWA, GNU General Public License version 3.0 (GPLv3), MIT License, Cambridge, MA, United States] (Li and Durbin, 2009). The duplicates were removed, and the quality of the sequencing was verified with the GATK program (Genome Analysis Toolkit). The coverage depth was exported in a BAM file with the Biobambam2 program[1], and the variants were identified as VCF files with the Freebayes program[2]. The BAM and VCF files for each pool were incorporated into the VarSeq® program (version 1.4.8; Golden Helix, Inc., Bozeman, MT, United States) for genetic variant annotation according to the public databases 1000 Genomes, GnomAD Exome, GnomAD Genome, and ExAC. A total of 102,927 variants were identified.

The selection of the variants of interest started with the exclusion of sequences that did not pass the quality control (coverage ≥ 20 and sequencing depth ≥ 100). After applying this filter, 61,398 variants were maintained. Next, the variants present in the control group were excluded, leaving only the variants contained in the pools of patients with NSCPO. The variants that did not show an allele frequency of at least 5% in the pool were also excluded, where in a universe of 20 possible alleles in each pool, at least one allele should be evidenced. The application of these filters reduced the number of variants to 5,129 variants in 3,360 genes. At this point, the GATACA database[3], VarElect database[4], and Online Mendelian Inheritance

[1]https://scfbm.biomedcentral.com/articles/10.1186/1751-0473-9-13
[2]https://arxiv.org/abs/1207.3907
[3]https://gataca.cchmc.org/gataca/
[4]http://varelect.genecards.org

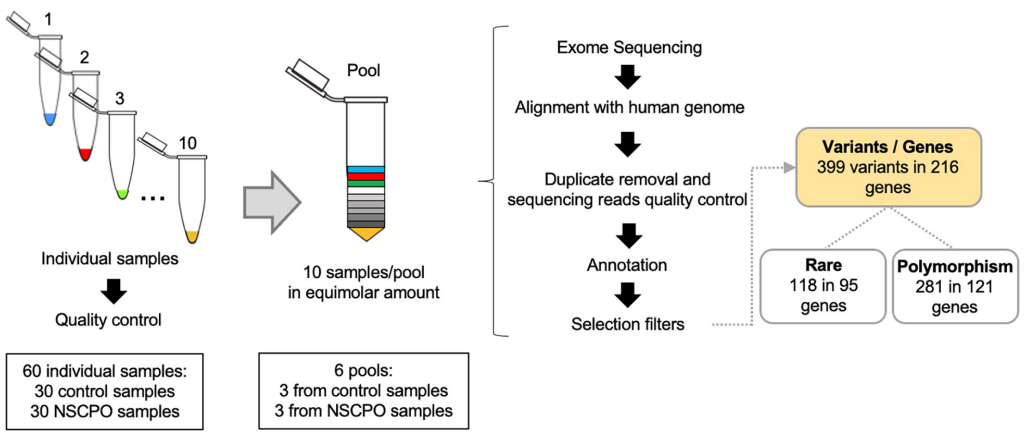

FIGURE 1 | Workflow of whole-exome pool sequencing applied to 30 samples of patients with non-syndromic cleft palate only (NSCPO) and 30 healthy controls. After sequencing and bioinformatic analyses, 399 variants distributed in 216 different genes were found, with 118 rare variants in 95 genes and 281 polymorphisms in 121 genes.

in Man (OMIM)[5] were used for identification of genes associated with cleft palate, including non-syndromic, syndromic, and CLP. The resulting list of genes was compared to 3,360 genes found in the exome (**Figure 1**). The polymorphism phenotyping (PolyPhen2[6]) (Adzhubei et al., 2013), sorting intolerant from tolerant (SIFT[7]) (Kumar et al., 2009), and mutation taster[8] were used for biological and functional effect prediction of the variants. STRING, protein–protein interaction networks functional enrichment analysis,[9] was used to investigate the functional significance of genes, including biological processes, pathways and interaction network. The *p*-Values were subjected to false discovery rate to correct multiple tests, and values ≤ 0.05 were considered significant.

RESULTS

Out of 3,360 cleft palate-related genes, 216 (6.43%) displayed at least a variation in the pools of NSCPO. Since phenotypic human gene classification also offers major insights into gene function (Frech and Chen, 2010), the identified genes were categorized on the basis of their previous association with NSCPO (**Table 1**), SCPO (**Supplementary Table 2**), and CLP (**Supplementary Table 3**). **Supplementary Table 4** depicts the variants identified in the pools of patients with NSCPO, but not located in the genes previously associated with palatogenesis or oral clefts.

Among genes previously described in association with NSCPO, 38 novel SNPs (except rs2229989 in *SOX9*, Jia et al., 2017) and 9 novel rare variants were identified in *ACACB*, *CDH1*, *COL11A1*, *COL11A2*, *COL2A1*, *CREBBP*, *FTCD*, *GRHL3*, *JAG2*, *LRP6*, *MSX1*, *MTHFD1*, *MTHFR*, *MTR*, *OFD1*, *POMGNT2*, *RFC1*, *SHMT1*, *SOX9*, *TBX1*, *TBX22*, *TCN2*, *TCOF1*, *TP63*, and *TYMS* (**Table 1**). The biological processes and pathways for these NSCPO-associated genes were generated by STRING (**Table 2** and **Supplementary Table 5**). The most significant biological processes were skeletal system development (GO:0001501, P = 1.96e-10), tetrahydrofolate interconversion (GO:0035999, P = 3.57e-09), and pteridine-containing compound metabolic process (GO:0042558, P = 3.88e-09) (**Supplementary Table 5**), and the pathways were of one carbon pool by folate (hsa00670, P = 3.63e-11) and antifolate resistance (hsa01523, P = 0.00038) (**Table 2**). Two main networks interconnected by interactions between *LRP6* and *MTR* were identified in NSCPO-associated genes (**Figure 2**).

Variations (n = 192) in 99 SCPO-associated genes were found in NSCPO samples, but not in the control (**Supplementary Table 2**). These genes participate in 437 biological processes and 31 pathways. The most significantly represented GO terms for biological processes and cellular component ontologies for the encoded proteins were developmental process (GO:0032502, P = 6.42e-12), anatomical structure development (GO:0048856, P = 6.42e-12), and multicellular organism development (GO:0007275, P = 8.60e-12) (**Supplementary Table 6**), and the pathways were thyroid hormone signaling (hsa04919, P = 0.00047), protein digestion and absorption (hsa04974, P = 0.00077), and proteoglycans in cancer (hsa05205, P = 0.0041) (**Supplementary Table 7**). The network involved in the SCPO-associated genes included 205 interactions (**Supplementary Figure 1**).

Since CLP results from failure of fusion of lip and palate, we have also looked into variations of genes related to CLP, and 160 variants in 92 genes were identified (**Supplementary Table 3**). Together, the CLP-associated genes identified exclusively in the NSCPO pools participate in 873 biological processes and 68 pathways, with the most significant being animal organ development (GO:0048513, P = 2.24e-20) (**Supplementary Table 8**) and human papillomavirus infection (hsa05165, P = 3.58e-06) (**Supplementary Table 9**), respectively. A complex network characterized by 244 interactions among these CLP-associated genes identified exclusively in the NSCPO pools was observed (**Supplementary Figure 2**).

As some genes were exclusive to the NSCPO phenotype and others coincided with the SCPO and CLP phenotypes (**Figure 3**), we investigated whether biological processes and pathways differ among genes related to NSCPO, SCPO, and CLP, and we compared the biological processes and pathways to identify those ones associated with NSCPO only. Although most genes/pathways are interrelated, 76 biological processes were enriched only for NSCPO-associated genes in the pools of NSCPO, and the most significant were tetrahydrofolate interconversion (GO:0035999, P = 3.57e-09) and pteridine-containing compound metabolic process (GO:0042558, P = 3.88e-09) (processes indicated with an * on **Supplementary Table 5**). In addition, the pathways of one carbon pool by folate (hsa00670, P = 3.63e-11), antifolate resistance (hsa01523, P = 0.00038), and biosynthesis of amino acids (hsa01230, P = 0.0460), formatted by *FTCD*, *MTHFD1*, *MTHFR*, *MTR*, *SHMT1*, and *TYMS*, were found only in NSCPO-associated genes (pathways indicated with an * on **Table 2**).

DISCUSSION

Although the palatogenesis is a complex process with involvement of many genes and cellular pathways, genetic variants in association with cleft palate have been identified in only a limited number of these genes. In the present study, after exome sequencing and bioinformatic analyses, we found 399 variants in 216 genes related to palatogenesis/cleft palate exclusively in the DNA pool of patients with NSCPO. Among variations in the 25 NSCPO-associated genes (**Table 1**), 13 are described in association with syndromes displaying cleft palate in the clinical spectrum (SCPO-associated genes) and 13 were previously associated with CLP. Therefore, variants in *ACACB* and *SHMT1* belonged exclusively to NSCPO. *ACACB*, encoding the acetyl-coenzyme-A-carboxylase β, an enzyme involved in the oxidation of fatty acids (Ma et al., 2011), was recently reported as a potential candidate for NSCPO by exome sequencing (Hoebel et al., 2017). *SHMT1* (serine hydroxymethyltransferase),

[5]http://omim.org
[6]http://genetics.bwh.harvard.edu/pph2/
[7]http://sift.jcvi.org/
[8]http://www.mutationtaster.org/
[9]http:/string-db.org

TABLE 1 | Novel variants in genes previously described in association with non-syndromic cleft palate only (NSCPO) found exclusively in the samples of patients with NSCPO.

Gene	Protein	Variants	Chr:Pos	MAF 1K	MAF gnomAD Exomes	MAF gnomAD Genomes	MAF ExAC	MAF ABraOM	Sequence Ontology	SIFT	Polyphen2	Mutation Taster	OMIM Number	References
ACACB	Acetyl-CoA Carboxylase Beta	rs60293430	12:109665242	0.0517173	0.0479439	0.0660566	0.049	0.066183	missense	Tolerated	Possibly damaging	Damaging	*601557	Hoebel et al., 2017
CDH1†	Cadherin 1	rs33969373	16:68856088	0.0227636	0.0103762	0.0177832	0.011	0.038588	synonymous	-	-	-	*192090	Song and Zhang, 2011
		rs33964119	16:68862165	0.0545128	0.0426288	0.0346343	0.04	0.037767	synonymous	-	-	-		
COL2A1*	Collagen Type II Alpha 1 Chain	rs34392760	12:48391657	0.0179712	0.0376268	0.0349919	0.038	0.047619	missense	Tolerated	Benign	Damaging	+120140	Li et al., 1995; Nikopensius et al., 2010
COL11A1*	Collagen Type XI Alpha 1 Chain	rs1012281	1:103427407	0.038139	0.0516874	0.0579359	0.053	0.068144	intron	-	-	-	*120280	Seegmiller et al., 1971
		rs771593293	1:103468856	-	-	-	-	0.087800	-	-	-	-		
		rs111841420	1:103470191	0.0183706	0.0245013	0.022501	0.023	0.025452	synonymous	-	-	-		
		rs3767272	1:103483329	0.0347444	0.0296967	0.0200607	0.03	0.026273	intron	-	-	-		
COL11A2*	Collagen Type XI Alpha 2 Chain	rs2229784	6:33136310	0.057508	0.0344903	0.0395325	0.034	0.051724	missense	Damaging	Possibly damaging	Damaging	*120290	Nikopensius et al., 2010
		rs73741526	6:33139635	0.0810703	0.0464905	0.0476175	0.047	0.064860	intron	-	-	-		
		rs2855430	6:33141280	0.102236	0.121898	0.106553	0.122	0.084565	missense	Tolerated	Probably damaging	Damaging		
		rs9280359	6:33142013	0.202476	0.162732	0.189819	0.1	0.178053	intron	-	-	-		
		rs41317098	6:33144466	0.102436	0.0473386	0.115006	0.052	0.077997	intron	-	-	-		
		rs2744507	6:33148878	0.102636	0.121967	0.106294	0.122	0.085386	intron	-	-	-		
CREBBP*	CREB Binding Protein	rs73491901	16:3781845	0.00139776	0.0003691	0.0021309	0.0004942	0.001281	missense	Tolerated	Possibly damaging	Damaging	*600140	Hoebel et al., 2017
		rs130004	16:3828207	0.0553115	0.0137934	0.0517921	0.017	0.027754	intron	-	-	-		
		rs130018	16:3831187	0.0780751	0.0281749	0.069947	0.033	0.052519	intron	-	-	-		
FTCD†	Formimidoyltransferase Cyclodeaminase	rs10432965	21:47557222	0.167532	0.0830084	0.0992947	0.087	0.091954	synonymous	Damaging	Benign	Damaging	*606806	Boyles et al., 2009
GRHL3*,†	Grainyhead Like Transcription Factor 3	rs34637004	1:24663184	0.0175719	0.0343092	0.0398771	0.033	0.033662	missense	Tolerated	Benign	Tolerated	*608317	Peyrard-Janvid et al., 2014; Leslie et al., 2016; Basha et al., 2018
JAG2†	Jagged Canonical Notch Ligand 2	rs78862296	14:105634205	0.00519169	0.00102047	0.0052073	0.001451	0.002467	synonymous	-	-	-	*602570	Jiang et al., 1998; Vieira et al., 2005; Jagomagi et al., 2010
		rs113906438	14:105613039	0.023762	0.0125495	0.0139761	0.011	0.018883	synonymous	-	-	-		
LRP6*,†	LDL Receptor Related Protein 6	rs34815107	12:12279735	0.00299521	0.00103964	0.0041338	0.001285	0.002463	missense	Tolerated	Bening	Damaging	*603507	Basha et al., 2018

(Continued)

TABLE 1 | Continued

Gene	Protein	Variants	Chr:Pos	MAF 1K	MAF gnomAD Exomes	MAF gnomAD Genomes	MAF ExAC	MAF ABraOM	Sequence Ontology	SIFT	Polyphen2	Mutation Taster	OMIM Number	References
MSX1†	Msh Homeobox 1	rs33929633	4:4864405	0.189696	0.216977	0.234219	0.215	0.206076	intron	-	-	-	*142983	Satokata and Maas, 1994; Jagomagi et al., 2010
MTHFD1†	Methylenetetrahydrofolate Dehydrogenase, Cyclohydrolase And Formyltetrahydrofolate Synthetase 1	rs60806768	14:64898459	0.0593051	0.0315681	0.0640463	0.036	0.047619	intron	-	-	-	*172460	Boyles et al., 2008; Murthy et al., 2014
		rs59770063	14:64898463	0.0593051	0.0315598	0.0639411	0.036	0.047619	intron	-	-	-		
MTHFR†	Methylenetetrahydrofolate Reductase	rs45496998	1:11852412	-	-	-	-	0.002463	-	-	-	-	*607093	Shaw et al., 1999
		rs2274976	1:11850927	0.0744808	0.055472	0.0408481	0.056	0.033662	missense	Tolerated	Benign	Tolerated		
MTR†	5-Methyltetrahydrofolate-Homocysteine Methyltransferase	rs113277607	1:236971983	0.0421326	0.0113392	0.0400116	0.015	0.032020	intron	-	-	-	*156570	Boyles et al., 2008
		rs7526063	1:236971998	0.0744808	0.0374526	0.051899	0.04	0.049261	splice region	-	-	-		
		rs12022937	1:237060850	0.215056	0.0764726	0.146143	0.085	0.113300	splice region	-	-	-		
OFD1**	OFD1 Centriole And Centriolar Satellite Protein	rs5979959	X:13769452	0.00503311	0.00163061	0.00527241	0.001738	0.002994	synonymous	-	-	-	*300170	Ferrante et al., 2006; Jugessur et al., 2012
		rs140369491	X:13779341	0.0362914	0.0130494	0.0185598	0.015	0.022954	intron	-	-	-		
POMGNT2**	Protein O-Linked Mannose N-Acetylglucosaminyl transferase 2 (Beta 1,4-)	rs115870061	3:43122162	0.00499201	0.00106109	0.00432956	0.001491	0.00243	synonymous	-	-	-	*614828	Huang et al., 2019
RFC1†	Replication Factor C Subunit 1	rs2066782	4:39303925	0.106829	0.115582	0.0985123	0.115	0.096880	synonymous	-	-	-	*600424	Shaw et al., 2003; Boyles et al., 2008, 2009
SHMT1	Serine Hydroxymethyltransferase 1	rs8080285	17:18234028	0.0924521	0.026609	0.0748126	0.031	0.068966	intron	-	-	-	*182144	Boyles et al., 2009
		rs2273026	17:18256979	0.135184	0.122439	0.109661	0.119	0.103448	splice region	-	-	-		
SOX9**	SRY-Box Transcription Factor 9	rs2229989	17:70118935	0.136581	0.193679	0.172156	0.192	0.157635	synonymous	-	-	-	*608160	Bi et al., 2001
TBX1**	T-Box Transcription Factor 1	rs139776757	22:19750797	0.000998403	0.0028023	0.0040708	0.003031	0.003284	synonymous	-	-	-	*602054	Basha et al., 2018
TBX22**	T-Box Transcription Factor 22	rs195293	X:79283509	0.101457	0.0254122	0.0901992	0.029	0.092814	synonymous	-	-	-	*300307	Pauws et al., 2009
TCN2†	Transcobalamin 2	rs2283873	22:31013296	0.167133	0.0871466	0.1164	0.087	0.100985	intron	-	-	-	*613441	Martinelli et al., 2006

(Continued)

TABLE 1 | Continued

Gene	Protein	Variants	Chr:Pos	MAF 1K	MAF gnomAD Exomes	MAF gnomAD Genomes	MAF ExAC	MAF ABraOM	Sequence Ontology	SIFT	Polyphen2	Mutation Taster	OMIM Number	References
		rs9621049	22:31013419	0.108626	0.114338	0.127767	0.112	0.148604	missense	Tolerated	Benign	Tolerated		
*TCOF1**	Treacle Ribosome Biogenesis Factor 1	rs73270831	5:149740772	0.00958466	0.00245265	0.00910853	0.003006	0.008210	synonymous	-	-	-	*606847	Dixon et al., 2000; Machado et al., 2016
		rs73270846	5:149756088	0.0091853	0.00238518	0.00898746	0.0029	0.008210	missense	Tolerated	Possibly damaging	Tolerated		
		rs2071240	5:149755744	0.0605032	0.0693377	0.0643264	0.069	0.045977	missense	Damaging	Probably damaging	Tolerated		
		rs11743855	5:149772932	0.0623003	0.0638	0.0878194	0.065	0.086207	splice region	-	-	-		
*TP63**	Tumor Protein P63	rs33979049	3:189584563	0.0145767	0.0164723	0.0142811	0.017	0.012315	synonymous	-	-	-	*603273	Basha et al., 2018
TYMS†	Thymidylate Synthetase	rs28602966	18:658170	0.0181709	0.027113	0.0262783	0.022	0.024752	stop gained	-	-	-	*188350	Boyles et al., 2009; Shaw et al., 2013

**Genes described in syndromes with cleft palate.* †*Genes described in cleft lip and palate. OMIM, Online Mendelian Inheritance in Man (http://omim.org). An asterisk (*) before an OMIM entry number indicates a gene. A plus sign (+) before an OMIM entry number indicates that the entry includes a description of a gene and a phenotype.*

located at 17p11.2, encodes the cytoplasmic SHMT enzyme consisting of 483 residues (Garrow et al., 1993). Although Shmt1 knockout mice are viable and fertile (MacFarlane et al., 2008), the incidence of neural tube defects among the offspring of Shmt1$^{-/-}$ females is significantly affected by a low-folate diet (Beaudin et al., 2012). Previous studies have also associated SNPs in *SMHT1* with NSCPO in a Norwegian population (Boyles et al., 2008), and with NSCL ± P risk in a Chilean population (Salamanca et al., 2020).

Our analyses also revealed novel variants in *GHRL3* and *LRP6*. *GRHL3* encodes a transcription factor member of the grainyhead family with significant roles during the embryogenesis of craniofacial structure (Dworkin et al., 2014; Peyrard-Janvid et al., 2014). *GRHL3* mutations were reported in patients with VWS (Peyrard-Janvid et al., 2014) and human spina bifida (Lemay et al., 2017), and polymorphisms were associated with both NSCL ± P and NSCPO phenotypes (Leslie et al., 2016; Mangold et al., 2016; Wang Y. et al., 2016; Eshete et al., 2018). In a recent study, we analyzed the previous *GRHL3*-associated variants (rs10903078, rs41268753, and rs4648975) in a large ancestry-structured case–control sample composed of 1,127 Brazilian participants, and none of the variants withstood the multiple logistic regression analysis with *p*-Values adjusted to multiple comparisons (Azevedo et al., 2020). As the common *GRHL3* variants identified as risk factors for NSCPO in European, Asian, and African populations (Leslie et al., 2016; Mangold et al., 2016; Wang Y. et al., 2016) were not confirmed in our previous study, it is suggested that NSCPO risk associated with particular variants in *GRHL3* may differ among ethnic groups and the variant identified in this study (rs34637004) may be the risk variant for the Brazilian population. *LRP6*, which encodes a central co-receptor in the WNT/β-catenin signaling pathway, has pleiotropic roles in both normal development and complex diseases (Wang et al., 2018). LRP6 controls the canonical WNT/β-catenin pathway promoting development of neural crests and participating in the craniofacial morphogenesis, including lip and palate formation (Tamai et al., 2000; Song et al., 2009; Jin et al., 2011). Variants in *LRP6* were associated with congenital neural tube defects (Allache et al., 2014; Lei et al., 2015), tooth agenesis (Massink et al., 2015; Ockeloen et al., 2016), and NSOC (Basha et al., 2018). Although the *LRP6*-variant rs34815107 (c.4202G > A; p.Arg1401His; MAF < 0.002) was predicted as benign and tolerated and to date no disease was associated with this variant, it is located in the LRP6 cytoplasmic domain, which is essential for Wnt phosphorylation of serine/threonine residues of target proteins (Chen et al., 2014). Further validation in large multiethnic cohort studies and functional analysis are warranted to clarify the association between the novel variants in *GRHL3* and *LRP6* and NSCPO.

Using ontology analysis, we found 243 biologic processes and 8 pathways formatted by NSCPO-associated genes that interact with each other constituting a large network with two large nodes interconnected by *LRP6* and *MTR*. *MTR* encodes the methionine synthase protein, which catalyzes the remethylation of homocysteine to form methionine and links of homocysteine cycle to folate metabolism (Leclerc et al.,

TABLE 2 | List of the overrepresented pathway formatted with the variant-containing-genes identified in patients with non-syndromic cleft palate only (NSCPO).

Pathway ID	Term description	Observed gene count	Background gene count	False discovery rate	Matching proteins in your network
hsa00670*	One carbon pool by folate	6	20	3.63e-11	MTHFD1, FTCD, TYMS, SHMT1, MTR, MTHFR
hsa01523*	Antifolate resistance	3	31	0.00038	TYMS, SHMT1, MTHFR
hsa01100	Metabolic pathways	8	1250	0.0027	MTHFD1, FTCD, TYMS, SHMT1, ACACB, POMGNT2, MTR, MTHFR
hsa04974	Protein digestion and absorption	3	90	0.0039	COL11A1, COL11A2, COL2A1
hsa04330	Notch signaling pathway	2	48	0.0262	CREBBP, JAG2
hsa01230*	Biosynthesis of amino acids	2	72	0.0460	SHMT1, MTR
hsa04520	Adherens junction	2	71	0.0460	CDH1, CREBBP
hsa05200	Pathways in cancer	4	515	0.0460	LRP6, CDH1, CREBBP, JAG2

**Pathway found only in NSCPO.*

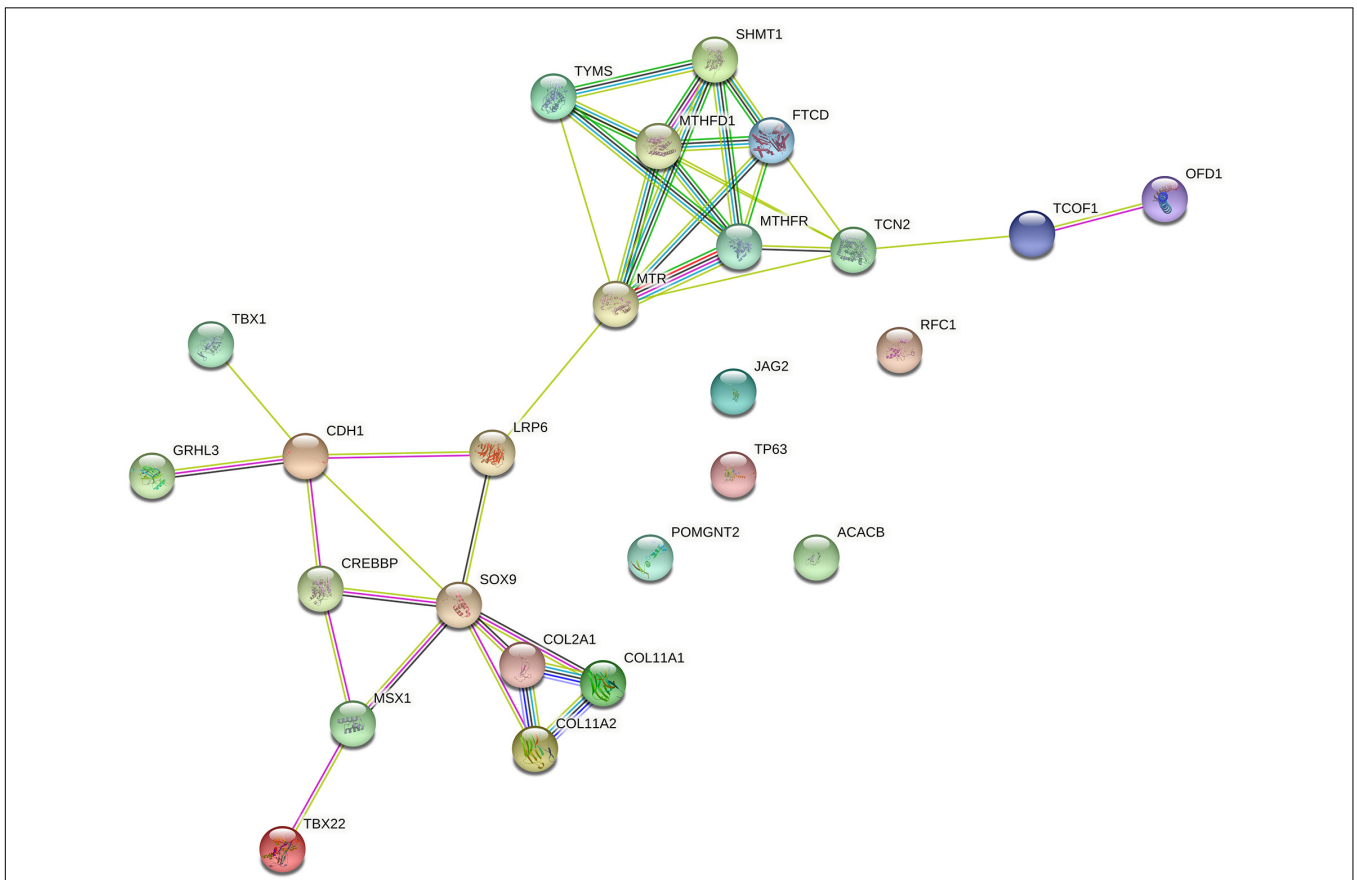

FIGURE 2 | Protein–protein interaction network with the genes associated with non-syndromic cleft palate only (NSCPO). Twenty out of 25 genes formed two nodes interconnected by a validated interaction between *LRP6* and *MTR*. The first encompassed nine genes, including *FTCD*, *MTHFD1*, *MTHFR*, *MTR*, *OFD1*, *SHMT1*, *TCN2*, *TCOF1*, and *TYMS* (P < 1.0e-16), and the second node involved *CDH1*, *COL2A1*, *COL11A1*, *COL11A2*, *CREBBP*, *GRHL3*, *LRP6*, *MSX1*, *SOX9*, *TBX1*, and *TBX22* (P < 1.0e-16). Both nodes were based on curated databases (light blue), experimentally (purple), gene neighborhood (green), gene fusions (red), gene co-occurrence (blue), text mining (light green), co-expression (black), and protein homology (violet). This analysis had an average confidence score of 0.588 (P < 1.0e-16), suggesting a low rate for false-positive interactions.

1996). Strong evidences suggest that the presence of accepted folate/homocysteine levels may not be the only requirement for NSOC prevention, since its absorption, transport, and metabolism, producing active derivatives essentials for DNA methylation and synthesis during embryonic processes, including craniofacial development, are also important to oral cleft predisposing (Desai et al., 2016). Indeed, variants in several genes related to transport and metabolism of folate and homocysteine, including *MTR*, have been shown to alter the disponibility of the active forms of those molecules

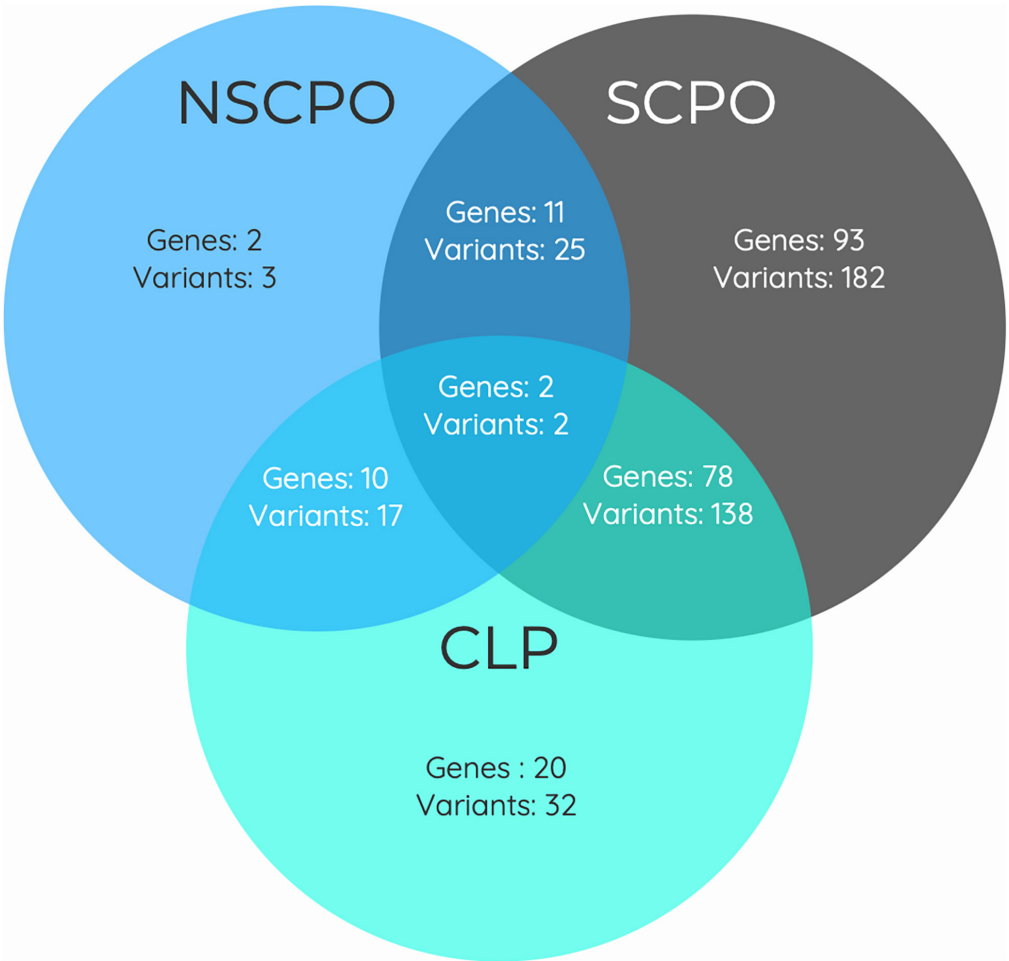

FIGURE 3 | Venn diagram showing the overlap between genes associated with the phenotypes of non-syndromic cleft palate only (NSCPO), syndromic cleft palate only (SCPO), and cleft lip and palate (CLP) found in patients with NSCPO. The numbers in each area represent the gene and variants count for the particular section.

and influence cleft risk (Wang W. et al., 2016; Lei et al., 2018). Interestingly, a recent study demonstrated that the methionine-depleted medium inhibits canonical Wnt/β-catenin signaling (Albrecht et al., 2019), and as LRP6 is an indispensable co-receptor for WNT signaling (Gray et al., 2010), our findings reinforce the interlink between *MTR* and *LRP6* and the risk of NSCPO through potential epistatic interactions. Furthermore, as cleft palate can be part of a syndrome or concomitant with cleft lip, indicating that variants in multiple genes may be shared by different conditions with a specific cleft palate phenotype, we applied genetic ontology analysis to identify common and specific pathways. We found 167 biological processes and 5 pathways consisting of *ACACB*, *CDH1*, *COL2A1*, *COL11A1*, *COL11A2*, *CREBBP*, *FTCD*, *LRP6*, *JAG2*, *MTHFD1*, *MTHFR*, *MTR*, *POMGNT2*, *SHMT1*, and *TYMS* enriched in SCPO and CLP. In relation to NSCPO, 76 biological processes and 3 pathways, led by *FTCD*, *MTHFD1*, *MTHFR*, *MTR*, *SHMT1*, and *TYMS*, were found. Thus, these findings suggest that although the genes form distinct biological processes and pathways, similar genes participated in both phenotypes, suggesting common etiologies among them.

The DNA sequencing of pooled patients proved to be an excellent and cost-effective strategy to identify genetic variants related to complex diseases (Collins et al., 2016; Popp et al., 2017; Özdoğan and Kaya, 2020), although it has never been applied to study oral clefts. We detected variants in 6.43% of the investigated genes, which is quite similar to the number of variants identified in the study conducted by Basha et al. (2018), applying individual exome sequencing in 46 multiplex families with NSCPO. Furthermore, we found variants in the same genes identified and validated by Basha et al. (2018) as of risk for NSCPO. However, this technique is associated with problems to be considered when analyzing and interpreting the results. One important problem is to correctly identify rare variants, since sequencing errors can be confused with alleles present at low frequencies, generating false-positive variants. Another potential problem is associated with the estimation of the allelic frequency of the polymorphic variants. The power of genetic analysis depends on the calculation of the allele frequency,

and in principle, the pool should provide a robust estimate of the allele frequencies, since it represents several samples, decreasing the general variances of the estimated frequencies. This hypothesis is well supported by mathematical models under the assumption that there are no sequencing errors and each individual contributes an equal amount of DNA to the pools (Anand et al., 2016). Therefore, the lack of validation in a large cohort and the non-characterization of the functional impact of the variants are the limitations of this study. Another limitation that should be noted when interpreting the results is that we did not control for environmental risk factors, although the major source of confounding for genetic studies is population stratification, and our results were adjusted for this.

In summary, our results support the findings of earlier epidemiological studies, indicating that specific variants in genes related to SCPO and CLP may cause NSCPO. Furthermore, gene ontology enrichment analysis identified the interconnection of *LRP6* and *MTR*, reinforcing that variants in the folate/homocysteine pathway may influence risk of NSCPO through potential epistatic interactions. While this study has explored novel variants in previously reported cleft palate genes, we have also identified and described a large group of variants in genes without previous association with NSCPO.

DATA AVAILABILITY STATEMENT

The datasets presented in this study can be found in online repositories. The name of the repository and accession number are as follows: European Nucleotide Archive PRJEB44884 and the samples (SAMEA8730854, SAMEA8730858, SAMEA8730857, SAMEA8730856, SAMEA8730855, SAMEA8730853).

ETHICS STATEMENT

The studies involving human participants were reviewed and approved by the Piracicaba Dental School, University of Campinas – 08452819.0.0000.5418. Written informed consent to participate in this study was provided by the participants' legal guardian/next of kin.

AUTHOR CONTRIBUTIONS

RM contributed to the conception, design, data acquisition, and interpretation, and drafted and critically revised the manuscript. HM-J, SR, EK, RS, and LN contributed to conception, design, data acquisition, and interpretation, and critically revised the manuscript. RC made substantial contributions to the study's conception and design, and manuscript review and editing. All authors gave their final approval and agreed to be accountable for all aspects of the work.

ACKNOWLEDGMENTS

We thank Dra. Ana Cristina Victorino Krepischi (Institute of Biosciences, University of São Paulo, São Paulo, Brazil) for her assistance during exome analysis.

SUPPLEMENTARY MATERIAL

The Supplementary Material for this article can be found online at: https://www.frontiersin.org/articles/10.3389/fcell.2021.638522/full#supplementary-material

Supplementary Figure 1 | Protein-protein interaction networks constructed with the previously syndromic cleft palate only (SCPO)-associated genes identified in the pools of patients with non-syndromic cleft palate only (NSCPO), but not in the control, using STRING. The networks include 205 edges (interactions) among 98 nodes based on curated databases (light blue), experimentally (purple), gene neighborhood (green), gene fusions (red), gene co-occurrence (blue), textmining (light green), co-expression (black) and protein homology (violet). The overall confidence score of this analysis was 0.446 ($P < 1.0e-16$), indicating a low change for false-positive interactions.

Supplementary Figure 2 | The protein-protein interaction networks with cleft lip-palate (CLP)-associated targets found in the pools of patients with non-syndromic cleft palate only (NSCPO), but not in the control. Networks include 244 interactions among 91 nodes (overall coefficient score = 0.557; $P < 1.0e-16$). Different colors represent different levels of evidence of connection between proteins. Light blue represents curated databases, purple experimental evidence, green gene neighborhood, red gene fusions, blue gene co-occurrence, light green evidence from textmining, black co-expression, and violet protein homology.

REFERENCES

Adzhubei, I., Jordan, D. M., and Sunyaev, S. R. (2013). Predicting functional effect of human missense mutations using PolyPhen-2. *Curr. Protoc. Hum. Genet.* 7, 7.20.1–7.20.41.

Aidar, M., and Line, S. R. (2007). A simple and cost-effective protocol for DNA isolation from buccal epithelial cells. *Braz. Dent. J.* 18, 148–152. doi: 10.1590/s0103-64402007000200012

Albrecht, L. V., Bui, M. H., and Robertis, W. M. (2019). Canonical Wnt is inhibited by targeting one-carbon metabolism through methotrexate or methionine deprivation. *Proc. Natl. Acad. Sci. U.S.A.* 116, 2987–2995. doi: 10.1073/pnas.1820161116

Allache, R., Lachance, S., Guyot, M. C., De Marco, P., Merello, E., Justice, M. J., et al. (2014). Novel mutations in Lrp6 orthologs in mouse and human neural tube defects affect a highly dosage-sensitive Wnt non-canonical planar cell polarity pathway. *Hum. Mol. Genet.* 23, 1687–1699. doi: 10.1093/hmg/ddt558

Anand, S., Mangano, E., Barizzone, N., Bordoni, R., Sorosina, M., Clarelli, F., et al. (2016). Next generation sequencing of pooled samples: guideline for variants' Filtering. *Sci. Rep.* 6:33735.

Azevedo, C. M. S., Machado, R. A., Martelli-Júnior, H., Reis, S. R. A., Persuhn, D. C., Coletta, R. D., et al. (2020). Exploring GRHL3 polymorphisms and SNP-SNP interactions in the risk of non-syndromic oral clefts in the Brazilian population. *Oral Dis.* 26, 145–151. doi: 10.1111/odi.13204

Basha, M., Demeer, B., Revencu, N., Helaers, R., Theys, S., Saba, S. B., et al. (2018). Whole exome sequencing identifies mutations in 10% of patients with familial non-syndromic cleft lip and/ or palate in genes mutated in well-known syndromes. *J. Med. Genet.* 55, 449–458. doi: 10.1136/jmedgenet-2017-105110

Beaty, T. H., Marazita, M. L., and Leslie, E. J. (2016). Genetic factors influencing risk to orofacial clefts: today's challenges and tomorrow's opportunities. *F1000Res.* 5:2800. doi: 10.12688/f1000research.9503.1

Beaty, T. H., Ruczinski, I., Murray, J. C., Marazita, M. L., Munger, R. G., Hetmanski, J. B., et al. (2011). Evidence for gene-environment interaction in a genome wide study of nonsyndromic cleft palate. *Genet. Epidemiol.* 35, 469–478.

Beaudin, A. E., Abarinov, E. V., Malysheva, O., Perry, C. A., Caudill, M., and Stover, P. J. (2012). Dietary folate, but not choline, modifies neural tube defect risk in Shmt1 knockout mice. *Am. J. Clin. Nutr.* 95, 109–114. doi: 10.3945/ajcn.111.020305

Bi, W., Huang, W., Whitworth, D. J., Deng, J. M., Zhang, Z., Behringer, R. R., et al. (2001). Haploinsufficiency of Sox9 results in defective cartilage primordia and premature skeletal mineralization. *Proc. Natl. Acad. Sci. U.S.A.* 98, 6698–6703. doi: 10.1073/pnas.111092198

Boyles, A. L., Wilcox, A. J., Taylor, J. A., Meyer, K., Fredriksen, A., Ueland, P. M., et al. (2008). Folate and one-carbon metabolism gene polymorphisms and their associations with oral facial clefts. *Am. J. Med. Genet. A* 146A, 440–449. doi: 10.1002/ajmg.a.32162

Boyles, A. L., Wilcox, A. J., Taylor, J. A., Shi, M., Weinberg, C. R., Meyer, K., et al. (2009). Oral facial clefts and gene polymorphisms in metabolism of folate/one-carbon and vitamin A: a pathway-wide association study. *Genet. Epidemiol.* 33, 247–255. doi: 10.1002/gepi.20376

Bureau, A., Parker, M. M., Ruczinski, I., Taub, M. A., Marazita, M. L., Murray, J. C., et al. (2014). Whole exome sequencing of distant relatives in multiplex families implicates rare variants in candidate genes for oral clefts. *Genetics* 197, 1039–1044. doi: 10.1534/genetics.114.165225

Butali, A., Mossey, P. A., Adeyemo, W. L., Eshete, M. A., Gowans, L. J. J., Busch, T. D., et al. (2019). Genomic analyses in African populations identify novel risk loci for cleft palate. *Hum. Mol. Genet.* 28, 1038–1051.

Carlson, J. C., Anand, D., Butali, A., Buxo, C. J., Christensen, K., Deleyiannis, F., et al. (2019). A systematic genetic analysis and visualization of phenotypic heterogeneity among orofacial cleft GWAS signals. *Genet. Epidemiol.* 43, 704–716.

Chen, Q., Su, Y., Wesslowski, J., Hagemann, A., Ramialison, M., Wittbrodt, J., et al. (2014). Tyrosine phosphorylation of LRP6 by Src and Fer inhibits Wnt/β-catenin signalling. *EMBO Rep.* 15, 1254–1267. doi: 10.15252/embr.201439644

Collins, D. W., Gudiseva, H. V., Trachtman, B., Bowman, A. S., Sagaser, A., Sankar, P., et al. (2016). Association of primary open-angle glaucoma with mitochondrial variants and haplogroups common in African Americans. *Mol. Vis.* 22, 454–471.

Desai, A., Sequeira, J. M., and Quadros, E. V. (2016). The metabolic basis for developmental disorders due to defective folate transport. *Biochimie* 126, 31–42. doi: 10.1016/j.biochi.2016.02.012

Dixon, J., Brakebusch, C., Fassler, R., and Dixon, M. J. (2000). Increased levels of apoptosis in the prefusion neural folds underlie the craniofacial disorder, Treacher Collins syndrome. *Hum. Mol. Genet.* 9, 1473–1480. doi: 10.1093/hmg/9.10.1473

Dixon, M. J., Marazita, M. L., Beaty, T. H., and Murray, J. C. (2011). Cleft lip and palate: understanding genetic and environmental influences. *Nat. Rev. Genet.* 12, 167–178. doi: 10.1038/nrg2933

do Rego, A. B., Saì, J., Hoshi, R., Viena, C. S., Mariano, L. C., de Castro Veiga, P., et al. (2015). Genetic risk factors for nonsyndromic cleft lip with or without cleft palate in a Brazilian population with high African ancestry. *Am. J. Med. Genet. A* 167A, 2344–2349. doi: 10.1002/ajmg.a.37181

Dworkin, S., Simkin, J., Darido, C., Partridge, D. D., Georgy, S. R., Caddy, J., et al. (2014). Grainyhead-like 3 regulation of endothelin-1 in the pharyngeal endoderm is critical for growth and development of the craniofacial skeleton. *Mech. Dev.* 133, 77–90. doi: 10.1016/j.mod.2014.05.005

Eshete, M. A., Liu, H., Li, M., Adeyemo, W. L., Gowans, L. J. J., Mossey, P. A., et al. (2018). Loss-of-function GRHL3 variants detected in African patients with isolated cleft palate. *J. Dent. Res.* 97, 41–48. doi: 10.1177/0022034517729819

Ferrante, M. I., Zullo, A., Barra, A., Bimonte, S., Messaddq, N., Studer, M., et al. (2006). Oral-facial-digital type I protein is required for primary cilia formation and left-right axis specification. *Nat. Genet.* 38, 112–117. doi: 10.1038/ng1684

Frech, C., and Chen, N. (2010). Genome-wide comparative gene family classification. *PLoS One* 5:e13409. doi: 10.1371/journal.pone.0013409

Funato, N., and Nakamura, M. (2017). Identification of shared and unique gene families associated with oral clefts. *Int. J. Oral Sci.* 9, 104–109. doi: 10.1038/ijos.2016.56

Garrow, T. A., Brenner, A. A., Whitehead, V. M., Chen, X. N., Duncan, R. G., Korenberg, J. R., et al. (1993). Cloning of human cDNAs encoding mitochondrial and cytosolic serine hydroxymethyltransferases and chromosomal localization. *J. Biol. Chem.* 268, 11910–11916. doi: 10.1016/s0021-9258(19)50286-1

Gray, J. D., Nakouzi, G., Slowinska-Castaldo, B., Dazard, J. E., Rao, J. S., Nadeau, J. H., et al. (2010). Functional interactions between the LRP6 WNT co-receptor and folate supplementation. *Hum. Mol. Genet.* 19, 4560–4572. doi: 10.1093/hmg/ddq384

He, M., Zuo, X., Liu, H., Wang, W., Zhang, Y., Fu, Y., et al. (2020). Genome-wide analyses identify a novel risk locus for nonsyndromic cleft palate. *J. Dent. Res.* 99, 1461–1468. (in press) doi: 10.1177/0022034520943867

Hecht, J. T., Mulliken, J. B., and Blanton, S. H. (2002). Evidence for a cleft palate only locus on chromosome 4 near MSX1. *Am. J. Med. Genet.* 110, 406–407. doi: 10.1002/ajmg.10497

Hoebel, A. K., Drichel, D., van de Vorst, M., Böhmer, A. C., Sivalingam, S., Ishorst, N., et al. (2017). Candidate genes for nonsyndromic cleft palate detected by exome sequencing. *J. Dent. Res.* 96, 1314–1321.

Huang, L., Jia, Z., Shi, Y., Du, Q., Shi, J., Wang, Z., et al. (2019). Genetic factors define CPO and CLO subtypes of nonsyndromic orofacial cleft. *PLoS Genet.* 15:e1008357. doi: 10.1371/journal.pgen.1008357

Ishorst, N., Francheschelli, P., Bohmer, A., Khan, M., Heilmann-Heimbach, S., Fricker, N., et al. (2018). Nonsyndromic cleft palate: an association study at GWAS candidate loci in a multiethnic sample. *Birth Defects Res.* 110, 871–882. doi: 10.1002/bdr2.1213

Jagomagi, T., Nikopensius, T., Krjutskov, K., Tammekivi, V., Viltrop, T., Saag, M., et al. (2010). MTHFR and MSX1 contribute to the risk of nonsyndromic cleft lip/palate. *Eur. J. Oral Sci.* 118, 213–220. doi: 10.1111/j.1600-0722.2010.00729.x

Jia, Z. L., He, S., Jiang, S. Y., Zhang, B. H., Duan, S. J., Shi, J. Y., et al. (2017). Rs12941170 at SOX9 gene associated with orofacial clefts in Chinese. *Arch. Oral Biol.* 76, 14–19. doi: 10.1016/j.archoralbio.2016.12.010

Jiang, R., Lan, Y., Chapman, H. D., Norton, C. R., Serreze, D. V., Weinmaster, G., et al. (1998). Defects in limb, craniofacial, and thymic development in Jagged2 mutant mice. *Genes Dev.* 12, 1046–1057. doi: 10.1101/gad.12.7.1046

Jin, Y. R., Turcotte, T. J., Crocker, A. L., Han, X. H., and Yoon, J. K. (2011). The canonical Wnt signaling activator, R-spondin2, regulates craniofacial patterning and morphogenesis within the branchial arch through ectodermal-mesenchymal interaction. *Dev. Biol.* 352, 1–13.

Jugessur, A., Skare, O., Lie, R. T., Wilcox, A. J., Christensen, K., Christiansen, L., et al. (2012). X-linked genes and risk of orofacial clefts: evidence from two population-based studies in Scandinavia. *PLoS One* 7:e39240. doi: 10.1371/journal.pone.0039240

Koillinen, H., Lahermo, P., Rautio, J., Hukki, J., Peyrard-Janvid, M., and Kere, J. (2005). A genome-wide scan of non-syndromic cleft palate only (CPO) in Finnish multiplex families. *J. Med. Genet.* 42, 177–184. doi: 10.1136/jmg.2004.019646

Kumar, P., Henikoff, S., and Ng, P. C. (2009). Predicting the effects of coding non-synonymous variants on protein function using the SIFT algorithm. *Nat. Protoc.* 4, 1073–1081. doi: 10.1038/nprot.2009.86

Leclerc, D., Campeau, E., Goyette, P., Adjalla, C. E., Christensen, B., Ross, M., et al. (1996). Human methionine synthase: cDNA cloning and identification of mutations in patients of the cblG complementation group of folate/cobalamin disorders. *Hum. Mol. Genet.* 5, 1867–1874. doi: 10.1093/hmg/5.12.1867

Lei, W., Xia, Y., Wu, Y., Fu, G., and Ren, A. (2018). Associations between MTR A2756G, MTRR A66G, and TCN2 C776G polymorphisms and risk of nonsyndromic cleft lip with or without cleft palate: a meta-analysis. *Genet. Test. Mol. Biomarkers* 22, 465–473. doi: 10.1089/gtmb.2018.0037

Lei, Y., Fathe, K., McCartney, D., Zhu, H., Yang, W., Ross, M. E., et al. (2015). Rare LRP6 variants identified in spina bifida patients. *Hum. Mutat.* 36, 342–349. doi: 10.1002/humu.22750

Lemay, P., De Marco, P., Emond, A., Spiegelman, D., Dionne-Laporte, A., Laurent, S., et al. (2017). Rare deleterious variants in GRHL3 are associated with human spina bifida. *Hum. Mutat.* 38, 716–724. doi: 10.1002/humu.23214

Leslie, E. J., and Marazita, M. L. (2013). Genetics of cleft lip and cleft palate. *Am. J. Med. Genet. C Semin. Med. Genet.* 163C, 246–258.

Leslie, E. J., Liu, H., Carlson, J. C., Shaffer, J. R., Feingold, E., Wehby, G., et al. (2016). A genome-wide association study of nonsyndromic cleft palate identifies an etiologic missense variant in GRHL3. *Am. J. Hum. Genet.* 98, 744–754. doi: 10.1016/j.ajhg.2016.02.014

Li, H., and Durbin, R. (2009). Fast and accurate short read alignment with burrows-wheeler transform. *Bioinformatics* 25, 1754–1760. doi: 10.1093/bioinformatics/btp324

Li, S. W., Prockop, D. J., Helminen, H., Fassler, R., Lapvetelainen, T., Kiraly, K., et al. (1995). Transgenic mice with targeted inactivation of the Col2 alpha 1 gene for collagen II develop a skeleton with membranous and periosteal bone but no endochondral bone. *Genes Dev.* 9, 2821–2830. doi: 10.1101/gad.9.22.2821

Liu, H., Busch, T., Eliason, S., Anand, D., Bullard, S., Gowans, L. J., et al. (2017). Exome sequencing provides additional evidence for the involvement of ARHGAP29 in Mendelian orofacial clefting and extends the phenotypic spectrum to isolated cleft palate. *Birth Defects Res.* 109, 27–37.

Ludwig, K. U., Böhmer, A. C., Bowes, J., Nikolić, M., Ishorst, N., Wyatt, N., et al. (2017). Imputation of orofacial clefting data identifies novel risk loci and sheds light on the genetic background of cleft lip ± cleft palate and cleft palate only. *Hum. Mol. Genet.* 26, 829–842.

Ma, L., Mondal, A. K., Murea, M., Sharma, N. K., Tönjes, A., Langberg, K. A., et al. (2011). The effect of ACACB cis-variants on gene expression and metabolic traits. *PLoS One* 6:e23860. doi: 10.1371/journal.pone.0023860

MacFarlane, A. J., Liu, X., Perry, C. A., Flodby, P., Allen, R. H., Stabler, S. P., et al. (2008). Cytoplasmic serine hydroxymethyltransferase regulates the metabolic partitioning of methylenetetrahydrofolate but is not essential in mice. *J. Biol. Chem.* 283, 25846–25853. doi: 10.1074/jbc.m802671200

Machado, R. A., Messetti, A. C., de Aquino, S. N., Martelli-Junior, H., Swerts, M. S., de Almeida Reis, S. R., et al. (2016). Association between genes involved in craniofacial development and nonsyndromic cleft lip and/or palate in the Brazilian population. *Cleft Palate Craniofac. J.* 53, 550–556. doi: 10.1597/15-107

Mangold, E., Böhmer, A. C., Ishorst, N., Hoebel, A.-K., Gültepe, P., Schuenke, H., et al. (2016). Sequencing the GRHL3 coding region reveals rare truncating mutations and a common susceptibility variant for nonsyndromic cleft palate. *Am. J. Hum. Genet.* 98, 755–762. doi: 10.1016/j.ajhg.2016.02.013

Martinelli, M., Scapoli, L., Palmieri, A., Pezzetti, F., Baciliero, U., Padula, E., et al. (2006). Study of four genes belonging to the folate pathway: transcobalamin 2 is involved in the onset of non-syndromic cleft lip with or without cleft palate. *Hum. Mutat.* 27:294. doi: 10.1002/humu.9411

Massink, M. P., Créton, M. A., Spanevello, F., Fennis, W. M., Cune, M. S., Savelberg, S. M., et al. (2015). Loss-of-function mutations in the WNT co-receptor LRP6 cause autosomal-dominant oligodontia. *Am. J. Hum. Genet.* 97, 621–626.

Messetti, A. C., Machado, R. A., Oliveira, C. E., Martelli-Júnior, H., Reis, S. R. A., Moreira, H. S. B., et al. (2017). Brazilian multicenter study of association between polymorphisms in CRISPLD2 and JARID2 and non-syndromic oral clefts. *J. Oral Pathol. Med.* 46, 232–239. doi: 10.1111/jop.12470

Murthy, J., Gurramkonda, V. B., and Lakkakula, B. V. (2014). Significant association of MTHFD1 1958G>A single nucleotide polymorphism with nonsyndromic cleft lip and palate in Indian population. *Med. Oral Patol. Oral Cir. Bucal* 19, e616–e621.

Nikopensius, T., Jagomagi, T., Krjutskov, K., Tammekivi, V., Saag, M., Prane, I., et al. (2010). Genetic variants in COL2A1, COL11A2, and IRF6 contribute risk to nonsyndromic cleft palate. *Birth Defects Res. A Clin. Mol. Teratol.* 88, 748–756. doi: 10.1002/bdra.20700

Ockeloen, C. W., Khandelwal, K. D., Dreesen, K., Ludwig, K. U., Sullivan, R., van Rooij, I., et al. (2016). Novel mutations in LRP6 highlight the role of WNT signaling in tooth agenesis. *Genet. Med.* 18, 1158–1162.

Özdoğan, G. O., and Kaya, H. (2020). Next-Generation sequencing data analysis on pool-seq and low-coverage retinoblastoma data. *Interdiscip. Sci. Comput. Life Sci.* 12, 302–310. doi: 10.1007/s12539-020-00374-8

Pauws, E., Hoshino, A., Bentley, L., Prajapati, S., Keller, C., Hammond, P., et al. (2009). Tbx22null mice have a submucous cleft palate due to reduced palatal bone formation and also display ankyloglossia and choanal atresia phenotypes. *Hum. Mol. Genet.* 18, 4171–4179. doi: 10.1093/hmg/ddp368

Pengelly, R. J., Arias, L., Martiìnez, J., Upstill-Goddard, R., Seaby, E. G., Gibson, J., et al. (2016). Deleterious coding variants in multi-case families with non-syndromic cleft lip and/or palate phenotypes. *Sci. Rep.* 6:30457.

Peyrard-Janvid, M., Leslie, E. J., Kousa, Y. A., Smith, T. L., Dunnwald, M., Magnusson, M., et al. (2014). Dominant mutations in GRHL3 cause Van der Woude syndrome and disrupt oral periderm development. *Am. J. Hum. Genet.* 94, 23–32. doi: 10.1016/j.ajhg.2013.11.009

Popp, B., Ekici, A. B., Thiel, C. T., Hoyer, J., Wiesener, A., Kraus, C., et al. (2017). Exome Pool-Seq in neurodevelopmental disorders. *Eur. J. Hum. Genet.* 25, 1364–1376. doi: 10.1038/s41431-017-0022-1

Salamanca, C., González-Hormazábal, P., Recabarren, A. S., Recabarren, P. A., Pantoja, R., Leiva, N., et al. (2020). A SHMT1 variant decreases the risk of nonsyndromic cleft lip with or without cleft palate in Chile. *Oral Dis.* 26, 159–165. doi: 10.1111/odi.13229

Satokata, I., and Maas, R. (1994). Msx1 deficient mice exhibit cleft palate and abnormalities of craniofacial and tooth development. *Nat. Genet.* 6, 348–356. doi: 10.1038/ng0494-348

Seegmiller, R., Fraser, F. C., and Sheldon, H. (1971). A new chondrodystrophic mutant in mice. Electron microscopy of normal and abnormal chondrogenesis. *J. Cell Biol.* 48, 580–593. doi: 10.1083/jcb.48.3.580

Shaw, G. M., Todoroff, K., Finnell, R. H., Rozen, R., and Lammer, E. J. (1999). Maternal vitamin use, infant C677T mutation in MTHFR, and isolated cleft palate risk. *Am. J. Med. Genet.* 85, 84–85. doi: 10.1002/(sici)1096-8628(19990702)85:1<84::aid-ajmg15>3.0.co;2-v

Shaw, G. M., Yang, W., Perloff, S., Shaw, N. M., Carmichael, S. L., Zhu, H., et al. (2013). Thymidylate synthase polymorphisms and risks of human orofacial clefts. *Birth Defects Res. A Clin. Mol. Teratol.* 97, 95–100. doi: 10.1002/bdra.23114

Shaw, G. M., Zhu, H., Lammer, E. J., Yang, W., and Finnell, R. H. (2003). Genetic variation of infant reduced folate carrier (A80G) and risk of orofacial and conotruncal heart defects. *Am. J. Epidemiol.* 158, 747–752. doi: 10.1093/aje/kwg189

Song, L., Li, Y., Wang, K., Wang, Y. Z., Molotkov, A., Gao, L., et al. (2009). Lrp6-mediated canonical Wnt signaling is required for lip formation and fusion. *Development* 136, 3161–3171. doi: 10.1242/dev.037440

Song, Y., and Zhang, S. (2011). Association of CDH1 promoter polymorphism and the risk of non-syndromic orofacial clefts in a Chinese Han population. *Arch. Oral Biol.* 56, 68–72. doi: 10.1016/j.archoralbio.2010.08.019

Tamai, K., Semenov, M., Kato, Y., Spokony, R., Liu, C., Katsuyama, Y., et al. (2000). LDL-receptor-related proteins in Wnt signal transduction. *Nature* 407, 530–535. doi: 10.1038/35035117

Vieira, A. R., Avila, J. R., Daack-Hirsch, S., Dragan, E., Félix, T. M., Rahimov, F., et al. (2005). Medical sequencing of candidate genes for nonsyndromic cleft lip and palate. *PLoS Genet.* 1:e64. doi: 10.1371/journal.pgen.0010064

Wang, W., Jiao, X. H., Wang, X. P., Sun, X. Y., and Dong, C. M. T. R. (2016). MTRR, and MTHFR gene polymorphisms and susceptibility to nonsyndromic cleft lip with or without cleft palate. *Genet. Test. Mol. Biomarkers* 20, 297–303. doi: 10.1089/gtmb.2015.0186

Wang, Y., Sun, Y., Huang, Y., Pan, Y., Jia, Z., Ma, L., et al. (2016). Association study between Van der Woude Syndrome causative gene GRHL3 and nonsyndromic cleft lip with or without cleft palate in a Chinese cohort. *Gene* 588, 69–73. doi: 10.1016/j.gene.2016.04.045

Wang, Z. M., Luo, J. Q., Xu, L. Y., Zhou, H. H., and Zhang, W. (2018). Harnessing low-density lipoprotein receptor protein 6 (LRP6) genetic variation and Wnt signaling for innovative diagnostics in complex diseases. *Pharmacogenomics J.* 18, 351–358. doi: 10.1038/tpj.2017.28

Wattanawong, K., Rattanasiri, S., McEvoy, M., Attia, J., and Thakkinstian, A. (2016). Association between IRF6 and 8q24 polymorphisms and nonsyndromic cleft lip with or without cleft palate: Systematic review and meta-analysis. *Birth Defects Res. A Clin. Mol. Teratol.* 106, 773–788. doi: 10.1002/bdra.23540

Yu, Y., Zuo, X., He, M., Gao, J., Fu, Y., and Qin, C. (2017). Genome-wide analyses of non-syndromic cleft lip with palate identify 14 novel loci and genetic heterogeneity. *Nat. Commun.* 8:14364.

Conflict of Interest: The authors declare that the research was conducted in the absence of any commercial or financial relationships that could be construed as a potential conflict of interest.

frontiers in Cell and Developmental Biology

REVIEW
published: 12 August 2021
doi: 10.3389/fcell.2021.632766

Depression and Antidepressants During Pregnancy: Craniofacial Defects Due to Stem/Progenitor Cell Deregulation Mediated by Serotonin

Natalia Sánchez[1†], Jesús Juárez-Balarezo[1†], Marcia Olhaberry[2,3], Humberto González-Oneto[4], Antonia Muzard[2,3], María Jesús Mardonez[2,3], Pamela Franco[2,3], Felipe Barrera[4] and Marcia Gaete[1]*

[1] Department of Anatomy, Faculty of Medicine, Pontificia Universidad Católica de Chile, Santiago, Chile, [2] Department of Psychology, Pontificia Universidad Católica de Chile, Santiago, Chile, [3] Millennium Institute for Research in Depression and Personality (MIDAP), Santiago, Chile, [4] School of Dentistry, Faculty of Medicine, Pontificia Universidad Católica de Chile, Santiago, Chile

OPEN ACCESS

Edited by:
Sebastian Dworkin,
La Trobe University, Australia

Reviewed by:
Gary Ten Eyck,
New York University, United States
Juliane Isaac,
Université de Paris, France

***Correspondence:**
Marcia Gaete
mgaets@uc.cl

[†] These authors have contributed equally to this work

Specialty section:
This article was submitted to Molecular and Cellular Pathology, a section of the journal Frontiers in Cell and Developmental Biology

Received: 24 November 2020
Accepted: 13 July 2021
Published: 12 August 2021

Citation:
Sánchez N, Juárez-Balarezo J, Olhaberry M, González-Oneto H, Muzard A, Mardonez MJ, Franco P, Barrera F and Gaete M (2021) Depression and Antidepressants During Pregnancy: Craniofacial Defects Due to Stem/Progenitor Cell Deregulation Mediated by Serotonin. Front. Cell Dev. Biol. 9:632766. doi: 10.3389/fcell.2021.632766

Depression is a common and debilitating mood disorder that increases in prevalence during pregnancy. Worldwide, 7 to 12% of pregnant women experience depression, in which the associated risk factors include socio-demographic, psychological, and socioeconomic variables. Maternal depression could have psychological, anatomical, and physiological consequences in the newborn. Depression has been related to a downregulation in serotonin levels in the brain. Accordingly, the most commonly prescribed pharmacotherapy is based on selective serotonin reuptake inhibitors (SSRIs), which increase local serotonin concentration. Even though the use of SSRIs has few adverse effects compared with other antidepressants, altering serotonin levels has been associated with the advent of anatomical and physiological changes *in utero*, leading to defects in craniofacial development, including craniosynostosis, cleft palate, and dental defects. Migration and proliferation of neural crest cells, which contribute to the formation of bone, cartilage, palate, teeth, and salivary glands in the craniofacial region, are regulated by serotonin. Specifically, craniofacial progenitor cells are affected by serotonin levels, producing a misbalance between their proliferation and differentiation. Thus, it is possible to hypothesize that craniofacial development will be affected by the changes in serotonin levels, happening during maternal depression or after the use of SSRIs, which cross the placental barrier, increasing the risk of craniofacial defects. In this review, we provide a synthesis of the current research on depression and the use of SSRI during pregnancy, and how this could be related to craniofacial defects using an interdisciplinary perspective integrating psychological, clinical, and developmental biology perspectives. We discuss the mechanisms by which serotonin could influence craniofacial development and stem/progenitor cells, proposing some transcription factors as mediators of serotonin signaling, and craniofacial stem/progenitor cell biology. We finally highlight the importance of non-pharmacological therapies for depression on fertile and pregnant women, and provide an individual analysis of the risk–benefit balance for the use of antidepressants during pregnancy

Keywords: craniofacial defects, antidepressant, depression, pregnancy, stem cells

INTRODUCTION

Maternal depression is one of the most frequent mood disorders occurring during and after pregnancy, affecting 7–12% of women in developed countries (Charlton et al., 2015; Huybrechts et al., 2015; Fairbrother et al., 2017; Field, 2017a; McAndrew, 2019). The depressive symptomatology during pregnancy has been identified as a predictor for postnatal depression (Field, 2011; Koutra et al., 2014; Raskin et al., 2016). On the other hand, the development of the fetus is affected by maternal depression, being correlated with fetus low heart rate baseline, premature births, protracted descent (Emory and Dieter, 2006), and low size and weight of the newborns (Field, 2011; Dadi et al., 2020; Hompoth et al., 2020). Also, the offspring of depressed mothers has a high risk of depression (Pawlby et al., 2009) and negative consequences in affective, cognitive, and behavioral development (Grace et al., 2003; Milgrom et al., 2008; Pearson et al., 2012).

The identification of risk factors associated with maternal depression can contribute to their prevention. The risk factors can be classified as prenatal factors, factors related to pregnancy, and factors related to the mother herself. Overall, the lack of a partner, absence of socio-familiar support network, low income, insecurity attachments, history of depression, and extreme ages (teenagers or>40 years), are prenatal risk factors for maternal depression (Faisal-Cury and Rossi Menezes, 2007; Olhaberry et al., 2014; Field, 2017b). Pregnancy-related risk factors are the lack of pregnancy planning, undesired pregnancy, and the ambivalence about maternity (Bowen and Muhajarine, 2006). Maternal-related risk factors include stress, drug consumption, violence, conflicts with partners, low educational level (Escribe-Aguir et al., 2008; Field, 2017b), insecure attachment to their own mother (Murray et al., 1996; Bifulco et al., 2006), and adverse or traumatic experiences during childhood and adolescence (Buist and Janson, 2001; Nelson et al., 2002).

The treatment for depression usually includes psychotherapy, pharmacotherapy, or a combination of both. Regarding psychotherapy, cognitive–behavioral therapy has been demonstrated to be effective in the decrease of symptoms and remission of depression during pregnancy (O'Connor et al., 2016). Nevertheless, the adherence to psychotherapy is difficult (Rojas et al., 2015), and the outcome depends on the individual traits of the mothers (Miranda et al., 2017). In the recent years, new behavioral interventions have emerged as an alternative treatment for maternal depression, such as interpersonal psychotherapy, mindfulness, peer support groups, massage, tai chi, yoga, aerobic exercise, and sleep interventions (Field, 2017b; Ladyman et al., 2020; Lucena et al., 2020).

Pharmacotherapy is frequently used to treat depression: approximately one-third of pregnant depressive women use antidepressants (Ramos et al., 2007; Goodman and Tully, 2009; Jimenez-Solem et al., 2013; Molenaar et al., 2020). In line with the serotonergic theory of depression, which proposes that diminished activity of serotonin pathways plays a causal role in the pathophysiology of depression (Kerr, 1994), the most commonly prescribed antidepressants belong to the family of the selective serotonin reuptake inhibitors (SSRIs). SSRIs act by blocking the serotonin transporter (SERT), preventing serotonin recapture, which increases the extracellular concentration of physiologically released serotonin (Stahl, 1998; Gershon and Tack, 2007). Fluoxetine, sertraline, and citalopram are the most prescribed SSRIs (Kern et al., 2020; Molenaar et al., 2020).

Apart from its role as a neurotransmitter related to mood, serotonin appears to have a relevant role during development (Shuey et al., 1993; Buznikov et al., 2001; Kaihola et al., 2016). From this, the question about whether depression or antidepressants interfere with developmental process during pregnancy emerges. As the abovementioned effects of maternal depression at birth, negative effects of the use of antidepressants during pregnancy have been reported, including non-optimal birth outcomes (i.e., preterm delivery and lower Apgar scores), persistent pulmonary hypertension of the newborn, neonatal withdrawal/toxicity syndrome, greater internalizing behaviors at toddler age, and greater risk for autism spectrum disorder (Meltzer-Brody et al., 2011; Huybrechts et al., 2015; Field, 2017b). Regarding the craniofacial region, the use of SSRI has also been associated with bone defects like craniosynostosis and dental malformations, affecting mainly the proliferation and differentiation equilibrium in progenitor cells, as described in different experimental models (Shuey et al., 1992; Moiseiwitsch et al., 1998; Cray et al., 2014; Calibuso-Salazar and Ten Eyck, 2015; Durham et al., 2019), and associated with an increased risk of craniofacial malformations in humans (Alwan et al., 2007; Berard et al., 2015, 2017; Reefhuis et al., 2015; Gao et al., 2018).

Depression and the use of SSRIs have increased over the last few years (Global Burden of Disease Study, 2017). Therefore, it is necessary to build a systematic model to allocate the current knowledge that links depression, SSRI treatment, and craniofacial development. In this review, we performed a bibliographic search using search engines such as PubMed and Google Scholar, looking for cellular, animal, and human research that associates the role of serotonin during craniofacial development with maternal depression or the use of antidepressants. To provide a background to understand this topic, we primarily will describe craniofacial development and the general origin of craniofacial defects, to introduce then the role of serotonin in the craniofacial region development, describing the craniofacial defects related to the use of SSRI. We finally propose a model to explain how depression or antidepressants, as environmental factors, could generate craniofacial developmental defects in the offspring, by altering the stem/progenitor cell biology.

CRANIOFACIAL DEVELOPMENT AND THE ORIGIN OF CRANIOFACIAL DEFECTS

Human craniofacial congenital defects vary between 1 and 4% in different countries (Dolk, 2005; Canfield et al., 2006) having serious functional, aesthetic, and social consequences. This makes it relevant to identify the developmental processes involved in craniofacial congenital defects, and how genetic and environmental factors can alter them.

Vertebrate craniofacial development is characterized by a rich crosstalk between the three germ layers and neural crest-derived

cells (NCCs) (Couly et al., 2002; Rinon et al., 2007; Grenier et al., 2009; Marcucio et al., 2011; **Figure 1A**). During development, NCCs show multipotency (stemness) and migratory capabilities (Abzhanov et al., 2003; Adameyko and Fried, 2016). They delaminate alongside the edge of the neural plate and populate the craniofacial region, forming the progenitors for most facial bones, cartilages, salivary glands, and dental mesenchyme at the craniofacial region (Le Douarin et al., 2004). The defects in generation, migration, and differentiation of NCCs could generate a variety of apparently non-related diseases named neurocristopathies (Bolande, 1974). The advance of research and general understanding of NCC development in recent years has led to an increase in the number of reported neurocristopathies (Bolande, 1997; Sato et al., 2019).

Regarding craniofacial tissues, among the malformations typically manifested at birth are maxillary, zygomatic, and mandibular hypoplasia, cleft palate, and auricular defects. The etiology of neurocristopathies includes genetic mutations in the genes *Tcof1* and *Polr1* in Treacher–Collins syndrome, *Sox9* in Pierre Robin sequence, *Sox10* in Waardenburg syndrome,

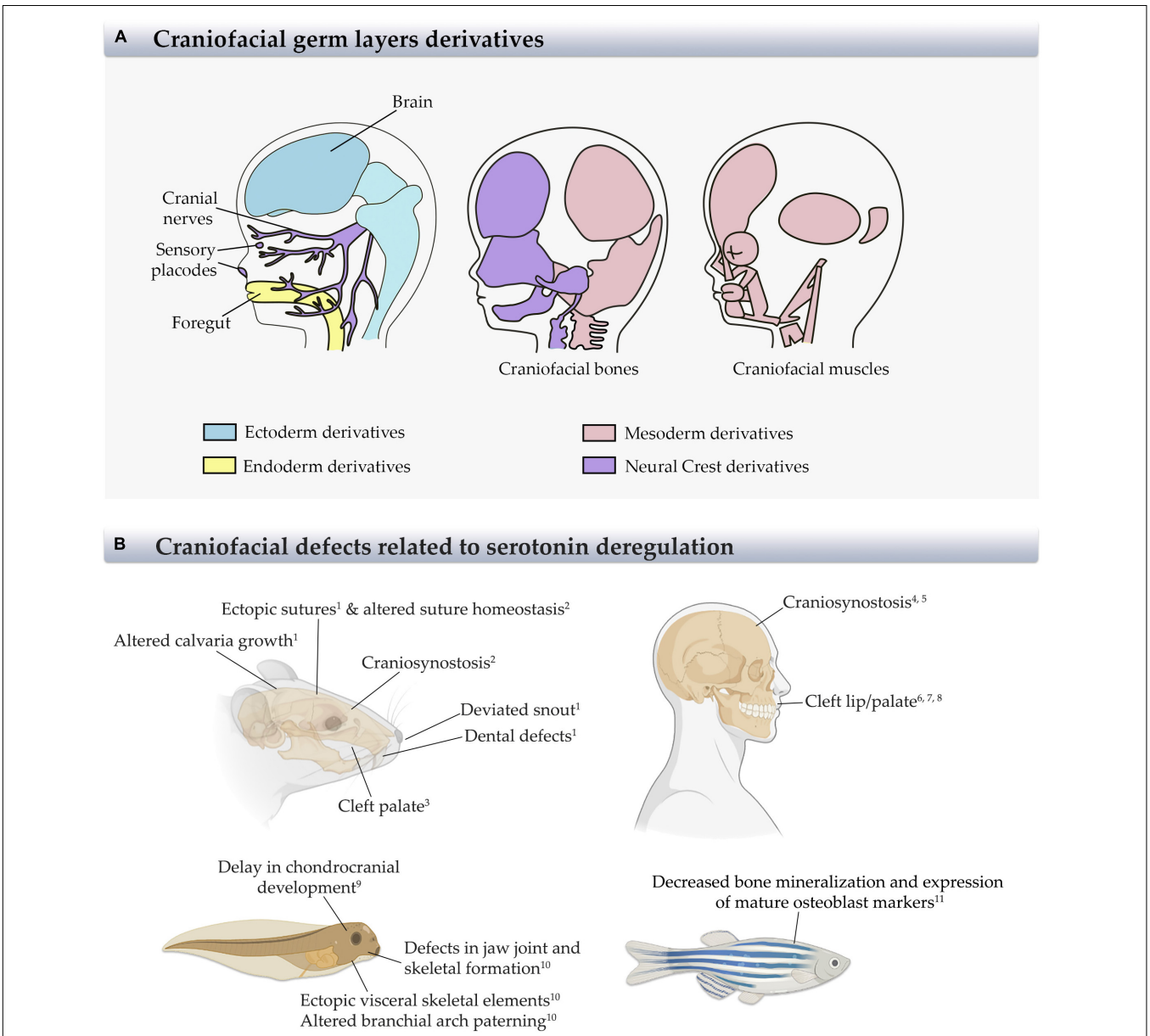

FIGURE 1 | Derivatives structures from germ layers and craniofacial defects in different animal models and humans. **(A)** Scheme of the craniofacial derivatives from ectoderm, mesoderm, endoderm, and neural crest (NCs) showing the main craniofacial structures and the germ layer from which they came. Modified from Carlson (2019). **(B)** Scheme of animal models and humans indicating the most relevant craniofacial defects generated by serotonin deregulation, as reported. References: [1]Cray et al., 2014; [2]Durham et al., 2019; [3]Cabrera et al., 2020; [4] Berard et al., 2017; [5]Alwan et al., 2007; [6]Colvin et al., 2011; [7]Louik et al., 2007; [8]Malm et al., 2011; [9]Calibuso-Salazar and Ten Eyck, 2015; [10]Reisoli et al., 2010; [11]Fraher et al., 2016.

and a region on chromosome 14q32 in Goldenhar syndrome. Additionally, environmental factors such as alcohol, folic acid deficiency, maternal diabetes, infection, and pharmaceutical agents, and their interaction with genetic mutations, have also been related to the development of neurocristopathies (reviewed in Sato et al., 2019; **Figure 1B**).

The growth of the skull is also an important process during craniofacial development. The skull sutures, zones in which flat bones contact, ossify during the first two postnatal decades, allowing the growth and expansion of the brain. When an imbalance between proliferation and differentiation in the suture cells and adjacent bones occurs, premature bone differentiation leads to premature closure of sutures and produces craniosynostosis (Twigg and Wilkie, 2015). Most of the craniosynostosis alter the shape of the skull, generating a secondary effect such as altered intracranial pressure, blindness, cognitive disabilities, and mental retardation; therefore, surgery is required as treatment (Durham et al., 2019). Craniosynostosis has a prevalence of 1:1,800–2,500 births, being associated to some genetic mutations (*Cdc45*, *Twist*, *Fgfr*, and *Tcf12*) and/or environmental factors including nicotine, hyperthyroidism in pregnant women, and importantly, the use of antidepressants (Twigg and Wilkie, 2015; Durham et al., 2017). The relationship between these environmental factors and craniosynostosis has been described in animal models, which show an altered proliferation and differentiation of stem/progenitor cells, and in humans, in which the newborns from mothers exposed to these disturbances have an increase in craniosynostosis prevalence (Shuey et al., 1992; Carmichael et al., 2008; Grewal et al., 2008; Browne et al., 2011; Berard et al., 2015, 2017; Durham et al., 2017, 2019; **Figure 1B**).

As the overall growth of the skull is important during craniofacial development, two characteristic craniofacial organs that can be affected during development and are extensively studied are teeth and salivary glands. Teeth and salivary gland development require a tight communication between the oral epithelium and the surrounding NCC-derived mesenchyme. Teeth develop through different stages including the initiation stage, bud stage, cup stage, bell stage, and posterior root formation (Ruch et al., 1995; Thesleff and Sharpe, 1997; Thesleff, 2003). During each stage, defects in the correct sequence of events that will form the teeth produce malformations such as agenesia, hypodontia, or tooth shape abnormalities, which can be presented alone or as part of a major syndrome. Similar to other craniofacial defects, teeth defects are related to well-characterized genetic mutations (*Msx1*, *Pax9*, *Axin2*, *Eda*, W*nt10A*, *Foxc1*, and *Pitx2*, among others) and/or environmental factors like ingestion of chemical substances (fluorides, tetracyclines, dioxins, and thalidomide), malnutrition, vitamin D deficiency, bilirubinemia, thyroid, and parathyroid disturbances, maternal diabetes, severe infections, and metabolic disorders (Brook, 2009; Klein et al., 2013; **Figure 1B**). As is observed for teeth, salivary gland development also proceeds through different stages: placode, bud, pseudoglandular, canalicular, and cytodifferentiation (Affolter et al., 2003; Patel et al., 2006; Knosp et al., 2012; Hauser and Hoffman, 2015; Chatzeli et al., 2017; Emmerson et al., 2017). Congenital genetic and/or environmental-caused defects during salivary gland development generate aplasic or ectopic glands, mainly associated to syndromes as Levy–Hollister syndrome, oculo–auriculo–vertebral spectrum (OAVS), Treacher–Collins syndrome, and Down syndrome (Togni et al., 2019).

In summary, craniofacial development is a highly sensitive process that occurs early during gestation. Congenital craniofacial defects are multifactorial and are associated with diverse genetic, environmental factors, and the interaction of both (Murray, 2002; Murray and Marazita, 2013; Nagy and Demke, 2014; Durham et al., 2017). Though most of the current research have focused on genetic factors, environmental factors need to be studied as well.

SEROTONIN SIGNALING COMPONENTS ARE PRESENT IN CRANIOFACIAL TISSUES

Serotonin is a monoamine synthesized intracellularly from L-tryptophan, released, and later degraded via monoamine oxidase action (Kirk et al., 1997; Sahu et al., 2018). The serotonin signaling is transduced to subcellular events by specific membrane receptors of different classes. Most of the serotonin receptors belong to the superfamily of G-protein-coupled receptors containing a predicted seven-transmembrane domain structure, coupled with Gαi, Gαq/11, or Gαs, given a plethora of biochemical pathways that could be influenced by serotonin receptor activation (Peroutka, 1994; Sahu et al., 2018). Conversely, the serotonin-3 receptor is a ligand-gated ion channel (Hoyer et al., 2002; Millan et al., 2008; Ori et al., 2013). Furthermore, serotonin can act intracellularly after being internalized by SERT or transported through the gap junction between neighboring cells. Then, it can act in two ways: binding to proteins such as Mad3 (protein related to checkpoint in cell division) and serotonin-2 receptor, or by serotonylation of several molecules (covalent addition of serotonin to glutamine residues) [reviewed in Berard et al. (2019)].

Serotonin controls a broad spectrum of biological process, including gastrointestinal motility and secretion, cardiovascular regulation, hemostatic processes, circadian rhythms, sleep–wake cycle, memory, and learning, perception of pain, and appetite and sexual behavior [reviewed in Berger et al. (2009)]. In the nervous system, serotonin has a well-known role as a neurotransmitter, whose imbalance is associated with human psychiatric disorders like depression, anxiety, obsessive–compulsive disorders, autism, and schizophrenia. The brain serotonin is mainly produced by neurons of the raphe nuclei and the pineal gland, in the latter, as a precursor of melatonin. Besides the brain, serotonin is produced by almost all cells, being enriched in the enterochromaffin and myenteric cells of the gut, representing about 95% of the total serotonin secretion (Tsapakis et al., 2012; Sahu et al., 2018).

In parallel to these roles in metabolism, serotonin has been implicated in several early developmental processes before the onset of neurogenesis, acting as a morphogen that regulates cell proliferation, migration, and differentiation. Some of the processes regulated by serotonin include left–right asymmetry

(Levin et al., 2006), neural crest cell formation and migration (Moiseiwitsch and Lauder, 1995; Vichier-Guerre et al., 2017), and heart, bone, and craniofacial development (Shuey et al., 1992, 1993; Yavarone et al., 1993; Moiseiwitsch and Lauder, 1996). In mammals, serotonin required for early development is produced by the embryo, as early as the two-cell stage (Amireault and Dube, 2005; Dube and Amireault, 2007; Kaihola et al., 2016), and from a source supplied by the maternal blood (Cote et al., 2007) and trophoblast placental cells (Bonnin and Levitt, 2011; Kaihola et al., 2015). Uptake of serotonin has been observed in cranial mesenchyme, heart, liver tissues, and, importantly, in migrating neural crest cells (Lauder and Zimmerman, 1988; Narboux-Neme et al., 2008; Vichier-Guerre et al., 2017; **Figure 2**).

Interestingly, in the craniofacial region, serotonin receptors are expressed at early stages, and their activation or inactivation are related with several developmental processes. In NCC explants and mouse embryos, the addition of an antagonist of the serotonin-1A receptor inhibited the migration of cranial NCCs (Moiseiwitsch and Lauder, 1995). In whole mouse embryo cultures, blocking the serotonin-2 receptor generates malformed embryos (Choi et al., 1997; Lauder et al., 2000; Bhasin et al., 2004), and in *Xenopus laevis*, it perturbs the development of the heart, face, and eyes (Reisoli et al., 2010). In embryonic mouse mandibular mesenchyme and explant cultures, antagonists for serotonin-2 and -3 receptors block the effects of serotonin on the expression of mandibular proteins (Moiseiwitsch and Lauder, 1997; **Figure 3**). Concomitantly, SERT is expressed in different regions of the mouse and rat craniofacial mesenchyme and cartilage from E14 to at least E18 (Moiseiwitsch and Lauder, 1997; Moiseiwitsch et al., 1998; Hansson et al., 1999; Lauder et al., 2000; Narboux-Neme et al., 2008; **Figure 2**). Similarly, sites of serotonin uptake and degradation are identified in mouse tooth germ (Lauder and Zimmerman, 1988; Shuey et al., 1992), and serotonin receptors are expressed in the epithelium of the tooth germ from the bud stage (Moiseiwitsch et al., 1998; Lauder et al., 2000). Serotonin synthesis and uptake have also been detected in palate shelves during palate formation (Wee et al., 1981; Zimmerman et al., 1981; Hirata et al., 2018; **Figure 2**).

The early expression of the serotonin pathway components and the developmental defects that produce their downregulation or upregulation, including the use of SSRIs, strongly indicate a role of serotonin in the development of craniofacial structures. This makes relevant to understand which cells are affected and what the underlying mechanism implied is.

SEROTONIN HAS A ROLE OVER STEM/PROGENITOR CELLS THAT INFLUENCES CRANIOFACIAL DEVELOPMENT

Different studies have shown that serotonin works as a dose-dependent growth regulatory signal for craniofacial progenitor cells. In neural crest mice explants (E9) and dissociated

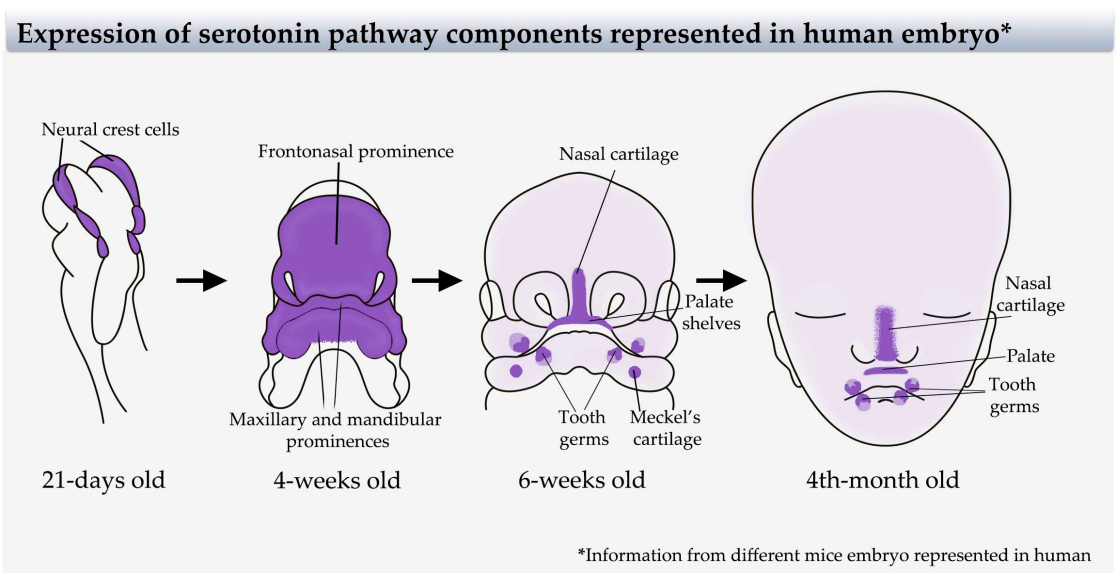

FIGURE 2 | Serotonin pathway component expression in the craniofacial region represented in the human embryo. Sites of serotonin signaling components expression [receptors and serotonin transporter (SERT)] extrapolated from mice embryo animal model (Moiseiwitsch and Lauder, 1995, 1996; Moiseiwitsch et al., 1998; Lauder et al., 2000) to a human embryo. *Left-to-right:* A 21-day-old human embryo (representing the information from E9.5 mice embryo) showing expression in neural crest cells. A 4-week-old human embryo (representing the information from E11.5 mice embryo) showing expression in the first pharyngeal arch and frontonasal prominence. A 6-week-old human embryo (representing the information from E13.5 mice embryo) showing specific expression in the tooth germ, palate, first arch cartilage, and nasal cartilage, and a wide light color representing the expression in the developing craniofacial skeleton. A 4-month-old human embryo (representing the information from E16.5 mice embryo) showing expression in tooth germ, palate, nasal cartilage, and wide light expression in the craniofacial skeleton. Modified from Adameyko and Fried (2016).

mandibular cells (E12), low levels of serotonin stimulate the migration of NCCs, mediated by serotonin-1A receptor. On the contrary, at high doses, serotonin inhibits the migration of less motile mandibular mesenchymal stem cells (MSCs) (Moiseiwitsch and Lauder, 1995). Similarly, the treatment with paroxetine (SSRI) in NCCs differentiated from human embryonic stem cells triggers an increased proliferation, migration, and AP2-α expression, an important gene involved in the bone plate fusion process in the skull. On the contrary, sertraline decreases the NCC proliferation and increases the expression of AP2-α, demonstrating that SSRIs alter the normal behavior of NCCs (Vichier-Guerre et al., 2017; **Figure 3** and **Table 1**).

In whole mice embryos and cultured frontonasal mass explants, the activation of serotonin-2B receptors promotes cell proliferation in the frontonasal mass (Bhasin et al., 2004) and mandibular mesenchyme cells exposed to serotonin (Buznikov et al., 2001). In mouse calvaria pre-osteoblastic cultured cells (MC3T3-E1), citalopram exposure produces an increase in markers of osteoblastic differentiation (Cray et al., 2014). Similarly, the proliferation rate increases in response to serotonin, and low concentrations of fluoxetine in human-derived induced osteoblast culture, and conversely, high levels of fluoxetine have an inhibitory effect on proliferation (Gustafsson et al., 2006). In ATDC5 cartilage cell line, SSRI treatment upregulates *Sox9* expression, a transcription factor that marks NCCs, and cartilage differentiation (Miyamoto et al., 2017). Interestingly, mice exposed to citalopram *in utero* (E13–E20) exhibit altered calvaria growth and craniofacial anomalies including ectopic sutures, single maxillary incisors, absence of incisor root, and deviated snout (Cray et al., 2014). Another study in mice determined that *in utero* exposure to citalopram increases the risk of craniosynostosis, due to a depletion of Gli1^{+} stem cells and altered homeostasis of the suture mesenchymal cells in the calvaria (Durham et al., 2019; **Figure 3** and **Table 1**).

Other animal models, different from mice and humans, show similar responses to serotonin imbalance. Frogs exposed to fluoxetine have a delay in chondrocranial development (Calibuso-Salazar and Ten Eyck, 2015). In *Xenopus laevis*, the

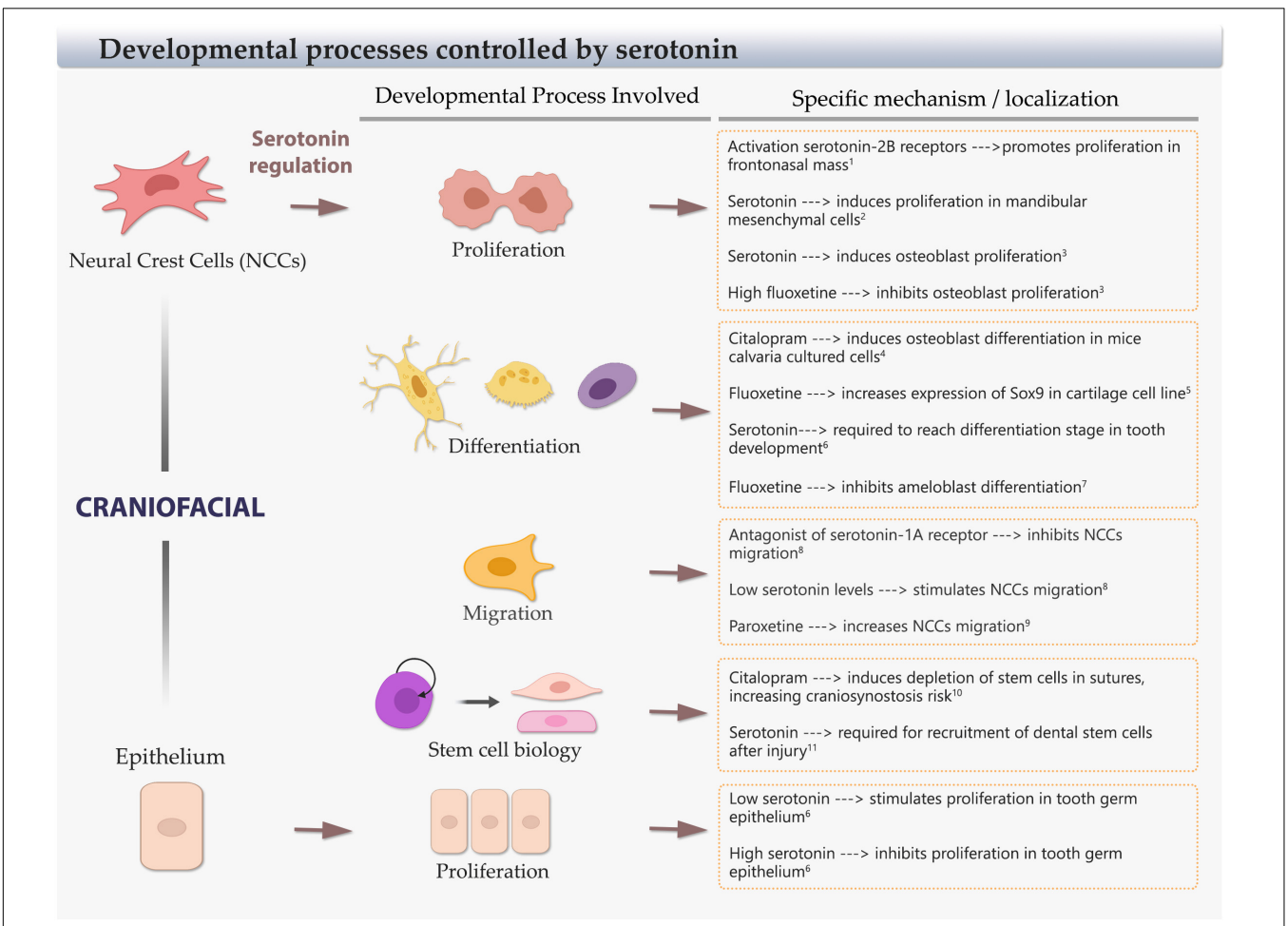

FIGURE 3 | Cellular developmental processes regulated by serotonin. Scheme of craniofacial neural crest cells (NCCs) and epithelial cells, and the main cellular processes controlled by serotonin: proliferation, differentiation, migration, and stem cell balance. The specific regulation, effect, and craniofacial territory/type of cell involved are included. References: [1]Bhasin et al., 2004; [2]Buznikov et al., 2001; [3]Gustafsson et al., 2006; [4]Cray et al., 2014; [5]Miyamoto et al., 2017;[6] Moiseiwitsch and Lauder, 1996; [7]Riksen et al., 2010; [8]Moiseiwitsch and Lauder, 1995; [9]Vichier-Guerre et al., 2017; [10]Durham et al., 2019; [11]Baudry et al., 2015.

TABLE 1 | Summary of main findings of research relating serotonin signaling pathway disruption and craniofacial development related effects.

Tissue Affected	Type of serotonin signaling disruption	Organ/tissue/cell effect	Involved/ affected factors	Model of study	Main methods	References
Bone (skull) and tooth	SSRI exposure	Smaller skull, shorter and narrower snout, skull ectopic suture, fusion of maxillary incisor and absence of root	FGFs	Mouse new-born	*In utero* exposition (E13 to E20) to SSRI. Analysis at P15. Citalopram dosage: 500 μg/day in drinking water.	Cray et al., 2014
Bone (skull)	SSRI exposure	Increased risk of craniosynostosis by depleting calvaria Gli1$^+$ stem cells	Gli1$^+$ calvaria stem cells	Mouse new-born	*In utero* exposition (E13 to E20) to SSRI. Analysis at P15. Citalopram dosage: 500 μg/day in drinking water.	Durham et al., 2019
Bone (Operculum)	SSRI exposure	Decreased bone mineralization and osteoblast-specific markers expression during embryogenesis. Reduced expression of osteoblast activity markers in cell culture	Runx2	Zebrafish embryo/hMSCs	SSRI exposition at 36 hpf - 130 hpf/hMSC 7d culture. Dosage: Citalopram 15 μM; Sertraline 30 μM.	Fraher et al., 2016
Bone (cell line)	SSRI exposure/Serotonin addition	Serotonin and low dose of SSRI promotes osteoblast proliferation. At high doses of SSRI proliferation is inhibited	Serotonin-2 receptor	MC3T3-E1 (murine pre-osteoblasts)	Fluoxetine dosage: 1 nM, 10 nM, 100 nM, 1 μM, 10 μM Serotonin addition: 1 nM, 10 nM, 100 nM, 1 μM, 10 μM, 50 μM	Gustafsson et al., 2006
-	SSRI exposure	Changes in migration and expression of bone plate fusion-associated factors	AP2-α	ESCs-derived NCCs	Paroxetine and sertraline dosage: 30 nM, 300 nM, 3 μM	Vichier-Guerre et al., 2017
Cartilage (Cell line and knees)	SSRI exposure	Increased Sox9 and decreased Axin2 and Mmp13 expression. Pro-chondrogenic effect on osteoarthritic (OA) model	Sox9	ATDC5/Osteoarthritic-induced rats	OA phenotype induced through surgical meniscus destabilization. OA model fluoxetine dosage: 50 μM, 100 μM, 200 μM injections Cell culture fluoxetine dosage:1 μM, 5 μM, 10 μM	Miyamoto et al., 2017
Hippocampus	SSRI exposure	Increased proliferation in hippocampal progenitors with reduced self-renewal and division	Sox2	Btg1 KO mouse (adult)	Fluoxetine (10 μM) injected intra peritoneal administered for 21 days, since 56 days or 15 months of age.	Micheli et al., 2018
-	Serotonin-2B receptor gain and loss of function	Loss of function leads to a loss of the jaw joint and altered first brachial arch. Gain of function produces abnormal craniofacial development	Serotonin-2B receptor	*Xenopus laevis* embryo	Loss of function viaserotonin-2B receptor morpholino. Gain of function using *in vitro* synthesized serotonin-2B receptor mRNA. Both microinjected at 2-4 cell stage embryos	Reisoli et al., 2010; Ori et al., 2013
Mandibular epithelium	SSRI exposure	Craniofacial defects: maxilla deficiency, absence of lens invagination and open cranial neural folds	-	Mouse embryo	E9 embryos were culture for 48h in presence of SSRI. Dosage: Fluoxetine 1 μM, 10 μM; Sertraline 5 μM, 10 μM, 20 μM.	Shuey et al., 1992
Tooth germ	SSRI exposure/Serotonin addition	Serotonin addition promoted transition between developmental stages.	-	Mouse embryo	E13 embryos mandible explants were culture up to 2 or 8 days. Fluoxetine dosage: 10 μM Serotonin addition: 10 nM, 1 μM, 100 μM	Moiseiwitsch and Lauder, 1996
Craniofacial mesenchyme and epithelia	Serotonin-2B receptor antagonists	Craniofacial malformations as hypoplastic forebrain/frontonasal process, hypoplastic maxilla/mandible, lack of lens invagination and neural tube defects	Serotonin-2B receptor	Mouse embryo	E9 embryos were culture for 48 h in presence of antagonists. Receptor Antagonists: Mianserin (1 μM, 10 μM), Ritanserin (0.1 μM, 1 μM), Ketanserin (1 μM, 10 μM)	Lauder et al., 2000
Craniofacial bone and cartilage	SSRI exposure	Delayed development of frontoparietal bones, mandible, nasal cartilage, and squamosal bones.	-	*Eleutherodactylus coqui* embryo	Embryos were culture from TS1 to TS15 (Townsend and Stewart staging). Fluoxetine dosage: 100 μM, 250 μM, 500 μM, 1 mM	Calibuso-Salazar and Ten Eyck, 2015

(Continued)

TABLE 1 | Continued

Tissue Affected	Type of serotonin signaling disruption	Organ/tissue/cell effect	Involved/ affected factors	Model of study	Main methods	References
Mandible	Serotonin-1A/2A-2C/3 receptors antagonists and serotonin addition	Serotonin addition stimulated tooth germ development at bud and bell stages. The same effect was inhibited by serotonin-1A receptor antagonist and reversed by the serotonin-3 receptor antagonist.	Serotonin-1A/2A-2C/3 receptors	Mouse embryo	E13 embryos mandible explants were culture up to 8 days. Serotonin addition: 10 nM, 1 μM, 100 μM. Receptor Antagonists (10 μM): NAN-190, Mianserin, Zofran	Moiseiwitsch et al., 1998
Dental pulp	Serotonin-2B/7 receptors antagonists	Altered tooth reparative process upon disrupted injury signals	Serotonin-2B/7receptors	Rat dental pulp injury	Gelatine hydrogel microspheres loaded with antagonists were implanted within the pulp just after lesion and followed up to 30 days. Receptor Antagonists (100nM): RS127445 (serotonin-2B receptor), SB269970 (serotonin-7 receptor)	Baudry et al., 2015
Ameloblast-like cell line	SSRI exposure/serotonin addition	Serotonin and SSRI treatment downregulated amelogenin, enamelin and MMP20 expression, as well as VEGF, MCP-1, and IP-10. Also, both treatments enhanced alkaline phosphatase activity	-	LS8	Cell cultures were analyzed at 1, 3 and/or 7 days. Fluoxetine dosage: 0.1 μM, 1 μM, 10 μM Serotonin addition: 0.1 μM, 1 μM, 10 μM	Riksen et al., 2010
Cranial neural crest and mandibular mesenchyme	Serotonin and serotonin-1A receptor antagonist addition	At higher concentrations of serotonin, the migratory capabilities of cranial neural crest were stimulated. The effect was reversed on mandibular mesenchyme cells	Serotonin and serotonin-1 Areceptor	Mouse embryo	NCCs and mandibular mesenchyme were obtained from E9 and E12 embryos, respectively. Serotonin addition: 10 nM, 100 nM, 1 μM, 10 μM, 100 μM. Receptor Antagonist (10 nM): NAN-190	Moiseiwitsch and Lauder, 1995

serotonin-2B receptor is the regulator of post-migratory NCCs without altering early steps of migration. Overexpression of this receptor induces ectopic visceral skeletal elements and alters the patterning of branchial arches. Additionally, loss-of-function experiments reveal that this receptor signaling is necessary for the formation of jaw joints and the mandibular arch skeletal elements (Reisoli et al., 2010). Incubation with SSRIs (citalopram and fluoxetine) during zebrafish development decreases bone mineralization and the expression of mature osteoblast-specific markers during embryogenesis (Fraher et al., 2016) (**Figure 3**, **Table 1**).

Mandible-forming cells and tooth germ development are also sensitive to fluctuations in serotonin levels. Serotonin exerts its effects through modifying the expression of growth factors, such as IGF-1, which is positively regulated by low-to-medium doses of serotonin, and activation of serotonin-1A and serotonin-4 receptors in micromass mandibular cell cultures (Lambert and Lauder, 1999). In addition, in mandibular micromass cultures and mandibular explants, serotonin and activation of specific serotonin receptors can modulate the extracellular matrix, increasing the expression of aggrecan and inhibiting the production of tenascin, two molecules relevant in craniofacial development (Moiseiwitsch and Lauder, 1997; Moiseiwitsch et al., 1998). In mouse mandibular explants, it has been described that serotonin facilitates the morphological transitions at the early stages of the tooth germ by regulating proliferation rates: whereas low concentrations of serotonin stimulate cell proliferation, high concentrations inhibit proliferation in different areas, shaping the dental epithelium and mesenchyme. Hence, in organ cultures without serotonin, tooth germ develops only up to the bud stage. When the medium is supplemented with serotonin, the cultured explants reach a late bell stage in a dose-dependent manner (Moiseiwitsch and Lauder, 1996). According to that, fluoxetine affects the interaction between epithelium and mesenchyme arresting tooth development at the early stages (Moiseiwitsch et al., 1998). Later, during the initial postnatal days, SSRI reduces the transcription of enamel proteins and secretion of vascular factors in mouse enamel organ and cultured ameloblast-like cells that indicate possible adverse effects of fluoxetine on amelogenesis (Riksen et al., 2010). In adult rats, platelet-derived serotonin has been related to the recruitment of dental stem cells after injury: when platelets come from rats with deficiency of serotonin storage, dentin reparation is impaired (Baudry et al., 2015). All the research presented suggests that the balance of serotonin signaling is important for the correct development of the mandible and teeth, potentially affecting the different developmental processes in which stem/progenitor cells and the differentiation of their progeny are involved (**Figure 3** and **Table 1**).

In the case of the salivary glands, they have a common progenitor with tooth germs generated from the same ectodermal-derived epithelium and NCC mesenchyme (Jimenez-Rojo et al., 2012; Chatzeli et al., 2017; Emmerson et al., 2017) and, therefore, being prone to be affected by a serotonin imbalance. Indeed, fluoxetine treatment modifies the salivary flow rate, mass, and cell volume, indicating its role in adult salivary gland function in rats and humans (Hunter and Wilson, 1995;

Turner et al., 1996; da Silva et al., 2009; Henz et al., 2009; Paszynska et al., 2013). Nevertheless, there are no studies showing the role of SSRI in salivary gland formation.

Palate formation has also been associated with serotonin signaling. Interestingly, one recent work indicates that mice exposed *in utero* to sertraline generate significantly more cleft palate than the control group (Cabrera et al., 2020). Thus, it is proposed that serotonin and antagonist of serotonin receptors alter the rotation of the palate shelves in mouse embryo culture (Wee et al., 1979, 1981; Zimmerman et al., 1981). Similarly, cleft lip with or without palate has an increasing risk in mothers that use SSRIs (Louik et al., 2007; Colvin et al., 2011; Malm et al., 2011).

Similar to the craniofacial tissues, serotonin also controls proliferation in the nervous system. Serotonin induces the proliferation of fetal hypothalamic neuroprogenitor cells *in vitro*, demonstrated by the increase in neurospheres and undifferentiated $Sox2^{+}$ stem cells, with a decrease in mature $NeuN^{+}$ neurons (Sousa-Ferreira et al., 2014). Importantly, on the adult dentate gyrus of *Btg1* knock-out mice, characterized by reduced self-renewal and proliferative capability, fluoxetine can reactivate the proliferation of neural stem cells in a similar manner that Sox2 overexpression does in these animals (Micheli et al., 2018) (**Table 1**). Interestingly, tooth germ, salivary glands, and palate have stem/progenitor cells that are positive for Sox2 and Sox9 transcription factors, which are affected by SSRI in chondrogenic and neural context, suggesting that these cells could be also affected in these organs (Gaete et al., 2015; Kawasaki et al., 2015; Chatzeli et al., 2017; Emmerson et al., 2017).

In conclusion, serotonin levels are associated with the regulation of proliferation, differentiation, and migration of craniofacial tissues and stem/progenitor cells including those that form bone, cartilage, tooth germ, salivary gland, and palate (**Figure 3**). All these processes are critical for the formation of the craniofacial region and can alter the cellular conditions with an outcome in craniofacial defects (**Figure 1**). Considering this, depression and antidepressants have the potential of causing craniofacial defects based on the interference in the extensive cellular and developmental process of the embryo (**Figure 3**).

FOX TRANSCRIPTION FACTORS AS A POTENTIAL CONNECTION BETWEEN SEROTONIN DEREGULATION AND DISRUPTED CRANIAL STEM CELL BIOLOGY

One interesting goal is to understand how the levels of serotonin are translated into transcription factor expression that leads to changes in proliferation, migration, and differentiation of craniofacial cells. Recently, the Forkhead transcription factor family, characterized by their DNA-binding domain called Forkhead box (Fox), has been associated with craniofacial development.

A modular expression of distinct subclasses of Fox proteins (Foxc/d/f) was observed in the zebrafish facial tissue, linked with important craniofacial signaling pathways like Fgf, Bmp, and Hh among others. Additionally, using TALENs (transcription-activator-like effector nuclease) and CRISPR/Cas9 technologies to generate mutant zebrafish embryos for specific Fox genes, different facial cartilage and tooth defects were detected depending on the specific mutated genes, showing that Fox proteins are required for craniofacial development (Xu et al., 2018). Foxc1 function is required for access to chondrocyte-specific enhancers in zebrafish face; within this subset of cartilage elements, approximately a third of them have Fox and Sox response elements, suggesting that Foxc1 could promote Sox9 binding to those enhancers by increasing chromatin accessibility (Xu et al., 2021). Foxc2 could cooperate with Foxc1 in the development of the cranial base, since both are co-expressed in this area during mouse craniofacial development. Foxc2 silencing through the Cre-recombinant system showed a lack of ossification in the presphenoid, while Foxc1 silencing exhibit a non-ossification of the presphenoid, a deformed alisphenoid, and severe loss in the anterior part of the basisphenoid (Takenoshita et al., 2021). These studies introduce Fox proteins as important players to consider during craniofacial development.

Among the Fox proteins, the FoxO subfamily transduces environmental signals, affecting gene expression associated with cell proliferation, differentiation, apoptosis, and metabolism, among other processes (Carlsson and Mahlapuu, 2002; Benayoun et al., 2011). In the last years, there has been increasing evidence linking FoxO proteins to the regulation of bone formation (Huang et al., 2020; Ma et al., 2020). It has been demonstrated that FoxO1 functions as an early regulator of osteogenic differentiation in MSCs. FoxO1 silencing leads to a 20% reduction in the size of the mandible, premaxilla, and nasal bones of mice embryos, in addition to a 40% decrease in ossification on the palatine process through direct interaction with Runx2, an important factor in craniofacial bone differentiation (Teixeira et al., 2010). Runx2 has been proposed as a mediator for the gut-derived serotonin suppressive action on the bone formation, with a bimodal action on the tissue. At the physiological circulating serotonin levels, there exists a balance in FoxO1 expression promoting osteoblast proliferation. On the contrary, at high serotonin levels, the balance is disrupted increasing its transcriptional activity that suppresses cell cycle progression genes (Kode et al., 2012; **Figure 4**). Using *C. elegans*, it was observed that a serotonin deficit promotes nuclear accumulation of Daf-16, a FoxO ortholog (Liang et al., 2006). An enhancement of serotoninergic activity by d-fenfluramine treatment increased the inhibitory phosphorylation of FoxO1 in several regions of the mouse brain (Polter et al., 2009), adding evidence of FoxO regulation by serotonin in the mammalian brain. On the other hand, serotonin can improve hematopoietic stem/progenitor cell survival through the inhibition of the AKT-FoxO1 signaling pathway during embryonic development (Lv et al., 2017).

FoxO1 acts as a pluripotency regulator in embryonic stem cells interacting with Sox2 and Oct4, strong pluripotency regulators, through modulating their expression (Zhang et al., 2011; Ormsbee Golden et al., 2013). Other regulatory actions have been reported for FoxO1 on the craniofacial stem/progenitor

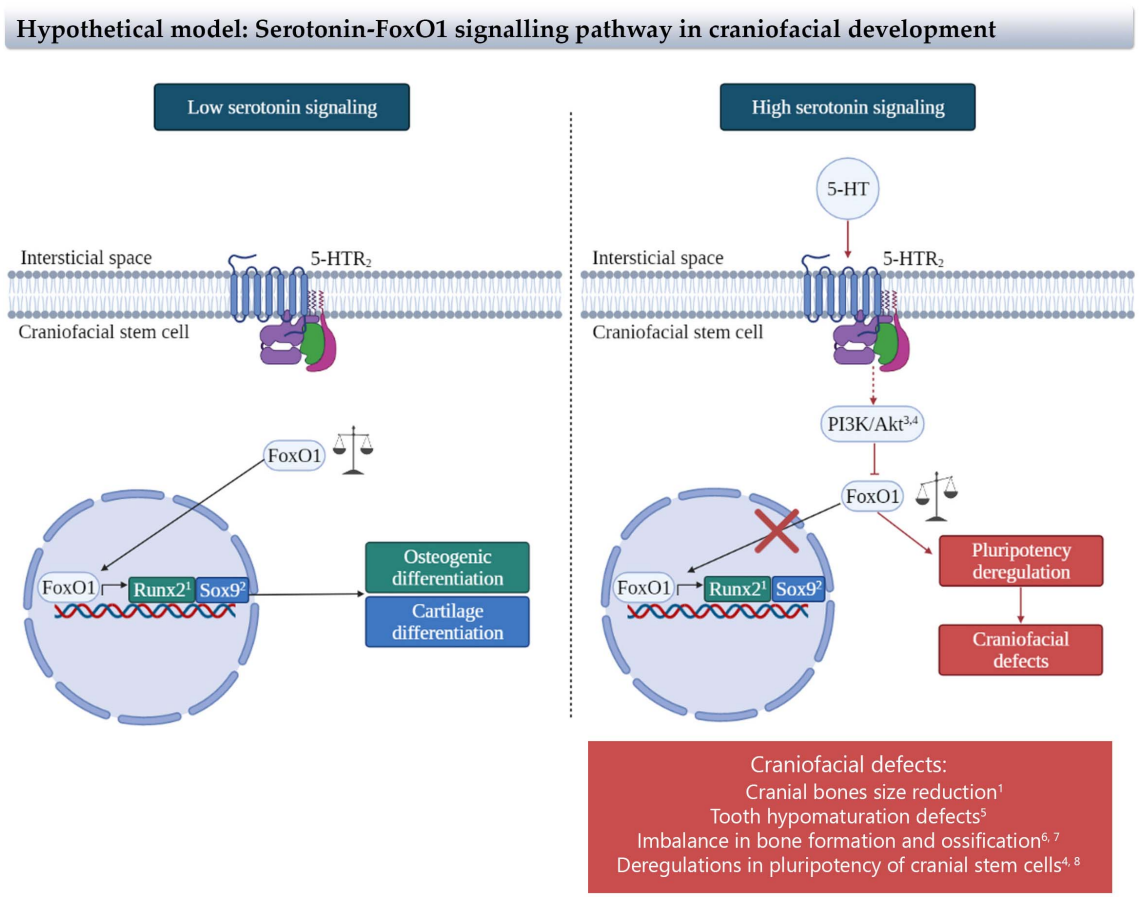

FIGURE 4 | Representation of the proposed link between serotonin and craniofacial defects mediated by FoxO1 transcription factor. Our hypothetical model proposes that under low serotonin signaling, FoxO1 enters to the nucleus generating the transcription of osteogenic (Runx2) and cartilage (Sox9) differentiation genes promoting the differentiation of bones and cartilages. On the contrary, under high serotonin signaling, the activation of the serotonin two receptor, through PI3K/AKT signaling pathway, impedes the entrance of FoxO1 to the nucleus, generating an imbalance in the pluripotency genes related to craniofacial defects. Craniofacial defects observed are included. References: [1]Teixeira et al., 2010; [2]Kurakazu et al., 2019; [3]Lv et al., 2017; [4]Ormsbee Golden et al., 2013; [5]Poche et al., 2012; [6]Almeida et al., 2007; [7]Iyer et al., 2013; [8]Zhang et al., 2011.

marker Sox9. Thus, *FoxO1* knock-down leads to a lower expression of Sox9 in ATDC5 cells (Kurakazu et al., 2019). The same study showed that both FoxO1 and Sox9 start to increase their expression at the same time during chondrogenic differentiation, suggesting that both transcription factors interact to contribute to the differentiation process. This cooperation between both transcription factors has been previously suggested by the identification of Fox consensus binding motifs highly enriched in Sox9-bound enhancers of chondrocytes genes (Ohba et al., 2015; **Figure 4**).

Furthermore, FoxO genes have the capacity to antagonize Wnt/β-catenin signaling through its association with β-catenin that blocks its interaction with TCF/LEF transcription factors, attenuating bone formation in bipotential osteoblast precursors. This effect has been proposed as a molecular mechanism for the possible loss of periodontal ligament, bone, and tooth derived from periodontal disease (Almeida et al., 2007; Galli et al., 2011; Iyer et al., 2013). Hence, tooth development could be also affected by serotonin-derived FoxO deregulation. Experiments using ameloblast-specific knock-out for *FoxO1* showed mice with enamel hypomaturation defects, resulting in faster attrition of the teeth during mice life (Poche et al., 2012).

Additionally, it has been reviewed that FoxO genes are involved in the regulation of the behavioral manifestation of depression. These proteins are not only expressed in brain areas that respond to emotional stimuli but also are related to circadian rhythm regulation, for which disruptions are associated with major depression (Wang et al., 2015). In a recent study, *FoxO1* mRNA and protein levels were reduced in the prefrontal cortex of depressive postpartum mice induced through chronic unpredictable stress treatments (Liu et al., 2020). Mice with brain knock-out for *FoxO1* display increased depressive behaviors and reduced anxiety (Polter et al., 2009).

Altogether, these studies suggest that FoxO1 could be part of the mechanism involved in the craniofacial defects due to the disrupted serotonin levels present in depressed mothers. Here, we propose a model in which FoxO1 acts as an integrator of

the serotonin signaling with the specific stem/progenitor cells involved in the craniofacial development (see **Figure 4**).

THE USE OF SEROTONIN-RELATED ANTIDEPRESSANTS INCREASES THE RISK OF CRANIOFACIAL DEVELOPMENT DEFECTS IN HUMANS

Although there is sufficient biological basis to establish an association between serotonin deregulation and SSRI use during pregnancy as environmental factors affecting craniofacial normal development, it remains a controversial topic in the clinical field. Various knowledge resources to investigate alterations in craniofacial development patterns such as genome-wide association studies (GWAS), dysmorphology, twin family, and animal and population studies are highly available. The last two approaches are the most suitable for elucidating the association between depression/SSRIs and craniofacial defects.

Prospective cohort investigations have been published with the aim of clarifying the association between antidepressant use during pregnancy and major congenital malformations. Berard et al. (2017) determined the association between first-term exposure to antidepressants and the risk of major congenital malformations in a cohort of depressed/anxious women. These data were obtained from the Quebec Pregnancy Cohort, including all pregnancies diagnosed with depression or anxiety, or exposed to antidepressants in the 12 months prior to pregnancy that ended with a live-born child. When looking at the specific types of antidepressants used during the first trimester, only the SSRI citalopram increased the risk of major congenital malformations [adjusted odds ratio (OR) 1.36, 95% CI 1.08–1.73], although there was a trend toward an increased risk for the most frequently used antidepressants. Regarding the craniofacial territory, citalopram increased the risk of craniosynostosis (adjusted OR 3.95, 95% CI 2.08–7.52), tricyclic antidepressants (TCA) were associated with eye, ear, face, and neck defects (adjusted OR 2.45, 95% CI 1.05–5.72), indicating that antidepressants with effects on serotonin reuptake during embryogenesis increased the risk of some craniofacial malformations in a cohort of pregnant women with depression (Berard et al., 2017). Using the same population-based cohort study in Quebec, the authors concluded that sertraline increases the risk of craniosynostosis (OR 2.03, 95% CI 1.09–3.75) when it is compared with depressed women not using pharmacological antidepressant therapy. In addition, non-sertraline SSRIs were associated with an increased risk of craniosynostosis (OR 2.43, 95% CI, 1.44–4.11) (Berard et al., 2015). In another cohort population study from Northern Denmark, SSRI treatments were associated with an increased risk of malformations (OR 1.3, 95% CI 1.1–1.6) (Kornum et al., 2010). These results were confirmed by a systematic review that analyzed different studies of major congenital malformation cohort populations. In general, the use of SSRIs was associated with an increased risk of overall major congenital anomalies (OR 1.11, 95% CI 1.03–1.19). Similar significant associations were observed using maternal citalopram exposure (OR 1.20, 95% CI 1.09–1.31), fluoxetine (OR 1.17, 95% CI 1.07–1.28), and paroxetine (OR 1.18, 95% CI 1.05–1.32) (Gao et al., 2018).

In a case-control study (major birth defects vs. control) using an expanded dataset from the National Birth Defects Study of the United States population, the mothers of the children were asked about the use of antidepressants during the first trimester of pregnancy. Maternal SSRI consumption was associated with craniofacial defects: anencephaly (adjusted OR 2.4, 95% CI 1.1–5.1) and craniosynostosis (adjusted OR 2.5, 95% CI, 1.5–4.0) (Alwan et al., 2007). These results were confirmed by the systematic review, determining an increased odds ratio for birth defects with paroxetine (anencephaly OR 3.2, 95% CI 1.6–6.2) and fluoxetine (craniosynostosis OR 1.9, 95% CI 1.1–3.0) (Reefhuis et al., 2015).

Most clinical studies have the difficulty to separate the effects of the underlying depression and the use of antidepressants. One control-case study that considers this variable, comparing the offspring defects of women with unmedicated depression, women with treated depression and women without depression, determined that compared with women without depression, major congenital anomalies were not associated with unmedicated depression (adjusted OR 1.07, 95% CI 0.96–1.18), SSRIs (adjusted OR 1.01, 95% CI 0.88–1.17), or TCAs (adjusted OR 1.09, 95% CI 0.87–1.38) (Ban et al., 2014). A previous work found an increased risk of major congenital anomalies in infants born from women who took SSRIs in the first trimester of pregnancy (adjusted OR 1.33, 95% CI 1.16–1.53), whereas the correlation was not significant for women who paused their SSRI intake (adjusted OR 1.27, 95% CI 0.91–1.78) (Jimenez-Solem et al., 2013). This issue was considered by the systematic review of Gao et al. (2018), in which they studied a population of women with a psychiatric diagnosis (depression or anxiety) as a different group of comparison. No significantly increased risk was observed in this group compared with the control group (major congenital anomalies, OR 1.04, 95% CI 0.95–1.13) (Gao et al., 2018). From these studies, we can infer that depression itself is not a risk factor for congenital anomalies. However, more research is still necessary to conclude this.

Despite the limitations and the different results between the cited studies, they all share the conclusion that SSRI usage during the first trimester of pregnancy is associated with a higher risk of congenital malformations and specifically craniofacial defects, in which a higher risk of craniosynostosis and other defects with some SSRIs are reported. All the studies presented here emphasized that an increasing number of women with depression during pregnancy is being diagnosed and that the use of SSRIs has been increased in the past years. Thus, it is important that to review its use in pregnant or reproductive-age women. Therefore, these results should have direct implications on their clinical management.

FUTURE PERSPECTIVES

The treatment of maternal depression during pregnancy with a combination of psychotherapy and antidepressants is widely

used, however, some studies reveal negative effects: The use of SSRI antidepressants increase the risk of congenital craniofacial defects in the newborn. It is important to highlight that maternal depression impacts the mother–fetus/baby dyad, and this should be considered during prevention, diagnosis, and treatment. An interdisciplinary approach that considers biological, clinical, psychological, social, and familiar aspects is also fundamental (**Figure 5**). New treatments should include the provision of a support network and the identification of lifestyle risk factors that may contribute to maternal depression (diet, physical activity, etc.), and weigh the possibility of adherence and prejudices about the selected treatment.

The application of early preventive intervention programs that increases wellness and promotes the mental health of mothers and their children, considering that the previous history and habits of the mother is of major relevance. To take the best decision for the treatment for each dyad, it is necessary to perform more longitudinal studies that consider the time and comorbidities of maternal depression and the impact on the offspring. These methods could include the implementation of scalable prenatal approach models: universal prevention→universal screening→prevention indicated for risk groups: early low-, medium-, and high-intensity specialized intervention (all based on evidence). This model can be represented as a pyramid to understand that the basics should be attended widely, escalating over more specific groups and therapies (**Figure 6**). Additionally, it is important to promote high-quality research in innovative treatments for depression, for instance, food supplements (Sparling et al., 2017) or transcranial magnetic stimulation (Kim et al., 2019). Finally, we think it is important to build, review, and recommend "decision aid protocols" to analyze individually the risk–benefit balance of the antidepressant treatment. Nowadays, this is of particular importance when the percentage of depressive women has increased over the last years (Global Burden of Disease Study, 2017).

As we described in this review, the craniofacial region appears to be especially sensitive to changes in serotonin signaling, where the imbalance generates defects in bone development, cartilage maturation, tooth germ, and palate formation. Even the effects of depression itself appear to be marginal in epidemiological studies; the use of SSRI that cross through the placenta (Rampono et al., 2009) could affect the development of the fetus, increasing the risk of craniofacial defects. Interestingly, at the time when the craniofacial region is actively forming, most women are not aware of being pregnant, so if they are using an SSRI, probably they will

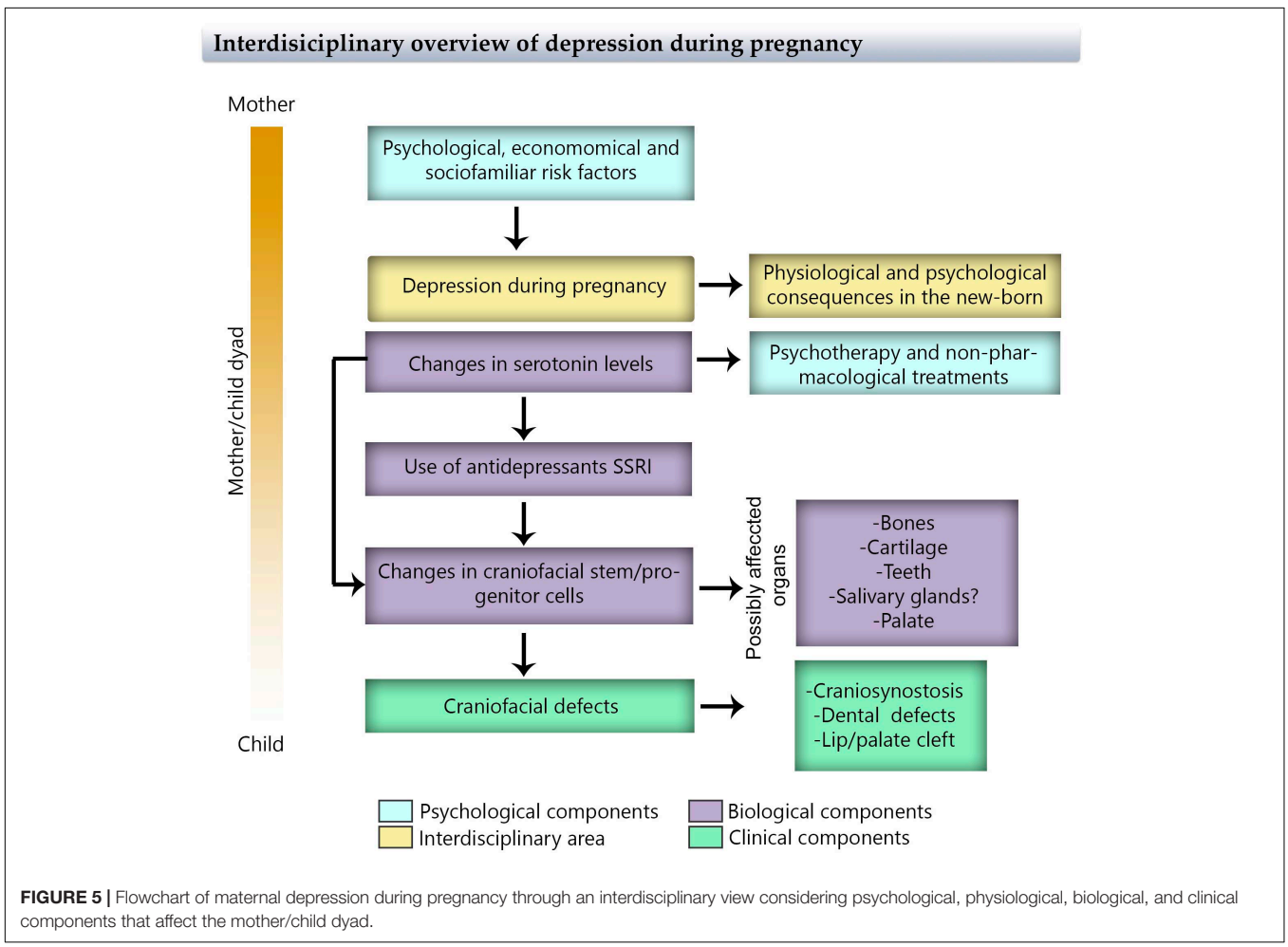

FIGURE 5 | Flowchart of maternal depression during pregnancy through an interdisciplinary view considering psychological, physiological, biological, and clinical components that affect the mother/child dyad.

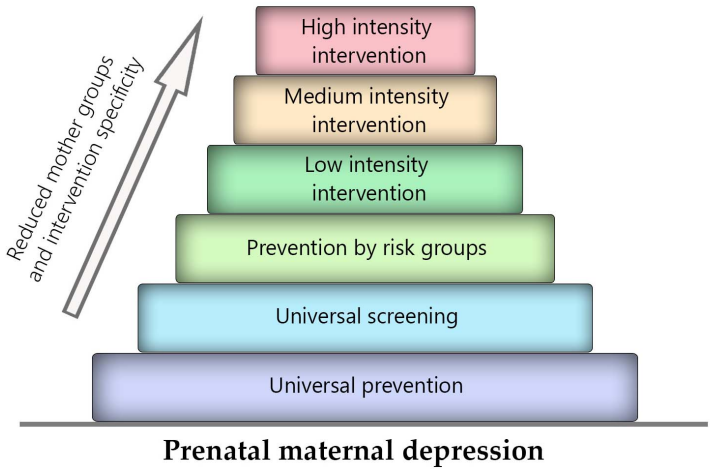

FIGURE 6 | Scale of proposed approaches for maternal depression interventions. This pyramid represents the size of the interventions for maternal depression, indicating that the basis should be attended wide and escalating over more specific groups and therapies.

continue to do so. Thus, the decision to prescribe antidepressant medication during pregnancy or on fertile women must be weighed against the risks of untreated maternal depression.

In our revision, we found limited research about biological aspects linking serotonin and craniofacial defects, indicating a great necessity to investigate this topic. This gained special relevance in light of the prevalence and clinical problems that the deregulation of serotonin implies during development. Importantly, most of the publications in the biological field are from decades ago, so the advantage of cutting-edge methods is not employed. New experimental models can be used to explain the underlying mechanisms of clinical problems related to craniofacial defects, including genetic and/or environmental etiology. Models like zebrafish and frog larva offer a great possibility to test not only pollutants such as bisphenol but also drugs such as SSRI, by adding them directly into the liquid growth medium, allowing to test different doses and drugs (fluoxetine, citalopram, and sertraline, etc.) (Calibuso-Salazar and Ten Eyck, 2015). Organ culture also offers similar advantages to test diverse doses and drugs by adding them directly to the culture medium (Sánchez et al., 2018). These experiments can provide valuable information about serotonin regulation in a quick and easy manner, which then can be complemented with *in vivo* studies using, for example, mice models for depression (Krishnan and Nestler, 2011; Planchez et al., 2019) or using SSRIs during pregnancy in murine models.

Here, we mentioned that the mechanism by which serotonin deregulation could affect craniofacial development is not totally elucidated, but that this includes developmental biology processes and the biology of stem/progenitor cells. Accordingly, NCCs and MSCs appear to be the most affected cells, especially given their proliferative and migrative capacities that impact over facial and skull bone, cartilage, palate, and tooth formation. The similarities between the tooth and salivary gland formation, and the influence of serotonin in the neural-crest derived mesenchyme, make evident the necessity of future studies about how serotonin deregulations could affect salivary gland development.

In this review, we propose that the transcription factor FoxO1 could be implicated linking the misregulation of serotonin levels with the different processes affected during craniofacial formation, disrupting the stem/progenitor cell biology. FoxO1 has a role in craniofacial tissue development (bone, cartilage, and tooth) and function within the stem cell regulation (Xu et al., 2018, 2021; Takenoshita et al., 2021). Moreover, it has a capacity to respond to changes in serotonin concentrations, being involved in the manifestation of major depressive disorders (Polter et al., 2009; Wang et al., 2015). All these together suggest that FoxO1 functions as a potential link between the craniofacial development and disrupted serotoninergic signaling by a specific context/environment. However, more studies are necessary to determine this hypothesis and the mechanism disrupted by the changes in serotonin levels by depression or SSRI use.

Regarding the clinical research field, we need to consider some limitations, such as difficulties on patient recruitment, withdrawal of patients, insufficient statistical power, issues with the classification of birth defects, the presence of confounders, or poor information about the medication exposure. Additionally, it is difficult to determine an SSRI dose-response effect because, in general, the information comes from maternal reports that are imprecise. A similar difficulty occurs with the type of antidepressants because the mothers were usually asked about the commercial name of the drug, generating an under- or over-representation of some antidepressants and possible bias in

the responses. Another important limitation is the presence of confounders such as smoking, folic acid, alcohol, or other drug intakes that are commonly present in the lifestyles of mothers with depression. Although the study design tried to consider these variables, it is not completely reliable given that these depends on patient reports.

Randomized clinical trials contrasting a group of depressed pregnant women with and without pharmacological treatment would allow us to further elucidate the relationship between antidepressants and congenital malformations. Currently, a randomized placebo-controlled trial on depressed mothers is being conducted in Stockholm; the results in the child exposed or not exposed to SSRI *in utero* will be analyzed (Heinonen et al., 2018). In this way, while current systematic reviews (Uguz, 2020) of meta-analyses examining the relationship between maternal use of SSRI during pregnancy and congenital anomalies have suggested a significant positive association between the use of SSRIs and the risk of major congenital anomalies, further large-scale prospective observational studies, and meta-analyses on the effects of SSRIs are required to reach definitive conclusions. However, since risk estimates for adverse events are similar in randomized trials and observational studies, the findings described in this review have implications for clinical practice (Golder et al., 2011).

In conclusion, serotonin appears to be involved in many developmental processes and the deregulation of its signaling, and the use of SSRI antidepressant leads to an increased risk of craniofacial development defects. Maternal depression during pregnancy needs to be carefully treated, diminishing the use of pharmacotherapy, and highlighting psychotherapy and alternative tools for the treatment, especially in minor and middle depression. Serotonin can affect the balanced role of NCCs and MSCs, but more research is necessary to determine the mechanism by which serotonin could influence the development of craniofacial tissues with special attention to stem/progenitor cells, aiming to discover alternative pathways to prevent the craniofacial development defects generated.

AUTHOR CONTRIBUTIONS

NS, JJ-B, and MG reviewed the literature, wrote the developmental biology sections of the review, and formulated the figures and tables. MO, AM, MM, and PF reviewed the literature and wrote the psychological sections of the review. HG-O and FB reviewed the literature and wrote the clinical section of the review. NS and MG edited all the sections. All authors contributed to the discussion of the document.

FUNDING

NS received funding from the Fondo Nacional de Desarrollo Científico y Tecnológico (FONDECYT) from the Agencia Nacional de Investigación y Desarrollo de Chile (ANID) Postdoctorate fellowship no. 3190798, in which MG is the Academic Researcher and JJ-B is Research Associate. AM received funding from the ANID, Scholarship Program Doctorado Nacional 2020 no. 21200074. PF received funding from the ANID, Scholarship Program, Doctorado Nacional 2019 no. 21190745. Article publication was partially financed by the Millennium Institute for Research in Depression and Personality (MIDAP), Chile, ICS13_005. NS, JJ-B, MO, HG-O, AM, MM, PF, FB and MG are researchers in the Interdisciplinary Research Funding II180016 from the Vicerrectoría de Investigación of Pontificia Universidad Católica de Chile (VRI).

ACKNOWLEDGMENTS

We thank the Interdisciplinary Research Funding II180016 from the Pontificia Universidad Católica de Chile in funding the project that gathered the interdisciplinary group that wrote this review. We also thank Esteban G. Contreras for critical review of the manuscript. We thank Constanza Daza (conny.daza.c@gmail.com), for performing **Figures 1A** and **2** illustrations. **Figures 1B**, **3** and **4** were created using BioRender.com under academic account license.

REFERENCES

Abzhanov, A., Tzahor, E., Lassar, A. B., and Tabin, C. J. (2003). Dissimilar regulation of cell differentiation in mesencephalic (cranial) and sacral (trunk) neural crest cells in vitro. *Development* 130, 4567–4579. doi: 10.1242/dev.00673

Adameyko, I., and Fried, K. (2016). The nervous system orchestrates and integrates craniofacial development: a review. *Front. Physiol.* 7:49. doi: 10.3389/fphys.2016.00049

Affolter, M., Bellusci, S., Itoh, N., Shilo, B., Thiery, J. P., and Werb, Z. (2003). Tube or not tube: remodeling epithelial tissues by branching morphogenesis. *Dev. Cell* 4, 11–18. doi: 10.1016/s1534-5807(02)00410-0

Almeida, M., Han, L., Martin-Millan, M., O'Brien, C. A., and Manolagas, S. C. (2007). Oxidative stress antagonizes Wnt signaling in osteoblast precursors by diverting beta-catenin from T cell factor- to forkhead box O-mediated transcription. *J. Biol. Chem.* 282, 27298–27305. doi: 10.1074/jbc.M702811200

Alwan, S., Reefhuis, J., Rasmussen, S. A., Olney, R. S., Friedman, J. M., and National Birth Defects Prevention Study (2007). Use of selective serotonin-reuptake inhibitors in pregnancy and the risk of birth defects. *N. Engl. J. Med.* 356, 2684–2692. doi: 10.1056/NEJMoa066584

Amireault, P., and Dube, F. (2005). Serotonin and its antidepressant-sensitive transport in mouse cumulus-oocyte complexes and early embryos. *Biol. Reprod.* 73, 358–365. doi: 10.1095/biolreprod.104.039313

Ban, L., Gibson, J. E., West, J., Fiaschi, L., Sokal, R., Smeeth, L., et al. (2014). Maternal depression, antidepressant prescriptions, and congenital anomaly risk in offspring: a population-based cohort study. *BJOG* 121, 1471–1481. doi: 10.1111/1471-0528.12682

Baudry, A., Alleaume-Butaux, A., Dimitrova-Nakov, S., Goldberg, M., Schneider, B., Launay, J. M., et al. (2015). Essential roles of dopamine and serotonin in tooth repair: functional interplay between odontogenic stem cells and platelets. *Stem Cells* 33, 2586–2595. doi: 10.1002/stem.2037

Benayoun, B. A., Caburet, S., and Veitia, R. A. (2011). Forkhead transcription factors: key players in health and disease. *Trends Genet.* 27, 224–232. doi: 10.1016/j.tig.2011.03.003

Berard, A., Levin, M., Sadler, T., and Healy, D. (2019). Selective serotonin reuptake inhibitor use during pregnancy and major malformations: the importance of serotonin for embryonic development and the effect of serotonin inhibition on the occurrence of malformations. *Bioelectricity* 1, 18–29. doi: 10.1089/bioe.2018.0003

Berard, A., Zhao, J. P., and Sheehy, O. (2015). Sertraline use during pregnancy and the risk of major malformations. *Am. J. Obstet. Gynecol.* 212, e791–e795. doi: 10.1016/j.ajog.2015.01.034

Berard, A., Zhao, J. P., and Sheehy, O. (2017). Antidepressant use during pregnancy and the risk of major congenital malformations in a cohort of depressed pregnant women: an updated analysis of the Quebec Pregnancy Cohort. *BMJ Open* 7:e013372. doi: 10.1136/bmjopen-2016-013372

Berger, M., Gray, J. A., and Roth, B. L. (2009). The expanded biology of serotonin. *Annu. Rev. Med.* 60, 355–366. doi: 10.1146/annurev.med.60.042307.110802

Bhasin, N., LaMantia, A. S., and Lauder, J. M. (2004). Opposing regulation of cell proliferation by retinoic acid and the serotonin2B receptor in the mouse frontonasal mass. *Anat. Embryol. (Berl.)* 208, 135–143. doi: 10.1007/s00429-004-0380-7

Bifulco, A., Kwon, J., Jacobs, C., Moran, P. M., Bunn, A., and Beer, N. (2006). Adult attachment style as mediator between childhood neglect/abuse and adult depression and anxiety. *Soc. Psychiatry Psychiatr. Epidemiol.* 41, 796–805. doi: 10.1007/s00127-006-0101-z

Bolande, R. P. (1974). The neurocristopathies: a unifying concept of disease arising in neural crest maldevelopment. *Hum. Pathol.* 5, 409–429.

Bolande, R. P. (1997). Neurocristopathy: its growth and development in 20 years. *Pediatr. Pathol. Lab. Med.* 17, 1–25.

Bonnin, A., and Levitt, P. (2011). Fetal, maternal, and placental sources of serotonin and new implications for developmental programming of the brain. *Neuroscience* 197, 1–7. doi: 10.1016/j.neuroscience.2011.10.005

Bowen, A., and Muhajarine, N. (2006). Prevalence of antenatal depression in women enrolled in an outreach program in Canada. *J. Obstet. Gynecol. Neonatal. Nurs.* 35, 491–498. doi: 10.1111/j.1552-6909.2006.00064.x

Brook, A. H. (2009). Multilevel complex interactions between genetic, epigenetic and environmental factors in the aetiology of anomalies of dental development. *Arch. Oral. Biol.* 54(Suppl. 1), S3–S17. doi: 10.1016/j.archoralbio.2009.09.005

Browne, M. L., Hoyt, A. T., Feldkamp, M. L., Rasmussen, S. A., Marshall, E. G., Druschel, C. M., et al. (2011). Maternal caffeine intake and risk of selected birth defects in the National Birth Defects Prevention Study. *Birth Defects Res. A Clin. Mol. Teratol.* 91, 93–101. doi: 10.1002/bdra.20752

Buist, A., and Janson, H. (2001). Childhood sexual abuse, parenting and postpartum depression–a 3-year follow-up study. *Child Abuse Negl.* 25, 909–921. doi: 10.1016/s0145-2134(01)00246-0

Buznikov, G. A., Lambert, H. W., and Lauder, J. M. (2001). Serotonin and serotonin-like substances as regulators of early embryogenesis and morphogenesis. *Cell Tissue Res.* 305, 177–186. doi: 10.1007/s004410100408

Cabrera, R. M., Linda Lin, Y., Law, E., Kim, J., and Wlodarczyk, B. J. (2020). The teratogenic effects of sertraline in mice. *Birth Defects Res.* 112, 1014–1024. doi: 10.1002/bdr2.1660

Calibuso-Salazar, M. J., and Ten Eyck, G. R. (2015). A novel whole-embryo culture model for pharmaceutical and developmental studies. *J. Pharmacol. Toxicol. Methods* 73, 21–26. doi: 10.1016/j.vascn.2015.02.003

Canfield, M. A., Honein, M. A., Yuskiv, N., Xing, J., Mai, C. T., Collins, J. S., et al. (2006). National estimates and race/ethnic-specific variation of selected birth defects in the United States, 1999-2001. *Birth Defects Res. A Clin. Mol. Teratol.* 76, 747–756. doi: 10.1002/bdra.20294

Carlson, B. (2019). *Human Embryology and Developmental Biology*, 6th Edn. Netherlands: Elsevier.

Carlsson, P., and Mahlapuu, M. (2002). Forkhead transcription factors: key players in development and metabolism. *Dev. Biol.* 250, 1–23. doi: 10.1006/dbio.2002.0780

Carmichael, S. L., Ma, C., Rasmussen, S. A., Honein, M. A., Lammer, E. J., Shaw, G. M., et al. (2008). Craniosynostosis and maternal smoking. *Birth Defects Res. A Clin. Mol. Teratol.* 82, 78–85. doi: 10.1002/bdra.20426

Charlton, R. A., Jordan, S., Pierini, A., Garne, E., Neville, A. J., Hansen, A. V., et al. (2015). Selective serotonin reuptake inhibitor prescribing before, during and after pregnancy: a population-based study in six European regions. *BJOG* 122, 1010–1020. doi: 10.1111/1471-0528.13143

Chatzeli, L., Gaete, M., and Tucker, A. S. (2017). Fgf10 and Sox9 are essential for the establishment of distal progenitor cells during mouse salivary gland development. *Development* 144, 2294–2305. doi: 10.1242/dev.146019

Choi, D. S., Ward, S. J., Messaddeq, N., Launay, J. M., and Maroteaux, L. (1997). 5-HT2B receptor-mediated serotonin morphogenetic functions in mouse cranial neural crest and myocardiac cells. *Development* 124, 1745–1755.

Colvin, L., Slack-Smith, L., Stanley, F. J., and Bower, C. (2011). Dispensing patterns and pregnancy outcomes for women dispensed selective serotonin reuptake inhibitors in pregnancy. *Birth Defects Res. A Clin. Mol. Teratol.* 91, 142–152. doi: 10.1002/bdra.20773

Cote, F., Fligny, C., Bayard, E., Launay, J. M., Gershon, M. D., Mallet, J., et al. (2007). Maternal serotonin is crucial for murine embryonic development. *Proc. Natl. Acad. Sci. U. S. A.* 104, 329–334. doi: 10.1073/pnas.0606722104

Couly, G., Creuzet, S., Bennaceur, S., Vincent, C., and Le Douarin, N. M. (2002). Interactions between Hox-negative cephalic neural crest cells and the foregut endoderm in patterning the facial skeleton in the vertebrate head. *Development* 129, 1061–1073.

Cray, J. J. Jr., Weinberg, S. M., Parsons, T. E., Howie, R. N., Elsalanty, M., and Yu, J. C. (2014). Selective serotonin reuptake inhibitor exposure alters osteoblast gene expression and craniofacial development in mice. *Birth Defects Res. A Clin. Mol. Teratol.* 100, 912–923. doi: 10.1002/bdra.23323

da Silva, S., de Azevedo, L. R., de Lima, A. A., Ignacio, S. A., Machado, M. A., ZacliKevis, M. V., et al. (2009). Effects of fluoxetine and venlafaxine and pilocarpine on rat parotid glands. *Med. Chem.* 5, 483–490. doi: 10.2174/157340609789117868

Dadi, A. F., Miller, E. R., Woodman, R., Bisetegn, T. A., and Mwanri, L. (2020). Antenatal depression and its potential causal mechanisms among pregnant mothers in Gondar town: application of structural equation model. *BMC Pregnancy Childbirth* 20:168. doi: 10.1186/s12884-020-02859-2

Dolk, H. (2005). EUROCAT: 25 years of European surveillance of congenital anomalies. *Arch. Dis. Child. Fetal Neonatal. Ed.* 90, F355–F358. doi: 10.1136/adc.2004.062810

Dube, F., and Amireault, P. (2007). Local serotonergic signaling in mammalian follicles, oocytes and early embryos. *Life Sci.* 81, 1627–1637. doi: 10.1016/j.lfs.2007.09.034

Durham, E., Howie, R. N., Larson, N., LaRue, A., and Cray, J. (2019). Pharmacological exposures may precipitate craniosynostosis through targeted stem cell depletion. *Stem Cell Res.* 40:101528. doi: 10.1016/j.scr.2019.101528

Durham, E. L., Howie, R. N., and Cray, J. J. (2017). Gene/environment interactions in craniosynostosis: a brief review. *Orthod. Craniofac. Res.* 20(Suppl. 1), 8–11. doi: 10.1111/ocr.12153

Emmerson, E., May, A. J., Nathan, S., Cruz-Pacheco, N., Lizama, C. O., Maliskova, L., et al. (2017). SOX2 regulates acinar cell development in the salivary gland. *Elife* 6:e26620. doi: 10.7554/eLife.26620

Emory, E. K., and Dieter, J. N. (2006). Maternal depression and psychotropic medication effects on the human fetus. *Ann. N. Y. Acad. Sci.* 1094, 287–291. doi: 10.1196/annals.1376.036

Escribe-Aguir, V., Gonzalez-Galarzo, M. C., Barona-Vilar, C., and Artazcoz, L. (2008). Factors related to depression during pregnancy: are there gender differences? *J. Epidemiol. Community Health* 62, 410–414. doi: 10.1136/jech.2007.063016

Fairbrother, N., Young, A. H., Zhang, A., Janssen, P., and Antony, M. M. (2017). The prevalence and incidence of perinatal anxiety disorders among women experiencing a medically complicated pregnancy. *Arch. Womens Ment. Health* 20, 311–319. doi: 10.1007/s00737-016-0704-7

Faisal-Cury, A., and Rossi Menezes, P. (2007). Prevalence of anxiety and depression during pregnancy in a private setting sample. *Arch. Womens Ment. Health* 10, 25–32. doi: 10.1007/s00737-006-0164-6

Field, T. (2011). Prenatal depression effects on early development: a review. *Infant Behav. Dev.* 34, 1–14. doi: 10.1016/j.infbeh.2010.09.008

Field, T. (2017a). Prenatal anxiety effects: a review. *Infant Behav. Dev.* 49, 120–128. doi: 10.1016/j.infbeh.2017.08.008

Field, T. (2017b). Prenatal depression risk factors, developmental effects and interventions: a review. *J. Pregnancy Child. Health* 4:301. doi: 10.4172/2376-127X.1000301

Fraher, D., Hodge, J. M., Collier, F. M., McMillan, J. S., Kennedy, R. L., Ellis, M., et al. (2016). Citalopram and sertraline exposure compromises embryonic bone development. *Mol. Psychiatry* 21:722. doi: 10.1038/mp.2015.155

Gaete, M., Fons, J. M., Popa, E. M., Chatzeli, L., and Tucker, A. S. (2015). Epithelial topography for repetitive tooth formation. *Biol. Open* 4, 1625–1634. doi: 10.1242/bio.013672

Galli, C., Passeri, G., and Macaluso, G. M. (2011). FoxOs, Wnts and oxidative stress-induced bone loss: new players in the periodontitis arena? *J. Periodontal Res.* 46, 397–406. doi: 10.1111/j.1600-0765.2011.01354.x

Gao, S. Y., Wu, Q. J., Sun, C., Zhang, T. N., Shen, Z. Q., Liu, C. X., et al. (2018). Selective serotonin reuptake inhibitor use during early pregnancy and congenital malformations: a systematic review and meta-analysis of cohort studies of more than 9 million births. *BMC Med.* 16:205. doi: 10.1186/s12916-018-1193-5

Gershon, M. D., and Tack, J. (2007). The serotonin signaling system: from basic understanding to drug development for functional GI disorders. *Gastroenterology* 132, 397–414. doi: 10.1053/j.gastro.2006.11.002

Global Burden of Disease Study (2017). Global, regional, and national incidence, prevalence, and years lived with disability for 354 diseases and injuries for 195 countries and territories, 1990–2017: a systematic analysis for the Global Burden of Disease Study 2017. *Glob. Health Metrics* 392, 1789–1858. doi: 10.1016/S0140-6736(18)32279-7

Golder, S., Loke, Y. K., and Bland, M. (2011). Meta-analyses of adverse effects data derived from randomised controlled trials as compared to observational studies: methodological overview. *PLoS Med.* 8:e1001026. doi: 10.1371/journal.pmed.1001026

Goodman, S. H., and Tully, E. C. (2009). Recurrence of depression during pregnancy: psychosocial and personal functioning correlates. *Depress. Anxiety* 26, 557–567. doi: 10.1002/da.20421

Grace, S. L., Evindar, A., and Stewart, D. E. (2003). The effect of postpartum depression on child cognitive development and behavior: a review and critical analysis of the literature. *Arch. Womens Ment. Health* 6, 263–274. doi: 10.1007/s00737-003-0024-6

Grenier, J., Teillet, M. A., Grifone, R., Kelly, R. G., and Duprez, D. (2009). Relationship between neural crest cells and cranial mesoderm during head muscle development. *PLoS One* 4:e4381. doi: 10.1371/journal.pone.0004381

Grewal, J., Carmichael, S. L., Ma, C., Lammer, E. J., and Shaw, G. M. (2008). Maternal periconceptional smoking and alcohol consumption and risk for select congenital anomalies. *Birth Defects Res. A Clin. Mol. Teratol.* 82, 519–526. doi: 10.1002/bdra.20461

Gustafsson, B. I., Thommesen, L., Stunes, A. K., Tommeras, K., Westbroek, I., Waldum, H. L., et al. (2006). Serotonin and fluoxetine modulate bone cell function in vitro. *J. Cell Biochem.* 98, 139–151. doi: 10.1002/jcb.20734

Hansson, S. R., Mezey, E., and Hoffman, B. J. (1999). Serotonin transporter messenger RNA expression in neural crest-derived structures and sensory pathways of the developing rat embryo. *Neuroscience* 89, 243–265. doi: 10.1016/s0306-4522(98)00281-4

Hauser, B. R., and Hoffman, M. P. (2015). Regulatory mechanisms driving salivary gland organogenesis. *Curr. Top. Dev. Biol.* 115, 111–130. doi: 10.1016/bs.ctdb.2015.07.029

Heinonen, E., Szymanska-von Schultz, B., Kaldo, V., Nasiell, J., Andersson, E., Bergmark, M., et al. (2018). MAGDALENA: study protocol of a randomised, placebo-controlled trial on cognitive development at 2 years of age in children exposed to SSRI in utero. *BMJ Open* 8:e023281. doi: 10.1136/bmjopen-2018-023281

Henz, S. L., Cognato Gde, P., Vuaden, F. C., Bogo, M. R., Bonan, C. D., and Sarkis, J. J. (2009). Influence of antidepressant drugs on Ecto-nucleotide pyrophosphatase/phosphodiesterases (E-NPPs) from salivary glands of rats. *Arch. Oral Biol.* 54, 730–736. doi: 10.1016/j.archoralbio.2009.04.010

Hirata, A., Imura, H., Sugahara, T., Natsume, N., Nakamura, H., and Kondo, Y. (2018). Serotonin effectors expressed during palatogenesis: an immunohistochemical study. *JSM Dent.* 6:1115.

Hompoth, E. A., Peto, Z., Fureszne Balogh, V., and Toreki, A. (2020). Associations between depression symptoms, psychological intervention and perinatal complications. *J. Clin. Psychol. Med. Settings* 27, 199–205. doi: 10.1007/s10880-019-09632-4

Hoyer, D., Hannon, J. P., and Martin, G. R. (2002). Molecular, pharmacological and functional diversity of 5-HT receptors. *Pharmacol. Biochem. Behav.* 71, 533–554. doi: 10.1016/s0091-3057(01)00746-8

Huang, J., Shen, G., Ren, H., Zhang, Z., Yu, X., Zhao, W., et al. (2020). Role of forkhead box gene family in bone metabolism. *J. Cell Physiol.* 235, 1986–1994. doi: 10.1002/jcp.29178

Hunter, K. D., and Wilson, W. S. (1995). The effects of antidepressant drugs on salivary flow and content of sodium and potassium ions in human parotid saliva. *Arch. Oral Biol.* 40, 983–989. doi: 10.1016/0003-9969(95)00079-5

Huybrechts, K. F., Bateman, B. T., Palmsten, K., Desai, R. J., Patorno, E., Gopalakrishnan, C., et al. (2015). Antidepressant use late in pregnancy and risk of persistent pulmonary hypertension of the newborn. *JAMA* 313, 2142–2151. doi: 10.1001/jama.2015.5605

Iyer, S., Ambrogini, E., Bartell, S. M., Han, L., Roberson, P. K., de Cabo, R., et al. (2013). FOXOs attenuate bone formation by suppressing Wnt signaling. *J. Clin. Invest.* 123, 3409–3419. doi: 10.1172/JCI68049

Jimenez-Rojo, L., Granchi, Z., Graf, D., and Mitsiadis, T. A. (2012). Stem cell fate determination during development and regeneration of ectodermal organs. *Front. Physiol.* 3:107. doi: 10.3389/fphys.2012.00107

Jimenez-Solem, E., Andersen, J. T., Petersen, M., Broedbaek, K., Andersen, N. L., Torp-Pedersen, C., et al. (2013). Prevalence of antidepressant use during pregnancy in Denmark, a nation-wide cohort study. *PLoS One* 8:e63034. doi: 10.1371/journal.pone.0063034

Kaihola, H., Olivier, J., Poromaa, I. S., and Akerud, H. (2015). The effect of antenatal depression and selective serotonin reuptake inhibitor treatment on nerve growth factor signaling in human placenta. *PLoS One* 10:e0116459. doi: 10.1371/journal.pone.0116459

Kaihola, H., Yaldir, F. G., Hreinsson, J., Hornaeus, K., Bergquist, J., Olivier, J. D., et al. (2016). Effects of fluoxetine on human embryo development. *Front. Cell Neurosci.* 10:160. doi: 10.3389/fncel.2016.00160

Kawasaki, K., Kawasaki, M., Watanabe, M., Idrus, E., Nagai, T., Oommen, S., et al. (2015). Expression of Sox genes in tooth development. *Int. J. Dev. Biol.* 59, 471–478. doi: 10.1387/ijdb.150192ao

Kern, D. M., Cepeda, M. S., Defalco, F., and Etropolski, M. (2020). Treatment patterns and sequences of pharmacotherapy for patients diagnosed with depression in the United States: 2014 through 2019. *BMC Psychiatry* 20:4. doi: 10.1186/s12888-019-2418-7

Kerr, C. W. (1994). The serotonin theory of depression. *Jefferson J. Psychiatry* 12:4.

Kim, D. R., Wang, E., McGeehan, B., Snell, J., Ewing, G., Iannelli, C., et al. (2019). Randomized controlled trial of transcranial magnetic stimulation in pregnant women with major depressive disorder. *Brain Stimul.* 12, 96–102. doi: 10.1016/j.brs.2018.09.005

Kirk, E. E., Giordano, J., and Anderson, R. S. (1997). Serotonergic receptors as targets for pharmacotherapy. *J. Neurosci. Nurs.* 29, 191–197. doi: 10.1097/01376517-199706000-00007

Klein, O. D., Oberoi, S., Huysseune, A., Hovorakova, M., Peterka, M., and Peterkova, R. (2013). Developmental disorders of the dentition: an update. *Am. J. Med. Genet. C Semin. Med. Genet.* 163C, 318–332. doi: 10.1002/ajmg.c.31382

Knosp, W. M., Knox, S. M., and Hoffman, M. P. (2012). Salivary gland organogenesis. *Wiley Interdiscip. Rev. Dev. Biol.* 1, 69–82. doi: 10.1002/wdev.4

Kode, A., Mosialou, I., Silva, B. C., Rached, M. T., Zhou, B., Wang, J., et al. (2012). FOXO1 orchestrates the bone-suppressing function of gut-derived serotonin. *J. Clin. Invest.* 122, 3490–3503. doi: 10.1172/JCI64906

Kornum, J. B., Nielsen, R. B., Pedersen, L., Mortensen, P. B., and Norgaard, M. (2010). Use of selective serotonin-reuptake inhibitors during early pregnancy and risk of congenital malformations: updated analysis. *Clin. Epidemiol.* 2, 29–36. doi: 10.2147/clep.s9256

Koutra, K., Vassilaki, M., Georgiou, V., Koutis, A., Bitsios, P., Chatzi, L., et al. (2014). Antenatal maternal mental health as determinant of postpartum depression in a population based mother-child cohort (Rhea Study) in Crete, Greece. *Soc. Psychiatry Psychiatr. Epidemiol.* 49, 711–721. doi: 10.1007/s00127-013-0758-z

Krishnan, V., and Nestler, E. J. (2011). Animal models of depression: molecular perspectives. *Curr. Top. Behav. Neurosci.* 7, 121–147. doi: 10.1007/7854_2010_108

Kurakazu, I., Akasaki, Y., Hayashida, M., Tsushima, H., Goto, N., Sueishi, T., et al. (2019). FOXO1 transcription factor regulates chondrogenic differentiation through transforming growth factor beta1 signaling. *J. Biol. Chem.* 294, 17555–17569. doi: 10.1074/jbc.RA119.009409

Ladyman, C., Signal, T. L., Sweeney, B., Gander, P., Paine, S. J., and Huthwaite, M. (2020). A pilot longitudinal sleep education intervention from early pregnancy and its effect on optimizing sleep and minimizing depressive symptoms. *Sleep Health* 6, 778–786. doi: 10.1016/j.sleh.2020.05.001

Lambert, H. W., and Lauder, J. M. (1999). Serotonin receptor agonists that increase cyclic AMP positively regulate IGF-I in mouse mandibular mesenchymal cells. *Dev. Neurosci.* 21, 105–112. doi: 10.1159/000017372

Lauder, J. M., Wilkie, M. B., Wu, C., and Singh, S. (2000). Expression of 5-HT(2A), 5-HT(2B) and 5-HT(2C) receptors in the mouse embryo. *Int. J. Dev. Neurosci.* 18, 653–662. doi: 10.1016/s0736-5748(00)00032-0

Lauder, J. M., and Zimmerman, E. F. (1988). Sites of serotonin uptake in epithelia of the developing mouse palate, oral cavity, and face: possible role in morphogenesis. *J. Craniofac. Genet. Dev. Biol.* 8, 265–276.

Le Douarin, N. M., Creuzet, S., Couly, G., and Dupin, E. (2004). Neural crest cell plasticity and its limits. *Development* 131, 4637–4650. doi: 10.1242/dev.01350

Levin, M., Buznikov, G. A., and Lauder, J. M. (2006). Of minds and embryos: left-right asymmetry and the serotonergic controls of pre-neural morphogenesis. *Dev. Neurosci.* 28, 171–185. doi: 10.1159/000091915

Liang, B., Moussaif, M., Kuan, C. J., Gargus, J. J., and Sze, J. Y. (2006). Serotonin targets the DAF-16/FOXO signaling pathway to modulate stress responses. *Cell Metab.* 4, 429–440. doi: 10.1016/j.cmet.2006.11.004

Liu, J., Meng, F., Dai, J., Wu, M., Wang, W., Liu, C., et al. (2020). The BDNF-FoxO1 Axis in the medial prefrontal cortex modulates depressive-like behaviors induced by chronic unpredictable stress in postpartum female mice. *Mol. Brain* 13:91. doi: 10.1186/s13041-020-00631-3

Louik, C., Lin, A. E., Werler, M. M., Hernandez-Diaz, S., and Mitchell, A. A. (2007). First-trimester use of selective serotonin-reuptake inhibitors and the risk of birth defects. *N. Engl. J. Med.* 356, 2675–2683. doi: 10.1056/NEJMoa067407

Lucena, L., Frange, C., Pinto, A. C. A., Andersen, M. L., Tufik, S., and Hachul, H. (2020). Mindfulness interventions during pregnancy: a narrative review. *J. Integr. Med.* 18, 470–477. doi: 10.1016/j.joim.2020.07.007

Lv, J., Wang, L., Gao, Y., Ding, Y. Q., and Liu, F. (2017). 5-hydroxytryptamine synthesized in the aorta-gonad-mesonephros regulates hematopoietic stem and progenitor cell survival. *J. Exp. Med.* 214, 529–545. doi: 10.1084/jem.20150906

Ma, X., Su, P., Yin, C., Lin, X., Wang, X., Gao, Y., et al. (2020). The roles of FoxO transcription factors in regulation of bone cells function. *Int. J. Mol. Sci.* 21:692. doi: 10.3390/ijms21030692

Malm, H., Artama, M., Gissler, M., and Ritvanen, A. (2011). Selective serotonin reuptake inhibitors and risk for major congenital anomalies. *Obstet. Gynecol.* 118, 111–120. doi: 10.1097/AOG.0b013e318220edcc

Marcucio, R. S., Young, N. M., Hu, D., and Hallgrimsson, B. (2011). Mechanisms that underlie co-variation of the brain and face. *Genesis* 49, 177–189. doi: 10.1002/dvg.20710

McAndrew, A. J. (2019). Emotional development in offspring from infancy to adolescence. *Early Child. Dev. Care* 189, 168–177.

Meltzer-Brody, S., Stuebe, A., Dole, N., Savitz, D., Rubinow, D., and Thorp, J. (2011). Elevated corticotropin releasing hormone (CRH) during pregnancy and risk of postpartum depression (PPD). *J. Clin. Endocrinol. Metab.* 96, E40–E47. doi: 10.1210/jc.2010-0978

Micheli, L., Ceccarelli, M., D'Andrea, G., Costanzi, M., Giacovazzo, G., Coccurello, R., et al. (2018). Fluoxetine or Sox2 reactivate proliferation-defective stem and progenitor cells of the adult and aged dentate gyrus. *Neuropharmacology* 141, 316–330. doi: 10.1016/j.neuropharm.2018.08.023

Milgrom, J., Gemmill, A. W., Bilszta, J. L., Hayes, B., Barnett, B., Brooks, J., et al. (2008). Antenatal risk factors for postnatal depression: a large prospective study. *J. Affect. Disord.* 108, 147–157. doi: 10.1016/j.jad.2007.10.014

Millan, M. J., Marin, P., Bockaert, J., and Mannoury la Cour, C. (2008). Signaling at G-protein-coupled serotonin receptors: recent advances and future research directions. *Trends Pharmacol. Sci.* 29, 454–464. doi: 10.1016/j.tips.2008.06.007

Miranda, A., Olhaberry, M., and Morales-Reyes, I. (2017). Intervención grupal en embarazadas: respuestas diferenciales de acuerdo al tipo de depresión y patrón de apego. *Revista Psykhe* 26, 1–17.

Miyamoto, K., Ohkawara, B., Ito, M., Masuda, A., Hirakawa, A., Sakai, T., et al. (2017). Fluoxetine ameliorates cartilage degradation in osteoarthritis by inhibiting Wnt/beta-catenin signaling. *PLoS One* 12:e0184388. doi: 10.1371/journal.pone.0184388

Moiseiwitsch, J. R., and Lauder, J. M. (1995). Serotonin regulates mouse cranial neural crest migration. *Proc. Natl. Acad. Sci. U. S. A.* 92, 7182–7186. doi: 10.1073/pnas.92.16.7182

Moiseiwitsch, J. R., and Lauder, J. M. (1996). Stimulation of murine tooth development in organotypic culture by the neurotransmitter serotonin. *Arch. Oral Biol.* 41, 161–165. doi: 10.1016/0003-9969(95)00117-4

Moiseiwitsch, J. R., and Lauder, J. M. (1997). Regulation of gene expression in cultured embryonic mouse mandibular mesenchyme by serotonin antagonists. *Anat. Embryol. (Berl.)* 195, 71–78. doi: 10.1007/s004290050026

Moiseiwitsch, J. R., Raymond, J. R., Tamir, H., and Lauder, J. M. (1998). Regulation by serotonin of tooth-germ morphogenesis and gene expression in mouse mandibular explant cultures. *Arch. Oral Biol.* 43, 789–800. doi: 10.1016/s0003-9969(98)00067-3

Molenaar, N. M., Bais, B., Lambregtse-van den Berg, M. P., Mulder, C. L., Howell, E. A., Fox, N. S., et al. (2020). The international prevalence of antidepressant use before, during, and after pregnancy: a systematic review and meta-analysis of timing, type of prescriptions and geographical variability. *J. Affect. Disord.* 264, 82–89. doi: 10.1016/j.jad.2019.12.014

Murray, J. C. (2002). Gene/environment causes of cleft lip and/or palate. *Clin. Genet.* 61, 248–256. doi: 10.1034/j.1399-0004.2002.610402.x

Murray, JC, and Marazita, ML. (2013). "Chapter 143 – clefting, dental, and craniofacial syndromes," in *Emery and Rimoin's Principles and Practice of Medical Genetics*, eds D. Rimoin, R. Pyeritz, and B. Korf (Cambridge, MA: Academic Press), 1–8. ISBN 9780123838346

Murray, L., Stanley, C., Hooper, R., King, F., and Fiori-Cowley, A. (1996). The role of infant factors in postnatal depression and mother-infant interactions. *Dev. Med. Child. Neurol.* 38, 109–119. doi: 10.1111/j.1469-8749.1996.tb12082.x

Nagy, L., and Demke, J. C. (2014). Craniofacial anomalies. *Facial Plast. Surg. Clin. North. Am.* 22, 523–548. doi: 10.1016/j.fsc.2014.08.002

Narboux-Neme, N., Pavone, L. M., Avallone, L., Zhuang, X., and Gaspar, P. (2008). Serotonin transporter transgenic (SERTcre) mouse line reveals developmental targets of serotonin specific reuptake inhibitors (SSRIs). *Neuropharmacology* 55, 994–1005. doi: 10.1016/j.neuropharm.2008.08.020

Nelson, E. C., Heath, A. C., Madden, P. A., Cooper, M. L., Dinwiddie, S. H., Bucholz, K. K., et al. (2002). Association between self-reported childhood sexual abuse and adverse psychosocial outcomes: results from a twin study. *Arch. Gen. Psychiatry* 59, 139–145. doi: 10.1001/archpsyc.59.2.139

O'Connor, E., Rossom, R. C., Henninger, M., Groom, H. C., and Burda, B. U. (2016). Primary care screening for and treatment of depression in pregnant and postpartum women: evidence report and systematic review for the US Preventive Services Task Force. *JAMA* 315, 388–406. doi: 10.1001/jama.2015.18948

Ohba, S., He, X., Hojo, H., and McMahon, A. P. (2015). Distinct transcriptional programs underlie Sox9 regulation of the mammalian chondrocyte. *Cell Rep.* 12, 229–243. doi: 10.1016/j.celrep.2015.06.013

Olhaberry, M., Zapata, J., Escobar, M., Mena, C., Farkas, C., Santelices, P., et al. (2014). Antenatal depression and its relationship with problem-solving strategies, childhood abuse, social support, and attachment styles in a low-income Chilean sample. *Ment. Health Prev.* 2, 86–97.

Ori, M., De Lucchini, S., Marras, G., and Nardi, I. (2013). Unraveling new roles for serotonin receptor 2B in development: key findings from Xenopus. *Int. J. Dev. Biol.* 57, 707–714. doi: 10.1387/ijdb.130204mo

Ormsbee Golden, B. D., Wuebben, E. L., and Rizzino, A. (2013). Sox2 expression is regulated by a negative feedback loop in embryonic stem cells that involves AKT signaling and FoxO1. *PLoS One* 8:e76345. doi: 10.1371/journal.pone.0076345

Paszynska, E., Linden, R. W., Slopien, A., and Rajewski, A. (2013). Parotid gland flow activity and inorganic composition in purging bulimic patients treated with fluoxetine. *World J. Biol. Psychiatry* 14, 634–639. doi: 10.3109/15622975.2013.795242

Patel, V. N., Rebustini, I. T., and Hoffman, M. P. (2006). Salivary gland branching morphogenesis. *Differentiation* 74, 349–364. doi: 10.1111/j.1432-0436.2006.00088.x

Pawlby, S., Hay, D. F., Sharp, D., Waters, C. S., and O'Keane, V. (2009). Antenatal depression predicts depression in adolescent offspring: prospective longitudinal community-based study. *J. Affect. Disord.* 113, 236–243. doi: 10.1016/j.jad.2008.05.018

Pearson, R. M., Melotti, R., Heron, J., Joinson, C., Stein, A., Ramchandani, P. G., et al. (2012). Disruption to the development of maternal responsiveness? The impact of prenatal depression on mother-infant interactions. *Infant Behav. Dev.* 35, 613–626. doi: 10.1016/j.infbeh.2012.07.020

Peroutka, S. J. (1994). Molecular biology of serotonin (5-HT) receptors. *Synapse* 18, 241–260. doi: 10.1002/syn.890180310

Planchez, B., Surget, A., and Belzung, C. (2019). Animal models of major depression: drawbacks and challenges. *J. Neural. Transm. (Vienna)* 126, 1383–1408. doi: 10.1007/s00702-019-02084-y

Poche, R. A., Sharma, R., Garcia, M. D., Wada, A. M., Nolte, M. J., Udan, R. S., et al. (2012). Transcription factor FoxO1 is essential for enamel biomineralization. *PLoS One* 7:e30357. doi: 10.1371/journal.pone.0030357

Polter, A., Yang, S., Zmijewska, A. A., van Groen, T., Paik, J. H., Depinho, R. A., et al. (2009). Forkhead box, class O transcription factors in brain: regulation and behavioral manifestation. *Biol. Psychiatry* 65, 150–159. doi: 10.1016/j.biopsych.2008.08.005

Ramos, E., Oraichi, D., Rey, E., Blais, L., and Berard, A. (2007). Prevalence and predictors of antidepressant use in a cohort of pregnant women. *BJOG* 114, 1055–1064. doi: 10.1111/j.1471-0528.2007.01387.x

Rampono, J., Simmer, K., Ilett, K. F., Hackett, L. P., Doherty, D. A., Elliot, R., et al. (2009). Placental transfer of SSRI and SNRI antidepressants and effects on the neonate. *Pharmacopsychiatry* 42, 95–100. doi: 10.1055/s-0028-1103296

Raskin, M., Easterbrooks, M. A., Lamoreau, R. S., Kotake, C., and Goldberg, J. (2016). Depression trajectories of antenatally depressed and nondepressed young mothers: implications for child socioemotional development. *Womens Health Issues* 26, 344–350. doi: 10.1016/j.whi.2016.02.002

Reefhuis, J., Devine, O., Friedman, J. M., Louik, C., Honein, M. A., and National Birth Defects Prevention Study (2015). Specific SSRIs and birth defects: Bayesian analysis to interpret new data in the context of previous reports. *BMJ* 351:h3190. doi: 10.1136/bmj.h3190

Reisoli, E., De Lucchini, S., Nardi, I., and Ori, M. (2010). Serotonin 2B receptor signaling is required for craniofacial morphogenesis and jaw joint formation in Xenopus. *Development* 137, 2927–2937. doi: 10.1242/dev.041079

Riksen, E. A., Stunes, A. K., Kalvik, A., Gustafsson, B. I., Snead, M. L., Syversen, U., et al. (2010). Serotonin and fluoxetine receptors are expressed in enamel organs and LS8 cells and modulate gene expression in LS8 cells. *Eur. J. Oral. Sci.* 118, 566–573. doi: 10.1111/j.1600-0722.2010.00778.x

Rinon, A., Lazar, S., Marshall, H., Buchmann-Moller, S., Neufeld, A., Elhanany-Tamir, H., et al. (2007). Cranial neural crest cells regulate head muscle patterning and differentiation during vertebrate embryogenesis. *Development* 134, 3065–3075. doi: 10.1242/dev.002501

Rojas, G., Santelices, M. P., Martinez, P., Tomicic, A., Reinel, M., Olhaberry, M., et al. (2015). [Barriers restricting postpartum depression treatment in Chile]. *Rev. Med. Chil.* 143, 424–432. doi: 10.4067/S0034-98872015000400002

Ruch, J. V., Lesot, H., and Begue-Kirn, C. (1995). Odontoblast differentiation. *Int. J. Dev. Biol.* 39, 51–68.

Sahu, A., Gopalakrishnan, L., Gaur, N., Chatterjee, O., Mol, P., Modi, P. K., et al. (2018). The 5-Hydroxytryptamine signaling map: an overview of serotonin-serotonin receptor mediated signaling network. *J. Cell Commun. Signal.* 12, 731–735. doi: 10.1007/s12079-018-0482-2

Sánchez, N., Inostroza, V., Perez, M. C., Moya, P., Ubilla, A., Besa, J., et al. (2018). Tracking morphological complexities of organ development in culture. *Mech. Dev.* 154, 179–192. doi: 10.1016/j.mod.2018.07.005

Sato, T. S., Handa, A., Priya, S., Watal, P., Becker, R. M., and Sato, Y. (2019). Neurocristopathies: enigmatic appearances of neural crest cell-derived abnormalities. *Radiographics* 39, 2085–2102. doi: 10.1148/rg.2019190086

Shuey, D. L., Sadler, T. W., and Lauder, J. M. (1992). Serotonin as a regulator of craniofacial morphogenesis: site specific malformations following exposure to serotonin uptake inhibitors. *Teratology* 46, 367–378. doi: 10.1002/tera.1420460407

Shuey, D. L., Sadler, T. W., Tamir, H., and Lauder, J. M. (1993). Serotonin and morphogenesis. Transient expression of serotonin uptake and binding protein during craniofacial morphogenesis in the mouse. *Anat. Embryol. (Berl.)* 187, 75–85. doi: 10.1007/BF00208198

Sousa-Ferreira, L., Aveleira, C., Botelho, M., Alvaro, A. R., Pereira de Almeida, L., and Cavadas, C. (2014). Fluoxetine induces proliferation and inhibits differentiation of hypothalamic neuroprogenitor cells in vitro. *PLoS One* 9:e88917. doi: 10.1371/journal.pone.0088917

Sparling, T. M., Henschke, N., Nesbitt, R. C., and Gabrysch, S. (2017). The role of diet and nutritional supplementation in perinatal depression: a systematic review. *Matern. Child. Nutr.* 13:e12235. doi: 10.1111/mcn.12235

Stahl, S. M. (1998). Mechanism of action of serotonin selective reuptake inhibitors. Serotonin receptors and pathways mediate therapeutic effects and side effects. *J. Affect. Disord.* 51, 215–235. doi: 10.1016/s0165-0327(98)00221-3

Takenoshita, M., Takechi, M., Vu Hoang, T., Furutera, T., Akagawa, C., Namangkalakul, W., et al. (2021). Cell lineage- and expression-based inference of the roles of forkhead box transcription factor Foxc2 in craniofacial development. *Dev. Dyn.* doi: 10.1002/dvdy.324 [Epub ahead of print]

Teixeira, C. C., Liu, Y., Thant, L. M., Pang, J., Palmer, G., and Alikhani, M. (2010). Foxo1, a novel regulator of osteoblast differentiation and skeletogenesis. *J. Biol. Chem.* 285, 31055–31065. doi: 10.1074/jbc.M109.079962

Thesleff, I. (2003). Epithelial-mesenchymal signalling regulating tooth morphogenesis. *J. Cell Sci.* 116, 1647–1648. doi: 10.1242/jcs.00410

Thesleff, I., and Sharpe, P. (1997). Signalling networks regulating dental development. *Mech. Dev.* 67, 111–123. doi: 10.1016/s0925-4773(97)00115-9

Togni, L., Mascitti, M., Santarelli, A., Contaldo, M., Romano, A., Serpico, R., et al. (2019). Unusual conditions impairing saliva secretion: developmental anomalies of salivary glands. *Front. Physiol.* 10:855. doi: 10.3389/fphys.2019.00855

Tsapakis, E. M., Gamie, Z., Tran, G. T., Adshead, S., Lampard, A., Mantalaris, A., et al. (2012). The adverse skeletal effects of selective serotonin reuptake inhibitors. *Eur. Psychiatry* 27, 156–169. doi: 10.1016/j.eurpsy.2010.10.006

Turner, J. T., Sullivan, D. M., Rovira, I., and Camden, J. M. (1996). A regulatory role in mammalian salivary glands for 5-hydroxytryptamine receptors coupled to increased cyclic AMP production. *J. Dent. Res.* 75, 935–941. doi: 10.1177/00220345960750031101

Twigg, S. R., and Wilkie, A. O. (2015). New insights into craniofacial malformations. *Hum. Mol. Genet.* 24, R50–R59. doi: 10.1093/hmg/ddv228

Uguz, F. (2020). Selective serotonin reuptake inhibitors and the risk of congenital anomalies: a systematic review of current meta-analyses. *Expert. Opin. Drug Saf.* 19, 1595–1604. doi: 10.1080/14740338.2020.1832080

Vichier-Guerre, C., Parker, M., Pomerantz, Y., Finnell, R. H., and Cabrera, R. M. (2017). Impact of selective serotonin reuptake inhibitors on neural crest stem cell formation. *Toxicol. Lett.* 281, 20–25. doi: 10.1016/j.toxlet.2017.08.012

Wang, H., Quirion, R., Little, P. J., Cheng, Y., Feng, Z. P., Sun, H. S., et al. (2015). Forkhead box O transcription factors as possible mediators in the development of major depression. *Neuropharmacology* 99, 527–537. doi: 10.1016/j.neuropharm.2015.08.020

Wee, E. L., Babiarz, B. S., Zimmerman, S., and Zimmerman, E. F. (1979). Palate morphogenesis. IV. Effects of serotonin and its antagonists on rotation in embryo culture. *J. Embryol. Exp. Morphol.* 53, 75–90.

Wee, E. L., Kujawa, M., and Zimmerman, E. F. (1981). Palate morphogenesis. VI. Identification of stellate cells in culture. *Cell Tissue Res.* 217, 143–154. doi: 10.1007/BF00233833

Xu, P., Balczerski, B., Ciozda, A., Louie, K., Oralova, V., Huysseune, A., et al. (2018). Fox proteins are modular competency factors for facial cartilage and tooth specification. *Development* 145:dev165498. doi: 10.1242/dev.165498

Xu, P., Yu, H. V., Tseng, K. C., Flath, M., Fabian, P., Segil, N., et al. (2021). Foxc1 establishes enhancer accessibility for craniofacial cartilage differentiation. *Elife* 10:e63595. doi: 10.7554/eLife.63595

Yavarone, M. S., Shuey, D. L., Tamir, H., Sadler, T. W., and Lauder, J. M. (1993). Serotonin and cardiac morphogenesis in the mouse embryo. *Teratology* 47, 573–584. doi: 10.1002/tera.1420470609

Zhang, X., Yalcin, S., Lee, D. F., Yeh, T. Y., Lee, S. M., Su, J., et al. (2011). FOXO1 is an essential regulator of pluripotency in human embryonic stem cells. *Nat. Cell Biol.* 13, 1092–1099. doi: 10.1038/ncb2293

Zimmerman, E. F., Wee, E. L., Phillips, N., and Roberts, N. (1981). Presence of serotonin in the palate just prior to shelf elevation. *J. Embryol. Exp. Morphol.* 64, 233–250.

Conflict of Interest: The authors declare that the research was conducted in the absence of any commercial or financial relationships that could be construed as a potential conflict of interest.

Publisher's Note: All claims expressed in this article are solely those of the authors and do not necessarily represent those of their affiliated organizations, or those of the publisher, the editors and the reviewers. Any product that may be evaluated in this article, or claim that may be made by its manufacturer, is not guaranteed or endorsed by the publisher.

frontiers in Cell and Developmental Biology

ORIGINAL RESEARCH
published: 10 February 2022
doi: 10.3389/fcell.2022.621261

Genome-wide Interaction Study Implicates *VGLL2* and Alcohol Exposure and *PRL* and Smoking in Orofacial Cleft Risk

*Jenna C. Carlson[1], John R. Shaffer[2], Fred Deleyiannis[3], Jacqueline T. Hecht[4], George L. Wehby[5], Kaare Christensen[6], Eleanor Feingold[1,2], Seth M. Weinberg[2,6], Mary L. Marazita[2,7] and Elizabeth J. Leslie[8]**

[1]Department of Biostatistics, Graduate School of Public Health, University of Pittsburgh, Pittsburgh, United States, [2]Department of Human Genetics, Graduate School of Public Health, University of Pittsburgh, Pittsburgh, United States, [3]UCHealth Medical Group, Colorado Springs, United States, [4]Department of Pediatrics, University of Texas Health Science Center at Houston, Houston, United States, [5]Department of Health Management and Policy, College of Public Health, University of Iowa, Iowa City, United States, [6]Department of Epidemiology, Institute of Public Health, University of Southern Denmark, Odense, Denmark, [7]Center for Craniofacial and Dental Genetics, Department of Oral Biology, School of Dental Medicine, University of Pittsburgh, Pittsburgh, United States, [8]Department of Human Genetics, Emory University School of Medicine, Atlanta, United States

OPEN ACCESS

Edited by:
Cornelia Braicu, Iuliu Haţieganu University of Medicine and Pharmacy, Romania

Reviewed by:
Jonathan Sandy, University of Bristol, United Kingdom
Heiko Martin Reutter, University of Erlangen Nuremberg, Germany

***Correspondence:**
Elizabeth J. Leslie
Ejlesli@emory.edu

Specialty section:
This article was submitted to Molecular and Cellular Pathology, a section of the journal Frontiers in Cell and Developmental Biology

Received: *25 October 2020*
Accepted: *18 January 2022*
Published: *10 February 2022*

Citation:
Carlson JC, Shaffer JR, Deleyiannis F, Hecht JT, Wehby GL, Christensen K, Feingold E, Weinberg SM, Marazita ML and Leslie EJ (2022) Genome-wide Interaction Study Implicates VGLL2 *and Alcohol Exposure and* PRL *and Smoking in Orofacial Cleft Risk. Front. Cell Dev. Biol. 10:621261. doi: 10.3389/fcell.2022.621261*

Non-syndromic cleft lip with or without cleft palate (NSCL/P) is a common birth defect, affecting approximately 1 in 700 births. NSCL/P has complex etiology including several known genes and environmental factors; however, known genetic risk variants only account for a small fraction of the heritability of NSCL/P. It is commonly suggested that gene-by-environment (G×E) interactions may help explain some of the "missing" heritability of NSCL/P. We conducted a genome-wide G×E interaction study in cases and controls of European ancestry with three common maternal exposures during pregnancy: alcohol, smoking, and vitamin use using a two-stage design. After selecting 127 loci with suggestive 2df tests for gene and G x E effects, 40 loci showed significant G x E effects after correcting for multiple tests. Notable interactions included SNPs of 6q22 near VGLL2 with alcohol and 6p22.3 near PRL with smoking. These interactions could provide new insights into the etiology of CL/P and new opportunities to modify risk through behavioral changes.

Keywords: orofacial cleft, gene-environement interactions, maternal exposures, GWAS, case- control

INTRODUCTION

Interest in identifying the causal factors for birth defects, including orofacial clefts (OFCs) can be traced back centuries (Marazita, 2012) and has often involved a debate as to the contribution of genetic versus environmental risk factors (Beames and Lipinski, 2020). Evidence for a multifactorial model for OFC etiology originated with Fraser's early studies exposing pregnant mice to cortisone showing that the incidence of corticosteroid induced cleft palate varied by strain. The multifactorial model is favored in human nonsyndromic OFCs, where twin and family studies provide evidence for a strong, but incomplete, genetic component. Many environmental factors have been postulated to modify risk of OFCs including maternal medications, smoking or alcohol consumption (Romitti et al., 2007; Grewal et al., 2008), nutrition (Kelly et al., 2012), obesity (Blomberg and Källén, 2009), gestational diabetes (Figueiredo et al., 2015), and occupational exposures. Of these, cigarette

smoking, alcohol consumption, and folic acid supplementation are the most widely studied, but, except for smoking (Hackshaw et al., 2011), these exposures have inconsistent results in epidemiological studies. Maternal smoking, on the other hand, has been shown to increase risk consistently across many studies with similar effect sizes (Little et al., 2004).

Over the last 10 years, 20 independent genome-wide association studies (GWAS) or meta-analyses have identified at least 50 loci associated with OFCs (Beaty et al., 2016). Cumulatively, these loci are estimated to account for 25–30% of the heritable risk attributed to additive genetic effects. Other approaches are needed to identify the "missing" heritability, some of which may be attributed to interaction effects. Leveraging published data from GWAS studies, gene-environment interaction (GxE) studies have become a popular approach to further elucidate OFC risk. Following one such GWAS study in European and Asian case-parent trios (Beaty 2010), candidate gene and pathway-based GxE analyses have suggested interactions between smoking and *RUNX2* (Wu et al., 2012), and between multiple exposures and *BMP4* (Chen et al., 2014). Genome-wide GxE using a variety of statistical approaches have identified interactions for maternal smoking, alcohol, or folate supplementation in cleft palate (Beaty et al., 2011; Wu et al., 2014; Haaland et al., 2017) and cleft lip with or without cleft palate (Haaland et al., 2018; Haaland et al., 2019).

In this study, we performed genome-wide GxE analyses in a case-control sample of European ancestry from the Pittsburgh Orofacial Cleft Study to identify interactions between genetic variants and three exposures (maternal smoking, alcohol consumption, or vitamin supplementation) during the periconceptional period that influence risk of OFCs.

MATERIALS AND METHODS

Study Samples and Genotyping

The sample for these analyses was derived from a larger multiethnic OFC cohort, which has been previously described (Leslie et al., 2016). Briefly, participants were recruited from 18 sites worldwide as part of ongoing genetic studies conducted by the University of Iowa and the University of Pittsburgh Center for Craniofacial and Dental Genetics. All sites obtained Institutional Review Board approval both locally and at the University of Iowa or the University of Pittsburgh. All participants gave informed consent. These data are available through dbGaP (accession number: phs000774. v2. p1).

This large multiethnic cohort contains OFC-affected probands and their unaffected relatives in addition to controls without a family history of OFC or other craniofacial anomalies. Additionally, data were obtained on three maternal periconceptional exposures: alcohol use, smoking, and vitamin use. Periconceptional exposures were gathered from maternal self-report of alcohol use, personal smoking, or vitamin use during the 3 months prior to pregnancy and during the first trimester for each child as were used as binary indicator variables in analyses.

From this larger cohort, a subset of unrelated cases and controls of European ancestry and with complete data for the three environmental exposure measures was drawn. It consisted of 344 NSCL/P cases and 194 controls of European descent from Denmark, Hungary, and the United States (**Supplemental Table S1**).

The genotyping, quality control procedures, imputation, and generation of principal components of ancestry (PCAs) have been previously described (Leslie et al., 2016). Briefly, samples were genotyped using the Illumina HumanCore + Exome chip (Illumina Inc., San Diego, CA), with approximately 97% of the genotyped SNPs passing quality control filters, resulting in a total of 539,473 genotyped SNPs. Genotype imputation for an additional 34,985,077 unobserved polymorphisms was performed using IMPUTE2 software with the multiethnic 1,000 Genomes Project Phase 3 reference panel (Howie et al., 2009). Imputed genotype probabilities were converted to most-likely genotypes using GTOOL; only most-likely genotypes with probabilities >0.9 were retained for statistical analysis. Imputed SNPs with INFO scores <0.5 or those deviating from Hardy–Weinberg equilibrium ($p < 1 \times 10^{-4}$ in a set of unrelated European controls) were also excluded from the analysis. The University of Washington, Genetics Coordinating Center released a full online report on the data cleaning, quality assurance, ancestry analyses, and imputation for this study (http://www.ccdg.pitt.edu/docs/Marazita_ofc_QC_report_feb2015.pdf, last accessed April 25, 2016). Additionally, we excluded variants with a minor allele frequency <10%, as the power to detect interaction effects among low-frequency variants is very limited and analysis of such variants is prone to type 1 errors. After these filtering steps, 5,165,675 variants were included in the genome-wide interaction analyses. Population structure was measured through generation of principal components of ancestry using the R package SNPRelate following the approach introduced by Patterson, Price, and Reich (Patterson et al., 2006).

Statistical Analyses

To assess the association between genetic variants and NSCL/P that may or may not be modified by an environmental factor, we used a two-stage approach for each of the three environmental exposure. First, we employed the strategy laid out in Kraft et al., 2007 a 2 degree of freedom (2df) joint test of the gene (G) and gene-environment interaction (GE) effects was employed genome-wide using logistic regression, adjusting for five principal components of ancestry (Kraft et al., 2007). This provides a sensitive test for two scenarios simultaneously: (Marazita, 2012) where there is a genetic effect that is similar across all environmental strata, and (Beames and Lipinski, 2020) where there is a genetic effect that is specific to a specific environmental stratum. Then, the GE effect was interrogated for variants demonstrating at least suggestive association from the G-GE joint test (i.e., $p < 0.05$) to identify regions in which there is a genetic effect differing across environmental stratum, not just a genetic effect alone. To estimate the dependence between the joint G-GE and GE alone tests and derive a significance threshold to use which accounts for this dependence, we performed simulation (details available in **Supplemental Note**). In simulation, using a first-stage threshold of $p < 0.05$, with a second-stage threshold of $p < 0.00275$, yielded a procedure with a properly controlled type-1 error rate of 0.05. To

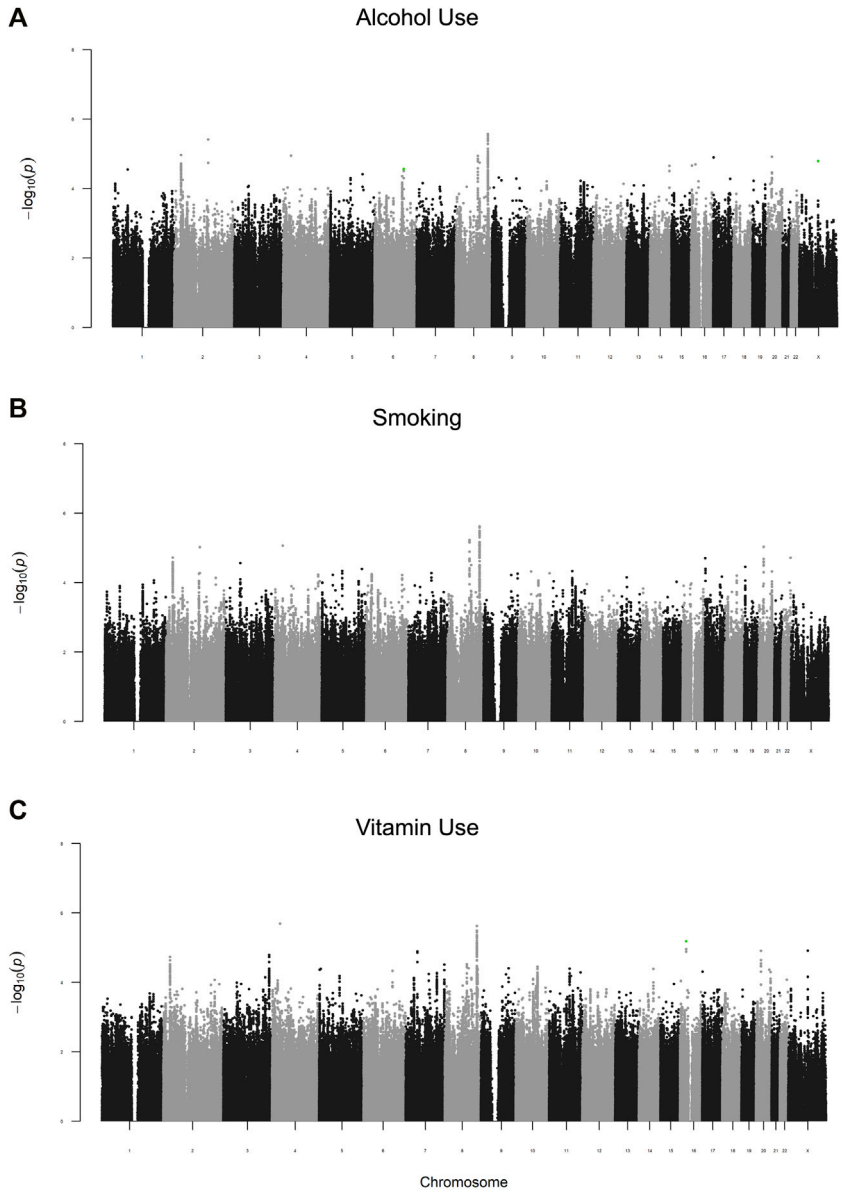

FIGURE 1 | Manhattan plots of the G-GE test for maternal periconceptional **(A)** alcohol use, **(B)** smoking, **(C)** vitamin use. SNPs highlighted in green are those with significant GE effects ($p_{2df} < 0.05$ and $p_{GE} < 4.8 \times 10^{-6}$).

account for multiple testing, we then Bonferroni-adjusted this second-stage significance level for interrogating the GE effect, adjusting for the number of regions with suggestive results from the G-GE joint test (i.e., $0.00275/572 = 4.8 \times 10^{-6}$). All analyses were conducted in PLINK v1.9 assuming an additive genetic model (Chang et al., 2015).

RESULTS

As a follow-up study to previous GWAS identifying marginal gene effects (G) increasing risk for NSCL/P, this study focused on identifying G x E interactions. We carried out a two-stage analysis, where we first examined the 2df joint test of G and G x E (GE). We observed suggestive evidence of association in the joint G-GE test for 572 loci (**Figure 1**). Several loci had multiple SNPs with $p < 0.05$ in each of the three analyses. These included 8q24, one of the most reliably associated loci with NSCL/P in European populations (Beaty et al., 2016). As expected, this locus showed strong G effects, but did not have a significant GE effect ($p > 0.05$). A locus on 2p23 with similarly strong G effects but no GE effects was identified in all three analyses but to our knowledge has not been reported before in GWAS of NSCL/P.

To identify gene-environment interactions, we next examined the GE effect alone for each variant with $p < 0.05$ in the joint test. Three regions (5 SNPs) had a significant GE p-value less than

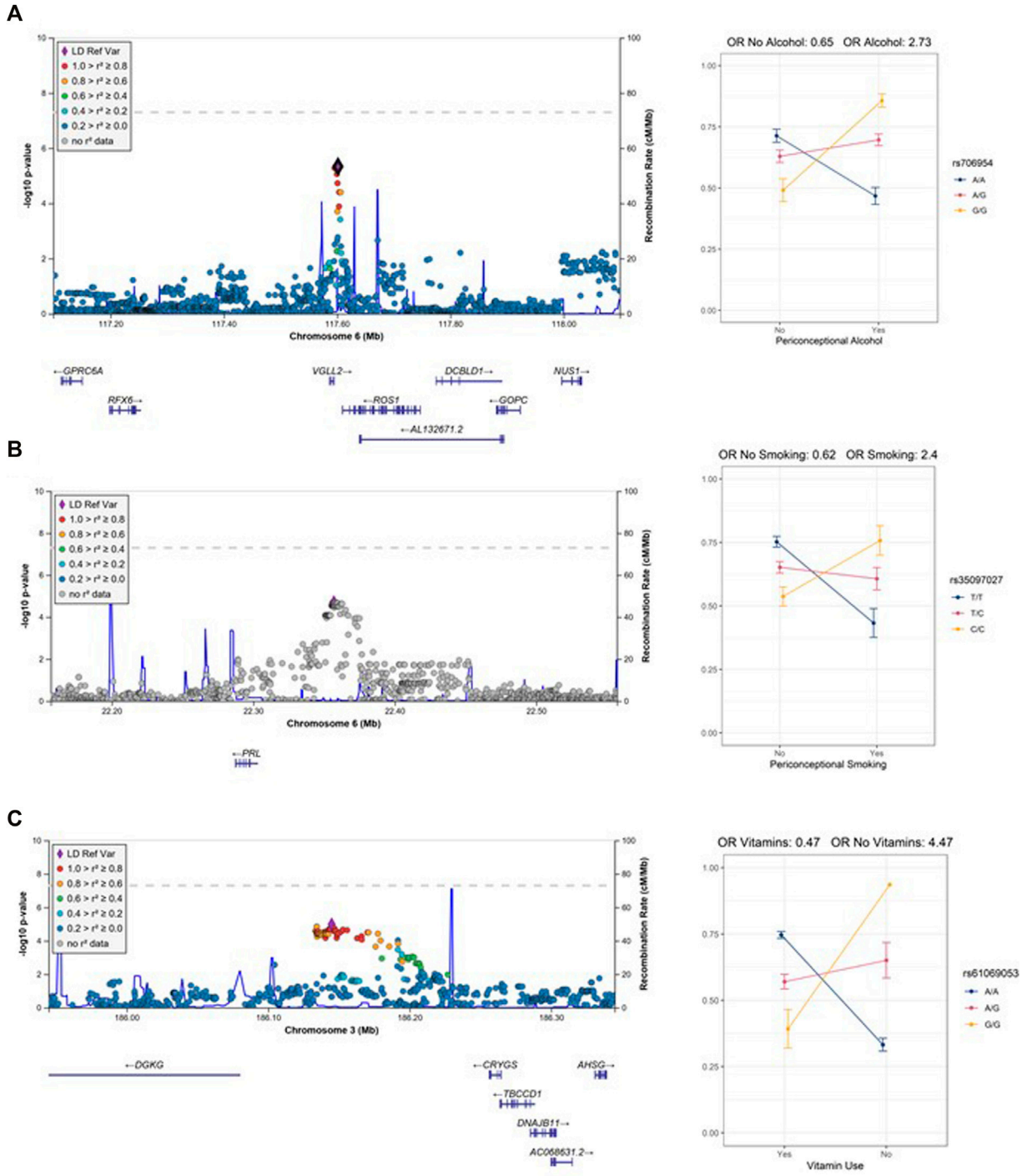

FIGURE 2 | Regional association plots of the GE test with interaction plots **(A)** 6q22 (rs706954) interaction with alcohol use. **(B)** 6p22.3 (rs35097027) interaction with smoking. **(C)** 3q27.3 (rs61069053) with vitamin use. Note, only one individual is homozygous for the G allele in the no vitamin use stratum.

4.8×10^{-6} (i.e., Bonferroni correction for 572 loci) and several more had suggestive results (GE *p*-value less than 5×10^{-4}) (**Supplementary Table S2**). Among these regions, we observed a significant interaction effect between rs706954, a variant <5 kb downstream of *VGLL2* on 6q22.1, and periconceptional alcohol exposure ($p_{GE} = 4.62 \times 10^{-6}$). The minor allele (G) of rs706954 was associated with higher odds of NSCL/P within individuals with periconceptional alcohol exposure, but lower odds with

individuals without periconceptional alcohol exposure (**Figure 2**). We also observed a significant GE effect with periconceptional alcohol exposure for a SNP on chrX (rs5912923, $p_{GE} = 3.71 \times 10^{-6}$).

Two additional loci had several SNPs per locus with suggestive GE *p*-values for alcohol exposures. These included 6q21 (lead SNP rs6929494, $p_{GE} = 1.18 \times 10^{-5}$) and 11q21 (lead SNP rs7116990, $p_{GE} = 1.80 \times 10^{-5}$). At the 6q21 locus, which included genes *REVL3* and *TRAF3IP2*, the major allele (A) of rs6929494 was associated with higher odds of NSCL/P within individuals with periconceptional alcohol exposure, but had an opposite (protective) effect for individuals without periconceptional alcohol exposure. The associated SNPs at the 11q21 locus, are located in an intergenic region between *CNTN5* and *JRKL*; for the lead SNP, rs7116990, the major allele (A) was associated with greater odds of NSCL/P in the individuals with periconceptional alcohol exposure and lower odds of NSCL/P for individuals without periconceptional alcohol exposure.

In the vitamin exposure analysis, one locus on 16p21.1 harbored a variant with a significant GE effect (rs9930171, $p_{GE} = 4.78 \times 10^{-6}$). While not statistically significant, several SNPs on 3q27.3 showed a suggestive interaction with vitamin exposure (lead SNP rs61069053, $p_{GE} = 1.05 \times 10^{-5}$). The minor allele (G) of rs61069053, located in an intergenic region between *CRYGS* and *DGKG*, had higher estimated odds of NSCL/P in the individuals without periconceptional vitamin exposure, but had lower odds of NSCL/P for the periconceptional vitamin exposure group. However, this result may be confounded by the distribution of vitamin use and allele frequency; only one individual was homozygous for the minor allele and did not have vitamin exposure.

In the periconceptional smoking analysis, no variants achieved statistical significance. However, at 6p22.3, several SNPs showed suggestive GE *p*-values for smoking (lead SNP rs35097027, $p_{GE} = 1.96 \times 10^{-5}$). These variants are upstream of *PRL*; the minor allele (C) of rs35097027 conferred higher odds of CL/P for individuals with maternal smoking exposure, but lower odds of NSCL/P for individuals without maternal smoking exposure (**Figure 2**).

DISCUSSION

The primary goal of this paper was to identify additional gene-environment interactions for NSCL/P and build on our previous work in this dataset (Leslie et al., 2016). These analyses were motivated by multiple studies reporting associations between OFCs and periconceptional smoking, alcohol use, and vitamin supplementation (Dixon et al., 2011; Beaty et al., 2016). Genome-wide interaction scans, however, have been limited for NSCL/P (Wu et al., 2014; Haaland et al., 2018). Our analyses add to a growing list of loci for which interactions between SNPs and maternal environmental exposures influence risk of OFCs.

While procedures for identifying GxE interactions have low power in general, the 2df joint G-GE test is nearly always more powerful than the marginal G and/or GE tests, even with a relatively small sample size, making it a useful screening tool, especially for common variants with strong effects (Kraft et al., 2007). Consistent with this, the loci in these analyses with statistically significant G-GE associations that were driven by the GE effect had markedly strong effect estimates. Notably, the estimated odds of NSCL/P were 2.73 times higher with each copy of the minor allele G of rs117083 (in linkage disequilibrium with rs706954, $R^2 = 0.88$) for individuals with maternal periconceptional alcohol exposure and was 35% lower for individuals without periconceptional alcohol exposure. For the only locus with more than one SNP with a significant GE *p*-value [i.e., 6q22.1 (alcohol)], the genotypic odds ratio ranged from 40% lower odds of CL/P to 178% higher odds. For alcohol and smoking exposures, we primarily identified scenarios described as "cross-over" interactions where the genotype group at lowest risk for NSCL/P without the exposure had high risk for NSCL/P with the exposure. In each of these interactions, the influence of genotype entirely depends on the exposure. The method we used to detect interactions is better suited for these "cross-over" interactions. However, it is limited in its ability to detect associations that are only present in one environmental context. For example, it is quite plausible that a genetic variant may only modify risk in the presence of a specific environment. This method has lower statistical power to detect such an association; additional methods are needed to explicitly search for these association signals.

We identified three loci with significant interactions and several loci with suggestive interactions. Of these, two loci have notable biological plausibility which we discuss in detail. The only locus with several variants demonstrating significant GE effects with periconceptional alcohol exposure was on 6q22.1, approximately 5 kb upstream of *VGLL2*, encoding vestigial-like 2. *Vgll2* is one of several Vestigial-like factors that plays a role in muscle fiber differentiation and the distribution of skeletal muscle fibers (Honda et al., 2017). Although its expression in adult tissues is restricted to skeletal muscle, during development, Vgll2 is more broadly expressed. In mice, its expression is enriched in the mandibular and maxillary prominences at embryonic day 10.5 and is localized to the epithelia of these structures (Johnson et al., 2011). In the zebrafish, Vgll2 is expressed in the pharyngeal pouches and somites (Maeda et al., 2002; Mielcarek et al., 2002). A role for *VGLL2* in craniofacial development is further supported by vgll2a zebrafish morphants, which induce death of neural crest cells in the pharyngeal arches causing hypoplasia of the Meckel's and palatoquadrate cartilages and truncation of the ethmoid plate (Johnson et al., 2011). Models for fetal alcohol syndrome indicate that ethanol exposure enhances cell death of cranial neural crest cells (Cartwright and Smith, 1995; Smith et al., 2014). Although a specific interaction between VGLL2 and ethanol has not been described *in vitro* or *in vivo*, these data, combined with our statistical interaction suggest this may be a fruitful area for future studies.

At the 6p22.3 locus, which was suggestively associated with exposure to maternal smoking, the lead SNP was located 60 kb upsteam of *PRL*, which encodes prolactin. Prolactin is a reproductive hormone primarily known for its ability to stimulate mammary gland development and lactation, but it also has a variety of functions in reproduction, growth, and development (Bole-Feysot et al., 1998). Prolactin receptor

transcripts and proteins have been detected in non-lactogenic tissues notably including the facial cartilage and olfactory epithelium in mammals (Freemark et al., 1997). Prolactin levels are known to be altered by both active smoking and exposure to secondhand tobacco smoke (Muraki et al., 1979; Ng et al., 2006; Xue et al., 2010; Benedict et al., 2012). Although smoking is associated with lower prolactin levels in pregnant women, the same is not true for fetal prolactin levels (Andersen et al., 1984). A role for prolactin in craniofacial development and OFCs is unclear as knockouts of mouse PRL receptors are viable and lack gross morphological defects (Ormandy et al., 1997). However, in amphibian models, prolactin signaling has been suggested as the pathway underlying the ability of pre-metamorphic *Xenopus laevis* tadpoles to correct craniofacial defects induced by thioridazine (Pinet et al., 2019). However, the same group also found that increased prolactin signaling during development alone does not cause craniofacial defects. Nonetheless, there is evidence linking smoking to prolactin levels and for prolactin signaling in craniofacial development; additional research will be needed to connect these results and determine a role for PRL and smoking in OFCs.

Our previous studies using this dataset have made use of the ancestral diversity that resulted from the 13 different recruitment sites worldwide. However, this study was limited to individuals of European descent as the number of unrelated participants with complete data from the other ancestry groups was quite small. In previous GWASs for gene-environment interactions, a lack of observations precluded the analysis of smoking and alcohol exposures in Asian trios (Haaland et al., 2018). The authors speculated that this was consistent with general trends of low alcohol and cigarette use among Asian women (Ng et al., 2014). This may also be true for other populations recruited into our study, but the incomplete data may also be due to changing study designs over the recruitment period. We also note that the recruitment of these participants was not population-based and thus does not reflect the population prevalence of NSCL/P nor the three environmental exposures we considered. In addition, a binary exposure variable does not capture or represent the range of possible environmental exposures that may influence development of NSCL/P. Therefore, the conclusions drawn here are limited to the study sample used in these analyses and cannot be used to draw conclusions at a broader level.

To summarize, we performed a genome-wide analysis to detect gene-environment interactions influencing risk of NSCL/P in individuals of European ancestry. We identified two notable interactions: near VGLL2 and PRL with maternal periconceptional alcohol use and smoking, respectively that are plausibly associated with risk of NSCL/P. These interaction effects are novel and warrant further investigations. If confirmed, these interactions provide new insights into the etiology of NSCL/P and could provide opportunities to modify risk through behavioral changes.

DATA AVAILABILITY STATEMENT

Publicly available datasets were analyzed in this study. This data can be found here: https://www.ncbi.nlm.nih.gov/projects/gap/cgi-bin/study.cgi?study_id=phs000774.v2.p1.

ETHICS STATEMENT

The studies involving human participants were reviewed and approved by Institutional Review Boards at the University of Pittsburgh and Emory University. Written informed consent to participate in this study was provided by the participants' legal guardian/next of kin.

AUTHOR CONTRIBUTIONS

JC and EL conceived the study and carried out the analyses. FD, JH, GW, KC, SW, MM contributed samples and data. JC and EL drafted the manuscript. All authors contributed to interpretation and critically reviewed and approved the manuscript.

FUNDING

This work was supported by grants from the National Institutes of Health (NIH): R00-DE025060 (EL), X01-HG007485 (MM, EF), R01-DE016148 (MM, SW). Genotyping and data cleaning were provided via an NIH contract to the Johns Hopkins Center for Inherited Disease Research: HHSN268201200008I.

ACKNOWLEDGMENTS

This project would not have been possible without the participation of families, field staff, and collaborators around the world. Special recognition to our colleague Andrew Czeizel (deceased).

SUPPLEMENTARY MATERIAL

The Supplementary Material for this article can be found online at: https://www.frontiersin.org/articles/10.3389/fcell.2022.621261/full#supplementary-material

REFERENCES

Andersen, A. N., Rønn, B., Tjønneland, A., Djursing, H., and Schiøler, V. (1984). Low Maternal but normal Fetal Prolactin Levels in Cigarette Smoking Pregnant Women. *Acta Obstet. Gynecol. Scand.* 63 (3), 237–239. doi:10.3109/00016348409155504

Beames, T. G., and Lipinski, R. J. (2020). Gene-environment Interactions: Aligning Birth Defects Research with Complex Etiology. *Development* 147 (21). doi:10.1242/dev.191064

Beaty, T. H., Marazita, M. L., and Leslie, E. J. (2016). Genetic Factors Influencing Risk to Orofacial Clefts: Today's Challenges and Tomorrow's Opportunities. *F1000Res* 5, 2800. doi:10.12688/f1000research.9503.1

Beaty, T. H., Ruczinski, I., Murray, J. C., Marazita, M. L., Munger, R. G., Hetmanski, J. B., et al. (2011). Evidence for Gene-Environment Interaction in a Genome Wide Study of Nonsyndromic Cleft Palate. *Genet. Epidemiol.* 35 (6), 469–478. doi:10.1002/gepi.20595

Benedict, M. D., Missmer, S. A., Ferguson, K. K., Vitonis, A. F., Cramer, D. W., and Meeker, J. D. (2012). Secondhand Tobacco Smoke Exposure Is Associated with Prolactin but Not Thyroid Stimulating Hormone Among Nonsmoking Women Seeking *In Vitro* Fertilization. *Environ. Toxicol. Pharmacol.* 34 (3), 761–767. doi:10.1016/j.etap.2012.09.010

Blomberg, M. I., and Källén, B. (2009). Maternal Obesity and Morbid Obesity: the Risk for Birth Defects in the Offspring. *Birth Defect Res. A.* 88 (1), 35–40. doi:10.1002/bdra.20620

Bole-Feysot, C., Goffin, V., Edery, M., Binart, N., and Kelly, P. A. (1998). Prolactin (PRL) and its Receptor: Actions, Signal Transduction Pathways and Phenotypes Observed in PRL Receptor Knockout Mice. *Endocr. Rev.* 19 (3), 225–268. doi:10.1210/edrv.19.3.0334

Cartwright, M. M., and Smith, S. M. (1995). Stage-dependent Effects of Ethanol on Cranial Neural Crest Cell Development: Partial Basis for the Phenotypic Variations Observed in Fetal Alcohol Syndrome. *Alcohol. Clin. Exp. Res.* 19 (6), 1454–1462. doi:10.1111/j.1530-0277.1995.tb01007.x

Chang, C. C., Chow, C. C., Tellier, L. C., Vattikuti, S., Purcell, S. M., and Lee, J. J. (2015). Second-generation PLINK: Rising to the challenge of Larger and Richer Datasets. *GigaSci* 4, 7. doi:10.1186/s13742-015-0047-8

Chen, Q., Wang, H., Schwender, H., Zhang, T., Hetmanski, J. B., Chou, Y.-H. W., et al. (2014). Joint Testing of Genotypic and Gene-Environment Interaction Identified Novel Association for BMP4 with Non-syndromic CL/P in an Asian Population Using Data from an International Cleft Consortium. *PLoS One* 9 (10), e109038. doi:10.1371/journal.pone.0109038

Dixon, M. J., Marazita, M. L., Beaty, T. H., and Murray, J. C. (2011). Cleft Lip and Palate: Understanding Genetic and Environmental Influences. *Nat. Rev. Genet.* 12 (3), 167–178. doi:10.1038/nrg2933

Figueiredo, J. C., Ly, S., Magee, K. S., Ihenacho, U., Baurley, J. W., Sanchez-Lara, P. A., et al. (2015). Parental Risk Factors for Oral Clefts Among Central Africans, Southeast Asians, and Central Americans. *Birth Defects Res. A: Clin. Mol. Teratology* 103 (10), 863–879. doi:10.1002/bdra.23417

Freemark, M., Driscoll, P., Maaskant, R., Petryk, A., and Kelly, P. A. (1997). Ontogenesis of Prolactin Receptors in the Human Fetus in Early Gestation. Implications for Tissue Differentiation and Development. *J. Clin. Invest.* 99 (5), 1107–1117. doi:10.1172/JCI119239

Grewal, J., Carmichael, S. L., Ma, C., Lammer, E. J., and Shaw, G. M. (2008). Maternal Periconceptional Smoking and Alcohol Consumption and Risk for Select Congenital Anomalies. *Birth Defect Res. A.* 82 (7), 519–526. doi:10.1002/bdra.20461

Haaland, Ø. A., Jugessur, A., Gjerdevik, M., Romanowska, J., Shi, M., Beaty, T. H., et al. (2017). Genome-wide Analysis of Parent-Of-Origin Interaction Effects with Environmental Exposure (PoOxE): An Application to European and Asian Cleft Palate Trios. *PLoS One* 12 (9), e0184358. doi:10.1371/journal.pone.0184358

Haaland, Ø. A., Lie, R. T., Romanowska, J., Gjerdevik, M., Gjessing, H. K., and Jugessur, A. (2018). A Genome-wide Search for Gene-Environment Effects in Isolated Cleft Lip with or without Cleft Palate Triads Points to an Interaction between Maternal Periconceptional Vitamin Use and Variants in ESRRG. *Front. Genet.* 9, 60. doi:10.3389/fgene.2018.00060

Haaland, Ø. A., Romanowska, J., Gjerdevik, M., Lie, R. T., Gjessing, H. K., and Jugessur, A. (2019). A Genome-wide Scan of Cleft Lip Triads Identifies Parent-Of-Origin Interaction Effects between ANK3 and Maternal Smoking, and between ARHGEF10 and Alcohol Consumption. *F1000Res* 8, 960. doi:10.12688/f1000research.19571.2

Hackshaw, A., Rodeck, C., and Boniface, S. (2011). Maternal Smoking in Pregnancy and Birth Defects: a Systematic Review Based on 173 687 Malformed Cases and 11.7 Million Controls. *Hum. Reprod. Update* 17 (5), 589–604. doi:10.1093/humupd/dmr022

Honda, M., Hidaka, K., Fukada, S.-i., Sugawa, R., Shirai, M., Ikawa, M., et al. (2017). Vestigial-like 2 Contributes to normal Muscle Fiber Type Distribution in Mice. *Sci. Rep.* 7 (1), 7168. doi:10.1038/s41598-017-07149-0

Howie, B. N., Donnelly, P., and Marchini, J. (2009). A Flexible and Accurate Genotype Imputation Method for the Next Generation of Genome-wide Association Studies. *Plos Genet.* 5 (6), e1000529. doi:10.1371/journal.pgen.1000529

Johnson, C. W., Hernandez-Lagunas, L., Feng, W., Melvin, V. S., Williams, T., and Artinger, K. B. (2011). Vgll2a Is Required for Neural Crest Cell Survival during Zebrafish Craniofacial Development. *Dev. Biol.* 357 (1), 269–281. doi:10.1016/j.ydbio.2011.06.034

Kelly, D., O'Dowd, T., and Reulbach, U. (2012). Use of Folic Acid Supplements and Risk of Cleft Lip and Palate in Infants: a Population-Based Cohort Study. *Br. J. Gen. Pract.* 62 (600), e466–e472. doi:10.3399/bjgp12X652328

Kraft, P., Yen, Y.-C., Stram, D. O., Morrison, J., and Gauderman, W. J. (2007). Exploiting Gene-Environment Interaction to Detect Genetic Associations. *Hum. Hered.* 63 (2), 111–119. doi:10.1159/000099183

Leslie, E. J., Carlson, J. C., Shaffer, J. R., Feingold, E., Wehby, G., Laurie, C. A., et al. (2016). A Multi-Ethnic Genome-wide Association Study Identifies Novel Loci for Non-syndromic Cleft Lip with or without Cleft Palate on 2p24.2, 17q23 and 19q13. *Hum. Mol. Genet.* 25 (13), ddw104–72. doi:10.1093/hmg/ddw104

Little, J., Cardy, A., and Munger, R. G. (2004). Tobacco Smoking and Oral Clefts: a Meta-Analysis. *Bull. World Health Organ.* 82 (3), 213–218. Available at: https://www.ncbi.nlm.nih.gov/pmc/articles/PMC2585921/.

Maeda, T., Chapman, D. L., and Stewart, A. F. R. (2002). Mammalian Vestigial-like 2, a Cofactor of TEF-1 and MEF2 Transcription Factors that Promotes Skeletal Muscle Differentiation. *J. Biol. Chem.* 277 (50), 48889–48898. doi:10.1074/jbc.M206858200

Marazita, M. L. (2012). The Evolution of Human Genetic Studies of Cleft Lip and Cleft Palate. *Annu. Rev. Genom. Hum. Genet.* 13, 263–283. doi:10.1146/annurev-genom-090711-163729

Mielcarek, M., Günther, S., Krüger, M., and Braun, T. (2002). VITO-1, a Novel Vestigial Related Protein Is Predominantly Expressed in the Skeletal Muscle Lineage. *Mech. Dev.* 119 (Suppl. 1), S269–S274. doi:10.1016/s0925-4773(03)00127-8

Muraki, T., Tokunaga, Y., Nakadate, T., and Kato, R. (1979). Inhibition by Cholinergic Agonists of the Prolactin Release Induced by Morphine. *Naunyn-schmiedeberg's Arch. Pharmacol.* 308 (3), 249–254. doi:10.1007/BF00501389

Ng, M., Freeman, M. K., Fleming, T. D., Robinson, M., Dwyer-Lindgren, L., Thomson, B., et al. (2014). Smoking Prevalence and Cigarette Consumption in 187 Countries, 1980-2012. *JAMA* 311 (2), 183–192. doi:10.1001/jama.2013.284692

Ng, S. P., Steinetz, B. G., Lasano, S. G., and Zelikoff, J. T. (2006). Hormonal Changes Accompanying Cigarette Smoke-Induced Preterm Births in a Mouse Model. *Exp. Biol. Med. (Maywood)* 231 (8), 1403–1409. doi:10.1177/153537020623100814

Ormandy, C. J., Camus, A., Barra, J., Damotte, D., Lucas, B., Buteau, H., et al. (1997). Null Mutation of the Prolactin Receptor Gene Produces Multiple Reproductive Defects in the Mouse. *Genes Dev.* 11 (2), 167–178. doi:10.1101/gad.11.2.167

Patterson, N., Price, A. L., and Reich, D. (2006). Population Structure and Eigenanalysis. *Plos Genet.* 2 (12), e190. doi:10.1371/journal.pgen.0020190

Pinet, K., Deolankar, M., Leung, B., and McLaughlin, K. A. (2019). Adaptive Correction of Craniofacial Defects in Pre-metamorphic *Xenopus laevis* Tadpoles Involves Thyroid Hormone-independent Tissue Remodeling. *Development* 146 (14). doi:10.1242/dev.175893

Romitti, P. A., Sun, L., Honein, M. A., Reefhuis, J., Correa, A., and Rasmussen, S. A. (2007). Maternal Periconceptional Alcohol Consumption and Risk of Orofacial Clefts. *Am. J. Epidemiol.* 166 (7), 775–785. doi:10.1093/aje/kwm146

Smith, S. M., Garic, A., Flentke, G. R., and Berres, M. E. (2014). Neural Crest Development in Fetal Alcohol Syndrome. *Birth Defect Res. C* 102 (3), 210–220. doi:10.1002/bdrc.21078

Wu, T., Fallin, M. D., Shi, M., Ruczinski, I., Liang, K. Y., Hetmanski, J. B., et al. (2012). Evidence of Gene-Environment Interaction for the RUNX2 Gene and Environmental Tobacco Smoke in Controlling the Risk of Cleft Lip With/without Cleft Palate. *Birth Defects Res. Part A: Clin. Mol. Teratology* 94 (2), 76–83. doi:10.1002/bdra.22885

Wu, T., Schwender, H., Ruczinski, I., Murray, J. C., Marazita, M. L., Munger, R. G., et al. (2014). Evidence of Gene–Environment Interaction for Two Genes on Chromosome 4 and Environmental Tobacco Smoke in Controlling the Risk of Nonsyndromic Cleft Palate. *PLoS One* 9 (2), e88088. doi:10.1371/journal.pone.0088088

Xue, Y., Morris, M., Ni, L., Guthrie, S. K., Zubieta, J.-K., Gonzalez, K., et al. (2010). Venous Plasma Nicotine Correlates of Hormonal Effects of Tobacco Smoking. *Pharmacol. Biochem. Behav.* 95 (2), 209–215. doi:10.1016/j.pbb.2010.01.007

Conflict of Interest: The authors declare that the research was conducted in the absence of any commercial or financial relationships that could be construed as a potential conflict of interest.

The reviewer ZJ declared a past collaboration with several of the authors EL and MM to the handling editor.

Publisher's Note: All claims expressed in this article are solely those of the authors and do not necessarily represent those of their affiliated organizations, or those of the publisher, the editors, and the reviewers. Any product that may be evaluated in this article, or claim that may be made by its manufacturer, is not guaranteed or endorsed by the publisher.

Advantages of publishing in Frontiers

OPEN ACCESS
Articles are free to read for greatest visibility and readership

FAST PUBLICATION
Around 90 days from submission to decision

HIGH QUALITY PEER-REVIEW
Rigorous, collaborative, and constructive peer-review

TRANSPARENT PEER-REVIEW
Editors and reviewers acknowledged by name on published articles

Frontiers
Avenue du Tribunal-Fédéral 34
1005 Lausanne | Switzerland

Visit us: www.frontiersin.org
Contact us: frontiersin.org/about/contact

REPRODUCIBILITY OF RESEARCH
Support open data and methods to enhance research reproducibility

DIGITAL PUBLISHING
Articles designed for optimal readership across devices

FOLLOW US
@frontiersin

IMPACT METRICS
Advanced article metrics track visibility across digital media

EXTENSIVE PROMOTION
Marketing and promotion of impactful research

LOOP RESEARCH NETWORK
Our network increases your article's readership